ADSORPTION PROPERTIES STUDIES OF THE NICKEL CATALYSTS FOR CARBON DIOXIDE REFORMING OF METHANE

Rong-Gang Ding[1, 2] *Zi-Feng Yan*[2]

[1]Department of Chemical Engineering, University of Queensland, Brisbane, 4072, Australia
[2]State Key Laboratory for Heavy Oil Processing, University of Petroleum, Dongying, Shandong 257062, CHINA

Introduction

Conversion of methane and carbon dioxide into useful products is an important area in the current catalytic research on hydrocarbon transformations. Carbon dioxide reforming with methane is not only very important for potential usefulness in industry and environment optimization[1-8] but also theoretically significant in understanding the nature of heterogeneous catalysis on hydrocarbon conversion. Heterogeneous catalysis occurs at active centers on a surface and it is recognized that a complete understanding of the catalytic process requires a detailed knowledge of the nature and function of active sites on the surface of the catalysts. The key to surveying the active centers of the metal catalysts is to evaluate and characterize the structure features and properties of the catalysts. The variation of the properties of catalysts can reflect the interaction among metal, support and promoter, and the agglomeration features of the active sites on the metal catalysts. The possible processes accompanying the carbon dioxide reforming with methane may be also speculated according to the changes of physical properties of catalysts. In this paper, physical and chemical adsorption methods are used to characterize the properties and structure of catalysts. The characterized results are used to correlate with the reforming reactivity on metal catalysts and to emphasize the importance of the special structure features in the reaction of this type.

Experimental

The surface properties such as surface area, average pore diameter, and pore volume are determined using an ASAP 2010 analyzer using N_2 adsorption at 77.5 K. Samples are degassed until the pressure in the tube was below 10 μmHg before analysis.

The total pore volume, V_t, is derived from the amount of adsorption at a relatively pressure close to unity, given that the pores were totally filled with the liquid adsorbate. The average pore size is estimated from the pore volume, assuming that a cylindrical pore geometry using the equation $D_p = 4V_t/S$. The mesopore distribution curve is obtained from the adsorption branch of the N_2 isotherm by BJH method. The micropore distribution is calculated from the gas adsorption using the Horvath-Kawazoe equation, with relative pressure (P/P_o) below 0.01.

The dispersion of nickel on the support is roughly estimated by static equilibrium chemisorption of H_2 at rather isothermal conditions of 308 K. A constant volume high-vacuum apparatus, ASAP 2010C, is used for this purpose. Samples are degassed until the pressure in the tube was below 10 μmHg before analysis.

The physisorbed gaseous impurities on the surfaces of the catalyst samples are cleaned away by ultra high pure N_2 (99.999%) at 973 K. Subsequently, the samples are reduced in ultra high pure H_2 (99.999%) flow at 973 K for 2 hrs. Finally, ultra high pure N_2 is introduced again to purge the samples for 30 minutes.

Results and Discussion

Effect of Active Component on Structure Variation of Catalysts. The catalysts are prepared by wetness impregnation method using $CoSO_4$ (Co-1), $Co(NO_3)_2$ (Co-2), and $Ni(NO_3)_2$ as the metal precursors, respectively. **Figure 1** shows the adsorption isotherms of the untreated alumina support and various calcined catalysts. All adsorption isotherms are similar to a type I isotherm. Impregnation results in an approached decrease in the amount adsorbed, with only slight modification of the knee corresponding to microporosity. A quantitative comparison of the variation of the textual structure, mesopore, and micropore distribution of the alumina support, fresh and used Co, Ni catalysts is given in **Table 1**. The results in **Table 1** show that impregnation of sulfate or nitrate on the support decreases its surface area and total pore volume. However, the average pore diameters of all catalysts are increased after impregnation and carbon dioxide reforming reaction. Of interest is that the mean micropore diameters of all catalysts are obviously decreased after impregnating of the metal component on the alumina support. It means that the impregnated metal species maybe mainly locate on the inner surface of the micropore of the alumina support and that the reforming active sites locate in these micropore metal sites. Simultaneously, the larger pores are generated after reaction.

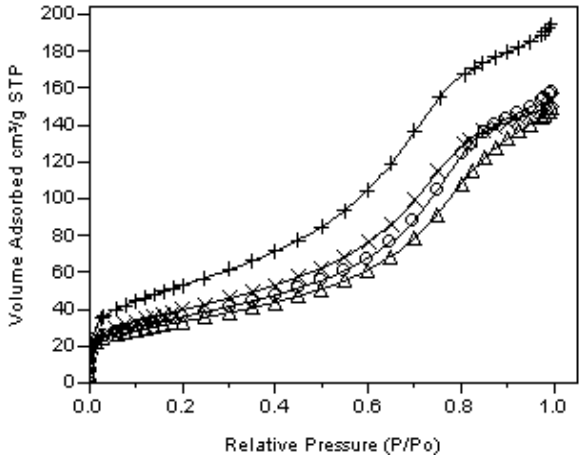

Figure 1. The adsorption isotherm of the untreated support and calcined catalysts.
×: 10 wt% Co-1/Al_2O_3 ($CoSO_4$ as the precursor) +: untreated γ-Al_2O_3 △ : 10 wt% Co-2/Al_2O_3 ($Co(NO_3)_2$ as the precursor) O: 10 wt% Ni/Al_2O_3

Table 1. Characterization of Catalyst Pore Structure*

Catalyst (10wt%)	state	S_{BET} (m^2/g)	D (Å)	D_{micro} (Å)	V_{total} (cm^3/g)
γ-Al_2O_3		192	62.5	7.20	0.300
Co-1/Al_2O_3	fresh	118	78.0	5.90	0.231
	used	114	85.7	6.31	0.244
Co-2/Al_2O_3	fresh	144	66.0	6.60	0.238
	used	174	97.1	6.67	0.422
Ni/Al_2O_3	fresh	130	75.2	6.50	0.244
	used	110	85.0	6.52	0.234

* D: average pore diameter $D_{micro:}$ mean micropore diameter

Effect of Promoter on Structure Variation of Catalysts. The variation of surface areas and total pore volumes of fresh and used catalysts with promoter addition are shown in **Table 2**. From the results shown in **Table 1**, it is deduced that nickel nitrate impregnate

is possibly distributed uniformly in the surface pores of the support with similar decrease in micropore and mesopore volume for various catalysts. Compared the results in **Table 2** with those in **Table 1**, it is easy to know that addition of oxide promoters results in the more decrease of the mesopore volume. Addition of promoters of $Mg(NO_3)_2$ and $Ce(NO_3)_2$ during the multiple-step impregnation process alters the deposition behaviors of $Ni(NO_3)_2$. The locations of the metal and oxide promoters are altered during the impregnation process and the oxide promoter are mostly concentrated on the outer layer of the alumina support while the nickel metal is generally dispersed in the support pores. Apparently, addition of promoters, which mostly deposit on the surface, contributes to more reduction in mesopore volume.

However, it is seen that the unpromoted and promoted 7wt% Ni catalysts show very slight difference in micro- and mesopore volume, but the variations are negligible and well within experimental errors. There is slight increase in surface area by promoter's addition. **Figure 2** indicates that the generation of the pores in the range of 10-30 Å results in the increase of surface area. The part blocking of the bigger mesopores by oxide promoters may be responsible for the generation of smaller mesopores.

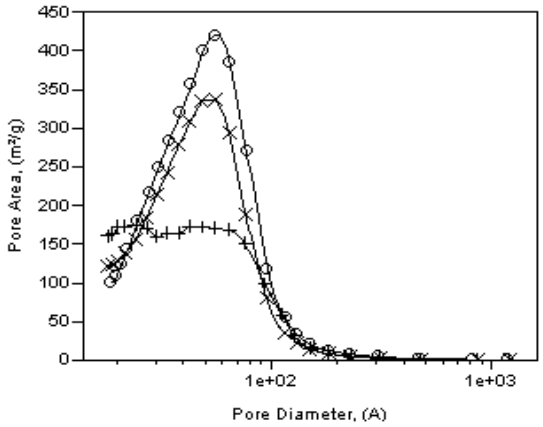

Figure 2. The mesopore distribution of the untreated support, fresh and used Ni supported catalysts.
O: untreated γ-Al_2O_3 ×: fresh 7wt%Ni/Al_2O_3 +: used 7wt%Ni/Al_2O_3

Table 2. Characterization of Catalyst Pore Structure*

Catalyst(wt%)	state	S_{BET} (m^2/g)	D (Å)	V_{total} (m^3/g)	V_{meso} (m^3/g)
γ-Al_2O_3		192	62.5	0.300	0.246
7%Ni/Al_2O_3	fresh	172	56.3	0.242	0.195
	used	143	53.6	0.192	0.154
7%Ni-1%Mg-1%Ce/Al_2O_3	fresh	180	55.3	0.240	0.195
8.5%Ni-2%Mg-3%Ce/Al_2O_3	fresh	150	59.4	0.227	0.189
	used	126	72.0	0.226	0.193
8.5%Ni-3%Mg-2%Ce/Al_2O_3	fresh	148	57.0	0.212	0.173
8.5%Ni-3%Mg-3%Ce/Al_2O_3	fresh	130	64.0	0.200	0.166
10%Ni-3%Mg-1%Ce/Al_2O_3	fresh	144	63.3	0.227	0.191
	used	123	69.0	0.212	0.181
11.5%Ni-1%Mg-2%Ce/Al_2O_3	fresh	145	61.7	0.223	0.186
	used	127	73.5	0.232	0.199
11.5%Ni-3%Ce/Al_2O_3	fresh	143	71.5	0.255	0.219

*D: average pore diameter

The pore structure variations of three kinds of 8.5 wt% Ni catalysts in **Table 2** show that more promoter addition results in more decrease in mesopore volume and the MgO addition exhibits stronger effect on this decrease. The data for 11.5 wt% Ni catalysts also indicate that MgO addition significantly influences pore structure. Too MgO addition may retard the reduction of NiO and cover the NiO layer on the support surface. Therefore, inappropriate MgO addition may decrease the nickel dispersion and surface nickel concentration, which will be described in the H_2 chemisorption.

Effect of Reaction on Structure Variation of Catalysts. Figure 2 shows that mesopore distribution of the untreated support, unpromoted and promoted catalysts before and after reaction. The variation of surface areas and total pore volumes of fresh and used catalysts are shown in **Table 2**.

Figure 2 indicates that the number of pores in catalysts decreases after nickel is loaded on the support remaining in approximately same range of pore diameters. However, the pore size distribution of various catalysts is quite different after reaction. **Figure 2** shows that the number of pores in the range of 30-80 Å in 7 wt%Ni/Al_2O_3 catalyst is significantly decreased after reaction. The total pore volume is also decreased from 0.242 to 0.192 cm^3/g. The mesopore volume decrease contributes primarily the decline of the total pore volume for 7 wt%Ni/Al_2O_3 catalyst. The pore volume decrease may be derived from the coverage of carbon deposition produced in the reforming reaction. That is to say, carbon deposition mainly covers the surface of the catalyst and blocks the mesopores. The unpromoted catalyst exhibits poor resistivity to carbon deposition compared with the alkaline oxide-promoted catalysts according to the pore volume results before and after reaction.

The results shown in **Table 2** indicate that the 8.5wt%Ni-2%MgO-3%CeO_2/Al_2O_3 provides almost unchanged total pore volume and decreased surface area after the reaction. The increased number of larger pores and decreased smaller pores generated in the reaction are responsible for these variations. The average pore diameter shifts toward larger pore size after reaction from 59.4 to 72.0 Å. The pore structure variation may be derived from the support crystalline phase change under high temperature.

H_2 Chemisorption. The metal dispersions of the nickel catalysts supported on alumina are estimated by assuming that each surface metal atom chemisorbs one hydrogen atom, i.e., $H/Ni_{surface}$= 1. Blank experiments show that the amount of H_2 chemisorbs on bare supports is negligibly small. The adsorption results are shown in **Table 3**.

It is found that the metal dispersions of Ni and metallic surface areas on all catalysts are not very high. The apparent low nickel dispersion on the high surface area of γ-Al_2O_3 carrier is probably due to the formation of $NiAl_2O_4$, which can not chemisorb hydrogen at room temperature. Incomplete reduction of Ni crystalline particles, as well as blocking and coverage of nickel crystallites by species originating from MgO and CeO_2 promoters, may also contribute to lowering the amount of hydrogen adsorbed.

Table 3. The Metal Dispersions of the Catalysts

Catalyst (wt %)	M_{disp} (%)	M_{sa} (m^2/g sample)	N_{sa} (m^2/g metal)
8.5%Ni-2%MgO-3%CeO_2/Al_2O_3	0.313	0.177	2.081
8.5%Ni-3%MgO-3%CeO_2/Al_2O_3	0.113	0.064	0.752
7%Ni-1%MgO-1%CeO_2/Al_2O_3	0.204	0.095	1.354
10%Ni-2%MgO/Al_2O_3	0.170	0.114	1.134

The results show that the 8.5%Ni-2%MgO-3%CeO_2/Al_2O_3 catalyst achieved best metal dispersion among the tested catalysts. The nickel dispersion declines form 0.313% to 0.113% with increased

MgO addition from 2 wt% to 3 wt%. This may be attributed partly to the catalyst preparation uncertainty. However, no doubt that the decrease of metal dispersion can be ascribed primarily to the inappropriate promoter addition.

Conclusions

1) The mean micropore diameters of all catalysts were obviously decreased after impregnating of the metal component on the alumina support. It means that the impregnated metal species maybe mainly locate on the inner surface of the micropore of the alumina support and that the reforming active sites also locate in these micropore metal sites.

2) The oxide promoter were mostly concentrated on the outer layer of the alumina support while the nickel metal was generally dispersed in the support pores. Addition of promoters contributed to more reduction in mesopore volume.

3) H_2 chemisorption revealed that the addition of the alkaline oxide MgO promoter significantly prohibits the metal dispersion on the catalyst. Inappropriate promoter addition can result in sharp decrease of the metal dispersion.

Acknowledgement. Financial supports by the Young Scientists Award Foundation of Shandong Province and China National Petroleum Corporation are gratefully acknowledged.

References

(1) Swaan, H. M.; Kroll, V. C. H.; Martin, G. A. and Mirodatos, C. *Catal. Today,* **1994**, *21,* 571.
(2) Hu, Y. H. and Ruckenstein, E. *Catal. Lett.,* **1997***, 43,* 71.
(3) Ruckenstein, E. and Hu, Y. H. *Appl. Catal*., **1995**, *133*, 149.
(4) Hu, Y. H. and Ruckenstein, E. *Catal. Lett,,* **1996**, *36,* 145.
(5) Horiuchi, T.; Sakuma, K.; Fukui, T.; Kubo, Y.; Osaki, T. and Mori, T. *Appl. Catal.,.* **1996**, *144*, 111.
(6) Zhang, Z. and Verykios, X. E. *Appl.Catal.,* **1996**, *138*, 109.
(7) Zhang, Z. and Verykios, X. E. *Catal. Today,* **1994**, *21*, 589.
(8) Tsipouriari, V. A.; Efstathiou, A. M. and Verkios, X. E. *Catal. Today,* **1994**, *21*, 579.

CH_4 DECOMPOSITION ON Co/SiO_2: INFLUENCE OF METAL PARTICLE SIZE AND GAS PHASE COMPOSITION ON DECOMPOSITION RATE

Yi Zhang and Kevin J. Smith

Department of Chemical & Biological Engineering
University of British Columbia, Vancouver, B.C.
Canada, V6T 1Z4

Introduction

Methane decomposition is important in a number of reactions that aim to convert natural gas to more valuable products using supported metal catalysts. These include methane steam reforming for synthesis gas production and methane decomposition for hydrogen production[1-4]. Also, initial CH_4 decomposition kinetics on Co catalysts have been reported at relatively mild conditions (450°C and 101kPa) relevant to CH_4 homologation: a two-step process in which CH_4 decomposition ($CH_4 \rightarrow CH_x \bullet S + H \bullet S$) at 350-450°C is followed by lower temperature hydrogenation ($CH_x \bullet S + H_2 \rightarrow S + C_2H_6$, C_3H_8). At these conditions[3], the initial high rate of CH_4 decomposition decreases rapidly but continues despite the nominal coverage of surface Co being greater than 1. A semi-empirical model that was developed to describe this observation assumed decomposition of CH_4 on a Co site with migration of the resulting CH_3 surface species from the metal to the support, thereby regenerating the metal site. This migration step was considered essential to explain the observed kinetics[3]. However, despite the low temperature, it is possible that filamentous carbon is formed during the reaction, in which case active metal sites would be regenerated as surface carbon is absorbed by the metal before diffusing through the metal particle.

The mechanism of catalyst deactivation during CH_4 decomposition is complex[4]. The deactivation rate depends on the rate of carbon build up on the surface of the catalyst, which in turn is a consequence of a number of interacting effects, including the effect of metal particle size on carbon diffusion rate, carbon gasification rate due to the presence of H_2 (whose evolution parallels CH_4 decomposition on the metal catalyst), and carbon morphology. The present work is aimed at clarifying some aspects of the deactivation during the decomposition of methane at moderate temperatures on low loaded Co/SiO_2 catalysts.

Experimental

Catalyst Preparation. Co catalysts were prepared by incipient wetness impregnation of the support using an aqueous solution of $Co(NO_3)_2 \bullet 6H_2O$ (+98% Aldrich) [3]. The catalysts were dried, calcined and reduced by temperature-programmed reduction (TPR) in a 100ml/min flow of 40% H_2/60%Ar to the reduction temperature. Co content was varied from 5-12wt%, and the degree of reduction of these catalysts was >83% in all cases, the reduction degree increasing to 96% for the 10 and 12wt%Co/SiO_2 catalysts.

Catalyst Characterization. The Co dispersion was determined by CO chemisorption using a thermogravimetric analyzer (Shimadzu TGA-50). The metal dispersion was calculated from the CO uptake and reported as a percent of reduced Co. The Co particle size was estimated from the equation d (nm)=0.962/Φ, where Φ is the percent metal dispersion. Carbon filament formation was confirmed by TEM using a Hitachi H-800 electron microscope, operated at 100-150 kV.

Methane Decomposition. Kinetic experiments were performed in a fixed-bed reactor system, details of which have been given elsewhere.[3] The reactor was operated in a differential mode (<10% CH_4 conversion), free of external and internal diffusional effects as confirmed by the methods of Froment and Bischoff [5].

Results and Discussion

The rate of methane decomposition over the 12% Co/SiO_2 catalyst at 500°C and 101 kPa shows a steady decrease in the period 0-60 minutes time-on-stream, as shown in Figure 1. The deactivation profile can be described by a 1st-order deactivation rate equation. Two parameters, the initial rate of reaction r_0 and the rate of the decay k_d, describe the deactivation rate according to the equations: $dr/dt = -k_d r$, such that $r = -k_d r_0 \exp(-k_d t)$. The solid line of Figure 1 shows the fit of this empirical equation to the measured data. Note that the equation does not include the migration of carbon from the catalyst surface as proposed previously[3], since here the deactivation is being considered over a longer time period. The migration step is relevant only at the initial stage of reaction[3] as evidenced by the data of Figure 2. CO is produced by reaction between CH_x (that has migrated from the metal to the support) and oxygen of the support. Within about 3 minutes of the start of the reaction, the CO has declined to a minimal amount, suggesting that the rate of CH_x migration has also decreased significantly.

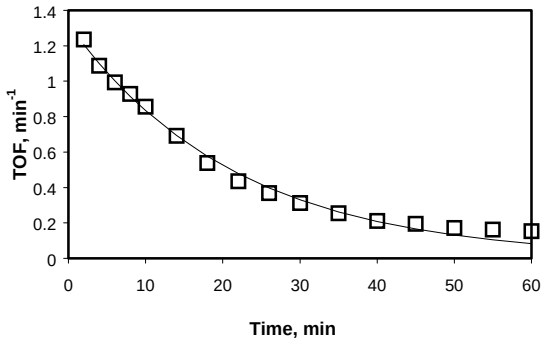

Figure 1. CH_4 TOF as a function of time at 500°C on 12wt% Co/SiO_2 with 5.16%CH_4 in Ar

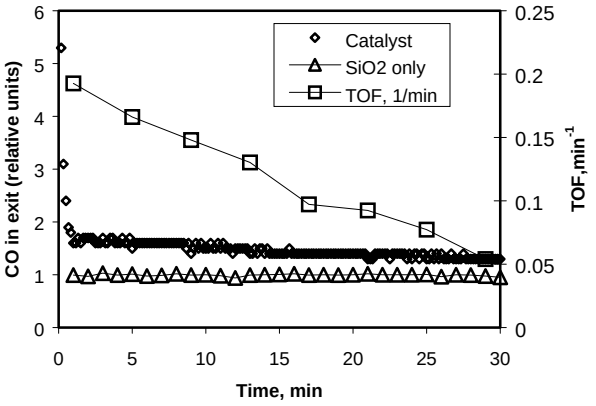

Figure 2. CO production during CH_4 decomposition at 450°C on 12%Co/SiO_2 catalyst (Feed 5.16% CH_4 in Ar).

Metal particle size effects. The influence of metal particle size on the CH_4 decomposition rate at 450ºC over Co/SiO_2 catalysts was investigated using catalysts with nominal metal loading of 5-12wt%. The Co particle size increased with metal loading in the range d = 5.8 – 11.4 nm. The dependency of initial TOF (r_o) and decay rate (k_d) on metal particle size were obtained by curve fitting the CH_4 decomposition rate versus time data to the empirical deactivation equation presented above. Data in Fig. 3 show that Co/SiO_2 catalyst exhibited structure sensitivity, where the initial TOF increased with

increasing Co particle size. Data in Fig. 4 show that an increase in Co particle size resulted in a minor decrease in deactivation rate.

Filamentous carbon formation on the 12wt% Co/SiO_2 (d=11.4 nm) catalyst, exposed to 5.16%CH_4/Ar for a reaction time of 120 minutes was confirmed by TEM of the used catalyst. Filament formation corresponds to a low value of k_d as reported in Fig. 4. The TEM micrograph showed that the filamentous carbon diameter was approximately 10 nm, in agreement with the particle size of 11.4 nm measured by CO chemisorption on the fresh catalyst.

Hence, both migration of carbon species and filamentous carbon formation occurred during CH_4 decomposition on 12wt%Co/SiO_2 catalyst. Fig 2 showed that the migration rate decreased to a very low level within a few minutes of the start of the reaction. Over longer reaction times (>10min) the absorption and diffusion of surface carbon into the metal particle must therefore be the main mechanism for sustained catalyst activity (and hence $k_d \rightarrow 0$).

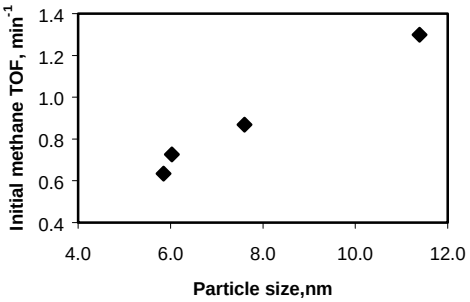

Figure 3. Effect of metal particle size on initial decomposition activity (TOF). (Feed gas 5.16 %CH_4/Ar at 450ºC.)

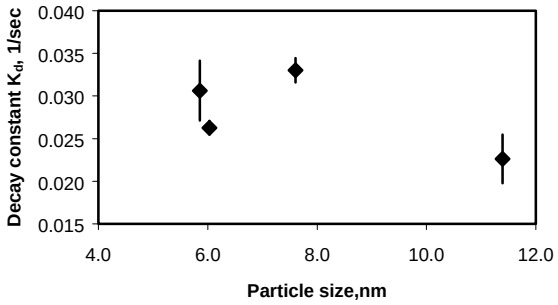

Figure 4. Effect of metal particle size on decay constant (k_d). (Feed gas 5.16 %CH_4/Ar at 450ºC.)

The above data can be interpreted using a simplified model for catalyst deactivation. Accordingly, the deactivation rate (r_d=dr/dt) for CH_4 decomposition is assumed dependent on the difference in the net rate of carbon formation ($r_{f,n}$, the rate of carbon formation minus the rate of gasification of carbon/coke precursor) and the net rate of carbon removal ($r_{r,n}$, mainly due to filamentous carbon formation) i.e. $r_d=r_{f,n}-r_{r,n}$. The rate of catalyst deactivation will depend on the difference between $r_{f,n}$ and $r_{r,n}$. From Fig. 3 we can conclude that $r_{f,n}$ must increase with metal particle size, and since k_d decreases marginally with particle size, we can also conclude that the net rate of carbon removal $r_{r,n}$ must increase with particle size. Considering size effects on the carbon diffusion mechanism, a similar conclusion can be reached.

Gas composition effects. The composition of the gas phase also affects the rate of catalyst deactivation and the formation of filamentous carbon. The presence of H_2 (1.2%) in the feed gas (5.16%CH_4/Ar) reduced the initial TOF and the deactivation rate of the catalyst (Fig.5). The difference between $r_{f,n}$ and $r_{r,n}$ (i.e. the deactivation rate) decreases because H_2 increases the hydrogenation of surface carbon and therefore, $r_{f,n}$ decreases. In the case of CO (0.36% in 5.16%CH_4/Ar), however, the initial TOF is not reduced significantly, whereas the deactivation rate remains low (Fig. 5). CO adsorption must therefore increase $r_{r,n}$, either by enhanced carbon diffusion due to CO surface modification[6], or displacement of surface H from the catalyst surface.

Conclusions

CH_4 decomposition kinetics on supported Co catalysts are strongly influenced by the metal particle size and gas phase composition. These effects have been explained in terms of the relative magnitudes of the net rate of carbon formation and the net rate of carbon removal from the catalyst surface. Filamentous carbon formation occurs when both rates are approximately equal, resulting in a low apparent deactivation rate.

Acknowledgement. Funding from the Natural Sciences and Engineering Research Council of Canada is gratefully acknowledged.

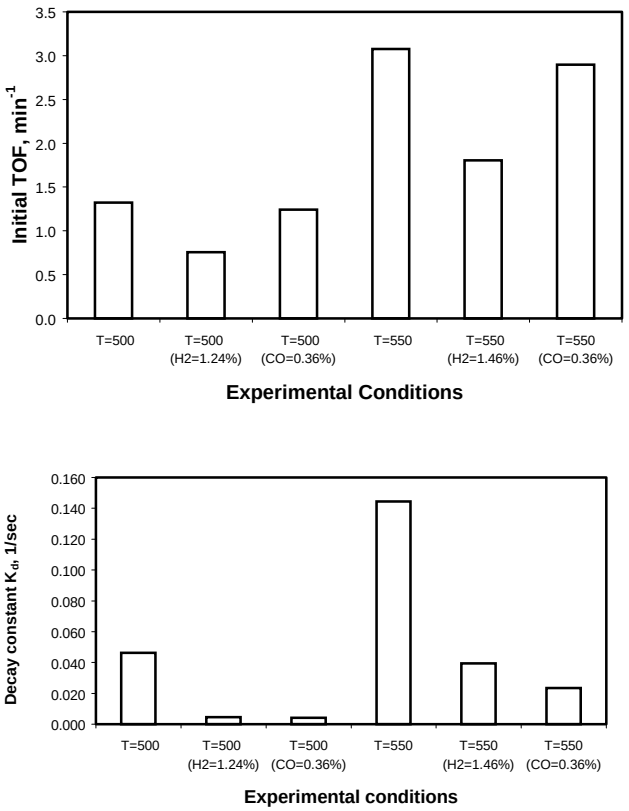

Figure 5. Effect of H_2 and CO on the initial activity and deactivation rate. (12wt% Co/SiO_2 catalysts with Co particle size 9.5 nm, exposed to 5.16%CH_4/Ar at temperature indicated).

References

(1) Amariglio, H.; Saint-Just, J.; Amariglio, A., *Fuel Processing Technology*, **1995,** *42*, 291.
(2) Guczi L.; Van Santen , R.A. and Sarma, K.V., *Catal. Rev.-Sci.*, **1996**, *38 (2)* 249.
(3) Zadeh, J.S.M. and Smith, K.J., *J. Catal.*, **1998,** *176,* 115.
(4) Snoek, J.W., Froment, G.F. and Fowles, M., *J. Catal.*, **1997**, *169*, 240 and *J. Catal.*, **1997**, *169*, 250.
(5) Froment, G.F. and Bischoff, K. B., "Chemical Reactor Analysis and Design" Wiley, New York, **1990**.
(6) Rodriguez ,N.M.; Kim M.S. and Baker R.T.K., J. Catal., **1993,** *144* , 93.

Challenges and Progress in the Conversion of Natural Gas to Fuels and Chemicals

Enrique Iglesia
Department of Chemical Engineering
University of California at Berkeley, Berkeley, CA 94720

Introduction

Its low heteroatom concentration and high hydrogen content make natural gas an ideal fuel in our continuing efforts to minimize the local and global environmental impact of energy use and of chemical syntheses. Gas reserves are more uniformly distributed than oil reserves, making supplies less sensitive to local disruptions or manipulative practices. Many gas reserves are located far from markets; and their use as fuels and petrochemical feedstocks is currently restricted by the limited availability of technology and infrastructure for efficient conversion of methane to liquid fuels, petrochemicals, and even electricity. In remote locations, gas conversion will produce predominately liquid fuels, because economies of scale and required depletion rates will involve the processing of large gas throughputs. With time, methane conversion to liquid fuels will be mostly replaced by direct use of gas as a fuel, as pipelines and local infrastructures and economies develop. The concurrent production of commodity and intermediate chemicals in large gas conversion plants can influence economic incentives by increasing margins and it can lead to earlier profitable implementations of emerging technologies. The synthesis of chemicals will continue even after the gas conversion to fuels window and it will provide the cleanest and most economical routes to many of the chemicals currently produced from oil.

Activation and Conversion of Methane

Natural gas conversion costs depend on gas prices, on thermal efficiencies, on chemical selectivities, and on capital costs. Maximum attainable (theoretical) thermal efficiencies depend only on the stoichiometry of the products formed. They are unaffected by whether direct or indirect routes are used to form a given product slate. Highest theoretical efficiencies are reached when product H/C ratios resemble those in CH_4. Practical (in contrast with theoretical) thermal efficiencies and capital costs depend for the most part on the temperature and pressure changes required throughout the process and on the product yield per pass. Thus, direct processes tend to minimize temperature (and pressure) fluctuations and to decrease second-law efficiency losses and capital costs, which depend strongly on the required amounts of heat exchange. High yields minimize the energy and capital costs of separation, recompression, and recycle.

Methane conversion can proceed via direct or indirect paths. Direct paths require C-H bond activation and the conversion of the CH_x species formed to products within a single vessel. Pyrolysis, oxidative coupling, selective oxidation (to methanol or formaldehyde), partial oxidation (to CO/H_2), and steam reforming are direct (one-step) methane conversion routes. Only a few desired products (CO/H_2, acetylene, ethylene, aromatics, methanol, formaldehyde) can be formed via these direct routes. Invariably, CH_4 reaction products are much more reactive than CH_4 itself and they progress along reaction paths leading to thermodynamically more stable carbon or CO_2 products. High product yields in direct routes require the continuous removal of desired products from the reaction zone or the thermodynamic or kinetic protection of these products against further reactions. In general, maximum attainable yields depend on the thermodynamic tendency of a given products to oxidize to CO_2 or to dehydrogenate to solid carbon. Weaker C-H bonds in products tend to favor their activation at low reaction temperatures in the absence of thermodynamic or kinetic protection. Although at first glance counterintuitive, low temperatures actually disfavor the desired products, because their subsequent reactions have much lower activation energies that the primary CH_4 activation reactions that form these desired initial products.

Many direct paths become indirect when desired products are made via the initial formation of chemically-protected intermediates, which are subsequently converted to the desired products. The first step forms a protected form of methane, which resists further conversion to CO_2 or carbon, and the second step "de-protects" this intermediate and forms the desired products in higher yields than via the corresponding direct routes. For example, synthesis gas (H_2/CO) is in effect a protected form of activated methane and it can be used to form a broad range of hydrocarbons and oxygenates useful as fuels and chemicals. High temperature reactions of CH_4 with H_2O, CO_2 and even O_2 do not form large amounts of CO_2 because of thermodynamic constraints imposed by the high reaction temperature and the stoichiometry of the reactants used. Kinetic protection can be achieved using methyl bisulfate or methyl chloride intermediates, both of which can be used to form methanol or hydrocarbons in subsequent steps. Synthesis gas routes require two steps, including a thermally efficient but costly synthesis gas generation process, but the oxidants, however, are O_2 or H_2O, which are readily available and require only their extraction from the environment in purified form. The bisulfate and chloride routes use expensive and toxic reagents (H_2SO_4, Cl_2, or HCl), which require careful handling. They also involve costly chemical regeneration in an additional third step. To some extent, these considerations have lead to the accepted use of synthesis gas routes in currently envisioned gas conversion technologies.

Intermediates can also be protected using physical rather than chemical means. Physical protection schemes require a device that extracts desired products continuously or which can separate CH_4 and O_2 within a chemical reactor. This separation can occur spatially or temporally. High ethylene and benzene yields can be obtained by rapid quenching of pyrolysis products; two-step cyclic processes involving methane decomposition to CH_x species on metals and hydrogenation of these fragments lead to larger alkanes. Endothermic CH_4 dimerization and pyrolysis reactions can be carried out at low temperatures by continuously removing hydrogen using absorption onto solids, transport through membranes, or reactions with lattice oxygen. High ethylene yields can be achieved by its continuous removal from a stream, using external absorbers in recycle or moving bed reactors and by the use of lattice oxygen in cyclic reactors for oxidative coupling. In all cases, the approaches are technically sound and practically feasible from engineering considerations, but they increase the complexity and cost of the reactors because of the multi-functional or transient nature of their operation. As a result, they do not really deliver the intended simplicity and low capital costs of direct methane conversion processes.

Direct and Indirect Methanol and Formaldehyde Synthesis

One-step homogeneous oxidation of methane at high pressures and temperatures has led to the synthesis of methanol with yields of ~4%. The rapid subsequent combustion reactions of methanol to form CO_2 limit conversions in practice, while the explosive nature of the required reactant mixtures creates engineering challenges in the design of mixing schemes and pressure vessels. Solid catalysts have not led to yield improvements, because surface sites activate C-H bonds in both methane and methanol. Staged O_2 introduction using multiple injectors or dense oxygen conducting

membranes are also unlikely to increase yields, because the rates of activation of C-H bonds in CH_3OH and CH_4 appear to depend similarly on O_2 concentrations. Continuous extraction of methanol can prevent combustion, but requires its selective absorption, adsorption, or permeation above ambient temperatures, none of which are currently possible, as well as a low conversion per pass. The introduction of sites for methanol conversion to hydrocarbons into homogeneous methane to methanol oxidation reactors may provide a less costly product separation scheme, as well as the protection of activated CH_4 (as methanol) as aromatic molecules that are considerably less reactive than methanol.

The direct conversion of methane to formaldehyde using O_2 has also been widely studied on heterogeneous catalysts and formaldehyde yields have been typically even lower that those reported for the direct methane conversion to methanol. Two recent studies have reported higher formaldehyde yields; one study uses NO/O_2 mixtures as the oxidant and homogeneous pathways and the other O_2 as the oxidant and supported silicomolybdic acids as heterogeneous catalysts.

Biological routes that convert methane selectively to methanol are often mentioned as the ultimate replacement for these other routes. Progress in this area will require enzymes or microorganisms that function selectively and efficiently in concentrated aqueous methanol solutions and the replacement of the co-reagents currently needed for effective energy transfer in these biochemical reactions.

Commercial methanol synthesis processes use indirect routes based on synthesis gas intermediates. These processes lead to much higher methanol yields (25-30% yield per pass) and >99% CH_3OH selectivity. Synthesis gas generation requires high temperatures and large capital investments but recent process improvements that combine partial oxidation and steam reforming in a nearly thermoneutral process have led to practical thermal efficiencies (71-72%) for the overall methanol synthesis process very close to theoretical thermal efficiency values (84.2%). Recent development in the use of adiabatic monolith reactors for partial methane oxidation to synthesis gas have provided a novel and useful approach, especially for small-scale methanol synthesis applications that cannot exploit the beneficial economies of scale of steam reforming and autothermal reforming processes. The chemical and structural integrity of noble metal catalytic coatings in these monolith reactors and the mixing and handling of explosive CH_4/O_2 mixtures remain challenging issues in the design of the short contact time reactors for the production of synthesis gas. Recent advances in the design of ceramic membranes for oxygen and hydrogen transport may become useful in decreasing or eliminating air purification costs and in driving endothermic steam reforming reactions to higher conversions or lower operating temperatures. Such ceramic membranes have advanced beyond their status as a laboratory curiosity and into developmental consortia, but their reliable practical implementation will require additional advances in the synthesis and stabilization of thin metal oxide films within novel reactor geometries as well as the development of faster proton conductors for the case of hydrogen separation schemes.

Methanol can also be formed via other indirect routes, such as via processes involving the formation of methyl bisulfate on Hg complexes followed by its conversion to methanol via hydrolysis, and by the regeneration of the sulfuric acid oxidant by SO_2 oxidation. Methyl bisulfate yields can reach 70-80%, because of the low reactivity of methyl bisulfate relative to methanol and even methane. Turnover rates are very low in the temperature tolerated by these homogeneous catalysts and Hg organometallic complexes and sulfuric acid are very toxic and difficult to handle and to regenerate. More recent studies have increased the stability of these catalysts by introducing more stable ligands and eliminated Hg-based materials with Pt-based homogeneous catalysts. This approach involves a new type of protected intermediate (methyl bisulfate) and leads to higher methanol yields than in commercial routes based on synthesis gas. It is, however, neither a direct route to methanol nor a process with low capital investment. It involves three steps, including a very costly oxidant regeneration step and a deprotection step limited by thermodynamics.

Oxychlorination provides another indirect route to methanol and to hydrocarbons via acid-catalyzed hydration or oligomerization of methyl chloride. It involves the use and the costly regeneration of Cl_2 and it requires corrosion-resistant vessels and significant temperature cycling of process streams. CH_3Cl yields of 25-30% have been achieved with yield losses predominately to CO_2 and CH_2Cl_2. An additional chemical hurdle in these process is the low selectivity to monochlorinated products. Higher yields will require more selective monochlorination and lower combustion rates of these desired intermediates. These improvements appear unlikely because of the kinetic instability of CH_3Cl relative to CH_4 and of the thermodynamic stability of the sequential CO_2 and CH_2Cl_2 products.

Synthesis of Hydrocarbons via Pyrolysis Reactions

The pyrolysis of methane to form alkynes, alkenes, and arenes is highly endothermic and requires very high temperatures and concurrent combustion of methane as a fuel in order to provide the enthalpy of reaction in a heat exchange furnace. At these high temperatures, homogeneous pathways lead to acetylene, polynuclear aromatics and soot as the preferred products for both kinetics and thermodynamic reasons. Thermal efficiencies are low because of the extreme temperature cycling required of process streams and because of the rapid quenching protocols used to restrict chain growth and soot formation. The low pressures required by thermodynamics and the slow homogeneous reactions lead to large reactor vessels, which must be protected against carbon deposition and metal dusting corrosion by using coatings or specialized materials of construction.

Recently, several approaches have addressed these limitations and they have led to significant control of methane pyrolysis selectivity. One approach involves the synthesis of benzene and ethylene with 30-40% yields per pass using homogeneous pyrolysis reactors and the rapid thermal quenching of reaction products. Another improvement uses shape-selective catalysts based on MoC_x and WC_x species held within shape-selective channels in pentasil zeolites (H-ZSM5), where chain growth to form polynuclear aromatics is spatially restricted and the presence of CH_4 activation sites on the surface of carbide clusters leads to CH_4 pyrolysis reactions at much lower temperatures (700 ^{0}C) than for homogeneous pathways. The addition of small amounts of CO_2 during CH_4 pyrolysis on these catalysts and the selective deactivation of acid sites on external zeolite surfaces have led to marked improvements in catalyst stability and to lower selectivity to hydrocarbons larger than naphthalene. The combination of such catalysts with hydrogen removal by ceramic membranes remains a promising but challenging approach to the direct conversion of methane to larger hydrocarbons.

A two-step cyclic process involving the deposition of CH_x fragments from methane on metal surfaces at 200-300 ^{o}C and the coupling of such fragments during a subsequent hydrogenation cycle has led to very low yields of C_2+ hydrocarbons. Yields are unavoidably constrained by the unfavorable thermodynamics of this overall process at low temperatures and by the selectivity losses to surface carbon, which also cause rapid deactivation and loss of methane reactants. A more promising and thermodynamically feasible cyclic strategy involves the formation of relatively pure H_2 streams using CH_4-H_2O cyclic processes on solids that can generate reactive

carbon and H_2 during the CH_4 cycle and remove the carbon as CO while producing additional H_2 during subsequent contact with steam.

Oxidative Coupling of Methane

Oxidative coupling combines at the molecular level methane dimerization via radical-like pathways with the removal of the hydrogen formed, often before recombinative desorption to form H_2, via oxidation steps. Ethane and ethylene are the predominant hydrocarbons formed. Heterogeneous catalysts improve the yields and selectivity attainable in homogeneous coupling reactions, but the active surface sites in these materials also activate C-H bonds in ethane and ethylene, leading to secondary combustion reactions, which limit attainable yields to 20-25% and lead to significant formation of CO_2. These secondary pathways are very exothermic and they place significant heat transfer loads on the catalytic reactors. The use of cyclic strategies using lattice oxygen and moving or fluid bed reactors provides an attractive alternate option, which avoids unselective homogeneous combustion pathways and uses the heat capacity of the solids to increase the efficiency to heat removal during reaction. Protecting strategies in oxidative coupling can lead to two-step processes similar to those for methanol synthesis. In principle, synthesis gas, methyl bisulfate, or methyl chloride intermediates can be used to form ethylene, but ethylene formation from these protected intermediates is not very selective and the overall processes is not environmentally benign.

Other protecting strategies have been attempted, or at least proposed, in order to increase C_2 yields in oxidative methane coupling. The separation of ethylene from the reactor effluent using cation-exchange zeolites has been carried out and it has led to slight C_2 yield improvements. The low adsorption temperatures required and the lack of adsorption selectivity for ethane, however, limit the practical applications of these approaches. The in situ conversion of ethane and ethylene to aromatics using cation-exchange zeolites after oxidative coupling can lead to the simpler separation of aromatics from the product stream, but in a process for the synthesis of aromatics instead of ethylene. Finally, yields improvements can result from the separation of methane and oxygen reactants in space (via membranes) or in time (via cyclic reactors). The first approach exploits any differences in kinetic oxygen response between the coupling and the product combustion reactions. O_2 is introduced along the reactor via multiple injectors or oxygen-conducting membrane walls. Low O_2 concentrations can also be achieved using backmixed fluidized beds operated at high oxygen conversion levels. The staging of the oxidant along a tubular reactor has not led to significant improvements, apparently as a result of the similar kinetic dependences of CH_4 and C_2 activation steps on O_2 concentration. Detailed kinetic simulations have shown that distributed oxygen introduction is unlikely to give C_2 yields above 35-40%. Laboratory tests have shown that poor radial dispersion of the oxygen feed can lead to high local O_2 concentrations, which can cause stable flames and structural damage at membrane walls.

Detailed kinetic and process simulations have suggested that continuous ethylene removal from a recycle stream can lead to 75-85% C_2 yields during oxidative coupling of methane. When the removal of ethylene requires temperatures significantly lower than for oxidative coupling, the required recycle ratios become impractical, because extensive thermal cycling leads to second-law inefficiencies and to large capital and operating costs associated with heat exchange and recompression. These constraints can be overcome by designing absorbers or membranes that remove ethylene selectively from dilute streams containing ethane, CH_4, CO_2, H_2O, and O_2 at typical oxidative coupling temperatures. A reaction-separation protocol using simulated chromatographic reactors has led to 65-70% ethylene yields. The practical use of these reactors as moving beds, however, requires porous solids that separate C_2 from methane and oxygen at elevated temperatures using adsorption, capillary condensation, or diffusion differences among these components. Cation-exchanged zeolites and microporous carbons are promising as materials for the separation of ethylene from such mixtures, but optimum operating temperatures remain well below those required for oxidative coupling.

Oxidative coupling of methane can be carried out without contact between hydrocarbons and O_2 using cyclic reactors or hydrogen-conducting membranes. High C_2 yields (25-28%) can be achieved by cycling reducible oxides between a methane activation reactor and a solids re-oxidation vessel. This cyclic process can maintain constant temperatures during solids recycle and uses air (instead of pure O_2) as the oxidant, but the process requires complex handling of solids in fluidized beds. Such redox cycles can be carried out within a single vessel by internally segregating a fluid bed into a reaction zone and an oxidative regeneration zone. The appropriate desing oxygen donor solids can be used to the amount of and rate of reaction of the available lattice oxygen. These cyclic oxidative coupling scheme remain of fundamental and practical interest in the activation and conversion of methane via oxidative routes.

Another type of cyclic reactor uses hydrogen absorption into a solid during methane pyrolysis and the removal of the absorbed hydrogen as water in subsequent oxidation cycles. This approach has been recently reported for dehydrogenation reactions of higher alkanes. In such cyclic schemes, pyrolysis and oxidation are separated temporally. In the mathematically analogous catalytic membrane process, reactants are separated spatially using a diffusion barrier that permits only hydrogen transport. Experimental tests using thick membrane disks of hydrogen-conducting perovskites led to very low methane conversion rates and C_2 yields. Significant improvements are possible by combining cation-exchanged zeolites for selective methane pyrolysis at low temperatures with much thinner oxide films, the successful synthesis of which has been recently reported. Hydrogen transport rates at the H_2 pressures prevalent during methane pyrolysis, however, must be improved significantly before practical applications of such schemes can be seriously considered.

Synthesis Gas Conversion Routes to Fuels and Chemicals

Synthesis gas conversion processes are significantly more advanced in development than direct or other two-step methane conversion schemes. Indirect gas conversion processes are currently practiced for methanol synthesis and for hydrocarbon formation via the Fischer-Tropsch synthesis. Diesel-range hydrocarbons (via FT synthesis) and gasoline (via MTG processes) can be produced thermal efficiencies as high as ~80% of their respective theoretical values (78% and 75%). These indirect processes have continued to evolve as continuous improvements have come about from advances in synthesis gas generation, from the design and deployment of three-phase bubble columns for synthesis gas conversion, and from the development of improved catalytic materials for the selective synthesis of paraffins, intermediate size α-olefins, and higher alcohols. Small modular gas conversion plants using catalytic partial oxidation in monolith reactors and CO hydrogenation in bubble columns may also create future opportunities for combining H_2 and power generation with the "small-scale" synthesis of commodity petrochemicals and even of liquid fuels.

Selective pathways for ethylene and propylene from synthesis gas remain unavailable, because Flory-type chain growth kinetics lead to broad carbon number distributions. The most promising approach uses acid-catalyzed chain growth reactions of methanol within shape-selective channels in pentasil zeolites and silicoaluminophosphate microporous materials in a three-step process

requiring synthesis gas generation, methanol synthesis, and methanol to olefins (MTO) or gasoline (MTG) conversion. The latter must be carried out in fluid bed or moving bed reactors because of the need for frequent regeneration. Currently available technologies use silicoaluminophosphate materials or modified pentasil zeolites in order to provide optimum shape-selective environments for the synthesis of light olefins. Intermediate range α-olefins (C_5-C_{15}) can be produced with modest selectivity from CO and H_2 on promoted Fe-based catalysts. Maximum yields are limited by Flory-type chain growth kinetics, but the valuable mid-range paraffins and the smaller olefins formed as by-products are much more valuable than the paraffins formed and useful only as fuels.

Higher alcohol synthesis is also restricted to broad product distributions governed by stochastic chain growth kinetics. Recently, bifunctional catalysts consisting of metal sites for hydrogenation reactions and basic sites for alcohol coupling steps have led to high selectivity to branched alcohols. Chain growth appears to be restricted to C_4 and C_5 alcohols by the chemical constraints of base-catalyzed aldol condensation reactions. High 2-methyl-1-butanol yields (200-300 g/kg-cat-h) have been recently reported on Pd-based bifunctional catalysts, but at very high pressures (>200 bar) and temperatures (400-450 ^{o}C). Dimethylether isomerization and aldol condensation of olefins with methanol using acid-base bifunctional catalysts provide alternate but unexplored pathways to overcome the C_1 to C_2 conversion bottleneck during CO hydrogenation to form higher alcohols.

CHARACTERIZATION AND APPLICATION OF Cr_2O_3-ZnO CATALYSTS FOR METHANOL SYNTHESIS

Michael C.J. Bradford, Mahesh V. Konduru, and Digna X. Fuentes

CeraMem Corporation
12 Clematis Avenue
Waltham, MA 02453

Introduction

The synthesis of methanol from mixtures of hydrogen and carbon oxides using mixed metals and metal oxides has been under investigation since at least 1914.[1] Both zinc oxide and chromium oxide, with or without promotion by alkali metal hydroxides, are described as preferred materials for oxygenate synthesis in this BASF patent. In addition, two later patents from BASF issued in 1925 [2] and 1926 [3] focused on the use of CuO/ZnO and Cr_2O_3/ZnO catalysts. By 1932, the industrial production of methanol was primarily undertaken through the use of these two catalyst types.[4] During this time, a series of papers was published by Frolich and coworkers that focused on methanol synthesis over CuO/ZnO/Al_2O_3,[5] CuO/ZnO,[6-8] and Cr_2O_3/ZnO[9] catalysts. Additional investigations of methanol synthesis over Cr_2O_3/ZnO catalysts were undertaken contemporaneously by Brown and Galloway.[10-11] However, CuO/ZnO/Al_2O_3 is currently (and has been since *ca.* 1960) the preferred industrial catalyst for methanol synthesis,[12-15] and academic research efforts on CuO/ZnO[16-18] and CuO/ZnO/Al_2O_3 [19-20] catalysts for methanol synthesis have continued essentially unabated.

Nevertheless, the use of alkali-promoted, Cr_2O_3/ZnO-based catalysts for higher alcohol synthesis (which can be inferred from the early BASF patent)[1] has been explicitly under investigation since at least 1928.[21-33] Mixed Cr_2O_3-ZnO/H-ZSM-5 catalysts have also been studied for the direct conversion of synthesis gas to C_2+ hydrocarbons and aromatics.[34-41] The mechanism of higher alcohol synthesis is reported to occur through the interaction of intermediate surface species (formate and methoxy) that also have the potential (via hydrogenation) to form methanol.[29,33] In addition, the mechanism for C_2+ hydrocarbon and aromatic formation over physical mixtures of Cr_2O_3-ZnO and H-ZSM-5 catalysts presumably involves the generation of intermediate alcohol species on the Cr_2O_3-ZnO function that migrate and react at Brönsted acid sites on the zeolite via the established methanol-to-olefin and methanol-to-gasoline mechanisms.[34-41] A common feature of both the higher alcohol and aromatic synthesis catalytic systems is the necessity for surface formate and methoxy species formation on the Cr_2O_3-ZnO catalyst function. Therefore, understanding the role of the Cr_2O_3-ZnO catalyst function on the kinetics of methanol formation is of fundamental importance to both higher alcohol and aromatics syntheses from synthesis gas..

Cryder and Frolich, in an early report on methanol synthesis over Cr_2O_3/ZnO catalysts, postulated that the apparent synergy observed between chromium oxide and zinc oxide when co-precipitated, in comparison to the pure component oxides, was mainly due to an increase in the catalyst surface area per unit mass;[9] however, they also explicitly lamented that in 1929 no satisfactory means of estimating the catalyst surface areas was available in order to report methanol synthesis rates on an areal basis. The subsequent development of a suitable and reproducible technique for the measurement of catalyst surface areas by Brunauer, Emmett and Teller,[42] now referred to commonly as the BET method, has since enabled researchers to measure catalyst surface areas, and thus to report kinetic data on an areal basis. Despite this fact that the BET method is widely available and relatively inexpensive, and areal rates are ultimately more suitable toward the elucidation of catalyst properties,[43] much experimental work in the areas of methanol, higher alcohol, and aromatics syntheses continues to be reported on either conversion or specific activity (per mass of catalyst) bases.

In the investigation reported herein, several Cr_2O_3-ZnO catalysts prepared via co-precipitation with either K_2CO_3 or $(NH_4)_2CO_3$ were characterized by X-ray diffraction, N_2-BET and activity for methanol synthesis at 593 K. Through the use of BET and areal rates it is demonstrated that the catalyst specific activities can be described well by a simple linear combination of areal rate data for the pure component oxides, indicating that no synergy is likely present between chromia and zinc oxide in these catalysts.

Experimental

Catalyst Preparation. Several K-Cr_2O_3/ZnO catalysts were prepared via co-precipitation using a procedure adapted from that reported by Ereña et al..[39] After defining the desired catalyst composition, a 0.14 M cation solution was prepared via addition of appropriate quantities of $Cr(NO_3)_3 \cdot 9H_2O$ (Acros, 99.98% Purity) and $Zn(NO_3)_2 \cdot 3H_2O$ (Acros, 99+% Purity) to distilled H_2O. In addition, a 0.5 M solution of K_2CO_3 was prepared as a precipitating agent. The cation (Cr^{3+} / Zn^{2+}) and anion (CO_3^{2-}) solutions were simultaneously added dropwise to a stirred beaker of distilled H_2O maintained at 7.0 ≤ pH ≤ 7.5 and 338±5 K. Analogous Cr_2O_3/ZnO catalysts with substantially lower potassium contents were prepared using a 0.5 M solution of $(NH_4)_2CO_3$. Co-precipitated materials were filtered, washed repeatedly with distilled water, dried in static air at 383 K, and subsequently calcined at 473 K for 2 h using 10% oxygen in argon at a Gas Hourly Space Velocity (GHSV) of 600 $cm^3/h \cdot g_{cat}$. Additional samples were prepared via subsequent calcination in 10% oxygen for 2 h at temperatures between 373 and 973 K.

Catalyst Characterization. All catalysts were characterized using direct current plasma emission spectroscopy (DCPES) to quantify the composition of elemental chromium, zinc, and potassium. N_2 BET analysis was used to determine the surface areas of the calcined samples after evacuation for 3-5 h at 473-573 K. In addition, powder X-ray diffraction (XRD) spectra were obtained using filtered CuK_α radiation (Materials Characterization Laboratory at the Pennsylvania State University). Volume-weighted crystallite sizes (d_v) were estimated from XRD spectra using the Scherrer equation, $d_v = 0.9\ \lambda\ /\ B\ cos\ \theta$, with Warren's correction for instrumental line broadening, $B = (B_M^2 - B_I^2)^{1/2}$, where λ = 1.54158 Å for weighted CuK_α radiation, B_M is the peak width at one-half maximum intensity, and B_I is the instrumental line broadening.

Selected catalyst samples were also characterized after reaction via temperature programmed oxidation (TPO). After reaction, catalysts were cooled to room temperature in flowing nitrogen, removed from the reactor, and subsequently transferred to a quartz tube packed with quartz wool. The quartz tube was placed in a horizontal tube furnace equipped with a carbon dioxide sensor (Vaisala) at the effluent. Catalyst TPO was thereafter performed using 10% oxygen in argon (GHSV = 100 $cm^3/h \cdot g_{cat}$) at *ca.* 4 K/min from 293 to 973 K to quantify total carbon deposition (as either carbonaceous deposits or adsorbed CO_x).

Apparatus for Methanol Synthesis. High purity N_2 (99.999%), H_2 (99.999%), and CO (99.3%) were used as-received without further purification and introduced independently using mass flow controllers (Porter) to a copper-lined, tubular reactor made of Inconel 600. The reactor was placed within a vertical split-tube furnace (Lindberg) equipped with a thermocouple for external reactor temperature control and a thermocouple inserted into the catalyst bed to monitor catalyst temperature. The temperature of the reactor effluent line was typically maintained at 240°C, and an electronic

back-pressure regulator (Tescom) was used to control reactor pressure up to 34 atm. The back-pressure regulator effluent was directly fed at 1 atm to the sampling valve of an on-line gas chromatograph (SRI Model 8610C), in which 0.2 cm^3 samples were subjected to simultaneous analysis with flame ionization (FID) and thermal conductivity (TCD) detectors. The FID was used for methanol, methane, and byproduct analyses, and the TCD was used for nitrogen, hydrogen, carbon monoxide, and methanol analyses. Carbon dioxide formation was not observed during the experiments reported herein. The absolute rate of methanol formation was determined with the TCD via reference to nitrogen, by-product formation rates were quantified via reference to methanol, and carbon monoxide conversion was quantified from an overall carbon balance assuming a negligible rate of carbon accumulation on the catalyst. TCD and FID response values obtained during in-house calibration were used in conjunction with those available in the literature.[44]

Procedures for Methanol Synthesis. Typically, *ca.* 1 gram of ground and sieved catalyst [0.125 ≤ particle diameter (mm) ≤ 0.25] was packed into the reactor between plugs of quartz wool, and thereafter purged for 15 min at 293 K in flowing nitrogen (1350 $cm^3/h \cdot g_{cat}$). The catalyst was then subject to a pretreatment procedure involving reduction for 2 h in flowing hydrogen (H_2/N_2 = 2/1; GHSV = 4050 $cm^3/h \cdot g_{cat}$) at 673 K. After completion of pretreatment, the reactor temperature was reduced to 393 K, and the catalyst was exposed to a mixture of hydrogen and carbon monoxide in nitrogen ($N_2/H_2/CO$ = 1/2/1, GHSV ≈ 5000 $cm^3/h \cdot g_{cat}$). After exposure to this gas composition for 15 min, the reactor pressure was raised at a rate of 0.34 atm/min from 1 to 34 atm, and then the reactor temperature was raised at a rate of 2.5 K/min to 593 K. Catalyst activity and selectivity at 593 K remained fairly constant during the initial 15 h on stream; therefore, time-weighted average of these data are reported herein.

Results and Discussion

Characterization of Prepared Catalysts. Catalyst chromium and zinc compositions determined via DCPES were in relatively good agreement with nominal composition values for the samples prepared with either ammonium or potassium carbonate. The potassium concentrations in the samples precipitated with ammonium carbonate are roughly three orders of magnitude lower than for those samples precipitated with potassium carbonate; however, the values are non-zero. Presumably, the trace potassium content in these ammonium-precipitated catalysts is a consequence of contamination from use of the same laboratory glassware for preparation of all samples.

Powder XRD spectra of the Cr_2O_3/ZnO catalysts after calcination for 2 h in flowing 10%O_2 at 973 K are shown in Figure 1. The bulk phase for the nominal Cr/Zn = 0 sample corresponds as expected to ZnO (JCPDS # 05-0664). Increase in catalyst Cr/Zn ratio from 0 to 1.86 resulted in a decrease in bulk ZnO and concomitant increase in bulk $ZnCr_2O_4$ (JCPDS #22-1107). Further increases in catalyst chromium content resulted in the appearance of Cr_2O_3 (JCPDS #6-0504) and a concomitant decrease in $ZnCr_2O_4$ content. Powder XRD spectra of the K-Cr_2O_3/ZnO catalysts after calcination for 2 h in flowing 10%O_2 at 973 K are similar (not shown), except that diffraction peaks due to the presence of K_2O (JCPDS 23-493) and $K_2Cr_2O_7$ (JCPDS 27-380) are also present.

Volume-weighted crystallite sizes for the catalysts were calculated through application of the Scherrer Equation to the (101) diffraction peak for ZnO, the (311) diffraction peak for $ZnCr_2O_4$, and the (110) diffraction peak for Cr_2O_3. The data for Cr_2O_3/ZnO catalysts prepared via co-precipitation with $(NH_4)_2CO_3$ demonstrate that addition of chromium to ZnO results in a decrease in the ZnO crystallite size (for Cr/Zn ≤ 1.86), which however tends to increase with increasing calcination temperature, as shown in Figure 2. Similar trends were obtained for the K-Cr_2O_3/ZnO catalysts.

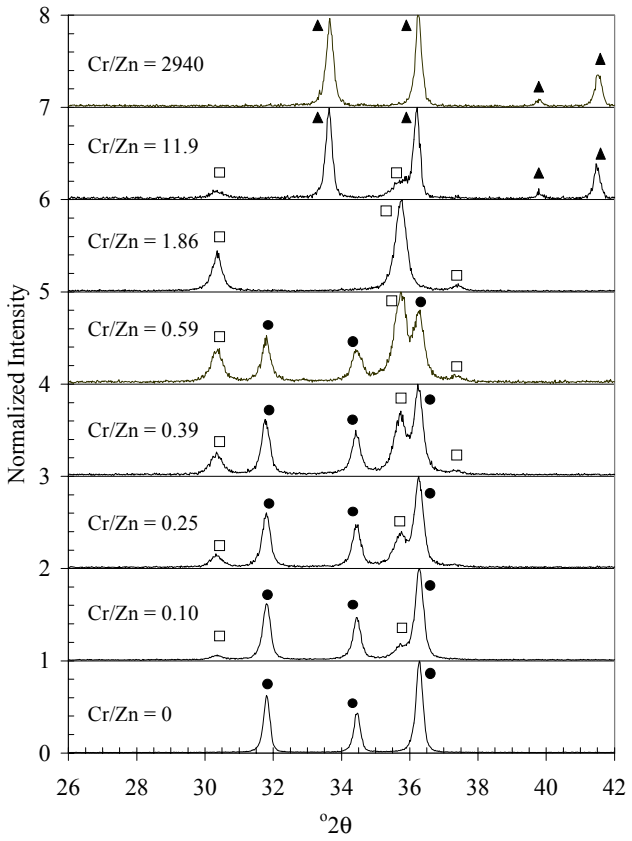

Figure 1. XRD spectra of Cr_2O_3/ZnO catalysts prepared via co-precipitation with $(NH_4)_2CO_3$ and calcined for 2 h in 10% O_2 at 973 K. Phases present include: (□) ZnO; (□) $ZnCr_2O_4$; and (□) Cr_2O_3.

Surface areas for the Cr_2O_3/ZnO catalysts prepared via co-precipitation with $(NH_4)_2CO_3$ reveal a similar trend; i.e., the addition of chromium to ZnO (or conversely, zinc to Cr_2O_3) results in an increase in catalyst surface area (Table 1). Surface areas of analogous K-Cr_2O_3/ZnO catalysts exhibited lower surface areas, presumably indicating that potassium oxides and potassium chromates induce an intrinsically low hydrothermal stability.

Table 1. Catalyst surface area after calcination for 2 h at 973 K.

	S (m^2/g)	
~ Nominal Cr/Zn	**$(NH_4)_2CO_3$**	**K_2CO_3**
0.00	5.3 ± 0.3	4.1 ± 0.1
0.10	17.0 ± 0.3	3.3 ± 0.7
0.25	19.1 ± 1.0	1.8 ± 0.3
0.39	19.00 ± 0.01	0.5 ± 0.2
0.42	23.9 ± 0.1	---
0.59	24.9 ± 0.9	7.9 ± 0.4
2.00	27.2 ± 0.3	2.4 ± 0.1
15.0	18.7 ± 0.7	0.16 ±0.11
∞	14.4 ± 0.1	< 0.05

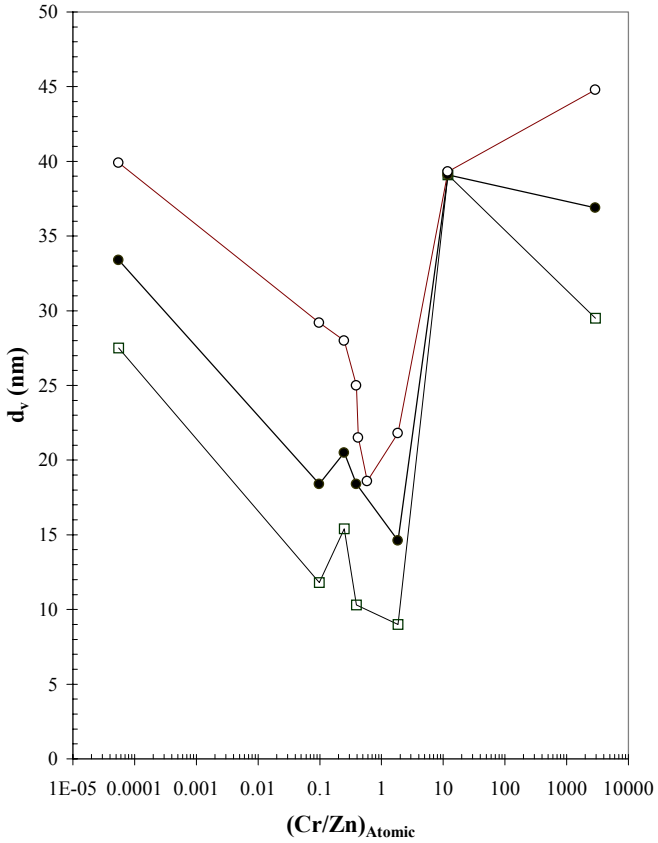

Figure 2. Catalyst volume-weighted crystallite size as a function of Cr/Zn ratio and calcination temperature for Cr_2O_3/ZnO catalysts prepared via co-precipitation with $(NH_4)_2CO_3$. (□) 773 K; (□) 873 K; (□) 973 K.

Catalyst activity for methanol synthesis was evaluated as a function of Cr/Zn ratio at 34 atm and 593 K, as shown in Tables 2-3 and Figure 3. It has been reported in the literature that internal mass transport limitations exist during methanol synthesis, and that the degree of this limitation increases with increasing catalyst particle diameter (> 1 mm) and temperature.[45] However, application of the Weisz-Prater criterion[46] indicated that the data reported herein are free from internal mass transfer limitations. Regardless, subject to the experimental conditions of this study, the maximum allowable conversion of CO to CH_3OH is only 4.2%. Therefore, although the conversions used in this study are low, the kinetic results for many catalysts are to some extent equilibrium-limited.

The specific activity of the Cr_2O_3/ZnO catalysts prepared via co-precipitation with $(NH_4)_2CO_3$ exhibited the expected volcano-type of relationship with the activity maximum observed for *ca.* Cr/Zn = 0.39 (Figure 3); however, the specific activity of the K/Cr_2O_3/ZnO catalysts decreased with increasing potassium content. Comparison of rates on an areal basis, however, reveals that the activities of ZnO and K/ZnO are effectively identical within experimental error, and that activities for catalysts with other Cr/Zn ratios are at least within an order of magnitude (Tables 2 and 3). In addition, it is important to note that the highest observed areal rate for catalysts prepared with either $(NH_4)_2CO_3$ or K_2CO_3 is for ZnO, and the lowest areal rate among the catalysts prepared with $(NH_4)_2CO_3$ is observed for Cr/Zn = 11.9 and Cr_2O_3. Although the limited analysis herein cannot preclude the formation and presence

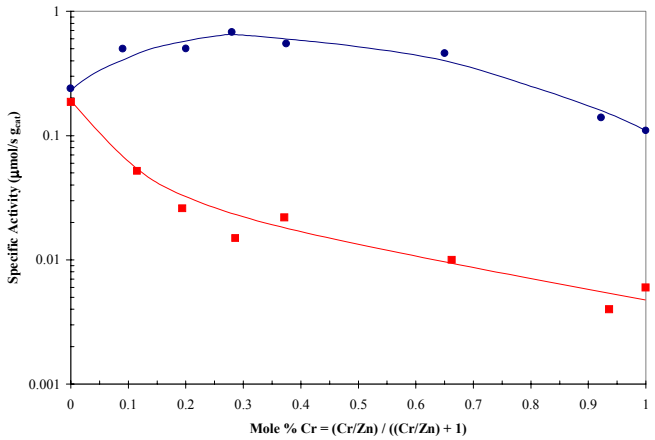

Figure 3. Specific activity of (□) K-free and (□) K-containing Cr_2O_3/ZnO catalysts for CH_3OH synthesis as a function of catalyst Cr/Zn content.

of active sites for methanol synthesis on the Cr_2O_3/ZnO catalysts that do not exist on either Cr_2O_3 or ZnO, the data indicate that, if they exist, they do not likely possess an intrinsic activity for methanol synthesis that exceeds the activity of sites present on the partially reduced ZnO surface.

Table 2.
Cr_2O_3/ZnO catalyst performance for CH_3OH synthesis.
(T=320±2°C, P=34.1±0.2 atm, $N_2/H_2/CO$=1/2/1, GHSV =5134±263 $cm^3/h \cdot g_{cat}$)

Cr/Zn (Actual)	CO Conversion (%)	Specific Activity (μmol/s·g_{cat})	Areal Rate (μmol/min·m^2)	Methanol In Product (wt%)
0.00	1.65	0.24 ± 0.01	2.72	97.8±0.1
0.10	2.98	0.50 ± 0.02	1.76	97.5±0.3
0.25	3.14	0.50 ± 0.03	1.57	97.5±0.2
0.39	4.13	0.68 ± 0.06	2.15	97.8±0.4
0.59	3.67	0.55 ± 0.02	1.32	96.7±0.4
1.86	2.72	0.46 ± 0.04	1.01	97.1±0.9
11.9	0.86	0.14 ± 0.04	0.45	96.5±0.7
2940	0.71	0.11 ± 0.02	0.46	91.6±0.3

Table 3.
K/Cr_2O_3/ZnO catalyst performance for CH_3OH synthesis.
(T=320±1°C, P=34.0±0.2 atm, $N_2/H_2/CO$=1/2/1, GHSV =5168±196 $cm^3/h \cdot g_{cat}$)

Cr/Zn (Actual)	CO Conversion (%)	Specific Activity (μmol/s·g_{cat})	Areal Rate (μmol/min·m^2)	Methanol In Product (wt%)
0.00	1.12	0.187±0.014	2.74	96.8 ± 0.3
0.13	0.31	0.052±0.003	0.94	74 ± 3
0.24	0.16	0.026±0.003	0.87	68 ± 6
0.40	0.09	0.015±0.002	1.80	42 ± 3
0.59	0.14	0.022±0.001	0.17	60 ± 4
1.96	0.06	0.010±0.006	0.25	67 ± 12
14.6	0.03	0.004±0.001	1.50	34 ± 6
1540	0.04	0.006±0.001	---	28 ± 3

Therefore, application of Occam's razor permits, to a first approximation, the expression of global reaction rates on a specific

activity basis as a linear combination of the intrinsic areal rates of the pure component oxides:

$$r_g = S_{ZnO} r_{ZnO} + (S_{Total} - S_{ZnO}) r_{Cr_2O_3}$$

where r_g is the observed global reaction rate (μmol/s·g_{cat}), r_{ZnO} is the intrinsic areal rate for ZnO (0.045 μmol/s·m^2), $r_{Cr_2O_3}$ is the intrinsic areal rate for Cr_2O_3 (0.008 μmol/s·m^2), S_{ZnO} is the surface area of ZnO, and S_{Total} is the total catalyst surface area measured via BET. Surface areas for ZnO in the Cr_2O_3/ZnO catalysts prepared via co-precipitation with $(NH_4)_2CO_3$ were calculated from this relationship using experimental values for r_g, r_{ZnO}, $r_{Cr_2O_3}$, and S_{Total}; see Table 4.

The results support the early hypothesis by Cryder and Frolich,[9] and indicate that the increase in the specific activity for CH_3OH synthesis observed for the Cr_2O_3/ZnO catalysts (for Cr/Zn ≤ 1.86) is due primarily to the increase in accessible ZnO surface area (Table 4). In addition, the results indicate that the observed decrease in specific activity for the Cr_2O_3/ZnO catalysts with Cr > 2 is likely due to the predominance of Cr_2O_3 on the catalyst surface.

Table 4. Estimated ZnO surface area in Cr_2O_3/ZnO catalysts.

	S (m^2/g)		
Cr/Zn	**Total**	**ZnO**	**Cr_2O_3**
0.00	5.3	5.3	0.0
0.10	17.0	9.8	7.2
0.25	19.1	9.4	9.7
0.39	19.0	14.2	4.8
0.59	24.9	9.5	15.4
1.86	27.2	6.7	20.5
11.9	18.7	0.0	18.7
2940	14.4	0.0	14.4

Summary

Several Cr_2O_3-ZnO catalysts prepared via co-precipitation with $(NH_4)_2CO_3$ were characterized by XRD, BET and activity for methanol synthesis at 593 K. Data reveal that addition of chromium to ZnO up to a level of Cr/Zn = 1.86 decreased the volume-weighted crystallite size of ZnO, increased the total catalyst surface area, and increased the available surface area of ZnO. It was also demonstrated that the catalyst specific activities could be described well by a simple linear combination of areal rate data for the pure component oxides. Although the limited analysis herein cannot preclude the formation and presence of active sites for methanol synthesis on the Cr_2O_3/ZnO catalysts that do not exist on either Cr_2O_3 or ZnO, the data indicate that, if they exist, they do not likely possess an intrinsic activity for methanol synthesis that exceeds the activity of sites present on the partially reduced ZnO surface. Therefore, there is likely no true synergy is present between chromia and zinc oxide in this catalyst system. Qualitatively similar results were obtained for catalysts prepared via co-precipitation with K_2CO_3. However, the presence of potassium in these catalysts induced hydrothermal instability and reduced the surface area for both the catalyst and ZnO, in comparison to the relatively K-free samples.

Acknowledgement

This work was funded by the U.S. Department of Energy under SBIR Grant No. DE-FG02-99ER82762. The authors thank CeraMem Corporation for permission to publish this work.

References

1. Mittasch, A. and Schneider, C., US Pat. 1,201,850, **1916.**
2. Mittasch, A., US Pat. 1,558,559, **1925**.
3. Mittasch, A., US Pat. 1,569,775, **1926**.
4. Dreyfus, H., US Pat. 1,868,096, **1932**.
5. Lewis,W.K. and Frolich,Per K., *Ind.Eng.Chem*., **1928**, *20(3),* 285.
6. Frolich,Per K., Fenske, M.R., and Quiggle,D., *Ind.Eng.Chem*., **1928**, *20(7)*, 694.
7. Frolich, Per K., Fenske,M.R., Taylor,P.S., and Southwich,C.A., *Ind.Eng.Chem*., **1928**, *20(12),* 1327.
8. Frolich,Per K., Davidson, R.L., and Fenske,,M.R., *Ind.Eng.Chem*., **1929**, *21(2),* 109.
9. Cryder, D.S.and Frolich,Per K., *Ind.Eng.Chem*., **1929**, *21(9),* 867.
10. Brown,R.L. and Galloway,A.E., *Ind.Eng.Chem*., **1928**, *20(9),* 960.
11. Brown,R.L. and Galloway,A.E., *Ind.Eng.Chem*., **1929**, *21(4),* 310.
12. Vannice,M.A., *Catal.Rev.-Sci.Eng*., **1976,** *14(2),*153.
13. Kung, H.H.,*Catal.Rev.-Sci.Eng*., **1980**, *22(2),* 235.
14. Rase,H.F., Handbook of Commercial Catalysts: Heterogeneous Catalysts, CRC Press: Boca Raton, 2000, p.432.
15. Synetix Brochure for the KATALCO 51-8 Methanol Synthesis Catalysts, available at: http://www.synetix.com/methanol/pdfs/productbulletins/pb51-8.pdf
16. King,D.S. and Nix,R.M., *J.Catal*., **1996,** *160,* 76.
17. Fujitani,T. and Nakamura,J., *Catal.Lett*., **1998**, *56,* 119.
18. Fujita,S.I., Moribe,S., Kanamori,Y., Kakudate,M. and Takezawa,N., *Appl.Catal.A.General*, **2001**, *207,* 121.
19. Skrzypek,J., Lachowska,M., Grzesik,M., S□oczy□ski,J. and Nowak,P., *Chem.Eng.J.,* **1995**, *58*, 101.
20. Lommerts,B.J., Graaf,G.H. and Beenackers,A.A.C.M., *Chem.Eng.Sci*., **2000**, *55*, 5589.
21. Frolich,Per K. and Lewis,W.K., *Ind.Eng.Chem*., **1928**, *20(4),* 354.
22. Frolich,Per K. and Cryder,D.S., *Ind.Eng.Chem*., **1930,** *22(10),*1051.
23. Graves, G.D., *Ind.Eng.Chem*., **1931**, *23(12),* 1382.
24. Anderson,R.B., Feldman,J. and Storch,H.H., *Ind.Eng.Chem*., **1952**, *44(10),* 2418.
25. Lunev,N.K., Artyukh,Y.N., Leonov,V.E., Yakubovich,M.N. and Ryzhak,I.A., *Kinet.Catal*., **1985**, *26(4)*, 752.
26. Tronconi,E., Ferlazzo,N., Forzatti,P. and Pasquon,I., *Ind.Eng.Chem.Res*., **1987,** *26,* 2122.
27. Lietti,L., Botta,D., Forzatti,P., Mantica,E., Tronconi,E. and Pasquon,I., *J.Catal*., **1988**, *111*, 360.
28. Calverley, E.M. and Smith,K.J., *J.Catal*., **1991**, *130,* 616.
29. Calverley, E.M. and Smith,K.J., *Ind.Eng.Chem.Res*., **1992**, *31,* 792.
30. Mawson,S., McCutchen,M.S., Lim,P.K. and Roberts,G.W., *Energy & Fuels*, **1993**, *7*, 257.
31. Campos-Martín,J.M., Guerrero-Ruiz,A. and Fierro,J.L.G., *J.Catal*., **1995**, *156*, 208.
32. Moser,W.R.and Connolly,K.E., *Chem.Eng.J*., **1996**, *64*, 239.
33. Beretta,A., Tronconi,E., Forzatti,P., Pasquon,I., Micheli,E., Tagliabue,L. and Antonelli,G.B., *Ind.Eng.Chem.Res*., **1996**, *35,* 2144.
34. Zahner,J.C., US Pat. 4,011,275, **1977.**
35. Chang,C.D.and Lang,W.H., US Pat. 4,180,516, **1979**.
36. Simard,F., Mahay,A., Ravella,A., Jean,G., and de Lasa,H., *Ind.Eng.Chem.Res*., **1991**, *30,*1448.
37. Simard,F., Mahay,A., Jean,G. and de Lasa,H., *Can.J.Chem.Eng*., **1991**, *69,* 898.
38. Simard,F., Sedran,U.A., Sepúlveda,J., Fígoli,N.S. and de Lasa,H.I., *Appl.Catal.A:General*, **1995**, *125,* 81.
39. Ereña,J., Arandes,J.M., Bilbao,J., Aguayo,A.T. and de Lasa,H., *AFINIDAD*, **1997**, *54(471),* 367.
40. Ereña,J., Arandes,J.M., Bilbao,J., Olazar,M. and de Lasa,H., *J.Chem.Technol.Biotechnol*., **1998**, *72,* 190.
41. Ereña,J., Arandes,J.M., Bilbao,J., Gayubo,A.G., and de Lasa,H., *Chem.Eng.Sci*., **2000**, *55,* 1845.
42. Brunauer,S., Emmett,P.H. and Teller,E., *J.Am.Chem.Soc*., **1938**, *60,* 309.
43. Boudart,M., *Chem.Rev*., **1995**, *95,* 661.
44. Dietz,W.A., *J.Gas Chromatography*, **1967**, *February*, 68.
45. Lommerts,B.J., Graaf,G.H. and Beenackers,A.A.C.M., *Chem.Eng.Sci*., **2000**, *55,* 5589.
46. Madon,R.J. and Boudart,M. *Ind.Eng.Chem.Fundam*., **1982**, *21*,438.

CHARACTERIZATION OF THE STRUCTURE FEATURES OF NICKEL CATALYSTS FOR CARBON DIOXIDE REFORMING OF METHANE

Rong-Gang Ding[1,2], and Zi-Feng Yan[2]

[1]Department of Chemical Engineering
University of Queensland, Brisbane 4072, AUSTRALIA
[2]State Key Laboratory for Heavy Oil Processing,
University of Petroleum,
Dongying, 257062, CHINA

Introduction

Conversion of methane and carbon dioxide into useful products is an important area in the current catalytic research on hydrocarbon transformations. Carbon dioxide reforming of methane is not only very important for potential usefulness in industry and environmental optimization[1-4] but also theoretically significant in understanding the nature of heterogeneous catalysis on hydrocarbon conversion. Heterogeneous catalysis occurs at active centers on a surface and it is recognized that a complete understanding of the catalytic process requires a detailed knowledge of the nature and function of active sites on the surface of the catalysts. The key to surveying the active centers of the metal catalysts is to evaluate and characterize the structure features and properties of the catalysts. The variation of the properties of catalysts can reflect the interaction among metal, support and promoter, and the agglomeration features of the active sites on the metal catalysts. The possible processes accompanying the carbon dioxide reforming of methane may be also speculated according to the changes of physical properties of catalysts. In this paper, XRD, TPR, SEM and EDX techniques are used to characterize the properties and structure of catalysts. The characterized results are used to correlate with the reforming reactivity on metal catalysts and to emphasize the importance of the special structure features in the reaction of this type.

Experimental

Catalyst preparation. Nickel catalysts were prepared by the incipient wetness impregnation method. The solids were dried overnight in air at 393K, then calcined at 773 K in air for 6 hrs for complete decomposition of the precursors. For the promoted catalysts, magnesium nitrate and cerous nitrate were added to the support by the same method.

Catalyst characterization. A BDX-3200 X-ray powder diffractometer was used to identify the main phases of nickel-based catalysts. Anode Cu Kα (40 kV, 20 mA) was employed as the X-ray radiation source, covering 2θ between 20° and 80°. The XRD patterns were monitored and processed by a computer.

The microscopic appearance observation was conducted using scanning electron microscope (JEM 5410LV, JEOL Technologies) with the accelerating voltage of 25 kV. The surface elemental composition of the catalysts was determined by energy distribution spectrum using X-ray microanalysis (ISIS, Oxford Instrument).

TPR experiments were carried out in an apparatus which consisted of a flow switching system, a heated reactor, and an analysis system. The reactor was a quartz tube of 6 mm diameter and 20 cm length. The outlet of the reactor was connected to a quadrupole mass spectrometer (DYCOR Quadrupole, Ametek Instrument) via a heated steel tube (diameter 3 cm). The pressure in the main chamber of the spectrometer was approximately 10^{-7} Pa. Calibration of the mass spectrometer was performed with a mixture of known composition. Ultra high purity gases (99.999%) were used in TPR experiments. The catalyst sample was firstly pretreated in a O_2 flow of 20 ml/min at 973 K for 30 min, then the sample was cooled to room temperature in the O_2 flow. Subsequently, the O_2 flow was switched to a H_2/He (10 ml/ 20ml) flow. After purging with H_2/He mixture for 10 min, temperature programming was initiated with a heating rate of 23 K/min and the TPR profiles were *on-line* recorded.

Results and Discussion

XRD characterization. The XRD patterns of support, promoted and unpromoted Ni-based catalysts were shown in **Figure 1**. From the XRD patterns of support and catalysts, it was clearly observed that NiO diffraction peak didn't appear in the patterns of unpromoted and promoted Ni-based catalysts. It was a good indication that high dispersion of nickel oxide was achieved over γ-Al_2O_3 support. However, it is difficult to estimate the effect of promoters on the metal dispersion on the support according to the XRD patterns.

As can be derived from the XRD patterns shown in **Figure 1**, no detectable solid reaction occurred between NiO and Al_2O_3 over promoted catalyst. However, certain amounts of nickel were found in the form of $NiAl_2O_4$, a compound resulting from the solid reaction between NiO and the acidic Al_2O_3 support in the Ni/Al_2O_3 catalyst. The $NiAl_2O_4$ crystalline phase, which has a stable spinel structure, is rather difficult to be reduced, as witnessed by the fact that it essentially survives H_2 reduction at 1023 K. However, addition of MgO (3 wt%) to γ-Al_2O_3 significantly affected the basicity/acidity of the support, leading to a profound change in the bulk phase composition. It was observed that the diffraction peak of $NiAl_2O_4$ disappeared over MgO-promoted catalyst. This is probably attributed the fact the basic MgO is preferably reacting with the acidic Al_2O_3 to form stable magnesium aluminate, thereby suppressing the reaction between NiO and Al_2O_3.

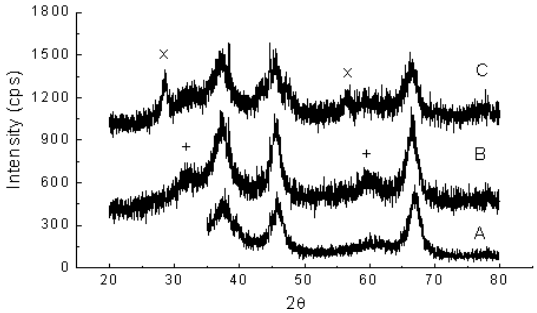

Figure 1. The XRD patterns of Al_2O_3 support, unpromoted and promoted catalysts. (+: $NiAl_2O_4$, ×: CeO_2) A: γ-Al_2O_3, B: 8.5wt%Ni/γ-Al_2O_3 C: 8.5wt%Ni-2wt%MgO-3wt%CeO_2/γ-Al_2O_3

The emergence of CeO_2 diffraction peak in Ni-Mg-Ce/Al_2O_3 catalyst indicated that the dispersion of CeO_2 was unsatisfactory. This may be related to the catalyst preparation processes and conditions. More series tests of the influence of CeO_2 addition on the dispersion of metal are absent now. The Ni-Mg-Ce/Al_2O_3 catalyst exhibited perfect performance in the catalyst evaluation experiments despite of unsatisfactory dispersion of CeO_2 promoter. The EDX analysis explains the emergence of the CeO_2 diffraction peak perfectly in following section. In the sharp contrast to CeO_2, the dispersion of MgO promoter was satisfactory and no diffraction peak appeared in the XRD patterns of the promoted catalyst.

SEM and EDX Analysis. The surface elemental compositions of the fresh and used catalysts were characterized by EDX analysis and the results were shown in **Table 1**. The high surface concentration of some element indicated that uniform dispersion of the element is achieved. The enrichment trend of the element may be effectively

retarded and various states of the element essentially exist in relatively small particles. From Table 1 it was observed that the surface concentration of the Ni over unpromoted catalyst significantly decreased by almost one time, from 5.29% to 2.37%, after carbon dioxide reforming reaction. The surface concentration of Ni element also declined to some extent, from 5.74% to 4.21% over the MgO-promoted catalyst after reaction. However, it was interesting that the surface concentrations of Ni element increased over CeO_2 promoted catalysts after reaction.

Table 1 Surface Composition of Fresh and Used Nickel Catalysts

catalyst(wt%)	state	Al (%)	Ni (%)	Mg (%)	Ce (%)
7 %Ni/Al_2O_3	fresh	94.71	5.29	-----	-----
	used	97.63	2.37	-----	-----
8.5%Ni-2%MgO-3%CeO_2/Al_2O_3	fresh	84.31	9.18	n.d.	6.51
	used	84.74	10.61	n.d.	4.65
10%Ni-2% MgO/Al_2O_3	fresh	94.26	5.74	n.d.	-----
	used	95.80	4.21	n.d.	-----
11.5%Ni-3% CeO_2/Al_2O_3	fresh	93.04	4.18	-----	2.78
	used	89.97	4.85	-----	5.19

Reaction conditions: P = 1 atm, T = 973 K, CH_4/ CO_2= 1.05, WHSV = 12.5 h^{-1}, used for 4 hrs. n.d.: not detected. %: atomic percentage

For the Ce-promoted catalysts, the nickel loadings on the support were higher than that of Ce-missing catalysts. High nickel loading does not favor the dispersion of Ni on the surface of the support. However, the surface concentration of Ni reached 4.18% on the fresh 11.5%Ni-3%Ce/Al_2O_3 catalyst, approached that on the fresh 7.5%Ni/Al_2O_3 catalyst. The uniform dispersion of nickel component over the 8.5%Ni loaded catalyst may be ascribed to appropriate nickel loading. Lu et al.[5] studied the optimum nickel loading on various supports. The results showed that two-dimensional surface compound was formed by the interaction between NiO and Al_2O_3 with nickl loading set at 9.0% under the specific conditions. The two-dimensional surface compound was highly dispersed on the surface of the support, and thus resulted in the maximum dispersion of Ni metal particles. Too high nickel loading may result in the formation of NiO crystalline phase on the support. The NiO crystalline phase submitted little contribution to the metal dispersion and large Ni particles were prone to formation in the reduction process. The large Ni particles provided less active metal surface area and caused rapid deactivation by carbon deposition on the Ni particles.

The high surface concentration of Ni on the 8.5%Ni-2%MgO-3%CeO_2/Al_2O_3 may be derived from two causes. The appropriate nickel loading was the key to obtaining uniform dispersion on the surface of the Al_2O_3 support. As mentioned above, two-dimensional surface compound may be formed by the interaction between NiO and Al_2O_3 on the catalyst and Ni particles were highly dispersed under the specific conditions. Additionally, the comparison of the surface compositions of the catalysts gave good indication that the addition of rare-earth metal oxide CeO_2 effectively promoted the Ni metal dispersion on the surface of the catalysts. Furthermore, the nickel component was gradually dispersed on the surface of the Ce-promoted catalysts following the exposure to reaction gas mixture for a period.

Chen et al.[6] investigated the influence of the rare-earth metal oxide on the nickel dispersion on the Al_2O_3 support. They reported that the active metal component was not directly sticked on the support, but adjacent to the surface of the rare-earth metal oxide. The interaction between them occurred and the specific filling structure was formed on the support. This structure inhibited the migration and enrichment of Ni and improved the nickel dispersion in the catalyst preparation and reaction processes. The formation of stable spinel $NiAl_2O_4$ was also retarded to a reasonable content.

It was also noteworthy that the variation of the self-dispersion of CeO_2 on the support. The surface concentration of Ce decreased from 6.51% to 4.65% on the MgO-containing catalyst and increased from 2.78% to 5.19% on the MgO-missing catalyst after reaction. The surface concentration of Ce decreased from 6.51% to 2.78% when the MgO addition increased from 2% to 3% for the fresh catalysts. Apparently, the addition of MgO inhibited the self-dispersion of CeO_2 on the catalysts. Therefore, the appearance of CeO_2 diffraction peak on the XRD patterns of 8.5% Ni-2%MgO-3%CeO_2/Al_2O_3 catalyst was indicative of the unsatisfactory self-dispersion of CeO_2 promoter. The EDX analysis result by scanning electron microscope was in good harmony with the XRD experiment result.

The surface concentration of Mg was not detected on the catalysts below 2% MgO-content added. It was observed that increased MgO addition inhibited the promotion effect of CeO_2 on Ni dispersion. Therefore, the optimum combination of the addition amount of the promoters is very important for perfect metal dispersion and desirable catalyst performance in the carbon dioxide reforming of methane.

TPR investigation. Figure 2, 3, and **4** showed the temperature programmed reduction profiles over promoted catalysts. Figure 2 indicated that appropriate MgO promoter may be a good solution to prohibiting the formation of $NiAl_2O_4$ spinnel phase. Addition of strong basic MgO significantly affected the basicity/acidity of the support, leading to a profound change in the bulk phase composition. It was observed that while the reduction peak of $NiAl_2O_4$ phase (1040 K) was significantly decreased, that of NiO (975 K) was greatly enhanced. This was probably ascribed to the fact that the basic MgO was preferably reacting with the acid Al_2O_3 to form stable magnesium aluminate, thereby suppressing the reaction between NiO and Al_2O_3. This was in agreement with the XRD results of promoted catalysts.

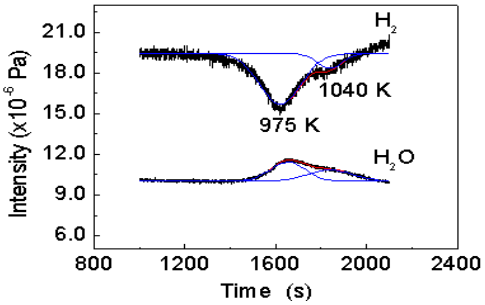

Figure 2. TPR profiles of 10wt% Ni-2wt%MgO/Al_2O_3 catalyst.

Addition of CeO_2 exhibited weak effect on retarding the formation of $NiAl_2O_4$ phase owing to its weak basicity (**Figure 3**). The reduction peak area of NiO was close to that of $NiAl_2O_4$ phase. However, the maximum reduction temperature of NiO on Ce-promoted catalyst was decreased from 975 K to 954 K, about 20 K reduction compared with that on Mg-promoted catalyst. The decreased reduction temperature may indicate that nickel dispersion on the support was improved by addition of CeO_2. The EDX analysis of the promoted nickel catalysts gave support for the description of promoting effect of CeO_2 on nickel dispersion.

The decreased reduction temperature of NiO and prohibition of formation of $NiAl_2O_4$ phase were obtained on the catalyst with appropriate addition amount of MgO and CeO_2 (**Figure 4).** It gave partial explanation for the perfect catalytic performance of the Mg-Ce-promoted catalyst. On the other side, the existence of appropriate amount of $NiAl_2O_4$ phase was beneficial to stabilization of Ni crystalline particles. Bolt et al.[7] reported that dispersed $NiAl_2O_4$ phase on the catalyst keep putting off the sintering and growth of nickel

particles. The backscattering spectra of specially treated catalyst with certain amount of $NiAl_2O_4$ on near-surface of the catalyst showed that unlapped Al_2O_3 reached 42%, while unlapped Al_2O_3 reached 83% on the near-surface of $NiAl_2O_4$-deficient catalyst. This indicated that the pronounced sintering of nickel particles on $NiAl_2O_4$-deficient catalyst occurred. The nickel particles were fixed and dispersed by $NiAl_2O_4$ and sintering was retarded on the treated catalyst.

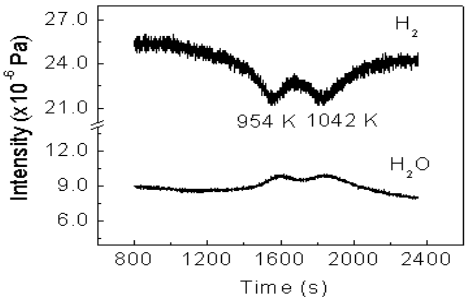

Figure 3. TPR profiles of 11.5wt% Ni-3wt%CeO_2/Al_2O_3 catalyst.

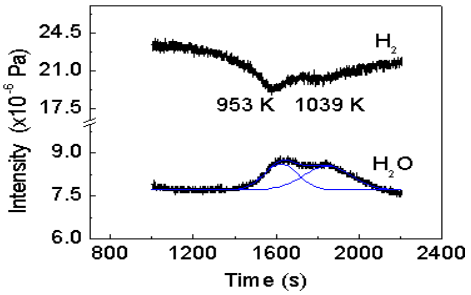

Figure 4. TPR profiles of 8.5wt% Ni-2wt%MgO-3wt%CeO_2/Al_2O_3 catalyst.

Conclusions

The chracterization results showed that addition of strong basic MgO promoter significantly retarded the formation of $NiAl_2O_4$ phase, while addition of rare-earth metal oxide CeO_2 effectively promoted the Ni metal dispersion on the surface of the catalysts despite of unsatisfactory self-dispersion of CeO_2 promoter. Furthermore, the nickel component was gradually dispersed on the surface of the support following the exposure to reaction gas mixture for a period. However, metal dispersion was not the unique factor that influenced the catalyst performance. Optimized combination of addition amount of different promoters was very important for perfect metal dispersion and desirable catalyst performance in the carbon dioxide reforming of methane.

Acknowledgement. Financial supports by the Young Scientists Award Foundation of Shandong Province and China National Petroleum Corporation are gratefully acknowledged.

References

(1) Trovarelli, A. *Catal. Rev. Sci. Eng.* **1996**, *38*, 439.
(2) Soria, J.; Coronado, J.M.; and Conesa, J.C. *J. Chem. Soc., Faraday Trans.* **1996**, *92*, 1619.
(3) Morterra C.; Bolis, V.; Magnacca, G. *J. Chem. Soc., Faraday Trans.* **1996**, *92*, 1991.
(4) Wang, C.Y.; Li, S.Y.; Yang, X.R.; Ren, J.; Chen, Y.G. *Energy Convers. Mgmt*. **1996**, *37*, 1357.
(5) Lu, Y.; Yu, C. C. *Chn. J. Catal.* **1996**, *17*(3), 212.
(6) Chen, Y. G.; Ren, J.; Wu, D.; Fan, W.H. *Petrochemical* **1994**, *23*(12), 771.
(7) Bolt P. H.; Habraken F. H. P. M.; Geus J. W. *J Catal.* **1995**, *151*, 300.

CO_2 Reforming and Partial Oxidation of Methane on Pt/Al_2O_3, Pt/ZrO_2 and $Pt/Ce\text{-}ZrO_2$ Catalysts

L.V. Mattos[1], E. R. de Oliveira[2], D. E. Resasco[3], F.B. Passos[2] and F.B. Noronha[1]

[1] Laboratório de Catálise, Instituto Nacional de Tecnologia, Rio de Janeiro, Brazil
[2] Departamento de Engenharia Química, Universidade Federal Fluminense, Niterói, Brazil
[3] School of Chemical engineering and Materials Science, University of Oklahoma, Norman, USA.

Introduction

Increasing concern about world dependence on petroleum oil has generated interest in the use of natural gas. However, the majority of these reserves are unmarketable since they are located in remote regions. The conversion of natural gas into transportation fuels such as gasoline and diesel is an alternative to the prohibitive transportation costs. The so-called gas-to-liquids technology (GTL) is based on the conversion of natural gas to a synthesis gas prior to the liquid production through the Fischer-Tropsch Synthesis (1).

Today, autothermal reforming (ATR) and catalytic partial oxidation (CPO) represent the technologies that fulfill the requirements to a gas with $H_2/CO = 2$, the ratio necessary to GTL plant. The ATR technology requires the addition of CO_2 or CO_2-rich gas in order to adjust the syngas composition to the desired H_2/CO ratio of the FT- synthesis (2).

The major obstacle associated with the CO_2 reforming reaction is the deactivation of the catalysts due to carbon deposition. Several studies have shown that Pt/ZrO_2 catalysts are very stable for the CO_2 reforming of methane (3,4). A mechanism involving two independent paths has been proposed to explain the CO_2 reforming of methane on Pt/ZrO_2 catalysts. In this mechanism, the support participates in the dissociative adsorption of CO_2 near the metal particles, transfering oxygen to the metal surface and accelerating the removal of carbon from the metal. More recently, we have reported that the use of promoters such as cerium oxide improves the activity and stability of Pt/ZrO_2 catalysts under severely deactivating reaction conditions (5,6). These results were attributed to the increase of the reducibility and oxygen transfer ability of the support by the addition of cerium oxide.

The aim of this work is to compare the performance of the $Pt/Ce\text{-}ZrO_2$ catalyst on the CO_2 reforming of methane and the partial oxidation of methane. The effect of the support reducibility on the catalytic activity of both reactions is evaluated.

Experimental

The ZrO_2 support was prepared by calcination of zirconium hydroxide (MEL) at 1073 K for 1h in flowing air. The alumina (Engelhard) was calcined at 1073K. The $Ce_{0.75}Zr_{0.25}O_2$ supports was synthesized following the method published by Hori et al. (7). The catalysts were prepared by incipient wetness impregnation of the supports with an aqueous solution of $H_2PtCl_6.6H_2O$ (Aldrich). Pt/ZrO_2 and $Pt/Ce_{0.75}Zr_{0.25}O_2$ samples were dried at 393K and calcined at 673K for 2h. Pt/Al_2O_3 sample was dried at 393K and calcined at 973K for 2h. The samples contained 1.5 wt.% of Pt.

Oxygen storage capacity (OSC) measurements were carried out in a micro-reactor coupled to a quadrupole mass spectrometer (Balzers, Omnistar). The samples were reduced under H_2 at 773K for 1h and then heated to 1073K in flowing He. Then, the samples were cooled to 723K and a $5\%O_2$/He mixture was passed through the catalyst until the oxygen uptake was finished. Then, the reactor was purged with He and the dead volume was obtained by switching the gas to the $5\%O_2$/He mixture. Finally, N_2 pulses were injected in order to calculate the amount of oxygen consumed on the catalysts taking into account a previous calibration of the mass spectrometer.

The dispersion was calculated from CO chemisorption by using pulses of a mixture containing 10%CO / He at room temperature. This experiment was performed on the same apparatus described to the OSC measurements and the same pretreatment was used.

Reactions were performed in a quartz reactor at atmospheric pressure. Prior to reaction, the sample was reduced under H_2 at 773K for 1h and then heated to 1073K in He. CO_2 reforming of methane was performed at 1073K with a $CH_4:CO_2$ ratio of 2:1 and a flow rate of 150 cm^3/min. The partial oxidation of methane was carried out at 1073K and a reactant mixture containing $CH_4:O_2$ ratio of 2:1 at a flow rate of 100 cm^3/min.

Results and Discussion

Table 1 presents the oxygen uptakes measured for the catalysts. The oxygen storage capacity of the $Pt/Ce_{0.75}Zr_{0.25}O_2$ catalyst is much higher than the one of the Pt/Al_2O_3 and Pt/ZrO_2 catalysts. The incorporation of ZrO_2 into CeO_2 lattice strongly increase the oxygen vacancies of the support due to the high oxygen mobility (8). The dispersion of the catalysts is also listed in Table 1. Pt/Al_2O_3 and $Pt/Ce_{0.75}Zr_{0.25}O_2$ catalysts exhibit approximately the same dispersion whereas the Pt/ZrO_2 catalysts had a higher dispersion.

Table 1. O_2 uptakes measured at 723K and dispersion calculated from the CO chemisorption at 298K.

Catalyst	O_2 uptake ($\mu mol/g_{catal}$)	Dispersion (%)
Pt/Al_2O_3	0.0	10
Pt/ZrO_2	8.5	24
$Pt/Ce_{0.75}Zr_{0.25}O_2$	625.6	8

The conversions of methane on the CO_2-reforming reaction at 1073K are shown in Figure 1. The Pt/Al_2O_3 catalyst had a low initial activity and rapidly deactivated due to coke deposition. The Pt catalysts supported on unpromoted zirconia and ceria-doped zirconia exhibited much higher activity and stability than the Pt/Al_2O_3 catalysts. The enhancement of the activity and the stability on the CO_2-reforming reaction could be assigned to the higher amount of oxygen vacancies in the proximity of metal particles as revealed by the OSC measurements (Table 1). According to the two-path mechanism proposed for the CO_2 reforming of methane (6), the addition of ceria to zirconia support greatly increases the rate of oxygen transfer and consequently the carbon removal.

Figure 1 shows the methane conversion on the partial oxidation of methane at 1073K. A strong deactivation is observed on the Pt/Al_2O_3 catalyst and less pronounced on the Pt/ZrO_2 catalyst. The $Pt/Ce_{0.75}Zr_{0.25}O_2$ catalyst practically did not loose their activity after 24 h time on stream (TOS).

Furthermore, a significant change in the selectivity towards CO and CO_2 was observed on the Pt/Al_2O_3 and Pt/ZrO_2 catalyst during the reaction (Figure 2). The production of CO_2 increased and the selectivity to CO decreased as the CH_4 conversion decreased. This effect is much less significant on the $Pt/Ce_{0.75}Zr_{0.25}O_2$ catalyst.

These results could be explained through the two step mechanism proposed for the partial oxidation of methane. According to this mechanism, in the first stage, combustion of methane occurs producing CO_2 and H_2. In the second one, synthesis gas is produced via carbon dioxide and steam-reforming reaction of the unreacted methane (9). Since the production of carbon and CO_2 increased on the Pt/Al_2O_3 and Pt/ZrO_2 catalyst during the reaction (Figure 2), the

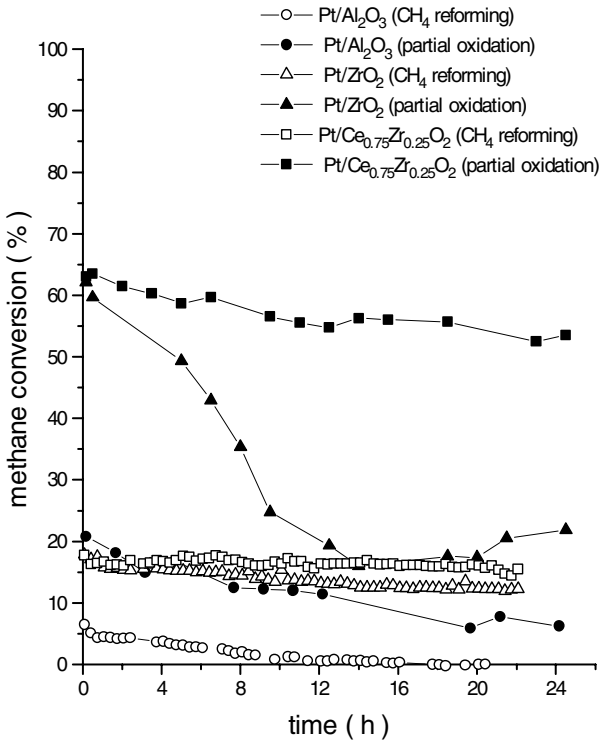

Figure 1. Catalytic activity on both CO_2-reforming of methane (open symbols) and partial oxidation of methane (solid symbols) versus time on stream for Pt/Al_2O_3, Pt/ZrO_2 and $Pt/Ce_{0.75}Zr_{0.25}O_2$ catalyst. Reaction conditions: T= 1073K; CH_4:CO_2 ratio = 2:1; CH_4:O_2 ratio = 2:1.

second step of the mechanism should be inhibited. From Figure 1, it is clear that the increase of carbon deposits around or near the particle metal affects the CO_2 dissociation and inhibits the CO_2 reforming of methane mainly on the Pt/Al_2O_3 catalyst and on less extent on the Pt/ZrO_2 catalyst. On the $Pt/Ce_{0.75}Zr_{0.25}O_2$ catalyst, the selectivity towards CO practically did not change during reaction due to the redox mechanism of carbon removal promoted by the support.

Conclusions

The results of catalytic activity on both the CO_2 reforming and the partial oxidation of methane revealed the important role of the support on the mechanism of these reactions. A strong deactivation was observed on the Pt/Al_2O_3 catalyst on both reactions. The addition of ceria to zirconia greatly promoted the stability of the catalyst due to higher oxygen exchange capacity of the support. The higher rate of oxygen transfer keep the metal surface free of carbon. This promotional effect on the CO_2 reforming of methane affects the partial oxidation of methane, which comprehends two steps: combustion of methane and CO_2 and steam reforming of unreacted methane.

Acknowledgement. The authors wish to acknowledge the financial support of the CNPq/CTPETRO (462530/00-0) and FNDCT/CTPETRO (65.00.0395.00) program. We also thanks MEL Chemicals for providing the zirconium hydroxide.

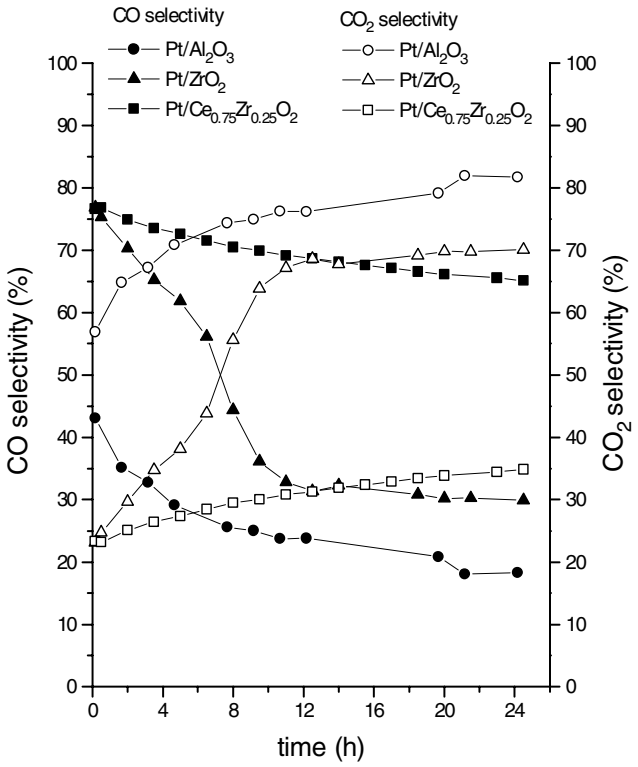

Figure 2. CO and CO_2 selectivity on partial oxidation of methane versus time on stream for: Pt/Al_2O_3, Pt/ZrO_2 and $Pt/Ce_{0.75}Zr_{0.25}O_2$ catalyst. Reaction conditions: T= 1073K; CH_4:O_2 ratio = 2:1.

References

(1) Venkataraman, V.K., Guthrie, H.D., Avellanet, R.A . and Driscoll, D.J., *Stud.Surf.Sci.Catal*. **1998**, *119*, 913.
(2) Dybkjaer, I. and Christensen, T.S., *Stud.Surf.Sci.Catal*. **2001**, *136*, 435.
(3) Van Keulen, A.N.J., Hegarty, M.E.S., Ross, J.R.H. e van den Oosterkamp, P.F., *Stud.Surf.Sci.Catal*. **1997**, *107*, 537.
(4) Stagg, S.M., Romeo, E., Padro, C., Resasco, D.E., *J.Catal.* **1998**, *178*, 139.
(5) Stagg-Willians, S.M., Noronha, F.B., Fendley, G. e Resasco, D.E., *J.Catal*. **2000**, *194*, 240.
(6) Noronha, F.B., Fendley, E.G., Soares, R.R., Alvarez, W.E. e Resasco, D.E., *Chem.Eng.Journal* **2001**, 82, 21.
(7) Hori, C.E., Permana, H., Simon Ng, K.Y., Brenner, A., More, K., Rahmoeller, K.M., Belton, D., *Appl. Catal. Envir. B* **1998**, 16, 105.
(8) Vlaic, G., Fornasiero, P., Geremia, S., Kaspar, J., Graziani, M., *J.Catal*. **1997**, *168*, 386.
(9) O'Connor, A ., M. and Ross, J.R.H., *Catal.Today* **1998**, 46, 203

CONTINUOUS PRODUCTION OF DIETHYL CARBONATE OVER A SUPPORTED $CuCl_2/PdCl_2$/KOH CATALYST

N. S. Roh, B. C. Dunn, and E. M. Eyring

Department of Chemistry
University of Utah
Salt Lake City, Utah 84112

J. Dworzanski, H. L. C. Meuzelaar, J. Z. Hu, M. S. Solum, and R. J. Pugmire

Department of Chemical and Fuels Engineering
University of Utah
Salt Lake City, Utah 84112

Introduction

Diethyl carbonate is a potential oxygen-containing additive for gasoline and diesel fuel to reduce pollutant emissions. Previous studies using a similar compound, dimethyl carbonate (DMC), as an oxygenate have shown reduction of carbon monoxide,[1] oxides of nitrogen,[2] hydrocarbons,[3] and particulate matter.[4] Our own research efforts[5] indicate that 5 wt. % DEC in diesel fuel can reduce the emission of particulate matter by as much as 50%. Additional factors make DEC an attractive oxygen-containing fuel additive, namely, its high oxygen content (40.6 wt. %), and more favorable gasoline/water distribution coefficient[3] when compared with ethanol or DMC. When in contact with soil, DEC should slowly decompose into ethanol and carbon dioxide,[6] two compounds with little or no environmental impact.

One promising method of producing DEC on an industrial scale is the oxidative carbonylation of ethanol using a heterogeneous catalyst. The overall reaction is:

$$2\,EtOH + CO + \frac{1}{2}O_2 \xrightarrow{Cu^{2+}/Pd^{2+}} O=C(OEt)_2 + H_2O$$

Previous studies[5] conducted with a batch reactor indicate an improvement in the yield of DEC when the $CuCl_2/PdCl_2$/activated carbon catalyst is treated with KOH after the support is loaded with the chloride salts. This post-treatment creates an additional phase of copper, atacamite, which creates a more active catalyst.[7]

Batch reactor studies[5] cannot predict the behavior of the chemical reaction due to the static nature of the system. Thus, studies employing a pulse-quench-flow reactor were conducted using the most active catalyst determined from the batch reactor experiments. These experiments have increased our understanding of the chemical reaction and may lead to the development of better catalysts.

Experimental

Pulse-quench-flow reactor. The reactor design was based on a previously published report[8] and consisted of three mass flow controllers (MKS) to deliver the gaseous reactants (CO and O_2) and N_2 carrier gas. The ethanol, with a 5 wt. % toluene internal standard, was delivered at a constant rate with a syringe pump (Isco) equipped with a preheater to ensure the ethanol was in the gas phase. The reactor consisted of a 5 inch long, ¼ inch id stainless steel tube, plugged at both ends with glass wool to contain the catalyst, and wrapped with a rope heater. A thermocouple was placed inside the catalyst bed for accurate temperature control. A backpressure regulator located downstream of the catalyst bed maintained pressure inside the system and the sampling port for the GC/MS was located on the low pressure side of the regulator. All components of the reactor were heated to maintain the reactants and products in the gas phase at all times. The GC/MS sampling line was also heated to prevent condensation.

Catalyst Preparation. The catalyst was prepared by dissolving suitable amounts of $CuCl_2$ and $PdCl_2$ in approximately 500 mL of methanol and adding sufficient activated carbon (Darco, 20-40 mesh) to yield 3 wt. % Cu and 0.25 wt. % Pd, both measured as metals. The mixture was refluxed for four hours to impregnate the carbon support and the methanol was removed by vacuum distillation. The catalyst was dried in a vacuum oven at 80 °C overnight. The catalyst was then treated with a methanolic solution of KOH, refluxed, vacuum distilled, and dried overnight. A fresh 2.00 g sample of the catalyst was loaded into the reactor for each experiment to ensure that any effects observed were due to the chemical reaction and not from catalyst deactivation.

Results and Discussion

The catalyst used for all of the studies consisted of $CuCl_2/PdCl_2$/KOH supported on activated carbon. This catalyst has proven to be more active[5] than those prepared without $PdCl_2$, with other copper salts ($Cu(NO_3)_2$, $Cu(CH_3COO)_2$, etc), with other hydroxide sources (NaOH, $Ca(OH)_2$, etc), or on other supports (alumina, silica, etc). Even with the most active catalyst, the reaction is quite slow, such that long residence times must be used to produce a suitable amount of DEC for GC/MS detection. The continuous flow reactor allows for simple adjustment of the residence time by modifying the flow rate of the N_2 carrier gas. The influence of residence time on DEC production is presented in **Figure 1** which shows the conversion of ethanol into DEC reaches a maximum of 12.5% at τ=17.4 s. Shorter residence times simply result in less DEC produced, and the selectivity for DEC remains constant at 100%. No additional products were detected in the GC/MS; however, conversion of CO into CO_2 was not considered.

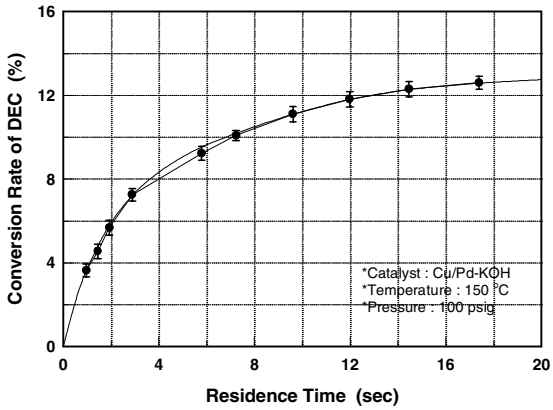

Figure 1. Influence of residence time on production of DEC. Conditions: 2.0 g catalyst, 3.2 standard cubic centimeters per minute (sccm) O_2, 48 sccm CO, 1.2 mL/hr ethanol (as liquid), 150 °C, 100 psig.

The reaction temperature was varied between 120 °C and 180 °C with five residence times and the results are presented in **Figure 2**. The two smallest residence times (1.44 s and 2.89 s) show very little temperature dependence presumably due to the short contact time with the catalyst, while the other three contact times show a linear dependence on the reaction temperature. No other organic products

were detected, thus the selectivity for DEC remained essentially constant at 100%. The maximum conversion of DEC reached almost 18% at 180 °C with 17.4 s contact time, and based on these data, further improvements may be possible with even higher temperatures.

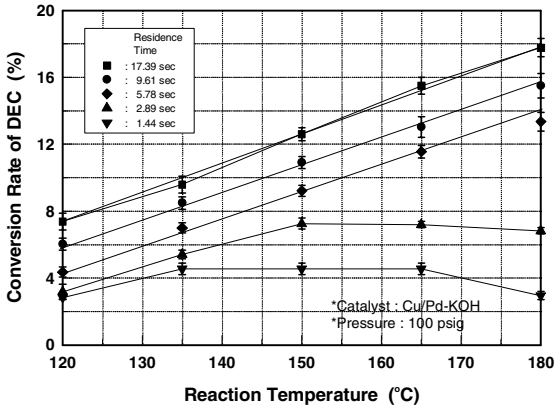

Figure 2. Impact of reaction temperature on the production of DEC. Conditions: 2.0 g catalyst, 3.2 sccm O_2, 48 sccm CO, 1.2 mL/hr ethanol (as liquid), 100 psig.

The flow rate of CO into the reactor showed unexpected behavior. As seen in **Figure 3**, the relationship between CO flow rate and production of DEC is not linear, but shows three distinct regions.

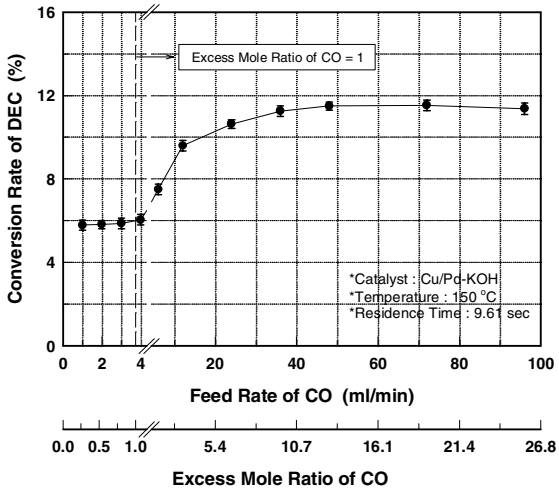

Figure 3. Influence of CO flow rate on conversion of ethanol to DEC. Conditions: 2.0 g catalyst, 3.2 sccm O_2, 1.2 mL/hr ethanol (as liquid), 150 °C, 9.61 s contact time.

In the region where CO is the limiting reactant, DEC production is independent of the flow rate of CO. Since the calculation of DEC conversion is based on the limiting CO reactant, this region indicates that a simple chemical equilibrium has been established. The ratio of DEC to CO is constant. At CO flow rates between 4 and 35 sccm, the results still indicate a simple chemical equilibrium because 100% conversion is based on ethanol rather than CO, as in the previous case. At CO flow rates above 35 sccm, the reaction has reached saturation in which all of the accessible catalytic sites are occupied by a CO molecule, and the yield is controlled by kinetics rather than by equilibrium.

The flow rate of ethanol was varied from 1.2 to 9.5 mL/hr while maintaining all other experimental parameters. The results can be seen in **Figure 4**. Rather than show simple chemical equilibrium as noted above, an additional product, diethoxymethane (DEM), is formed when ethanol is in stoichiometric excess. Since the amount of DEM increases independently of the amount of DEC, the reaction which produces DEM must be independent from the DEC reaction, not a sequential mechanism.

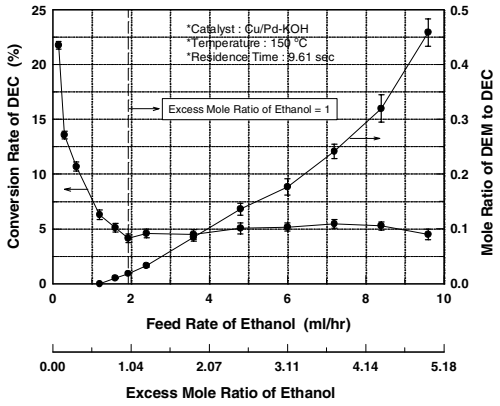

Figure 4. The impact of ethanol flow rate on DEC yield. Conditions: 2.0 g catalyst, 3.0 sccm O_2, 6.0 sccm CO, 150 °C, 9.61 s contact time.

Conclusions

Diethyl carbonate can be produced with high selectivity using a $CuCl_2/PdCl_2/KOH$ catalyst supported on activated carbon. The reaction behaves as predicted with respect to temperature and contact time, but unusual effects have been observed when the flow rate of CO and ethanol are varied. The reaction reaches kinetic saturation when CO is present in large excess, and when ethanol is in excess, the formation of a byproduct is favored.

Acknowledgement. Financial support by the US Department of Energy through the Consortium for Fossil Fuel Liquefaction Sciences (University of Kentucky, Lexington) is gratefully acknowledged.

References

1. Imoura, S.; Matsushita, D. Japan Patent 61[1986]-207496, **1986**
2. Stoner, M.; Litzinger, T. *SAE Technical Paper Series* **1999**, 1999-1901-1475.
3. Pacheco, M. A.; Marshall, C. L. *Energy & Fuels* **1997**, *11*, 2-29.
4. Dillon, D. M.; Iwamoto, R. Y. US Patent 4,891,049, **1990**
5. Dunn, B. C.; Guenneau, C.; Hilton, S. A.; Pahnke, J.; Eyring, E. M.; Dworzanski, J.; Meuzelaar, H. L. C.; Hu, J. Z.; Solum, M. S.; Pugmire, R. J. *Energy & Fuels* **2001**, *in press.*
6. Crandall, J. W.; Deitzler, J. E.; Kapicak, L. A.; Poppelsdorf, F. US Patent 4,663,477, **1987**
7. Punnoose, A.; Seehra, M. S.; Dunn, B. C.; Eyring, E. M. *Energy & Fuels* **2001**, *in press*.
8. Goguen, P. W.; Xu, T.; Barich, D. H.; Skloss, T. W.; Song, W.; Wang, Z.; Nicholas, J. B.; Haw, J. F. *J. Am. Chem. Soc.* **1998**, *120*, 2650-2651.

THE COUPLING OF CATALYTIC STEAM REFORMING AND OXIDATIVE REFORMING OF METHANE TO PRODUCE PURE HYDROGEN IN A NOVEL CIRCULATING FAST FLUIDIZATION BED MEMBRANE REFORMER

Zhongxiang Chen, Pradeep Prasad, and Said Elnashaie

Chemical Engineering Department
Auburn University, Auburn, AL 36849

Introduction

Steam reforming of natural gas represents the principal commercial route to hydrogen production. The classical industrial steam reformer (1st generation) consists of hundreds of parallel catalyst tubes of about 10 inches diameter, surrounded by a very large furnace. This process suffers from a number of limitations making it extremely inefficient e.g.:

(1) Diffusion Limitations: The effectiveness factors of the large catalyst pellets have been found to be as low as $10^{-2} - 10^{-3}$. [1,2]
(2) Thermodynamic Limitations: The reversibility of the reforming reactions limits the conversion to thermodynamic equilibrium.
(3) Catalyst Deactivation: Carbon formation increases with the increase in the temperature, leading to catalyst deactivation.

The most successful milestone to date in the development of a more efficient reformer was the bubbling fluidized bed membrane steam reformer (BFBMSR) for natural gas, where powdered catalyst was used to overcome the diffusion limitations and hydrogen selective membranes were used to overcome the thermodynamic equilibrium barrier.[3,4,5] Roy et al[6] have experimentally studied the addition of oxygen to the BFBMR to provide all of the heat required for the endothermic reforming reactions, and found that autothermal conditions could be reached and maintained.

The BFBMSR, although very efficient, still suffers from a number of important limitations. The present work suggests a novel, more efficient and flexible process consisting of a fast fluidization riser reactor where steam reforming and partial oxidation reactions are carried out. The riser reactor also has a number of hydrogen selective membranes for hydrogen removal and oxygen selective membranes to introduce a part of the oxygen into the reactor for partial oxidation of the feed. A gas solid separator is used to separate the solids and they are recycled to the riser reactor after regeneration of the catalyst. A preliminary schematic diagram of the proposed novel reformer is shown in Figure 1.

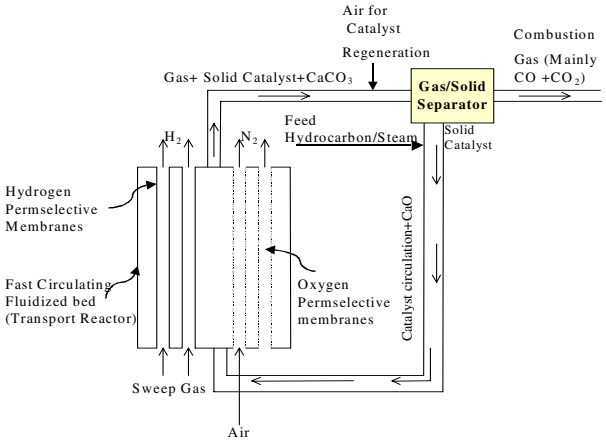

Figure 1. Schematic diagram of the proposed novel configuration.

Modeling

In the present paper, preliminary modeling and simulation are carried out on the reactor section alone of the circulating fast-fluidized bed reformer. The cases with and without hydrogen selective membranes are considered and are compared with industrial fixed bed reformers and bubbling fluidized bed reformers. Oxygen input to the reactor directly or through membranes is investigated.

Reaction Kinetics. The rate expressions proposed by Xu and Froment [7] for the steam reforming of methane using Ni/Al_2O_3 catalyst will be used in the present study. They were analyzed in some detail by Elnashaie et al [8] and found to be the most general rate equations.

A number of supported metal catalysts such as Ni, Rh, Pt, etc have been reported for partial oxidization of methane.[9] Dissanayake et al.[10] examined the oxidation state and phase composition of the Ni/Al_2O_3 catalyst as a function of axial position in the catalyst bed. Their results strongly support the mechanism of methane combustion followed by steam and carbon dioxide reforming.

Model Equations. The fast-fluidized bed reformer is modeled as a plug flow reactor with co-current flow in the reactor and membrane (sweep gas) sides. Ideal gas law is used to calculate the partial pressures on the reactor and the membrane sides. The mass and energy balances can be obtained at steady state as follows.

$$\frac{dF_i}{dl} = \rho_c A_c (1-\varepsilon) R_i + J_i \qquad (1)$$

$$\sum_i F_i \frac{d(H_i)}{dl} = A_c \rho_c (1-\varepsilon) \sum_j r_j (-\Delta H_j) + Q \qquad (2)$$

where $J_i=0$ for all components, except hydrogen and oxygen for which J_i is the corresponding molar permeation term depending on the type of membrane used. For a supported dense Pd membrane, the hydrogen permeation term is:[11]

$$J_{H_2} = -\frac{Q_{H_2}}{\delta_{H_2}} \exp\left(\frac{-E_{H_2}}{RT}\right)\left(\sqrt{p_{H_2,r}} - \sqrt{p_{H_2,m}}\right) \qquad (3)$$

For a dense perovskite oxygen permeable membrane, the oxygen permeation term is:[12]

$$J_{O_2} = Q_{O_2} \exp\left(\frac{-E_{O_2}}{RT}\right)\frac{T}{\delta_{O_2}} \ln\left(\frac{P_{O_2,m}}{P_{O_2,r}}\right) \qquad (4)$$

The set of initial value differential equations is solved using initial conditions to be the same as the feed conditions per tube of an industrial reactor described in Elnashaie and Elshishini.[13]

The method given by Kunii and Levenspiel[14] has been used to verify that the reactor is operating in the fast fluidization or the pneumatic transport regime.

Results and Discussion

Figure 2 shows the effect of the hydrogen permeable membrane on the conversion of methane in the isothermal reactor with only hydrogen selective membranes. The removal of hydrogen from the reactor side breaks the equilibrium barrier resulting in almost complete conversion of methane. This is achieved in a very short length of reactor (≈ 1 m) as compared to the much higher lengths (> 10 m) that are typically used for fixed bed steam reformers.

Table 1 compares the fast-fluidized membrane steam reformer (FFMSR) with the industrial fixed bed and the BFBMSR. The value hydrogen yield per m^3 of the reactor gives us a strong and direct indication of the improvement in the efficiency of the reactor.

Figure 3 shows the yield of hydrogen obtained for different amounts of oxygen introduced into an adiabatic reformer along with the feed, when no oxygen permeable membranes are present. Both, the cases with and without hydrogen permeable membranes are

investigated. We find a general increase in the yield of hydrogen for increased oxygen in the feed. The oxygen conversion via combustion causes an increase in hydrogen yield due to the higher equilibrium yield of the endothermic reforming reaction at higher temperatures. The use of hydrogen permeable membrane causes further increase in hydrogen yield by shifting the equilibrium.

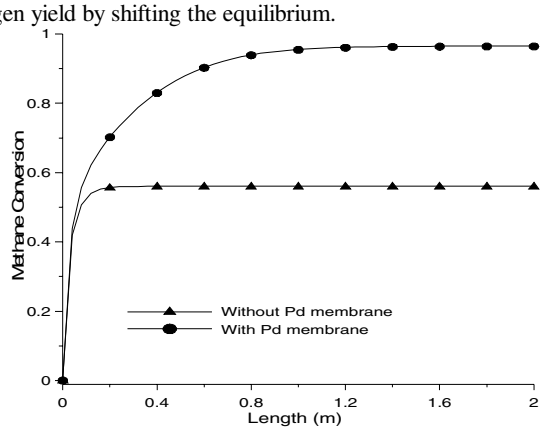

Figure 2. With membrane vs. without membrane for T=900 K, Reactor pressure=5atm, Membrane side pressure=1atm.

Table 1. Comparison between FFMSR and (a) Industrial Fixed Bed and (b) BFBMSR

(a)	Fixed Bed[12]	FFMSR	(b)	BFBMSR[5]	FFMSR
X_{CH4}	0.853	0.964	X_{CH4}	0.419	0.582
H_2 yield per m^3 of reactor	27.27	246.8	H_2 yield per m^3 of reactor	109	302.7

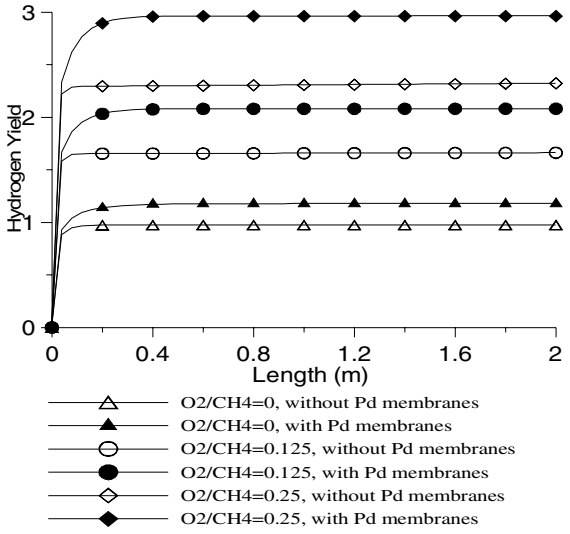

Figure 3. Yield of hydrogen with oxygen as part of reactor feed, T_{inlet}=1000K, Reactor pressure=5atm, Membrane side pressure=1atm.

An alternate approach is to introduce oxygen through oxygen permeable membranes. It allows us to distribute the supply of oxygen along the length of the reactor and thus optimize the extent of the oxidation reaction so as to maximize the productivity of hydrogen. Figure 4 shows the results of a simulation of an adiabatic reformer with both hydrogen and oxygen permeable membranes. Presently the permeability of the available oxygen permeable membranes seems to be a limiting factor. It necessitates the use of a reduced reactant feed rate as compared to the earlier cases, and high membrane surface area for oxygen permeation. The use of oxygen permeable membranes increases the yield of hydrogen because of the higher equilibrium conversion at higher temperature. The use of hydrogen permeable membrane causes a further increase in hydrogen yield by breaking the thermodynamic equilibrium barrier.

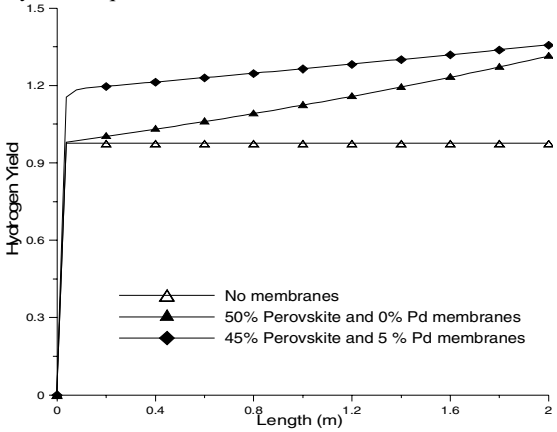

Figure 4. Yield of hydrogen vs length of reactor, T_{inlet}=1000K, Reactor pressure=5atm, Membrane side pressure=1atm. Percentage values denote percentage of reactor cross-sectional area occupied by the membrane.

Nomenclature

A_c	area of cross-section of the reactor (m^2)
E_i	apparent activation energy of membrane permeable to i ($kJ.mol^{-1}$)
F_i	molar flowrate of species i ($kmol.hr^{-1}$)
ΔH_j	heat of reaction for reaction j ($kJ.mol^{-1}$)
H_i	molar enthalpy of species i ($kJ.mol^{-1}$)
J_i	permeation flux of i ($kmol.hr^{-1}.m^{-2}$)
l	length of reactor (m)
P_i,r ,P_i,m	partial pressure of species i on the reaction and membrane sides respectively (kPa)
Q_i	pre-exponential factor in the Arrhenius relationships for permeability of hydrogen and oxygen ($kJ.m^{-1}.hr^{-1}.kpa^{-n}$)
Q	rate of heat input ($kJ.hr^{-1}.m^{-3}$)
R	gas constant (8.314 $kJ.kmol.^{-1}.K^{-1}$)
R_i	rate of production of species i ($kmol.hr^{-1}$)
T	temperature (K)
δ_i	thickness of membrane (m)
ε	void fraction
ρ_c	density of catalyst ($kg.m^{-3}$)

References

(1) De Deken, J.C.; Devos, E.F.; Froment,G.F., *Am. Chem. Soc. Symp. Ser.*, **1982**, 196, 181.
(2) Soliman, M.A.; Elnashaie, S.S.E.H.; Al-Ubaid, A.S.; Adris, A.M., *Chem. Eng. Sci.*, **1988**, 43, 1803.
(3) Adris, A.M.; Elnashaie, S.S.E.H.; Hughes, R., *Can. J. Chem. Eng.*,. **1991**, 69, 1061.
(4) Adris, A.M.; Lim, C.J.; Grace. J.R., *Chem. Eng. Sci.*,. **1994**, 49, 5833.
(5) Adris, A.M.; Lim, C.J.; Grace. J.R., *Chem. Eng. Sci.*,. **1997**, 52, 1609.
(6) Roy, S.; Pruden, B.B.; Adris, A.M.; Lim, C.J.; Grace, J.R., *Chem. Eng. Sci.* **1999**, 54, 2095.
(7) Xu, J.; Froment, G.F., *AIChE. J.*, **1989**, 35, 88.
(8) Elnashaie, S.S.E.H.; Adris, A.M.; Al-Ubaid, A.S.; Soliman, M.A., *Chem. Eng. Sci.*, **1990**, 45(2), 491.
(9) Ashcroft, A.T.; Cheetham, A.K.; Foord, J.S.; Green, M.L.H.; Grey, C.P.J.; Murrell , A. and Vernon, P.D.F., *Nature*, **1990**, 344, 319.
(10) Dissanayake, D.; Rosynek, M.P.; Kharas, K.C.C.; Lungsford, J.H., *J. Catal.*, **1991**, 132, 117.
(11) Barbieri, G.; Maio, F.P.D., *Ind. Eng. Chem. Res.* **1997**, 36, 2121.
(12) Tsai, C.; Dixon, A.G.; Moser, W.R.; Ma, Y.H., *J. AIChE*, **1997**, 43(11A), 2741.

(13) Elnashaie, S.S.E.H.; Elshishini, S.S., Modelling, simulation and optimization of industrial fixed bed catalytic reactors, Gordon and Breach Science Publishers: London, 1993.
(14) Kunii, D; Levenspiel, O., *Chem. Eng. Sci.*, **1997**, 52, 2471.

DEHYDRO-OLIGOMERIZATION OF METHANE TO BENZENE AND NAPHTHALENE WITHOUT ADDING OXYGEN: PROMOTIONAL EFFECT OF IN OVER MO/HZSM-5 CATALYST

Jinfeng Zhao, Xiaodong Wang, Tao Zhang, Lin Li, Ning Li, Mingyuan Zheng, Liwu Lin*

* State Key Laboratory of Catalysis,
Dalian Institute of Chemical Physics,
Chinese Academy of Sciences,
P.O.Box 110, Dalian 116023, China

Introduction

Methane dehydro-oligomerization and aromatization without adding oxygen over Mo/HZSM-5 catalyst have been widely studied.[1-8] However, the existing problem in this route is the low yield of aromatics, due to the high stability of methane. Recently, introduction of second metal species has been believed to be a promising route to improve methane non-oxidative transformation on the Mo/HZSM-5 catalyst.[9-13] Our previous work reported on the studies of the structures of Mo/HZSM-5 catalysts and the enhancing stability of Mo/HZSM-5 with incorporation of platinum in the process of dehydro-oligomerization of methane to benzene and ethylene.[9, 14] In the meanwhile, we found that indium took great effect on the activation of methane in the reaction of selective catalytic reduction of NO by methane over In/HZSM-5.[15,16] Therefore, in this paper, indium was used to be expected to promote the catalytic performance of Mo/HZSM-5 for methane non-oxidative reaction. Indeed, it was found that Mo-In/HZSM-5 exhibited much higher conversion of methane and production of benzene and naphthalene than Mo/HZSM-5.

Experimental

Catalysts preparation. Mo/HZSM-5, Mo-In/HZSM-5, In/Mo/HZSM-5 and Mo/In/HZSM-5 catalysts were prepared by impregnation, co-impregnation and successive impregnation methods, respectively. The component of catalysts were denoted by the weight ratio.

Catalytic tests. Methane conversion test was carried out in the fixed-bed continuous-flow micro-reactor system, with a 6.4mm i.d. quartz tubular reactor containing 0.2g catalyst (24-32 mesh). The catalysts were first heated to 973K under Ar stream (30ml/min) and held for 30 min. Then, the stream was switched to the feed gas mixture of 90% CH_4 (99.999%) with 10% N_2 as internal standard. The reaction was conducted at 973K under a total pressure of 1 atm. The hydrocarbon products were analyzed by on-line HP 6890 gas chromatograph.

An internal standard analyzing method similar to that reported by Liu et al. was used to calculate CH_4 conversion and selectivity toward hydrocarbon products according to mass balance for carbon. The selectivity of coke, including undetected heavy aromatics, would be obtained.[11]

Results and discussion

Table1 shows that the addition of 0.3-2% In to 6% Mo/HZSM-5 catalyst induces a significant effect on the catalytic performance. It is clear to see that the selectivity of aromatics increase remarkably after the introduction of small amount of In to Mo/HZSM-5. When In content reaches 0.7% in Mo-In/HZSM-5, the catalyst exhibits the best catalytic activity, leading to an increase in methane conversion from 11.13 to 13.14% and yield of aromatics from 7.25 to 9.42 as compared with Mo/HZSM-5. Meanwhile, it is observed that the selectivity of coke decreased considerably from 27.10 to 21.98%. This indicates that the improvement of catalyst activity and selectivity by In additives to Mo/HZSM-5 most probably originates from the alleviation of coke deposition. It is interesting to note that catalytic behavior of Mo-In/HZSM-5 catalyst is sensitive to the additive amount of In. Further increase in In content up to 2% causes methane conversion to slightly decrease, however, the yield of aromatics is higher and the selectivity of coke is less than Mo/HZSM-5. These results show that a proper amount of In introduced into Mo/HZSM-5 can evidently improve its catalytic activity for methane dehydro-oligomerization.

Fig.1 shows a comparison of the catalytic performances of both Mo/HZSM-5 and In-promoted Mo/HZSM-5 on time on stream. It can be seen that the methane conversion and the yield of aromatics on Mo-0.7In/HZSM-5 are always significantly higher than those on Mo/HZSM-5 in the range of time on stream. It is demonstrated that the addition of In is favorable for the dehydrogenation of methane

Table 1 Catalytic performances of Mo-In/HZSM-5 catalysts.

Catalysts	CH_4 Conv. (%)	Selectivity (%)					Yield of aromatics (%)
		C2	Benz.	C7-C8	Nap.	Coke	
6Mo/HZ	11.13	3.71	50.66	2.92	11.54	27.10	7.25
6Mo-0.3In/HZ	11.60	3.24	54.15	3.03	12.62	23.55	8.10
6Mo-0.7In/HZ	13.14	3.64	54.32	2.73	14.66	21.98	9.42
6Mo-1.0In/HZ	12.14	3.45	56.05	3.04	13.08	20.73	8.76
6Mo-1.5In/HZ	11.45	3.64	53.18	3.12	12.28	24.05	7.85
6Mo-2.0In/HZ	11.00	2.89	52.89	3.03	14.36	23.15	7.73

T=973K, P=1atm, t=60min, space velocity=1500ml$g^{-1}h^{-1}$,HZSM-5=HZ.

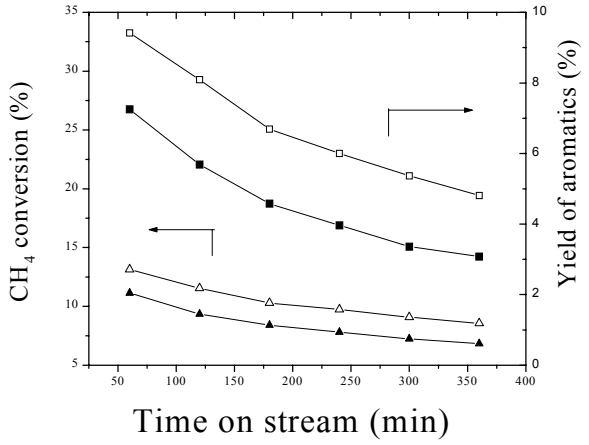

Fig.1 CH_4 conversion (triangle) and yield of aromatics (square) on Mo-0.7In/HZSM-5 (open) and Mo/HZSM-5 (solid) versus time on stream.

and the formation of aromatic hydrocarbons.

The impregnation sequence of Mo and In species during the catalyst preparation is also important for good catalytic performance. The result is summarized in **Table 2**. It is easy to find that the Mo-In/HZSM-5 catalyst prepared by co-impregnation method exhibits the best catalytic activity among the three different catalysts. The possible reason is that the catalyst prepared by co-impregnation method allows the two metal components to interact with the zeolite support simultaneously and evenly, thus inhibiting the formation of coke and resulting in higher activity and selectivity. However, for the successive impregnating method, the interaction between one metal and zeolite can be weakened when another metal component has united with HZSM-5 firmly.

Table 2 The effect of impregnation sequence on the catalytic performance of In promoted Mo/HZSM-5.

Catalysts	CH_4 Conv. (%)	Selectivity (%)					Yield of aromatics (%)
		C2	Benz.	C7-C8	Nap.	Coke	
6Mo/HZ	11.13	3.71	50.66	2.92	11.54	27.10	7.25
Mo/In/HZ	9.08	4.26	42.14	2.74	6.88	39.82	4.70
In/Mo/HZ	10.85	3.90	54.42	3.13	14.82	20.31	7.85
Mo-In/HZ	13.14	3.64	54.32	2.73	14.66	21.98	9.42

T=973K, P=1atm, t=60min, space velocity=1500ml$g^{-1}h^{-1}$, HZSM-5=HZ, Mo:In:HZ=6:0.7:93.3.

4. Conclusions

Introduction of a proper amount of In into Mo/HZSM-5 greatly enhances the catalyst activity and the selectivity of aromatics in methane non-oxidative reaction. In addition, the improvement of In over Mo/HZSM-5 is also due to the catalyst preparation method.

References

1 L. Wang, J. Hang, L. Tao, M. Xie and G. Xu, Catal. Lett., 1993,21,35.

2 Y. Xu, S. Liu, L. Wang, M. Xie and X. Guo, Catal. Lett., 1995,30,135.

3 F. Solymosi, A.Erdohelyi and A. Szoke, Catal. Lett., 1995,32,43.

4 L. Chen, L. Lin, Z. Xu, X. Li and T Zhang, J. Catal., 1995,157,190.

5 D. Wang, J.H. Lunsford and M.P. Rosynek, J. Catal., 1997,169,347.

6 R. Ohnishi, S. Liu, Q. Dong, L .Wang and M. Ichikawa, J. Catal.,1999,182,92.

7 L. Wang , Y. Xu, M. Xie, S. Liu and L.Tao, Stud. Surf. Sci. Catal.,1995,94,495.

8 S. T. Wong, Y. Xu, L. Wang and M. Xie, Catal. Lett., 1996,38,39.

9 L. Chen, L. Lin, Z. Xu, T. Zhang and X. Li, Catal. Lett., 1996,39,169.

10 Y. Shu, Y. Xu, S. Wong, L. Wang and X. Guo, J. Catal.,1997,170,11.

11 S. Liu, Q. Dong, R. Ohnishi and M. Ichikawa, Chem. Commun., 1997,1455.

12 R. Meriaudeau and C. Naccache, J. Catal., 1995,157,283.

13 B. Liu, Y. Yang and A. Sayari, Appl. Catal. A: General, 2001,214,95.

14 L. Chen, L. Lin, Z. Xu, X. Li and T, Zhang, J. Catal. 1995,157,190.

15 X. Zhou, T. Zhang, and L.Lin, Catal. Lett., 1996,40,35.

16 X. Zhou, Z, Xu, T. Zhang, and L.Lin, J. Mol. Catal. A, 1997,122,125

DEVELOPMENT OF A PRESSURE DEPENDENT REACTION MODEL FOR METHANE/METHANOL MIXTURES UNDER PYROLYTIC AND OXIDATIVE CONDITIONS AND COMPARISON WITH EXPERIMENT

Chad Sheng, Joseph W. Bozzelli and Wen-chiun Ing

Dept of Cheml Engrg, Chem and Envir Sci
New Jersey Institute of Technology, Newark, NJ 07102

ABSTRACT

Methanol experimental data are obtained under pyrolysis, fuel lean ($\phi = 0.75$) and stoichiometric mixtures with methane in a flow reactor. Methanol pyrolysis experiments are performed under isothermal conditions of 1073K over a pressure range from 1 to 10 atm. Oxidation environments are performed over a temperature range from 873 - 1073K and a pressure range from 1 - 5 atm. Oxidation experiments consisting of methane/methanol mixtures are performed under stoichiometric conditions, with varying ratios of the two fuels. A pressure dependent mechanism for methane/methanol oxidation and pyrolysis reaction system is developed and compared with experimental data. Pathways for formation of higher molecular weight species, such as methyl-ethers, are also incorporated in this mechanism. The mechanism consists of about 150 species and 450 elementary reaction steps, with over 200 elementary reactions being pressure dependent. Pressure and temperature dependent rate constants are determined by utilizing quantum RRK (QRRK) analysis on bimolecular (chemical activation) association, addition and insertion reactions and in unimolecular dissociation and isomerization reaction systems, combined with "modified strong collision" treatment for fall-off. Pressure and temperature dependent rate constants are determined by the QRRK code and expressed in the form of an 7 x 3 Chebyshev polynomial formalism over the pressure range of 0.001 to 100 atm and a temperature range of 250 to 2500K. Methane oxidation increased significantly with addition of methanol.

INTRODUCTION

Oxygenated hydrocarbons play an important role in both industrial and environmental chemistry. Alcohols, such as methanol and ethanol, are in use as alternative motor fuels and as additives to conventional transportation fuels to improve performance. Ethers, such as methyl tert-butyl ether (MTBE), are in use as oxygen additives as anti-knock components in gasoline and other ethers are being considered as additives for diesel fuels. The oxidation and pyrolysis of gas phase methanol has been reported in a number of studies over the past half century by different experimental methods, which range from laser induced fluorescence, diffusion flame, shock-tube and static or flow reactors. Both De Avillez Pereira *et. al* and Held and Dryer present recent experimental data on this system, as well as a thorough compilation of previous works done on this system.[5,10]

Three different wide ranges of experimental conditions are performed: methanol pyrolysis, methanol oxidation and methanol/methane oxidation. A reaction mechanism model is also developed, which includes about 200 pressure dependent reaction steps. Pressure and temperature dependent rate constants are represented in Chebyshev polynomial form over a pressure range from 0.001 - 100 atm and a temperature range of 250 – 2500K. Included in the mechanism are pressure effects on important unimolecular and bimolecular reactions plus negative temperature dependence and pressure effects on hydrocarbon (HC) and oxy-hydrocarbon (OHC) species reactions. Pathways for formation and oxidation of higher molecular weight products, such as C2 hydrocarbons and methyl-ethers, which we observe in this study, are also included.

EXPERIMENTAL SETUP:

The reactor used in the experiment is a 6mm ID (12mm OD) quartz tube, housed in a 75 cm three-zone clamshell 3 cm ID electric tube furnace equipped with three independent digital temperature controllers. A 200 psi back pressure regulator is used to maintain the desired pressure within the reactor. (Refer to Figure 1 for experimental setup).

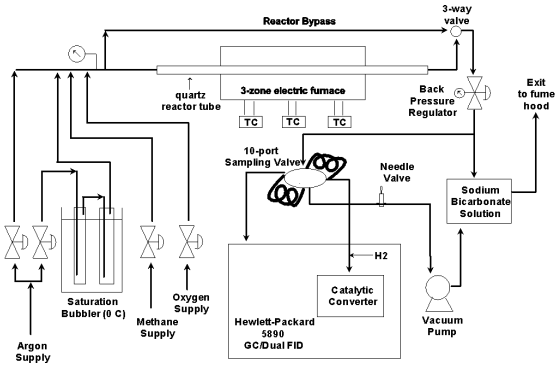

Figure 1. Schematic of experimental flow reactor and analytical system.

The feed mixtures are preheated to about 373ºK to prevent condensation and improve reactor temperature control. Gas samples are drawn through by a mechanical vacuum pump. An HP-5890 Series II gas chromatograph (GC) with two flame ionization detectors (FID) is used on-line for analysis. A packed column is used for the separation of CO, CO_2 and light HC's and a capillary column is used for heavier HC's and OHC's separation. A catalytic converter is used to improve quantitative analysis of CO and CO_2 by converting the mixture to methane, which can be detected by the FID. Batch samples of reactor gas drawn from the reactor are collected into evacuated 25 cm^3 stainless steel sample cylinders for verification of products using a GC/MS.

Methanol pyrolysis experiments are all performed under isothermal condition at 1073ºK, with varying concentrations of CH_3OH over a pressure range from 1 to 10 atm. Experimental data on the decomposition of methanol in presence of oxygen and argon were obtained for both fuel lean ($\phi = 0.75$) and stoichiometric ($\phi = 1.0$) conditions over a temperature range from 873 to 1073ºK and a pressure range of 1 to 5 atm. All methanol/methane oxidation experiments are carried out under overall stoichiometric conditions. Experimental data for methanol/methane oxidation experiments at two different temperatures and pressure combination conditions are collected: either 873ºK and 5 atm or 1073 and 1 atm. Various methanol/methane concentration ratios, ranging from 0:2 to 2:0, were studied for each of the two temperature/pressure conditions.

COMPUTATIONAL METHODS

Thermodynamic properties. Thermodynamic properties of species are from literature, theoretical and estimation techniques, such

as group additivity[2], hydrogen bond increment (HBI)[12] and *ab initio* or density function calculations. The molecular properties for the explicit CH_3OH dissociation system, including methanol, transition states (TS) and products, are determined by the high level composite CBS-APNO *ab initio* calculations. The *ab initio* calculations are performed using Gaussian94.[6] The CBS-APNO calculations are performed in accordance to the method outlined by Montgomery *et al*[15]. Vibrational frequencies, ZPVE and thermal correction contributions are calculated at the HF/6-311G(d,p) level of theory, with scaling factors consistent with the recommended values by Scott and Radom.[18] The optimized geometry is calculated at the QCISD/6-311G(d,p) level of theory. Figure 2 illustrates the potential energy diagram of the CH_3OH subsystem. The enthalpies of the two biradicals in the system are determined by use of isodesmic working reactions[9] with group balance.

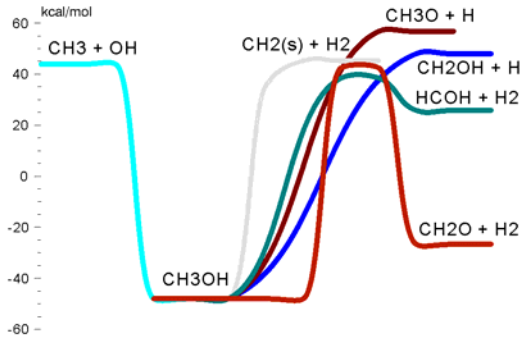

Figure 2. Potential energy diagram of the methanol subsystem calculated at CBS-APNO level of theory.

Conventional statistical mechanics analysis was employed to determine the vibrational, external rotational and translational contributions to entropy and $C_p(T)$. Unpaired electrons are also included in the S^{298} and $C_p(T)$ calculations accordingly. Contributions of internal rotation to S^{298} and $C_p(T)$ are incorporated based on the Pitzer-Gwinn formalism.[17]

Calculation of High-Pressure Rate Constants. Abstraction reaction rate constants are not pressure dependent and are usually taken from evaluated literature when available. Evans-Polanyi analysis is used on the reaction in the exothermic direction to estimate the energy of activation (E_a) for rate constant.

The high-pressure forward rate constants in the CH_3OH subsystem are determined by application of macrocanonical transition state theory (CTST) for temperatures from 300 – 2500 K. Forward rate constants from 300 – 2500 K are calculated and fitted by a nonlinear least squares method to the form of a modified Arrhenius rate expression. The rate constants for the three combination and dissociation reaction in the CH_3OH system are calculated by variational transistion state theory (VTST), with thermochemical properties determine at the CBS-Q//B3LYP/6-31G(d,p) level of theory.[16,1,13] The combination reaction rate constant is determined by satisfying the microscopic reversibility criteria.

Kinetic Analysis. Pressure and temperature dependent rate constants are determined by a modified quantum RRK (QRRK) formalism for *k(E)*. Two methods to analyze the collisional deactivation of the energized adduct are used: master equation analysis and the modified strong collision model. Chang *et al* described a modified QRRK analysis that is used in this paper.[4] Master equation analysis is used for fall-off in this analysis as described by Sheng *et al*[19] and follows Gilbert and Smith[7].

Pressure Dependent CHEMKIN Mechanism.: Both the modified strong collision and master equation codes incorporate a temperature and pressure dependent output formalism for the rate constants, in the form of an N x M Chebyshev polynomial expression. The temperature-pressure dependent rate coefficients in Chebyshev format for the current system of interest are derived from application of the methodology described by Venkatesh *et al*[21,20]. The CHEMKIN interpreter is modified to accept the N x M Chebyshev polynomial formalism of rate constant.[11]

RESULTS AND DISCUSSION

Enthalpies of CH3OH Subsystem. The sum of enthalpies for the respective product sets are compared with data from the study of Walch[22] and Harding *et al*[8]. Harding *et al*'s data are calculated at the RMP4/6-31G(d,p) level of theory and Walch's data are derived using complete-active-space self-consistent-field (CASSCF) / internally contracted configuration-interaction (CCI), *ab initio* calculations.

Table 1. Comparison of Product Enthalpies in the Methanol System with Literature Data.

	CBS-APNO	Walch[22]	Harding *et al*.[8]
CH_3OH	0	0.0	0.0
$CH_3O + H$	104.1		
$CH_2OH + H$	95.1		
$^1CH_2 + H_2O$	91.8	88.8	94.9
$^3CH_2 - {}^1CH_2$	-8.99	-9.0	
$CH_3 + OH$	90.5		
$^1HCOH + H_2$	72.8	71.1	71.1
$CH_2O + H_2$	20.1	18.1	16.4
$[H_2CO\cdots H_2]^‡$	90.7	91.9	96.5
$[HCOH\cdots H_2]^‡$	86.5	85.0	91.0
$[^1CH_2\cdots H_2O]^‡$	83.6	82.3	84.6

The enthalpy for the transition state of $^1CH_2 + H_2O$ channel, as reported also by Walch and Harding *et al*, is lower than the enthalpy of $^1CH_2 + H_2O$. The CH_3OH dissociation barrier, through the $^1CH_2 + H_2O$ channel is calculated form canonical transition state theory, based on an excited state of TS that has the same enthalpy as the enthalpy of $^1CH_2 + H_2O$ with a corresponding entropy at the same energy level as the "excited" TS. The high-pressure limit rate constants are shown in Table 2.

Table 2. High-Pressure Limit Rate Coefficient for the CH_3OH System.

Reaction	A	n	Ea (kcal/mol)	
$CH_3 + OH \rightarrow CH_3OH$	3.3133E6	2.0765	-1.7551	a
$CH_3OH \rightarrow CH_3 + OH$	3.2591E10	2.05451	90.347	b
$CH_3OH \rightarrow CH_2OH + H$	1.6369E7	2.54513	91.951	b
$CH_3OH \rightarrow CH_3O + H$	1.1908E7	2.38792	99.614	b
$CH_3OH \rightarrow CH_2O + H_2$	1.1004E9	1.28149	90.233	c
$CH_3OH \rightarrow {}^1HCOH + H_2$	2.0299E10	1.22342	86.411	c
$CH_3OH \rightarrow {}^1CH_2 + H_2O$	2.8735E11	1.60030	92.538	d

(a) Microscopic reversibility (b) Variational transition state theory calculation, based on CBS-Q//B3LYP/6-31G(d,p) (c) Canonical transition state theory calculation, based on CBS-APNO (d) Adjusted canonical

transition state theory calculation – thermochemical properties of the transition state taken at the corresponding energy level of the sum of the products.

After methanol decomposition occurs (refer to Figure 1), $CH_3OH + OH$ is the critical reaction responsible for methanol decay. The formation of $CH_2O + HO_2$ adduct is the dominant channel for pressures < 1 atm and temperature < 2000ºK. Formaldehyde then decays mostly by the reaction of $CH_2O + OH \rightarrow HCO + H_2O$. The decomposition reaction of $HCO + M \rightarrow CO + H + M$ is found to be the dominant channel to form carbon monoxide and $CO + O + M \rightarrow CO_2 + M$ to form final product of carbon dioxide.

The comparison of methane and methanol oxidation can be described in three stages: initiation, propagation and oxidation. During initiation, formation of key radicals is determined by the most favorable thermochemical kinetic of the respective elementary reaction. Several channels of CH_3OH unimolecular decomposition are much lower in energy than CH_4 and, therefore, faster than CH_4 decomposition. Therefore, propagation reactions in CH_3OH oxidation occur more rapidly than CH_4 oxidation.

CH_3 is the initial radical intermediate in CH_4 oxidation. The major reaction of CH_3 at low CH_3 concentration is reaction with O_2. CH_3 reaction with O_2 to form the $[CH_3OO]^*$ complex which can isomerize to $[CH_2OOH]^*$ and then form the products $CH_2O + OH$.

Formation of C2 Species. The current mechanism also includes the kinetics of several C2 species. The formation of C2 species is from the combination of two methyl radicals to form ethane. Abstraction of hydrogen from ethane by radicals from the radical pool forms ethyl radicals, which can undergo addition reaction to form ethylperoxy radical. The dominant products is $C_2H_4 + HO_2$.

Vinyl radicals are formed from the loss of hydrogen in the ethylene molecule, via abstraction reaction with radicals. The vinyl oxidation system used is from Chang *et al.*[4] This vinyl oxidation subsystem includes 5 possible stabilized adducts with multiple exit channels, including the formation of the 3-member ring dioxiranyl radical, which has recently been recognized to be an important channel.[3] The lowest energy process is peroxy radical attack on the ipso carbon, forming a di-oxirane methylene radical, which then isomerizes through an epoxide and cleaves the weak peroxy O—O bond. A further beta scission opens this epoxide ring to form the H_2C•-O-CHO isomer. This isomer beta scissions to form $CH_2O +$ HCO before stabilization can occur. The peroxy radical can also undergo a concerted elimination to form acetylene + HO_2, isomerize via a hydrogen shift to form the vinyl hydroperoxide radical or isomerize to form a 4-member ring. The 4-member ring can ring open to form product pairs such as $HCO + H_2CO$ or H + glyoxal, or redissociate to reactants.

CH_3C●$O + O_2$ and ●$CH_2CHO + O_2$ subsystems are obtained from Lee and Bozzelli[14] where thermochemical and kinetic properties are calculated at CBS-Q level of theory. Both reaction systems initiate by the addition of oxygen onto the radical site forming a peroxy radical. One product set resulting from both systems is the formation of ●$CH_2CO + HO_2$. In both oxidation systems, the ●$CH_2CO + HO_2$ products can be formed through two channels; direct molecular elimination or β-scission of the hydroperoxy radical formed from isomerization. The other channel that can occur with the hydroperoxy radical is ring closure to form a carbonyl-oxirane specie plus OH. In the ●$CH_2CHO + O_2$ subsystem, the hydroperoxy ethyl-aldehyde radical can also undergo a fast reaction, albeit complex, to form the product set consisting of $OH + CO + H_2CO$.

Comparisons with Experimental Results. Methanol pyrolysis comparisons between the model with experimental results at 1 atm is illustrated in Figure 3. Comparisons of the methanol oxidation model and the experimental results at 5 atm at an equivalence ratio of $\phi = 1$ is shown in Figures 4. These show reasonable agreement for reactant decay and main product formation.

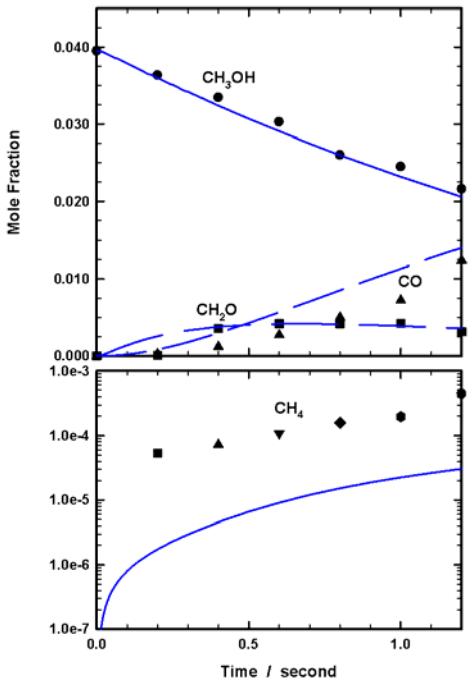

Figure 3. Comparison of experimental data with model for CH_3OH pyrolysis at 1073 K, 1 atm, $X_0 = 3.95$ %

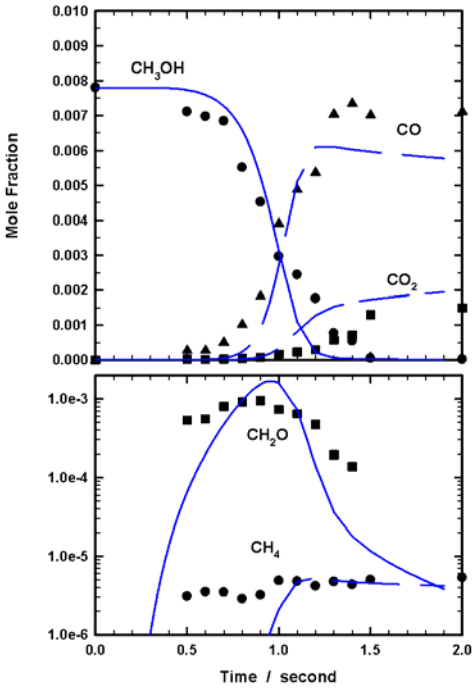

Figure 4. Comparison of experimental data with model for CH_3OH oxidation at 873 K, 5 atm, X_0 = 0.78 %

Figures 5 and 6 shows comparison of methane/methanol mixture experiment at 873ºK, 5 atm and equal initial concentration of methane/methanol, with a fuel equivalence ratio of unity. The initial methane concentration in Figure 5 is 0.78% and in Figure 6 it is 0.39%. Agreements between model and experimental data on methane and methanol predictions are relatively well matched. The model predicts methanol reacts slightly faster than experimental data. The model under predicts CO at both conditions, while CO_2 is over predicted. Formaldehyde formation between the model and experimental data has very good agreement. The model is able to predict a maximum inflection point in the concentration profile, which is observed in the experimental data as well. Trace product concentrations of ethane and ethylene, as predicted by the model, are higher than expected compared to experimental data.

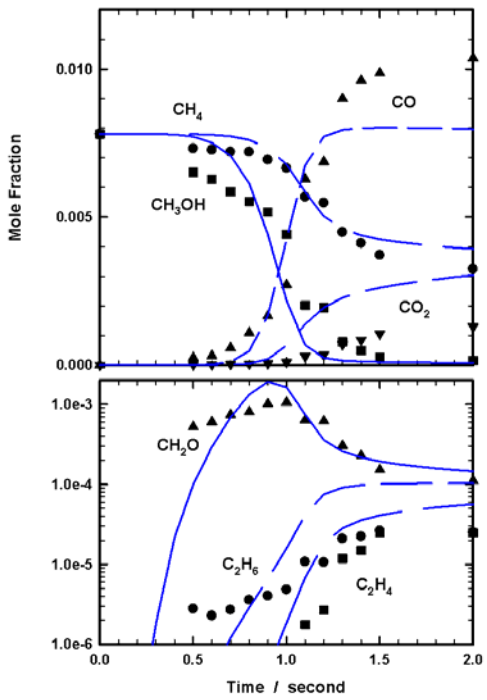

Figure 5. Comparison of experimental data with model for CH_3OH/CH_4 oxidation at 873 K, 5 atm, $X_{CH3OH,0}$ = 0.78%, X_{CH40} = 0.78%

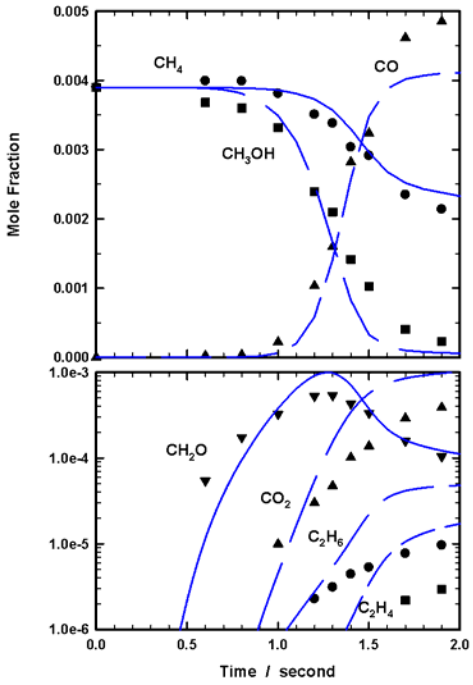

Figure 6. Comparison of experimental data with model for CH_3OH/CH_4 oxidation at 873 K, 5 atm, $X_{CH3OH,0}$ = 0.39%, X_{CH40} = 0.39%

CONCLUSION:

Experimental data and a kinetic model has been developed and tested for various types of reaction system (i.e. pyrolysis, fuel lean, stoichiometric and fuel additive) at different system conditions (temperature, pressure and initial fuel concentration). Comparison between experimental and the kinetic model shows relatively good agreement. This mechanism can serve as a basis for future studies on other higher molecular weight hydrocarbon and oxy-hydrocarbon system, especially since data on addition of oxy-hydrocarbon to hydrocarbon specie significantly accelerates the decay of the hydrocarbon specie.

REFERENCES

(1) Becke, A. D. *J. Chem. Phys.* **1993**, *98*.

(2) Benson, S. W. *Thermochemical Kinetics*, 2nd ed.; Wiley-Interscience: New York, 1976.

(3) Carpenter, B. K. *J. Phys. Chem.* **1995**, *99*, 9801.

(4) Chang, A. Y.; Bozzelli, J. W.; Dean, A. M. *Zeit. Phys. Ch.* **2000**, 1533-1568.

(5) De Avillez Pereira, R.; Baulch, D. L.; Pilling, M. J.; Robertson, S. H.; Zeng, G. *J. Phys. Chem. A* **1997**, *101*, 9681-9693.

(6) Frisch, M. J.; Trucks, G. W.; Head-Gordon, M.; Gill, P. M. W.; Wong, M. W.; Foresman, J. B.; Johnson, B. G.; Schlegel, H. B.; Robb, M. A.; Replogle, E. S.; Gromperts, R.; Andres, J. L.; Raghavachari, K.; Binkley, J. S.; Gonzalez, C.; Martin, R. L.; Fox, D. J.; Defrees, D. J.; Baker, J.; Stewart, J. J. P.; Pople, J. A.; Eds. *Gaussian 94 computer program, Revision C.2*; Gaussian Inc.: Pittsburgh, 1995.

(7) Gilbert, R. G.; Smith, S. C. *Theory of Unimolecular and Recombination Reactions*; Blackwell Scientific Publications: Oxford, 1990.

(8) Harding, L. B.; Schlegel, H. B.; Krishnan, R.; Pople, J. A. *J. Phys. Chem.* **1980**, *84*, 3394-3401.

(9) Hehre, W. J.; Radom, L.; Schleyer, P. R.; Pople, J. A. *Ab initio Molecular Orbital Theory*; Wiley & Sons: New York, 1986.

(10) Held, T. J.; Dryer, F. L. *Internation Journal of Chemical Kinetics* **1998**, *30*, 805-830.

(11) Kee, R. J.; Miller, J. A.; Jefferson, T. H. CHEMKIN: Fortran Chemical Kinetics Code Package, 1980.

(12) Lay, T. H.; Bozzelli, J. W.; Dean, A. M.; Ritter, E. R. *J. Phys. Chem.* **1995**, *99*, 14514-14527.

(13) Lee, C.; Yang, W.; Parr, R. G. *Phys. Rev. B* **1988**, *37*.

(14) Lee, J. W.; Bozzelli, J. W. "CH3CjO and CjCHO oxidation"; 5th International Conference on Chemical Kinetics, 2001, Gaithersburg, MD.

(15) Montgomery, J. A., Jr.; Ochterski, J. W.; Petersson, G. A. *J. Chem. Phys.* **1994**, *101*, 5900-5909.

(16) Ochterski, J. W.; Petersson, G. A.; Montgomery, J. A. *J. Chem. Phys.* **1996**, *104*, 2598.

(17) Pitzer, K. S.; Gwinn, W. D. *J. Chem. Phys.* **1942**, *10*, 428.

(18) Scott, A. P.; Radom, L. *J. Phys. Chem.* **1996**, *100*, 16502-16513.

(19) Sheng, C.; Bozzelli, J. W.; Dean, A. M.; Chang, A. Y. *Submitted to J. Phys. Chem. A* **2001**.

(20) Venkatesh, P. K.; Chang, A. Y.; Dean, A. M.; Cohen, M. H.; Carr, R. W. *AIChE Journal* **1997**, *43*, 1331-1339.

(21) Venkatesh, P. K.; Dean, A. M.; Cohen, M. H.; Carr, R. W. *Reviews in Chemical Engineering* **1997**, *13*.

(22) Walch, S. P. *J. of Chem. Phys.* **1993**, *98*, 3163-3167.

EFFECT OF THE AMOUNT OF BASE SITE ON CATALYTIC BEHAVIOR OF CAO FOR SYNTHESIS OF DIMETHYL CARBONATE FROM PROPYLENE CARBONATE AND METHANOL

Tong Wei Wei Wei Mouhua Wang Yuhan Sun Bing Zhong*

State Key Laboratory of Coal Conversion Institute of Coal Chemistry Chinese Academic of Sciences, Taiyuan, 030001

Introduction

Dimethyl carbonate (DMC) is a unique molecule having versatile chemical property and has been used mainly as methylating and methoxycarbonylating agent substituting for toxic phosgene, dimethyl sulfate, or methyl iodide [1-3]. It can be synthesized by transesterification method, in which CO_2 reacts with propylene oxide to yield propylene carbonate (PC), which continually reacts with methanol (MeOH) to yield DMC[4,5]. The reaction of PC with MeOH can be catalyzed by solid base with high conversion and selectivity [6]. On the basis of the discussion in the other paper submitted to this meeting, the effect of the amount of base site on catalytic behavior of CaO for synthesis of DMC from PC and MeOH was investigated in detail.

Experimental

CaO was prepared from $CaCO_3$ calcined at1073K or 1173K in N_2 atmosphere. The reaction was carried out in a 250mL flask equipped with reflux condenser, water bath and magnetic stirring. Catalyst was added into the flask accompanied with violent magnetic stirring after the temperature reached to the expected one. Reaction product was analyzed by Gas Chromatograph after centrifugal separation of solid catalyst from liquid.

Results and discussion

It was reported that CaO calcined from $CaCO_3$ was super base. Thus in present paper, CaO was prepared from $CaCO_3$ calcined at 1073K and 1173K respectively. BET surface area of CaO was listed in Tab. 1; XRD and CO_2TPD results of CaO were illustrated in Fig.1, 2. It can be seen from Fig.1 that $CaCO_3$ was totally dissociated when calcined at 1073K for 1hr and yields cubic CaO. Both the extendedness of calcinations time and the increase of temperature result in surface area increase as shown in Tab.1. From Fig.2 we can see that there is four kinds of base site with CO_2 desorption temperature being 430K, 470K, 640K and 890K respectively. With the extendedness of time and the increase of temperature, the amount of base site increases greatly with the sequence being 1173K/2hr> 1073K/2hr> 1073K/1hr.

Tab.1 BET Surface area of CaO obtained from $CaCO_3$ calcined under different condition(m^2/g)

Calcinition temperature/K	Calcinition time /hr	BET Surface Area /$m^2 . g^{-1}$
1073	1	3.848
1073	2	12.706
1173	1	12.166

* To whom corresponding should be addressed. Fax: +86 351 4041153
E-Mail: yhsun@sxicc.ac.cn or weiwei@sxicc.ac.cn

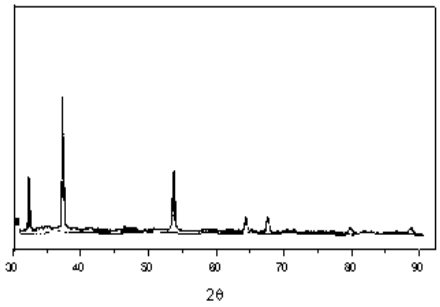

Fig.1 XRD of CaO calcined from $CaCO_3$ at 1073K for 1hr

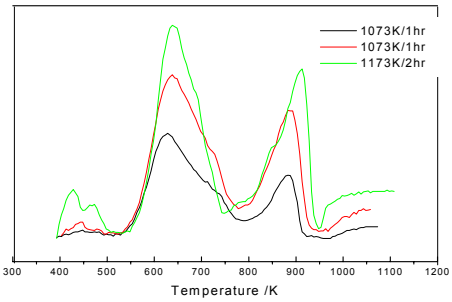

Fig. 2 CO_2 TPD of CaO calcined from $CaCO_3$

Since this reaction usually catalyzed by strong base, the effective base site may be that with CO_2 desorption temperature being 640K and 890K respectively. The effect of the amount of base site on DMC yield, DMC selectivity and reaction rate was shown in Fig. 3-5. It can be seen that with the increase of the amount of base site, the time need to reach equilibrium was shortened while equilibrium DMC yield was unchanged , which means the increase of the amount of base site can result in the increase of reaction rate but not change the equilibrium. On the other hand, the DMC selectivity decreases gradually with the increase of the amount of base site. The base site can catalyze both the subject reaction and the polymerization of PC, therefore the increase of bas site will also promote the side reaction and consequently make the DMC selectivity decrease. Fig. 5 shows the effect of the amount of base site on the reaction rate, with the increase of the amount of base site, the maximum rate increase and the induction time was shortened. As side in the other paper, the induction time comes from the activation of MeOH, the increase of base site amount can not only promote the activation of MeOH, but also make the surface concentration of activated MeOH increase and consequently promote the surface reaction of PC with activated MeOH.

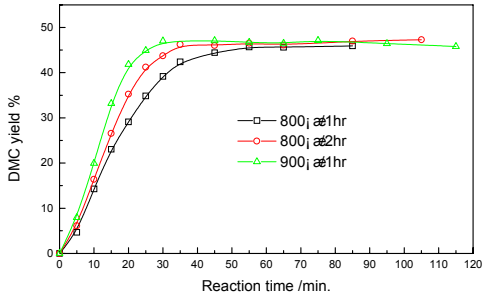

Fig. 3 Effect of basicity on DMC yield

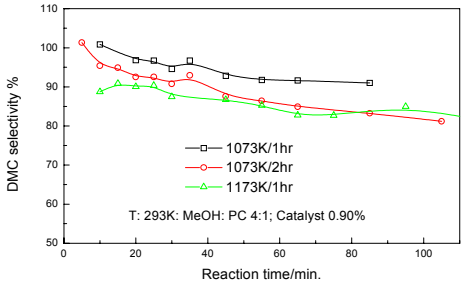

Fig.4 Effect of basicity on DMC selectivity

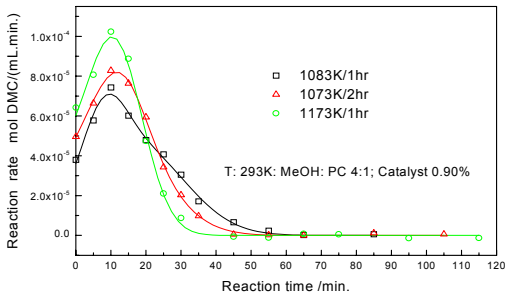

Fig. 5 Effect of basicity on reaction rate

Conclusion

1. $CaCO_3$ calcined at 1073K and 1173K can yield cubic CaO, which shows excellent catalytic activity for synthesis of DMC from PC and MeOH.
2. Both the surface area and the amount of base site of CaO increase with the increase of calcinatio temperature and the extendedness of calcination time for $CaCO_3$.
3. The increase of the amount of base site can promote both subject reaction and side reaction, therefore although the reaction rate increases, the DMC selectivity decreases with the increase of the amount of base site.

Reference

(1) Watanabe, Y.; Tatsumi, T. Microporous and mesoporous materials 1998, 22,399~407

(2) Pacheco, M. A.; Marshall, C. L. *Energy & Fuels* 1991, 11, 2~29

(3) Shaikh, A.G. *Chem. Rev.* 1996, 96, 951~976

(4) Ono, Y. Appl. Cata. A: General 1997, 155, 133~166

(5) Knifton, J.F., Duranleau, R.G. *Journal of molecular Catalysis*, 1991, 67, 389~399

(6) Zhao, T. *Dr Dissertation,* Shanxi Institute of Coal Chemistry, Chinese Academy of Sciences, 1999

Effect of Water on the Fischer-Tropsch Synthesis on Supported Cobalt Catalysts

S. Storsæter[1] ,Chr. Aaserud[1] A-.M.Hilmen[2] , O.A. Lindvåg[2] , E. Bergene[2] , D. Schanke[3] , S. Eri[3] and A. Holmen[1]

[1]Dept. of Chemical Engineering, Norwegian University of Science and Technology (NTNU). N-7491 Trondheim , Norway. [2]SINTEF Applied Chemistry, N-7465 Trondheim, Norway, [3]Statoil, R&D Centre, Postuttak, N-7005 Trondheim, Norway.

Introduction

The Fischer-Tropsch synthesis is an interesting pathway for converting natural gas to transportation fuels. A key element in improved Fischer-Tropsch processes is the development of active catalysts with high wax selectivity. Supported cobalt is the preferred catalysts for the Fischer-Tropsch synthesis of long chain paraffins from natural gas due to their high activity and selectivity, low water-gas shift activity and a comparatively low price. Water is produced during the Fischer-Tropsch synthesis and will be present in varying quantities during synthesis, depending on the conversion and reactor system.

Different results have been reported on the effect of water on the activity of cobalt Fischer-Tropsch catalysts[1,2,3]. The effect of water seems to depend mainly on the support although promoters may also be important. It has been shown that Al_2O_3-supported cobalt catalysts deactivate when water is added during the synthesis[4]. It has also been shown that water inhibits secondary hydrogenation of olefins on Al_2O_3-supported cobalt catalysts[5].

The present work aims at studying the effect of water on the activity and selectivity for cobalt catalysts using different supports and promoters as well as unsupported cobalt. In the following the main emphasis is on Al_2O_3 supported cobalt catalysts.

Experimental

Catalysts. The supported catalysts were prepared by incipient wetness (co)impregnation of the different supports as described elsewhere[6]. The unsupported cobalt catalyst was prepared by precipitation by adding NH_3 to an aqueous solution of $Co(NO_3)_2{\cdot}6H_2O$ with continuous stirring until there were an excess of NH_3. The precipitate was washed several times, dried and calcined in flowing air at 698 K for 3h.

Reactorsystem. The catalysts were tested in an isothermal fixed-bed microreactor[6] as shown below in **Figure 1**:

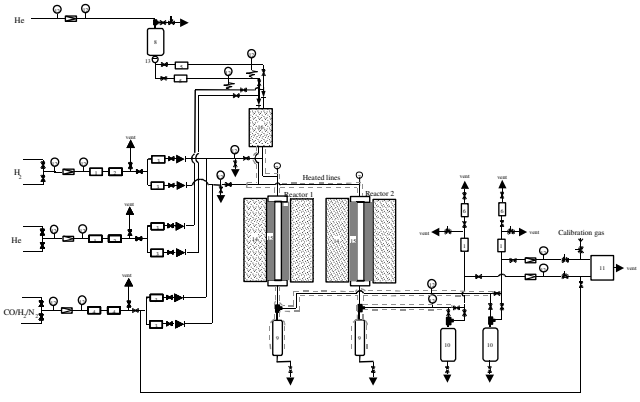

Figure 1. Experimental apparatus

Experimental procedure: The catalyst (1.0-1.6 g diluted with SiC) was loaded to the reactor, flushed with He and reduced in hydrogen at 350 ^{0}C for 16h. After reduction the reactor was cooled to 170 ^{o}C, the pressure increased to 20 bar and premixed synthesis gas (31.3 % CO, 65.7 % H_2 and 3 % N_2) was introduced. The reactor temperature was slowly increased to 483 K in order to prevent runaway. The feed and the products were analysed using an on-line HP 5890 gas chromatograph equipped with thermal conductivity (TCD) and flame ionization (FID) detectors.

Catalyst characterization: The catalysts were characterized by Temperature Programmed Reduction (TPR), chemisorption, and BET surface area. Model studies of catalysts exposed to different H_2O/H_2 ratios in a gravimetric microbalance have also been performed.

Results and Discussion

Previous results show that Co-Re/Al_2O_3 catalysts deactivate as a result of reoxidation of small cobalt particles. When water is added to the feed for Al_2O_3 supported cobalt catalysts the rate of deactivation increases. This behavior is clearly demonstrated in **Figure 2** below.

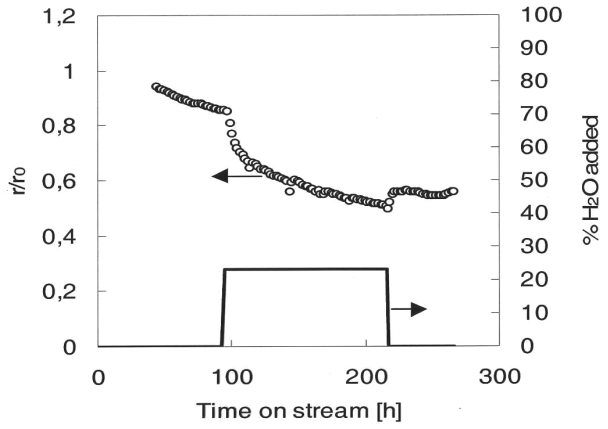

Figure 2. Rate of hydrocarbon formation relative to the initial rate for 20%Co-1%Re/Al_2O_3 at 210 ^{o}C, 20 bar and H_2/CO=2.1 [4].

Figure 2 also shows that the rate does not return to the same level as before water was added. It has been shown that the loss in activity can only partly be recovered by rereduction due to increased cobalt-alumina interactions. Both XPS and TPR indicate that a phase interacting more strongly with the alumina is formed upon exposure to water.

The effect of conversion on the selectivity is shown in **Figure 3**. The C_{5+} selectivity increases as the CO conversion is increased. It can also be added that the CH_4 selectivity decreases with increasing conversion and that the selectivity to olefins decreases with increasing CO conversion. In **Figure 3** the selectivity to C_{5+} is also given when water is added to the feed. The results show that the selectivity increases only slightly with the conversion when water is added. In the case of CH_4 the selectivity does almost not depend on the conversion when water is added to the feed (**Figure 4**).

It has been suggested[2] that the increase in C_{5+} selectivity as a function of conversion is to a large extent caused by secondary reactions of primary olefin products at longer residence times i.e.

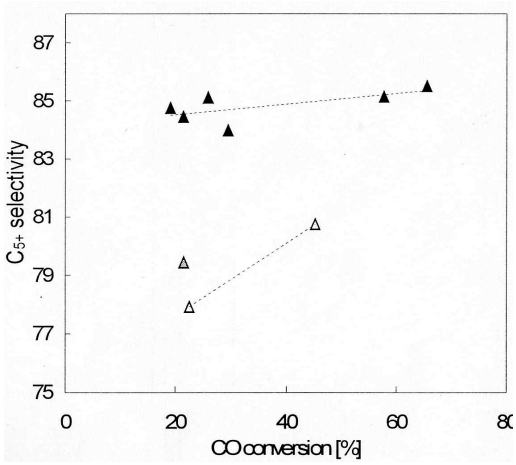

Figure 3. The effect of CO conversion on the selectivity of C_{5+} in the presence of added water (▲) compared with runs without water addition (Δ) for 12%CO-0.5%Re/Al_2O_3 at 210 °C, 20 bar and H_2/CO=2.1.

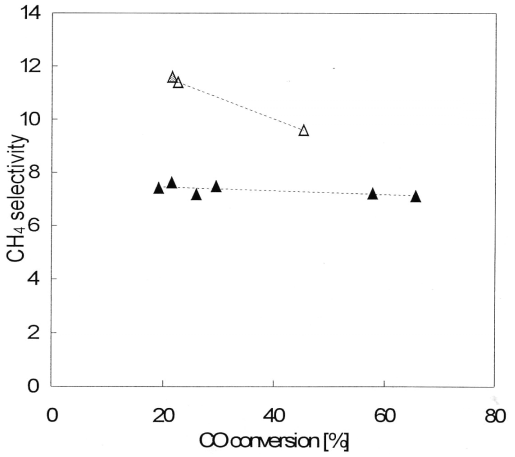

Figure 4. The effect of CO conversion on the selectivity of CH_4 in the presence of added water (▲) compared with runs without water addition (Δ) for 12%CO-0.5%Re/Al_2O_3 at 210 °C, 20 bar and H_2/CO=2.1.

readsorption and further chain growth. The present results also indicate that the increasing partial pressure of water with increasing CO conversion contributes to the increase in C_{5+} selectivity by inhibiting hydrogenation reactions.

The Fischer-Tropsch reaction network is indicated on **Figure 5** and the observed changes in selectivity can be interpreted in terms of the reaction network. It has been shown[5] that the hydrogenation reactions on active Fischer-Tropsch catalysts are inhibited by water. In one case the conversion of propene to propane dropped from 70% to below 40 % when water was added to the feed. (It should be noted that these results are obtained at different conditions (1 bar pressure, high dilution) but with an active Fischer-Tropsch cobalt catalyst). Even though the hydrogenation reactions are inhibited by water, the olefin selectivity decreases (except for C_2) suggesting also increased further chain growth.

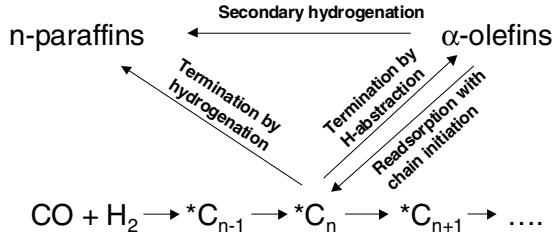

Figure 5. Fischer-Tropsch reaction network

Similar experiments have also been performed on different supports and on unsupported catalysts. The effect of water on the activity depends on the catalytic system, but the C_{5+} selectivity increases when water is added to the feed for all the systems studied.

Mass transfer effects are very important in Fischer-Tropsch synthesis. Even though the reactants are in the gas phase, the pores will be filled with liquids. Since diffusion in the liquid phase is about 3 order of magnitude slower than in the gas phase, even slow reactions may become mass transfer limited. For the Co/Al_2O_3 catalyst referred to above, the C_{5+} selectivity starts to decrease and the CH_4 selectivity increases at diffusion distances of roughly 0.2-0.3 mm[4].

Conclusions

- The C_{5+} selectivity increases with increasing conversion. Water is a main product of the Fischer-Tropsch synthesis and the amount increases with increasing conversion.
- Adding water to the feed increases the selectivity to C_{5+}. When water is added to the feed the selectivity to C_{5+} depends only slightly on the conversion
- The effect of water on the activity depends on the support. For cobalt supported on Al_2O_3 the addition of water results in deactivation.

Acknowledgement. Statoil and the Norwegian Research Council (NFR) are acknowledged for financial support and for the permission to publish these results.

References

(1) Hilmen, A.M.; Schanke, D.; Hanssen, K.F.; Holmen, A. Appl. Catal. A: General. **1999** 186, 169.
(2) Iglesia, E. Appl. Catal. A: General 1997, 161, 59.
(3) Schultz, M; Claeys, M; Harms, S. Stud. Surf. Sci. Catal. **1997** 107, 193.
(4) Hilmen, A.M.; Lindvåg, O.A.; Bergene, E.; Schanke, D; Eri, S.; Holmen. A. Stud. Surf. Sci. Catal, **2001** 136 295.
(5) Aaserud, Chr.; Hilmen, A.M.; Bergene, E.; Schanke, E.; Eri, S.; Holmen, A. Submitted.
(6) Schanke. D.; Hilmen, A.M.; Bergene, E.; Kinnari, K.; Rytter, E.; Ådnanes, E.; Holmen, A. Catal. Lett. **1995** 34 269.

Fischer-Tropsch Synthesis: Effect of Activation on Potassium Promoted Iron Catalysts

Mingsheng Luo and Burtron H. Davis

Center for Applied Energy Research,

2540 Research Park Drive, Lexington, KY 40511

Introduction

In the Fischer-Tropsch Synthesis (FTS) process, the hydrocarbon is produced from CO and H_2 by a reaction that can be expressed as

$$(2n+1)\ H_2 + n\ CO \rightarrow C_nH_{2n+2} + n\ H_2O \qquad (1)$$

When an iron catalyst is used for FTS, the water gas shift (WGS) reaction can also occur. This side reaction consumes CO and water formed by the FTS reaction and produces additional hydrogen as well as carbon dioxide.

$$H_2O + CO \rightarrow CO_2 + H_2 \qquad (2)$$

Potassium has long been used as a promoter for iron catalysts. It provides an increase in the alkene yield and a decrease in the CH_4 selectivity [1-3]. Potassium can also increase the catalytic activity for FTS and water-gas shift (WGS) reactions [3-9].

Pretreatment of iron catalysts can have important influence on FTS activity and selectivity. A cobalt catalyst is usually activated with H_2 and metallic cobalt is believe the active phase for FTS, but the pretreatment of iron catalyst is not as simple as that of a cobalt catalyst. Carbides are probably the active phase for FTS. Reduction of Fe_3O_4 with H_2 to zero valence was claimed by Rao and Bukur at al. [10-17]. It is also found that 20% metallic iron was obtained by treating iron catalyst with H_2 at 220EC. Pretreatment of iron catalyst with CO or syngas can result in the presence of P-carbide [13-15]. Bukur studied the activation effect on K/Fe=0.8/100 (mass) catalyst in a fixed bed reactor and concluded that CO activation at 280EC led to higher initial FTS activity and higher long chain hydrocarbons than H_2 activated catalysts.

Experimental

In this study, an Fe/Si/K=100/5.1/1.25 (atomic ratio) potassium promoted iron catalysts were pretreated with CO, syngas(H_2:CO=0.7) or H_2 at 230-270EC for 24 hours. Carbon monoxide activation was carried out at 1.3MPa while H_2 activation was at atmospheric pressure. To investigate the effect of syngas activation pressure on FTS activity, both atmospheric and 1.3MPa pressure were used. The CO flowed through a catalyst slurry containing 10% solids in 300 mL of Ethylflow (a mixture of decene trimers). A one-liter continuous stirred tank reactor (CSTR) was used in this study. A sintered metal filter was installed to remove the wax samples from the catalyst slurry. The wax sample was extracted through the internal filter and collected in the hot trap held at 200EC. A warm trap (100EC) and cold trap (0EC) were used to collect light wax and the water plus oil samples, respectively, by condensing from the vapor phase that was continuously withdrawn from the reactor vapor space.

Daily gas, water, oil, light and heavy wax samples were collected and analyzed. Table 1 gives a summary of the instruments for gas and liquid product analysis. A heavy wax sample was taken from the 200EC hot trap connected to the filter. The vapor phase above the slurry passed continuously to the warm (100EC) and the cold (0EC) traps outside the reactor. The light wax and water mixture was collected from the warm trap and an oil plus water sample from the cold trap. Tail gas from the cold trap was analyzed with an online HP Quad Series Micro GC, providing molar compositions of C_1-C_7 olefins and paraffins as well as for H_2, CO and CO_2. Hydrogen and carbon monoxide conversions were calculated based on the gas product GC analysis results and the gas flow measured at reactor outlet. The oil and light wax samples were mixed before analysis with an Agilent 6890 Series GC. The heavy wax was analyzed with an HP5890 Series II Plus GC while the water sample was analyzed using an HP5890 Series II GC.

Results and Discussion

Activity Carbon monoxide activated catalyst yielded the highest activity at 270EC, as indicated by Figure 1. A stabilized CO conversion of 80% was obtained at only 200 hours of time on stream and deactivated slightly after 600 hours of time on stream. Syngas activation yielded a stabilized CO conversion of 80% at 250 hours of time on stream while H_2 activation generated a CO conversion of 59% at 320 hours of time on stream. Increase in activation temperature from 250 to 270EC significantly improved the FTS activity regardless of the gas type used in the activation process, suggesting that higher temperature enhanced the activation process.

As claimed by other researchers, activation conditions can also influence the FTS activity [1, 3, 14]. Figure 2 shows the effect of activation pressure on FTS activity over syngas activated catalyst. Under atmospheric pressure, CO conversions of 42, 62 and 80% were achieved at 230, 250 and 270EC, respectively while a low CO conversion of less than 15% was obtained at all temperatures using 1.3MPa pressure. This result indicates that pressure had a detrimental effect on FTS activity with syngas activation. A higher temperature yielded a higher stabilized CO conversion. Figure 3 shows the effect of H_2 activation temperature on CO conversion. When temperature increased from 230 to 250EC, the peak CO conversion in the initial induction period was increased from 42 to 58%, while the stabilized CO conversion did not change. After 400 hours on stream, a stabilized CO conversion of 40% was obtained at both 230 and 250EC. At 270EC, however, both peak CO conversion and stabilized CO conversion were increased dramatically. A 76% initial peak conversion and a 55% stabilized CO conversion were generated at 270EC. Thus a higher activation temperature of 270EC is necessary for hydrogen activated iron catalyst.

Selectivity Higher activation temperature can produce a higher hydrocarbon rate when CO or syngas is used as activation gas, as shown in Figure 4. When CO was used as activation gas, hydrocarbon rate remained unchanged when activation temperature increased from 230 to 250EC. When activation temperature increased form 250 to 270EC, however, hydrocarbon rate improved from 1.67 to 1.75 g h^{-1} g-Fe^{-1}. Activation temperature with syngas showed a greater effect on hydrocarbon rate than for CO activation. An increase in activation temperature from 230 to 250EC improved the hydrocarbon rate form 1.16 to 1.29, and an increase in activation temperature from 250 to 270EC increased the hydrocarbon rate form 1.29 to 1.64. When H_2 was used as activation gas, an increase in activation temperature from 230 to 250EC resulted in little change in hydrocarbon rate, while an increase in activation temperature from

250 to 270EC yielded a significant hydrocarbon rate increase from 0.84 to 1.24. Carbon monoxide activation yielded a higher overall hydrocarbon rate than either syngas or H_2, regardless of the activation temperature.

Figure 5 gives the methane selectivity for the FTS with three different activation gases at 230, 250 and 270EC. With CO activation, methane selectivity did not change as activation temperature increased in the range of 230 to 270EC. Best overall methane selectivity was also obtained with CO activation and 8% methane was produced when CO was used as activation gas. Syngas activation gave 12.2% methane selectivity at 250EC and ~8% at 250 and 270EC. Hydrogen activation yielded a methane selectivity of 8, 9 and 10% at 230, 250 and 270EC, respectively. The lowest methane selectivity of 7.6% was obtained at 250EC with CO activation and 270EC with syngas activation while the highest methane selectivity of 12.2% was produced at 250EC with syngas activation

Highest olefin fraction was obtained from H_2 activation and the lowest from CO activation, as shown in Figure 6. With the exception of ethylene, all olefin ratios decreased linearly with increasing carbon number, regardless of the activation temperature. Ethylene is believed to possess rapid readsorption ability in the FTS system [18-20]. Other explanations for the low ethylene are incorporation of ethylene into the growing chain [21-22], hydrogenolysis of ethylene [19] and hydrogenation of ethene [20, 23-24].

Water gas shift Water-Gas shift (WGS) is an important reaction in an FTS process when iron catalyst was utilized. In this reaction, CO reacts with water, which is generated from FTS and produces CO_2 and H_2. WGS produces the majority of the CO_2 from FTS system, as given by equation [2]. Figure 7 shows the influence of activation temperature and activation gas type on CO_2 selectivity. This indicates that activation temperature did not affect the CO_2 selectivity with CO activation. With syngas and H_2 activation, however, CO_2 selectivity was affected by activation temperature. Carbon monoxide activation generated a CO_2 selectivity of 45% regardless of the activation temperature. As activation temperature increased from 230 to 250EC, CO_2 selectivity increased from 41to 45% with syngas activation, and from 43 to 47% with H_2 activation. Further increase in activation temperature slightly raised the CO_2 from 45 to 46% with syngas activation, but lowered the CO_2 selectivity from 47 to 44.5% with H_2 activation. The highest CO_2 of 47% was produced with H_2 activation at 250EC while the lowest of 41%obtained with syngas activation at 230EC.

Figure 8 shows that the effect of activation gas type and activation temperature on water-gas shift quotient. With syngas and H_2 activation, water-gas shift quotient increased monotonously as activation temperature increased from 230 to 270EC. Increase in activation temperature from 230 to 250EC shows a slight decrease in water-gas shift quotient from 12.6 to 11, but an increase of water-gas shift quotient from 11 to 15.8 as activation temperature increased from 250 to 270EC. The highest water-gas shift quotient was obtained with CO activation at 250EC while the lowest obtained with syngas activation at 230 to 250EC.

Conclusions

The highest CO conversion was obtained from CO activated catalyst, regardless of the activation temperature. Although higher initial CO conversion was obtained, stabilized CO conversion (80%) is independent of the activation temperature when CO was used as activation gas. In contrast, hydrogen activation yielded the lowest CO conversion among the three activation gases. Syngas activation temperature increased the CO conversion as activation temperature increased from 230 to 270EC. The results indicated that activation temperature and activation gas type showed a different influence on FTS activity. Syngas pretreatment showed a great dependency of FTS activity on the activation pressure. For high pressure, a low CO conversion was obtained, regardless of the activation temperature. At atmospheric pressure, however, FTS activity was noticeably increased and activation temperature showed a significantly influence on CO conversion

In addition to the FTS activity, CO activation showed the best overall hydrocarbon productivity and the best methane selectivity. The lowest hydrocarbon rate was obtained from H_2 activation.

Syngas activation generated the lowest water-gas shift activity while CO activation produced the highest. It was also found that activation temperature favored the WGS activity. The higher WGS activity from CO activated catalyst resulted in a lower H_2/CO usage as the WGS consumes CO and generated additional H_2 in the FTS system.

Acknowledgement. Funding from the Department of Energy (DE-FC-26-98FT40308) and the Commonwealth of Kentucky are acknowledged.

References

(1) Dry, M.E.; in *Catalysis: Science and Technology*, Vol. 1, 159-255, (1981)
(2) O'Brien, R.J.; Xu, L.;R. Spicer L; and Davis, *B.H; Symposium on Syngas Conversion to High Value Chemcials, 252-253*, Presented at the 211th ACS Annual Meeting, New Orleans, March 24-29, 1996.
(3) Dictor, R. A.; and Bell, A. T.; *J. Catal.*, 1986, 97, 121-136.
(4) Bukur, D. B.; Mukesh, D.; and Patel, S. A.; *Ind. Eng. Chem. Res.*, 1990, 29, 194.
(5) Dry, M. E. ; Shingles, T. ; Boshoff, L. J.; and Oosthuizen, G. J.; *J. Catal.* 1969, 15, 190.
(6) Benziger, J.; and Madix, R. J. ; *Surf. Sci.* 1980, 94, 119.
(7) Arakawa, H.; and Bell, A. T.; *I&EC Proc. Des. Dev.* 1993, 22, 97.
(8) Luo M; and Davis, B. H.; *in Studies in Surface Science and Catalysis*, Elsevier Science, 2001, 133, Vol. 139.
(9) O'Brien, R.J.; Xu, L.;R. Spicer L; and Davis, *B.H; Energy & Fuels*, 1996, 10, 921.
(10) Bukur, D. B.; Nowichi, L.; and Lang, X.; *Energy & Fuels*, 1995, 9, 620.
(11) Rao, K. R. P. M.; Huggins, F. E.; Mahajan, V.; Huffman, G. P.; Rao, B. L. Bhatt, V. U. S.; Bukur, D. B.; Davis, B.; and O'Brien, R. J.; *Top. Catal.*, 1995, 2, 71.
(12) Bukur, D. B.; Koranne, M.; Lang, X.; Rao, K. R. P. M.; and Huffman, G. P.; *Applied Catalysis A: General*, 1995, 126, 1, 85-113.
(13) E. S. Lox, G. B. Marin, E.De Graeve, and P. Bussiere, *Applied Catalysis A: General*, 40, 1, 197 (1988).
(14) O'Brien, R. J.; Zhang, Y.; Hamdeh, H. H.; Davis, B. H.; *"Mossbauer study of precipitated unpromoted iron Fischer-Tropsch catalyst," Preprints*, 44(1) ACS, Division of Petroleum Chemistry, Mar. 21-25, 1999, Anaheim, CA, 100-102.

(15) Raje, A. P.; O'Brien, R. J.; and Davis, B. H.; *J. Catal.*, 1998, 180, 36.
(16) Iglesia, E. ; Reyes, S. C.; and Madon, R. J.; *J. Catal.*, 1991, 129, 238.
(17) Komaya, T.; and Bell, A. T.; *J. Catal.*, 1994, 146, 237.
(18) Jordon, D. S.; and Bell, A. T.; *J. Phys. Chem*., 1986, 90, 4797.
(19) Novak, S.; Madon, R. J.; and Shul, H.; *J. Catal.,* 1982, 77, 141.
(20) Novak, S.; Madon, R. J.; and Shul, H.; *J. Phys. Chem.,* 1981, 74, 6083.
(21) Kuiper, E. W.; Vinkenburg, I. H.; and Oosterbeek, H.; *J. Catal.,* 1995, 152, 137.
(22) Kuiper, E. W.; Scheper, C.; Wilson, J. H.; and Oosterbeek, H.; *J. Catal.,* 1996, 158, 288.
(23) Dry, M. E.; *Appl. Catal. A: General,* 1999, 189, 1850.
(24) Forney, A. J.; Haynes, W. P.; Elliot, J. J.; Zarochak, *Am. Chem. Soc., Div. Fuel*, 1975, 20, 3.

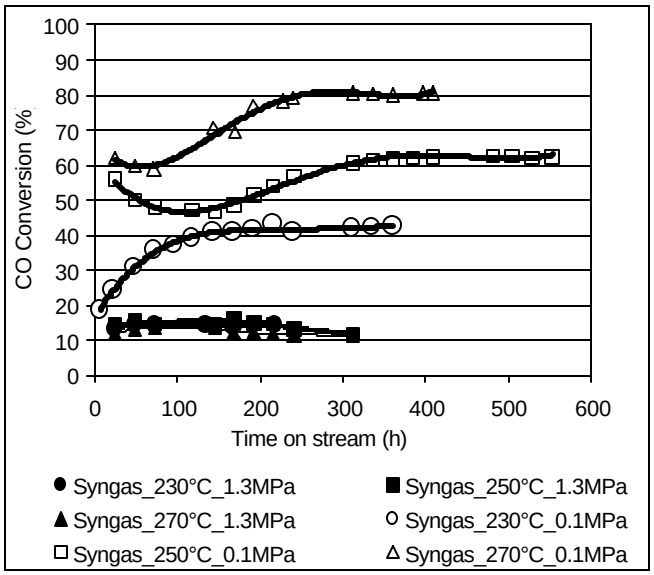

Figure 2. Influence of syngas activation pressure and temperature on CO conversion (FTS conditions: 270°C, 1.3MPa)

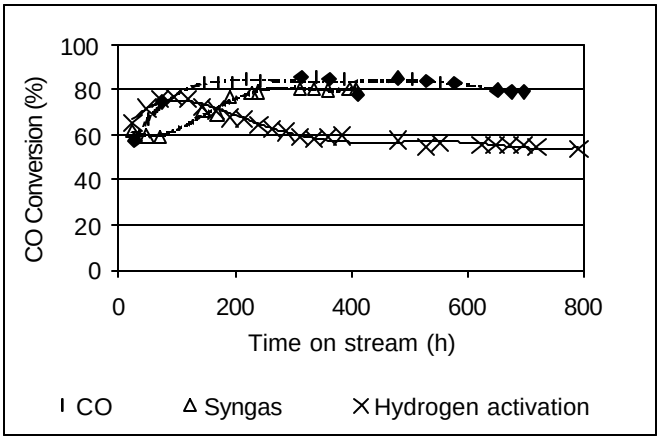

Figure 1. Influence of activation gas on CO conversion (activated at 270°C; FTS conditions: 270°C, 1.3MPa)

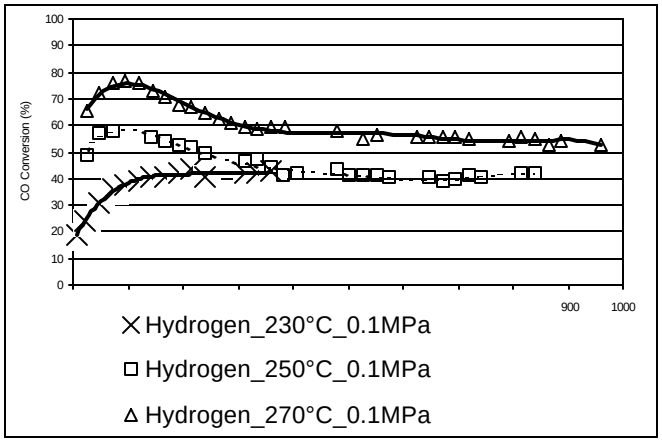

Figure 3. Influence of hydrogen activation temperature on CO conversion
(FTS conditions: 270°C, 1.3MPa)

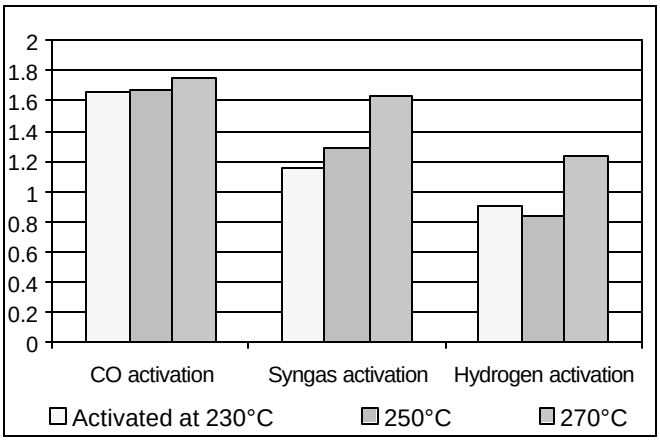

Figure 4. Influence of activation gas on hydrocarbon rate
(FTS conditions: 270°C, 1.3MPa)

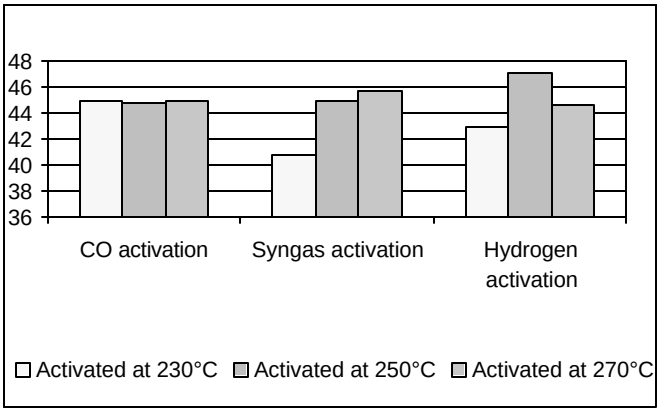

Figure 5. Influence of activation gas on methane selectivity
(FTS conditions: 270°C, 1.2MPa)

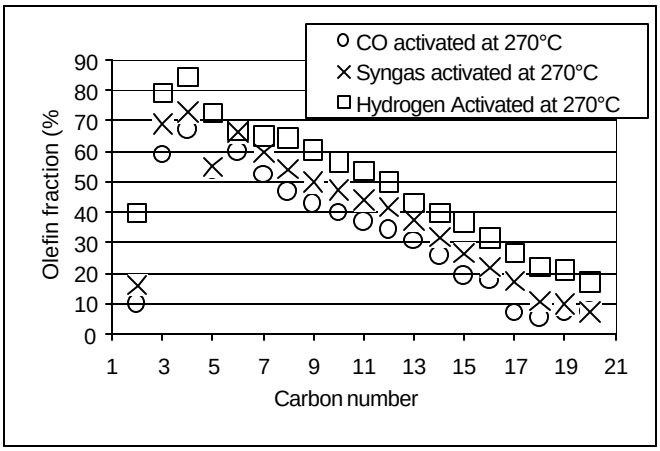

Figure 6. Influence of activation gas on olefin ratio
(FTS conditions: 270°C, 1.3MPa)

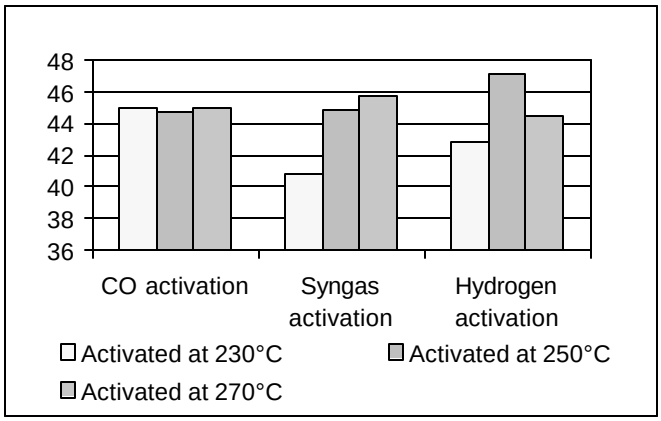

Figure 7. Influence of activation gas on CO_2 selectivity
(FTS conditions of 270°C, 1.3MPa)

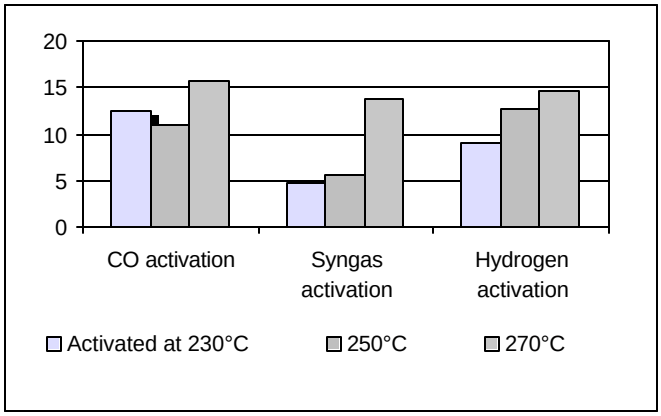

Figure 8. Influence of activation gas type on WGS quotient
$Q_{WGS} = P[CO_2]*P[H_2] / P[CO]*P[H_2O]$
(FTS conditions: 1.3MPa, 270°C)

INVESTIGATION OF HYDROFORMYLATION OF OLEFINS IN SUPERCRITICAL CARBON DIOXIDE USING PHOSPHINE MODIFIED RHODIUM CATALYST

Can Erkey, Daniel R. Palo, and Shaker Haji

Department of Chemical Engineering
University of Connecticut
191 Auditorium Road, U-3222
Storrs, CT 06269

Introduction

Over 6 million tons of aldehydes are produced annually by homogeneous catalytic hydroformylation of olefins. The shares of various aldehydes are C_3 (2%), C_4 (73%), C_5-C_{13} (19%) and C_{13}-C_{18} (6%).[1] The catalysts are of the form $H_xM_y(CO)_zL_n$; the two transition metals utilized are rhodium and cobalt and the most commonly utilized ligands are phosphines (PR_3 where R=C_6H_5 or n-C_4H_9). Production of C_4 aldehydes from hydroformylation of propene are dominated by rhodium based catalysts whereas higher aldehydes are produced mainly by catalysts based on cobalt. Since rhodium is about 10,000 times more active than cobalt, processes based on Rh catalysts operate at significantly lower temperatures and pressures than processes based on Co catalysts. For example, the UCC liquid recycle process for hydroformylation of propene which uses $HRh(CO)(P(C_6H_5)_3)_3$ operates in the temperature range 85-90 ^oC and at 18 bar. On the other hand, the BASF process for hydroformylation of 1-octene which uses $HCo(CO)_4$ operates in the temperature range 160-190 ^oC and in the pressure range 250-300 bar. Therefore, substantial savings in operating and capital costs can be achieved if hydroformylation of higher olefins are conducted using Rh based catalysts.

One of the difficulties associated with switching to Rh is the difficulty of the separation of products and catalyst by distillation of the aldehydes. The high boiling points of aldehydes beyond C_7 makes such an operation impractical even under reduced pressure due to thermal stability considerations for the catalyst. A relatively recent development in this field has been the commercialization of a biphasic hydroformylation process by RCH/RP.[1] In this process, the hydroformylation reaction is conducted in the aqueous phase using water-soluble rhodium complexes as catalysts, thus eliminating the problem of separating the catalyst from the product mixture. The process is utilized for production of C_4 and C_5 aldehydes, however application of this concept to higher olefins is highly unlikely due to extremely low solubilities of higher olefins in water. An alternative may be to utilize supercritical fluids as solvents in hydroformylation reactions.

A supercritical fluid (SCF) is a fluid that has been heated and compressed above its critical temperature and pressure. At these conditions, SCFs have densities that are greater than those of gases but comparable to those of liquids, which enable them to function as solvents. Using SCFs as solvents may have great advantages in catalyst recovery. The solubility of solutes in SCFs are strong functions of temperature and pressure in the vicinity of the critical point. Therefore, the catalyst, products and reactants may be separated in an efficient manner through temperature and/or pressure programming. Among the SCFs, supercritical carbon dioxide ($scCO_2$) is particularly attractive as a solvent since it is non-toxic, environmentally acceptable, cheap, readily available in large quantities and has a low critical temperature and a moderate critical pressure. It is non-flammable unlike some other SCFs such as ethane and propane, thus its use does not constitute a safety hazard. Today, there are many $scCO_2$ extraction plants operating around the world thereby indicating the technical and economical feasibility of carbon dioxide based processes. In this preprint we report the results of our investigations of hydroformylation of higher olefins in $scCO_2$ using $HRh(CO)L_3$ where L is a fluoroalkyl- or fluoroalkoxy-substituted arylphosphine.

Experimental

Experimental apparatus. A schematic diagram of the experimental apparatus is given in Figure 1. Hydroformylation reactions were conducted batchwise in a custom manufactured, 51.5 mL stainless steel reactor fitted with two sapphire windows (1" ID, Sapphire Engineering, Inc.), poly-ether-ether-ketone o-rings (Valco Instruments, Inc.), a T-type thermocouple assembly (Omega Engineering, DP41-TC-MDSS), a pressure transducer (Omega Engineering, PX300-7.5KGV), a vent line, and a rupture disk assembly (Autoclave Engineers). The reactor rests on a magnetic stir plate and heated to appropriate temperatures by a circulating heater (Fisher Scientific) via a machined internal heating coil. The reactor is pressurized with CO_2 from a syringe pump (ISCO, 260D) equipped with a cooling jacket to the desired reaction pressure. Samples can be obtained via a sampling loop with the arrangement shown below. A high-pressure-high temperature FTIR sampling head can be screwed through the reactor body to reach inside the reactor.

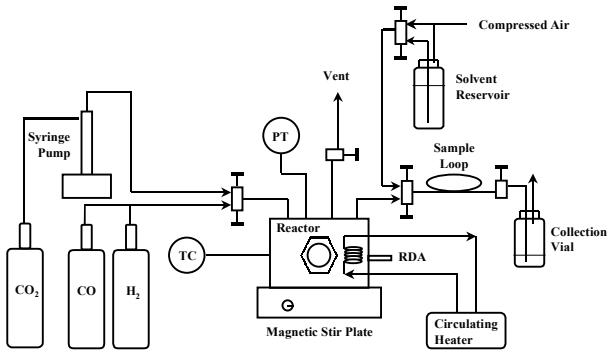

Figure 1. Schematic diagram of the experimental setup.

Catalysts preparation and the hydroformylation experiments. All the phosphines were synthesized from the corresponding perfluoroalkyl- or perfluoroalkoxy-substituted aryl bromides as described earlier.[2] The different forms of the catalyst $HRh(CO)L_3$ were formed in situ under hydroformylation conditions from $Rh(CO)_2(acac)$ and the specified ligand. For each hydroformylation experiment, $Rh(CO)_2(acac)$ (0.65×10^{-5} mol), ligand (2.0×10^{-5} mol), and 1-octene (0.054 mol) were charged to the reactor under nitrogen. The reactor was then sealed, heated to reaction temperature (50 ^oC), and charged with H_2/CO (0.055 mol each). Finally, CO_2 was charged to the reactor, bringing the total pressure to 273 atm. Periodic samples taken during each reaction were analyzed by gas chromatography.

Results and Discussion.

We synthesized and characterized several fluoroalkyl- or fluoroalkoxy-substituted arylphosphines and investigated the effect of ligand modification for homogeneous hydroformylation of 1-octene in $scCO_2$. The variation of 1-octene concentration with time for all the different phosphines are given in Figure 2.

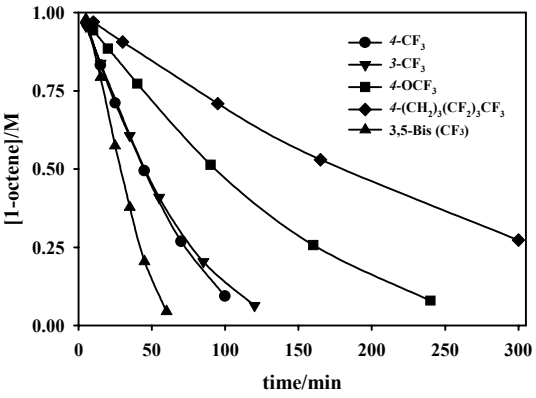

Figure 2. Hydroformylation of 1-octene using $HRh(CO)L_3$: P = 273 atm, T = 50 °C, $[1\text{-octene}]_0$ = 0.95 M, $[H_2]_0 = [CO]_0$ = 1.1 M, [Rh] = 1.27 mM, [P]/[Rh] = 3.0.

The activity of the rhodium complex (formed *in situ* from $Rh(CO)_2(acac)$ and L) increased with decreasing basicity of the phosphine according to the series $P[3,5\text{-}(CF_3)_2C_6H_3]_3$ > $P(4\text{-}CF_3C_6H_4)_3$ ≈ $P(3\text{-}CF_3C_6H_4)_3$ > $P(4\text{-}CF_3OC_6H_4)_3$ > $P[4\text{-}F(CF_2)_4(CH_2)_3C_6H_4]_3$. Among the various catalyst systems, the initial rates of reaction differed more than 5-fold between the fastest and the slowest. The rate of hydroformylation correlated very well with the IR stretching frequency of metal carbonyls, ν(CO), for the various catalysts, showing a linear dependence. The ν(CO) is a sensitive indicator of electron density at the metal center, yielding a relative measure of the amount of π-backbonding from an occupied metal d-orbital to the empty π*-orbital of the carbonyl. The trend in ν(CO) corresponded well with the amount and proximity of the electron-withdrawing fluoroalkyl or fluoroalkoxy groups of the phosphines, with $P[3,5\text{-}(CF_3)_2C_6H_3]_3$ having the greatest effect and $P[4\text{-}F(CF_2)_4(CH_2)_3C_6H_4]_3$ having the least effect relative to the value for PPh_3. The phosphines $P(4\text{-}CF_3C_6H_4)_3$ and $P(3\text{-}CF_3C_6H_4)_3$ showed identical electronic behavior, and almost identical activity/selectivity behavior, while $P[3,5\text{-}(CF_3)_2C_6H_3]_3$, with a much higher ν(CO) value also had a significantly higher activity. The results were in agreement with an earlier report that the electronic effect of trifluoromethyl-substitution is independent of *ortho*-, *meta*-, or *para*- placement, and that the effects of multiple trifluoromethyl-substitutions are cumulative.[3] The ability of oxygen and methylene groups to insulate against the electron-withdrawing effects of the fluoroalkyl moieties could be observed for phosphines $P(4\text{-}CF_3OC_6H_4)_3$ and $P[4\text{-}F(CF_2)_4(CH_2)_3C_6H_4]_3$, where significant decreases in ν(CO) were accompanied by 50% and 70% decreases in activity, respectively. The results confirmed the observation by Leitner that methylene spacers effectively insulated the phosphorus lone pair from the electron-withdrawing effect of the fluoroalkyl chain,[4] and also showed that oxygen spacers exhibited a similar though less profound effect. While these spacers are effective insulators, they actually decrease the catalytic activity relative to "non-insulated" phosphines.

Extensive in situ FTIR studies were carried out for the catalyst with the highest activity, the one with $P[3,5\text{-}(CF_3)_2C_6H_3]_3$ as ligand. The intermediates of the reactions of $RhH(CO)[P(3,5\text{-}(CF_3)_2C_6H_3)_3]_3$ **1** with CO, H_2, C_2H_4 and mixtures of these in dense carbon dioxide were monitored. The results were compared to the behavior of the conventional catalyst, $RhH(CO)(PPh_3)_3$ **2**, in organic solvents.[5,6,7] Comparing the IR spectra of **1** in solid form with that in solution in $scCO_2$ at 50 °C and 115 bar (2039 and 1952 cm^{-1} vs. 2041 and 1964 cm^{-1}), its concluded that $RhH(CO)L_3$ **1** does not dissociate in $scCO_2$ like **2** does in organic solvents. This indicates a stronger metal-ligand bond in **1** compared to **2**. The strong bond could be attributed to a strong π-backbonding from an occupied metal d-orbital to the empty π*-orbital of the ligand caused by the high electronegative trifluoromethyl groups attached to it. However, **1** was converted to $RhH(CO)_2L_2$ **3** and to $[Rh(CO)_2L_2]_2$ **4** in the presence of CO in $scCO_2$. When hydrogen was added to such mixture, $RhH(CO)L_2$ **5** was produced. The last three species (**3**,**4**, and **5**) existed in equilibrium with each other. Another strange behavior was noticed in the reaction of **1** with an equimolar mixture of CO and H_2. In the presence of 1:1 mixture of CO/H_2, **1** underwent ligand dissociation to form $RhH(CO)L_2$ **5**, however, the presence of equimolar H_2 prevented further coordination of CO to form the dicarbonyl species $RhH(CO)_2L_2$ **3**. In the presence of CO and C_2H_4, the peaks observed in the acyl region and the terminal carbonyl region indicated the formation of $Rh(CO)_2L_2(COEt)$ **6**. In the ethylene hydroformylation reaction, **6** was observed again at 14 °C, however, its concentration reduced as the reaction proceeded with heating. After the completion of the reaction both $RhH(CO)_2L_2$ **3** and $RhH(CO)L_2$ **5** co-existed in the presence of excess CO/H_2. After depressurizing the reaction mixture, NMR spectra showed that most of the catalyst species, presented in the reaction mixture, converted back to the original form of **1**. The carbonyl stretching frequencies of all of the rhodium-carbonyl species were shifted to higher wave numbers due to a reduction of electron density at the metal center by the CF_3 groups.

Acknowledgement

This work was partially supported by Petroleum Research Fund, administered by the ACS (ACS-PRF 32299-AC1). The authors also gratefully acknowledge the National Science Foundation for its grant (CTS-0080823).

References

[1] Frohning, C. D.; Kohlpaintner, C. W. In *Applied Homogeneous Catalysis with Organometallic Compounds*; Cornils, B., and Herrmann, W. A., Eds.; VCH: Weinheim, 1996; pp. 29.

[2] Palo, Daniel R.; Erkey. C. *Organometallics* **2000**, 19, 81.

[3] Howell, J. A. S.; Lovatt, J. D.; McArdle, P.; Cunningham, D.; Maimone, E.; Gottlieb, H. E.; Goldschmidt, Z. *Inorg. Chem. Commun.* **1998**, 1, 118.

[4] Kainz, S.; Koch, D.; Baumann, W.; Leitner, W. *Angew. Chem., Int. Ed. Engl.* **1997**, 36, 1628.

[5] Evans, D.; Wilkinson, G. *J. Chem. Soc. (A)* **1968**, 2660.

[6] Brown, C. K.; Wilkinson, G. *J. Chem. Soc. (A)* **1970**, 2753.

[7] Moser, W.R.; Papile, C.J.; Brannon, D.A.; Duwell, R.A.; Weininger, S.J. *J.Mol.Catal.* **1987**, 41, 271.

METHANE AND METHANOL STEAM REFORMING TO PRODUCE HYDROGEN USING CATALYTIC MICROCHANNEL REACTORS

Yong Wang, Robert Dagle, Ya-Huei Chin, Daniel Palo, Jianli Hu, and Jamie Holladay

Chemical and Biological Processing Group
Environmental Technology Division
Pacific Northwest National Laboratory
902 Battelle Blvd, Richland, WA 99352

Introduction

Steam reforming of hydrocarbons is conventionally used in fuel processing to produce hydrogen. A fuel processor is a critical reactor technology for the deployment of PEM-based fuel cells for portable, on-board, and stationary applications. Over the past several years, PNNL has developed microchannel chemical reactors for fuel processing applications, ranging from the power required for remote electronic device to that for automobile applications [1,2]. In particular, a series of steam reforming catalysts suitable for microchannel reactors have been developed [3-5]. In this presentation, we will present methane and methanol steam reforming catalyst work recently developed at PNNL.

Experimental

Pd/ZnO catalysts were prepared from impregnating aqueous $Pd(NO_3)$ solution containing 20.19 wt% Pd (Engelhard) onto ZnO powder (Aldrich, 99%) using a solution/solid ratio of 0.58 ml/g. The impregnated samples were dried under vacuum at 110 ^oC for at least 8 hrs prior to calcining in air. The calcination was conducted under a 2 ^oC/min ramp followed by holding isothermally at 350 ^oC for 3hs.

Activity tests were carried out in a 4 mm I.D. quartz tube reactor. Approximately 0.200 g of catalyst was loaded between two layers of quartz wool inside the reactor. A thermocouple was placed in the middle of the catalyst bed. A premixed 1:1wt % methanol-water feed was introduced into the reactor by using a syringe pump. The feed rate was adjusted such that the reaction was conducted under 100 ms contact time, which is in equivalent to a standard GHSV of 36000 h^{-1}. Prior to entering the reactor, the feed was fully vaporized through a vaporizer, operated at 200 ^oC. Prior to activity testings, the catalysts were reduced *in-situ* under a 10 % H_2/N_2 at 350 ^oC. A glass condenser at 0 ^oC was used to separate liquid products from gaseous products. The product gases, CO, CO_2, and H_2, were separated using MS-5A and PPQ columns, and analyzed on-line by means of a Hewlett Packard Quad Micro GC (Model Q30L) equipped with a TCD.

Results and Discussions

Methanol and methane are two popular and readily available hydrocarbons. One way to extract hydrogen from methanol or methane is via steam reforming reactions. Conventionally, CuZnAl catalysts are used for methanol steam reforming and methane steam reforming catalysts are based on Ni. Although these two types of catalysts are suitable for conventional fixed bed-type reactors where heat transfer is limiting, more active and selective catalysts are needed for mcirochannel reactor applications where heat and mass transfer advantages are exploited.

Methanol is a unique fuel since it is sulfur-free and can be activated at relatively low temperature (under 300 ^oC). This could be a significant advantage from system simplification and process heat recovery points of view. We have investigated the steam reforming of methanol with Pd/ZnO under high throughput conditions (GHSVs ranging from 18,000 to 144,000 hr^{-1}). Pd, like other transition metals (Pt, Rh), exhibits high methanol decomposition activity to CO and H_2. This is not surprising, since precious metal based catalysts typically exhibit different catalytic function than the Cu based catalytic materials. However, when supporting the Pd on ZnO, the catalytic function of Pd can be greatly modified, resulting in a highly active and selective catalyst for methanol steam reforming, which was not found previously on precious metal catalysts. Under steam reforming conditions, the Pd/ZnO catalyst produces mainly CO_2 and H_2 along with minimal amount of CO. The concentration of CO in the product stream was found to be at least as low as what reported for the well-studied Cu based catalyst. Hydrogen rich stream with low CO content is highly desired since the electrocatalyst at the anode is extremely sensitive to CO poisoning at the operating temperature of PEM fuel cells.

The methanol conversion and CO selectivity over 5, 10 and 20 wt% Pd/ZnO catalysts are shown in Figure 1a and 1b, respectively. The experiments were repeated with the same catalyst, and no noticeable catalyst deactivation was observed. As can be seen from Figure 1a and 1b that increasing Pd loading from 5 wt% to 20 wt% results in a 10 ^oC shift of the conversion profile to the lower temperatures. A complete conversion of methanol can be achieved at around 300 ^oC. The CO selectivities of these catalysts were less than 7 % over the entire temperature range studied. At 300 ^oC, this corresponds to a dry effluent consisting of approximately 1% CO, 26% CO_2, and 73% H_2. Of the three catalysts examined, the 20% Pd/ZnO catalyst exhibited the lowest CO selectivity. In addition to catalytic activity studies, we also attempted to elucidate the chemical and physical properties of Pd/ZnO catalysts using TPR, TEM, H_2 chemisorption and XRD. It was found that PdZn alloy formed under reducing environment at moderate temperatures (<300 ^oC). This species is highly selective for the steam reforming of methanol, which is not normally observed on precious metal based catalysts.

Methane steam reforming catalysts were also developed based on Rh [4]. This type of catalysts exhibited extremely high activity as evidenced by equilibrium conversion reached at a very high GHSV (as high as 1,000,000 hr^{-1}). Catalyst life was also evaluated under stoichiometric steam to carbon ratio, and no noticeable catalyst deactivation was observed under the conditions studied and the catalyst was shown to be coke resistance at low steam to carbon ratios.

Conclusions

A highly active and selective Pd/ZnO catalyst was developed for methanol steam reforming. Complete conversion was achieved at 300^{o}C with a CO concentration in the dry effluent around 1%. This catalyst was evaluated by various catalyst characterization techiniqes including TEM, TPR, chemisorption, and XRD. It was found that PdZn alloy formed under reducing environment at moderate temperatures (<300 ^oC). This species is highly selective for the steam reforming of methanol, which is not normally observed on precious metal based catalysts. A highly active and coke resistant methane steam reforming catalyst was developed and its life performance was evaluated under low steam to carbon ratios.

Acknowledgement. This work was performed in the Environmental Molecular Sciences Laboratory, a national scientific

user facility sponsored by the US Department of Energy's Office of Biological and Environmental Research and located at Pacific Northwest National Laboratory in Richland, WA.

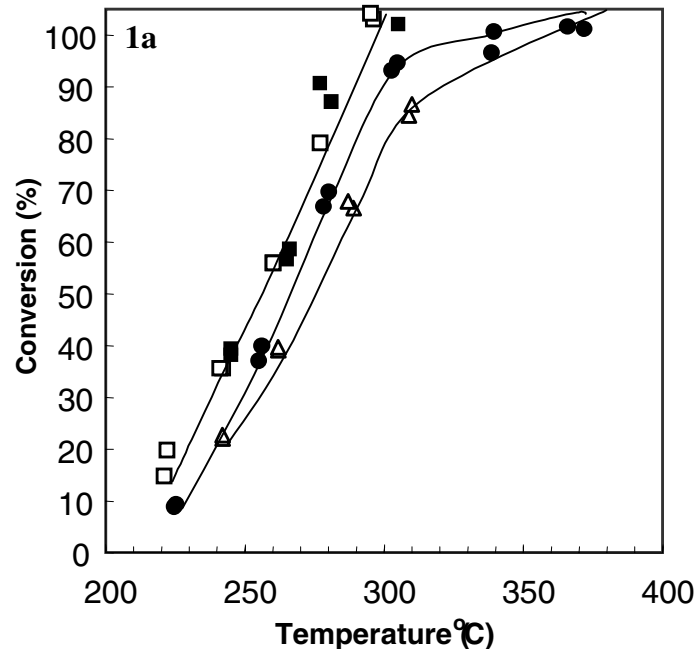

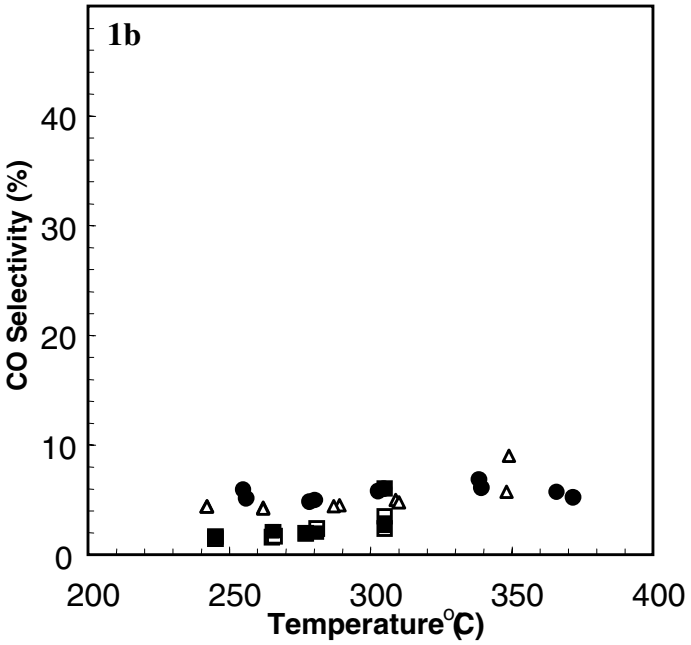

Figure 1a and 1b. Methanol conversion temperature profile under steam reforming of methanol (a) and the corresponded CO selectivity (b) for 5 wt% (triangle), 10 wt% (circle), and 20 wt% Pd on ZnO (both filled and open square). For 20%Pd/ZnO, the conversion profiles were acquired after two separate reduction temperatures: reduction at 125 °C (open square) and after reduction at 350 °C (filled square). All other catalysts were tested after reduction at 350 °C. Reaction conditions: 0.1925g catalyst, 100 ms contact time or 36000 GHSV, $H_2O/C = 1.8$, 1 atm.

References

1. D.R. Palo, J.D. Holladay, R.T. Rozmiarek, C.E. Guzman-Leong, Y. Wang, J.Hu, Y.Chin, R.A. Dagle, and E.G. Baker, *J. Power Sources* (in press).
2. J.D. Holladay, E.O. Jones, M.R. Phelps, and J. Hu, submitted to *Journal of Power Sources*
3. Y. Chin, R. Dagle, J. Hu, A. C. Dohnalkova, and Y. Wang, submitted to *Catalysis Today*.
4. Y. Wang, D. VanderWiel, A.L. Tonkovich, U.S. Pat., 6,284,17B1 (2001).
5. J.Hu , Y. Wang, D.P. VanderWiel, Y. Chin, D.R.Palo, R. Rozmiarek, R.A. Dagle, J.D. Holladay, and E.G.Baker, submitted to *Chemical Engineering and Technology.*
6. N. Iwasa, S. Masuda, N. Ogawa, N. Takezawa, *Appl. Catal*. 125 (1995) 145.

METHANOL SYNTHESIS ACTIVITY OF ALKALINE EARTH AND LANTHANOID METAL ADDED SULFIDED PD/SiO_2 AND THEIR SURFACE FINE STRUCTURES INVESTIGATED BY DRIFT SPECTROSCOPY

Naoto Koizumi, Kazuhito Murai, Satoshi Takasaki and Muneyoshi Yamada

Department of Applied Chemistry, Graduate School of Engineering, Tohoku University, 07Aoba, Aramaki, Aoba-ku, Sendai 980-8579, Japan

Introduction

Because of the potential use of dimethyl ether as a substituted diesel fuel, methanol synthesis from CO/H_2 (syngas) is one of attractive technologies for the production of high-quality transportation fuels. Cu/Zn-type catalyst is currently applied for the industrial methanol production using a feed containing both syngas and CO_2.[1] For a feed containing only the syngas, reduced Pd catalysts show a high activity. The turnover frequency of reduced Pd/CeO_2 at 443 K and 3.0 MPa has been reported to be equivalent to that of Cu/Zn catalyst at 523 K and 5.1 MPa from $CO/H_2/CO_2$ feed.[2]

To develop methanol synthesis catalysts with a sulfur tolerance, authors investigated CO hydrogenation activity of various transition metal sulfides and found that $Rh_{17}S_{15}$[3] and $Pd_{16}S_7$[4] yield methanol from the syngas feed even in the presence of H_2S. In the absence of H_2S, the space-time yield (STY) of methanol obtained with $Rh_{17}S_{15}$ reached 800 g/kg-cat/h at 593 K and 5.1 MPa, which is comparable with that obtained with a commercial Cu/Zn/Al catalyst at 523 K and 5.1 MPa from $CO/H_2/CO_2$ feed. $Pd_{16}S_7$, on the other hand, yielded only 77 g/kg-cat/h of methanol at 613 K and 5.1 MPa. To improve the methanol synthesis activity of Pd sulfide, authors investigated the activity of Pd sulfide supported on various metal oxides and found that SiO_2 is most effective support among the metal oxides examined. The STY of methanol obtained with sulfided Pd/SiO_2 was 1.6 times higher than that obtained with $Pd_{16}S_7$. Besides, the STY of methanol obtained with SiO_2 supported Pd sulfide changed depending on the kinds of SiO_2.[5] It was suggested that alkaline and alkaline earth metal impurities in SiO_2 act as promoters.

Thus, to improve the methanol synthesis activity of Pd sulfide further, the present work investigated effects of alkaline, alkaline earth or lanthanoid metal additives on the activity of SiO_2 supported Pd sulfide. DRIFT measurements under the reaction conditions were also performed to make clear active adsorbed species formed on SiO_2 supported Pd sulfide.

Experimental

Catalyst preparation. Precursor materials for SiO_2 supported Pd sulfide with or without the additive were prepared by the impregnation method. SiO_2 supported Pd oxide was prepared by impregnating pre-calcined SiO_2 powder (Fuji Silysia, 560 m^2/g) with an aqueous $Pd(NH_3)_4(NO_3)_2$ solution followed by drying and calcination (Pd/SiO_2). A weight ratio of Pd (as metal) to SiO_2 was 0.045. Then, Pd/SiO_2 with the additive was prepared by impregnating Pd/SiO_2 with an aqueous $M(NO_3)_x$ solution (M: Li, K, Cs, Mg, Ca, Sr, Ba, La or Nd) followed by drying (M-Pd/SiO_2 (D)). M/Pd atomic ratio was varied in a range from 0.1 to 1.0. To examine effects of calcination, part of M-Pd/SiO_2 (D) was calcined (M-Pd/SiO_2 (C)).

Activity measurement. The precursor material thus prepared was charged into a stainless steel reactor and was sulfided in a stream of H_2S 5%/H_2 at 673 K. The cumulative amount of H_2S fed during the sulfiding pretreatment was 160 mol-H_2S/mol-Pd. Methanol synthesis was then performed using the syngas feed (CO 33%/H_2 62%/Ar). Cu/Zn/Al catalyst supplied by ICI Corp. was also used as a reference.

DRIFT measurement. To obtain DRIFT spectra of adsorbed species formed under the high-pressure reaction conditions, DRIFT chamber equipped with ZnSe window (Spectra-Tech Inc.) was utilized in the present work. After the sulfidation of the precursor material in the chamber, methanol synthesis was performed at 613 K and 5.1 MPa using the same feed as that employed for the activity measurements. DRIFT spectra were recorded on FTS 6000 spectrometer (Digilab) with a resolution of 4 cm^{-1} and accumulation of 128.

Results and Discussion

Methanol synthesis was performed at 613 K, 5.1 MPa and 20 m^3 (STP)/kg-cat/h using sulfided Pd/SiO_2 and sulfided M-Pd/SiO_2 (D) having M/Pd atomic ratio of 0.5. Methanol, CH_4 and CO_2 were formed under these conditions. The products obtained with sulfided Pd/SiO_2 and sulfided M-Pd/SiO_2 (D) (M: Mg, Ca, Sr, La or Nd) were mainly composed of methanol while the remainder of the catalysts mainly yielded methane. Methanol selectivity of sulfided Pd/SiO_2 and M-Pd/SiO_2 (D) (M: Mg, Ca, Sr, La or Nd) was 90 mol% and 60-70 mol%, respectively. **Figure 1** shows the STY of methanol obtained with these catalysts. The STY of methanol obtained with sulfided M-Pd/SiO_2 (C) is also shown in **Figure 1**. Except for K and Cs additives, all the additives examined here show promoting effects. Especially, the higher STY is obtained with the sulfides containing Ca, Sr, La or Nd additive. The calcination of the precursor material increases the activity slightly in the case of sulfided Sr-Pd/SiO_2. Among the catalysts examined here, the maximum STY is obtained with sulfided Ca-Pd/SiO_2 (D), which is about 4 times higher than that obtained with sulfided Pd/SiO_2.

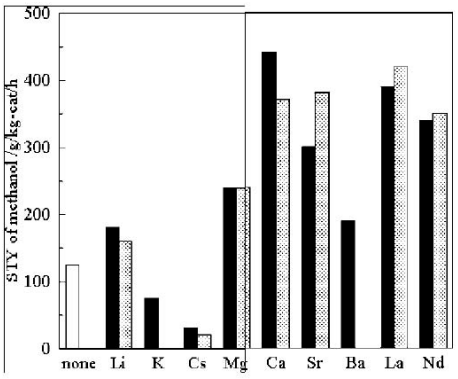

Figure 1. STY of methanol obtained with sulfided Pd/SiO_2 ( ), sulfided M-Pd/SiO_2 (D) ( ) and sulfided M-Pd/SiO_2 (C) ( ): Reaction conditions, CO 33%/H_2 62 %/Ar, 613 K, 5.1 MPa, 20 m^3 (STP)/kg-cat/h.

Then, methanol synthesis was performed using sulfided Ca-Pd/SiO_2 (D) at 5.1 MPa and 30 m^3 (STP)/kg-cat/h in a temperature range from 473 K to 613 K. The STY of methanol increases with increasing the temperature from 473 K to 593 K and was 700 g/kg-cat/h at 593 K. For comparison, the commercial Cu/Zn/Al catalyst was also subjected to the reaction. Cu/Zn/Al catalyst yielded 900 g/kg-cat/h of methanol at 523 K, 5.1 MPa and 6.0 m^3/kg-cat/h from $CO/H_2/CO_2$ feed. Thus, at the higher reaction temperature and gas-hourly space velocity, the STY of methanol obtained with sulfided Ca-Pd/SiO_2 (D) reaches 80% of that obtained with the commercial Cu/Zn/Al catalyst.

To make clear active species on sulfided Ca-Pd/SiO_2 (D), DRIFT spectra were recorded as a function of time when sulfided Ca-

Pd/SiO_2 (D) was exposed to the stream of the syngas at 613 K and 5.1 MPa (**Figure 2**). The spectra show IR bands at 1820, 1600, 1450, 1270, 1110, 1062, 1031, 1007 and 957 cm^{-1}. A shoulder band is also visible at 1304 cm^{-1}. The bands at 1062, 1031 and 1007 are assigned to C-O stretching vibration of the gas-phase methanol while the shoulder band at 1304 cm^{-1} is assigned to C-H bending vibration of the gas-phase methane. The appearance of the bands due to the gas-phase methanol clearly indicates that methanol synthesis takes place in the chamber.

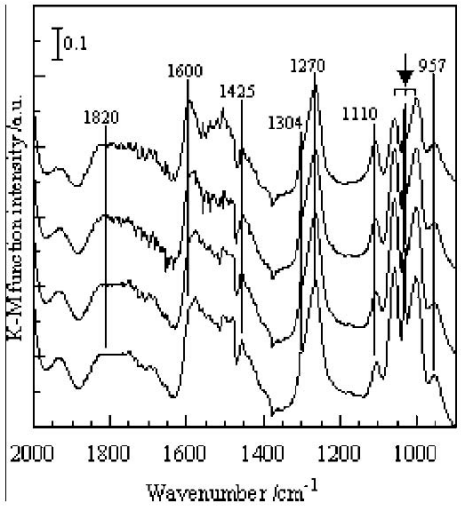

Figure 2. DRIFT spectra of sulfided Ca-Pd/SiO_2 (D) under the high-pressure methanol synthesis conditions as a function of time-on stream (from top to bottom, *t*=0, 5, 30, 93 min): The arrow indicates the IR bands due to the gas-phase methanol.

To facilitate assignments of the remainder of the bands observed during methanol synthesis, the catalyst temperature was reached down to 298 K under the high-pressure syngas flow and then the pressure of the syngas flow was reached down to 0.3 MPa followed by the flushing with helium. Although the bands of the gas-phase methanol, methane and CO completely disappeared, the bands at 1600, 1425 and 1270 cm^{-1} were still visible in the spectrum recorded under these conditions. IR bands were also visible at 2060 and 1925 cm^{-1}, which are assigned to C-O stretching vibration of adsorbed CO species. Thus, the bands at 1600, 1425 and 1270 cm^{-1} observed during methanol synthesis originate from adsorbed species, not the gas-phase products. Several authors have reported that IR bands of adsorbed formate species are observed when a reduced Na-Pd/SiO_2[6] or reduced PdCu/KL[7] is exposed to the stream of the syngas at elevated temperatures. The formate species shows IR bands at 1600-1550 cm^{-1}, 1400-1380 cm^{-1}, 1380-1340 cm^{-1} and 1090-1060 cm^{-1}.[8] The bands at 1600, 1425 and 1270 cm^{-1} observed during methanol synthesis, therefore, are not due to the adsorbed formate species. Except for the bands of the gas-phase methanol and methane, all the bands appeared in the spectra in **Figure 2** were also observed when sulfided SiO_2 was exposed to the stream of the syngas at 613 K and 5.1 MPa. This observation indicates that the bands at 1600, 1425 and 1270 cm^{-1} observed during methanol synthesis originate from some kinds of adsorbed species formed on SiO_2 and this species is not involved in the formation of methanol.

Then, attention was given to the nature of the adsorbed CO species. As mentioned above, IR bands of the adsorbed CO species appear at 2060 and 1925 cm^{-1} when sulfided Ca-Pd/SiO_2 (D) is exposed to the stream of helium after methanol synthesis. From the literature data,[8] these bands are assigned to CO species linearly adsorbed on Pd^0 sites (2060 cm^{-1}) and CO species adsorbed on Pd^0 sites in the form of bridge (1925 cm^{-1}), respectively. To investigate the reactivity of these adsorbed CO species toward hydrogen, helium flow was replaced by hydrogen flow. The catalyst temperature was then ramped from 298 to 613 K at the rate of 10 K/min. DRIFT spectra were recorded at each temperature (Temperature Programmed Surface Reaction, TPSR). The pressure of hydrogen flow was maintained at 1.6 MPa during the TPSR. The obtained spectra are shown in **Figure 3**. With increasing the temperature, the intensities of the bands of the adsorbed CO species decrease and disappear at the temperature above 473 K, which is accompanied with the increase of the intensities of the bands at 1271, 1099 and 950 cm^{-1}. Careful inspections of the spectra also show the appearance of the bands due to the gas-phase methanol at 1062, 1031 and 1007 cm^{-1}.

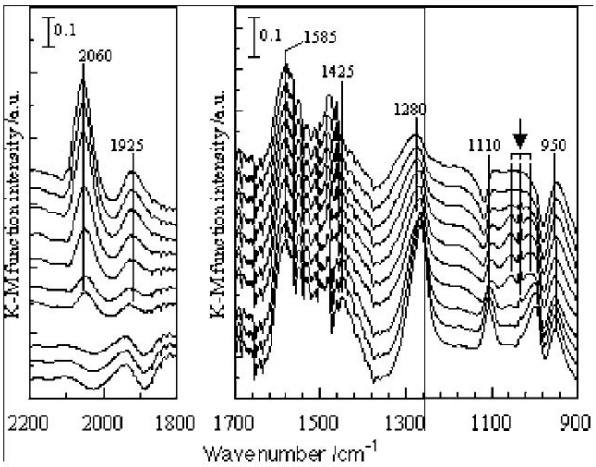

Figure 3. DRIFT spectra of sulfided Ca-Pd/SiO_2 during the TPSR (from top to bottom, *T*=303, 323, 343, 373, 393, 423, 473, 523, 573, 613 K): The arrow indicates the IR bands due to the gas-phase methanol.

The intensities of the bands at 1271, 1099 and 950 cm^{-1} increase with increasing the temperature until it reaches 613 K while those of the bands due to the gas-phase methanol showed the maximum at around 400 K. This indicates that the adsorbed CO species observed after methanol synthesis react with hydrogen to form the gas-phase methanol during the TPSR. It is suggested that Pd^0 sites are formed on sulfided Ca-Pd/SiO_2 under methanol synthesis conditions and CO species adsorbed on these sites is hydrogenated to yield methanol.

Acknowledgement

This work was supported by Research for the Future Program of JSPS under the project "Synthesis of Ecological High Quality of Transportation Fuels" (*JSPS-RFTF98P01001*).

References

(1) Chinchen, G. C.; Mansfield, K.; Spencer, M. S. *CHEMTECH* **1990**, 699.
(2) Matsumura, Y.; Shen, W. J.; Ichihashi Y.; Okumura, M. *.J. Catal.* **2001**, *197*, 267.
(3) Yamada, M.; Koizumi, N.; Miyazawa, A.; Furukawa, T. *Catal. Lett.*, *in print*
(4) Koizumi, N.; Miyazawa, A.; Furukawa, T; Yamada, M. *Chem. Lett., in print.*
(5) Koizumi, N. ; Murai, K.; Takasaki, S.; Yamada, M. Prepr. Pap. - *Am. Chem. Soc., Div. Fuel Chem.*, **2001**, *46* (2), 437.
(6) Kikuzono, Y.; Kagami, S.; Naito, S.; Onishi T.; Tamaru, K. *Faraday Discuss. Chem. Soc.* **1981**, *72*, 135.
(7) Anderson, J. A.; Lopez-Granados, M.; Fernandez-Garcia, M. *J. Catal.* **1998**, *176*, 235.
(8) Gopal, P. G.; Schneider, R. L.; Watters, K. L. *J. Catal.*, **1987**, *105,* 366.
(9) Sheppard, N.; Nguyen, T. T. *Adv. IR and Raman Spectrosc.* **1987**, *5*, 67.

PRODUCT ANALYSIS OF A NOVEL SYN-CRUDE SYNTHESIS DIRECTLY FROM A COMBINED CONVERSION OF COAL AND METHANE

Yu Wang[1], Yang Li[1], Jijun Zou, Baldur Eliasson[2], and Chang-jun Liu[1]*

1. State Key Laboratory of C1 Chemistry and Chemical Technology,School of Chemical Engineering and Technology, Tianjin University,Tianjin 300072, China
2. Energy & Global Change, ABB Corporate Research Ltd., Baden, CH5405, Switzerland

Introduction

Mankind has been used to an ever-growing supply of cheap and abundant fossil energy including coal, oil and natural gas for more than 150 years. Especially, cheap oil has played an important role in the booming economic all over the world. The consumption of fossil energy is challenging us due to some global problems. The first problem is the degradation of the environment. The second one is the lack of availability and security of oil. To solve these problems, one has to improve the efficiency of energy consumption and develop alternative fuels simultaneously. Since the safe nuclear energy technology is still in the development, alternative fuels and renewable energy become very important in the present world.

Methane is a principal component of natural gas, coalbed methane, associated gas of oil field and some by-product gases of chemical plants. There is a plentiful resource of methane. The utilization of methane is very important to keep the safe and reliable energy supply in the coming new century. On the other hand, there is a huge reserve of coal all over the world. Especially, the major fossil fuel consumed in China is coal. An intensive investigation has been conducted to develop technologies for the clean use of coal in China. Due to its low H/C, it is still difficult to chemically utilize coal. Since methane owns a higher heat value, with its high H/C ratio, it is very promising to combine the utilization of methane and coal. Especially, it will be very promising if we can produce liquid fuels directly from conversions of coal and methane. However, few work has been conducted in this field.

The industrialized synthetic fuel production from coal or methane claims a multi-step process. First, the syngas ($CO+H_2$) is produced and the liquid fuel is then produced from syngas.

However, there exist some difficulties in such fuel production. First, the process of the production of syngas is an endothermic reaction and requires a high temper-ature for a favoured equilibrium. This is a very energy-intensive process. Second, further reactions of syngas, like F-T synthesis, need high-pressure operation for a reasonable conversion. Therefore, the produced syngas has to be compressed. This also consumes extra energy. For the comercialised set-up of fuel synthesis from syngas, more than 60% of the cost goes to the production and compression of syngas [1]. The high-energy consumption and high investment in set-up limit the application of multi-step conversion. Especially, such multi-step utilization is not suitable for *on site* coal or methane conversion at remote sites by far. It is very necessary to improve such multi-step utilization of coal or methane simultaneously exploits new techniques. Among all the new technologies under developing, the non-thermal plasma conversion is very promising. Since non-thermal plasma is a mixture of electrons, highly excited atoms and molecules, ions, radicals, photons, etc, the chemistry is very complex. A very selective product from this plasma chemistry could become very expensive. This character determines that non-thermal plasma is feasible for the synthesis of liquid fuel that is a mixture of higher hydrocarbons. Here we report a direct liquid fuel synthesis from the combination of conversions of coal and methane using dielectric-barrier discharge (DBD) that has led to a significantly high yield of higher hydrocarbons.

Experimental

The DBD reactor we used in this investigation was similar to that reported previously [2,3]. The gap for the discharge was 1.8 mm and the length of the discharge zone was 250 mm. The pure methane feed was used for this investigation. The flow rates of feed gas were about 20 ml/min and 40 ml/min, respectively. The high voltage electrode was an aluminum foil attached to the inner surface of the quartz tube. And a stainless steel tube around the quartz tube served as the grounded electrode. The width of discharge gap was equal to the distance between the steel tube and the quartz tube. The temperature of all the reactions was adjusted at about 65 °C with circulating oil. All the experiments were operated at atmospheric pressure.

The feed gas (methane) was introduced into the reactors via mass flow controllers. The gaseous products were analyzed using an online gas chromatograph (HP 5890, TCD and FID) with a mass selective detector (HP 5971) equipped with a HP-PLOT Q column (30 m × 0.53 mm). The liquid products were collected in a trap cooled by a mixture of ice and water. The liquid hydrocarbons were analyzed using the same GC with a CBP-1 column (50 m × 0.25 mm).

The loading of coal (anthracite coal; purchased from Beijing Institute of Coal Science,product code: GBW11103b) in the discharge space was the same as the approach described elsewhere [3,4].

Results

The product from such DBD plasma methane conversion in the presence of coal contains gaseous hydrocarbons (mainly ethane and propane with some small amount of ethylene, propylene, butane, iso-butane and benzene) and syn-crude. It is clear that the product includes products from the decomposition of methane, products from the conversion of coal and products of reactions of discharge species with components in the coal. The decomposition of methane leads to the formation of higher hydrocarbons. The conversion of coal principally leads to the formation of aromatics and also higher hydrocarbons (from the hydrogenation of coal). The reactions of discharge species and components of coal lead to the production of hydrocarbons and oxygen-containing and nitrogen-containing hydrocarbons. The formation of nitrogen-containing hydrocarbons will induce extra purification of syn-crude that is a major drawback of the present DBD conversions.

The decomposition of methane was initiated from the formation of methyl radicals in the DBD discharges

$$CH_4 + e \rightarrow CH_3 + H \quad (4)$$

The reactions of propagating the length of carbon chain, which took place in the bulk gases, could be expressed as:

$$CH_3 + CH_3 \rightarrow C_2H_6 \quad (5)$$

$$C_2H_6 + e \rightarrow CH_3 + CH_3 \quad (6)$$

$$C_2H_6 + e \rightarrow C_2H_5 + H \quad (7)$$

$$CH_3 + C_2H_5 \rightarrow C_3H_8 \quad (8)$$

$$C_3H_8 + e \rightarrow C_3H_7 + H \quad (9)$$

$$CH_3 + C_3H_7 \rightarrow C_4H_{10} \quad (10)$$

$$C_2H_5 + C_2H_5 \rightarrow C_4H_{10} \quad (11)$$

…… …… ……

The chain reactions lead to the formation of syn-crude. In the presence of coal, the components in the coal will also involve in the chain growth reactions for the syn-crude production to lead to the production of aromatics and nitrogen-containing hydrocarbons. Figure *1* shows a MS spectrum of syn-crude produced. The peaks at

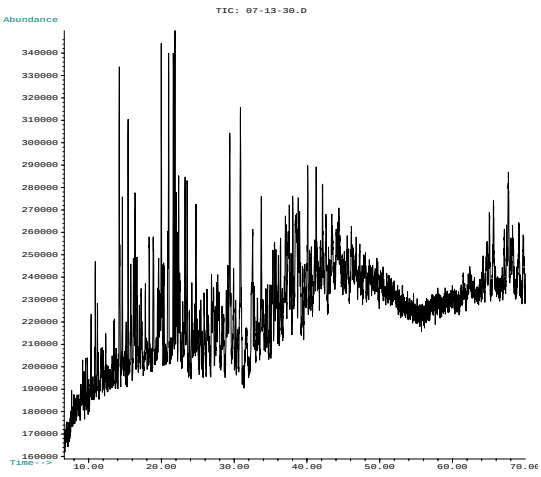

Figure*1*. MS spectra of syn-crude produced from the DBD plasma methane conversion in the presence of coal (*flow rate of feed methane: 20 Nml/min; Input power: 50 W; Conversion of methane: 28.2% (after 15 min); 35.0% (after 70 min)*)

the first 50 minutes in the Figure *1* are principally hydrocarbons. A large amount of branched hydrocarbons have been detected in these hydrocarbons, which means a better fuel production. The peaks present in the range of 60 to 70 minutes are mostly nitrogen-containing hydrocarbons. It is obviously that the nitrogen species in the coal are easily involved in the reactions for the production of higher hydrocarbons. Further investigation is being conducted for the understanding of reactive mechanisms.

Conclusion

The present investigation has confirmed a syn-crude production from the combined conversions of methane and coal. Such produced syn-crude contains a large amount of branched higher hydrocarbons. Some nitrogen-containing hydrocarbons have also been detected that requires a further purification of syn-crude. The syn-crude production from the combined conversions of methane and coal employs three kinds of reactions: (1) decomposition of methane; (2) conversion of coal, including hydrogenation, decomposition of volatiles under the condition of DBD plasmas (3) the reactions of methane plasma species with the components of coal. Compared to methane conversion in the absence of coal, the addition of coal in the discharge gap induces a significantly higher yield (more than 200% higher) of liquid fuel (syn-crude exactly). This means that the addition of coal is favoured for the syn-crude formation under the condition of DBD plasmas. This enhanced yield would be from the hydrogenation of coal (there is a plentiful of hydrogen species in the methane DBD plasmas). Since DBD plasma is a cold plasma phenomenon and can be operated at the ambient conditions, it is very potential to develop such combined conversions of coal and methane.

Acknowledgment

The support from the National Natural Science Foundation (under the contract number 29806011) is very appreciated. This investigation has been conducted using ABB donated instrument and the author is also grateful to ABB Corporate Research Ltd., Switzerland for the donation of instrument.

Reference

1. Pasquon, I. New trends in methane conversion and basic petrochemicals. *Bull. Soc. Chim. Fr.* **131**, 452-462(1994).
2. Liu, C.-J., Xue, B., Eliasson, B., He, F., Li, Y. and Xu, G.-H. Methane conversion to higher hydrocarbons in the presence of carbon dioxide using dielectric-barrier discharge plasmas, Plasma Chemistry & Plasma Processing，V.21, No.3,301-310, 2001
3. Eliasson, B., Liu, C.-J. and Kogelschatz, U. Direct Conversion of Methane and Carbon Dioxide to Higher Hydrocarbons Using Catalytic Dielectric-Barrier Discharges with Zeolites, Ind. Eng. Chem. Res., V.39, No.5, pp.1221-1227, 2000
4. Liu, C.-J., Eliasson, B., Xue, B., Li, Y. and Wang, Y.-Q. Zeolite-Enhanced Plasma Methane Conversion to Higher Hydrocarbons with Dielectric-barrier Discharges, Reaction Kinetics and Catalysis Letters (accepted)

PRODUCTION OF RICH HYDROGEN GASES IN FUEL CELLS

Zhang Xinrong[1], Shi Pengfei[1], Zhao Jianxi[2], Zhao Mengyue[3], and Liu Chuntao[1]

1.Applied of Chemical Department
Harbin Institute of Technology
No 92 Xidazhi Street ,Harbin, China
2.78 Cedar St. #1R, Wakefield, MA 01880
3.College of Chemical Engineering
Zhengzhou University
Wenhua road, Zhengzhou, China

Introduction

Currently, increasing attention is being paid to the low temperature steam reforming of methanol to produce high purity hydrogen to use as fuels in fuel cells for on-board power generation for vehicles. The favor for methanol as a chemical carrier for hydrogen is mainly due to its ready availability, high energy density, and easy storage and transportation. Hydrogen can be extracted in three different processes from methanol: (i)methanol decomposition (ii)steam reforming of methanol(SRM) and (iii) partial oxidation of methanol (POM; equations (1) – (3),respectively):

$CH_3OH \leftrightharpoons 2H_2+CO$ (1)

$\triangle H^0_{298}= + 92.0$ kJ mol^{-1}

$CH_3OH+H_2O \leftrightharpoons 3H_2+CO_2$ (2)

$\triangle H^0_{298}= + 49.4$ kJ mol^{-1}

$CH_3OH +(1/2)O_2 \leftrightharpoons 2H_2+CO_2$ (3)

$\triangle H^0_{298}= - 192.2$ kJ mol^{-1}

So far, the steam reforming of methanol reaction (equation(2)) was the only process considered for hydrogen production for fuel cell applications. Unfortunately, the reaction produces a considerable amount of CO (＞100ppm) as a by-product. As for the application of PEFC, even traces of CO(＞20ppm) in the reformed gas deteriorate a Pt electrode and the cell performance is lowered dramatically. A second-stage catalytic reactor has been suggested to remove the CO by water-gas shift reaction($CO+H_2O \leftrightharpoons CO_2+H_2$,WGSR, equation (4)) or CO oxidation which, in turn , requires additional space and equipment cost.

An ideal method to produce high concentration hydrogen with lower amount of CO is by steam reforming of methanol reaction over the high activity and selectivity catalysts. Now the most widely used catalysts for this reaction are copper containing catalysts since copper has been found to be highly active and selective for hydrogen. In the present study, we have prepared $Cu/ZrO_2/Al_2O_3$ ternary catalyst by coprecipitation method. Our studies were aimed at investigating the effects of ZrO_2 concentration, reaction temperature, H_2O/CH_3OH molar ratio, methanol space velocity and reaction time on the activity and selectivity and stability of the cataysts. The results show that the catalysts display great activity for methanol conversion and high selectivity for hydrogen and long stability. Maximum conversion of methanol 95.0 %, 100 mol.% hydrogen selectivity and CO molar fraction $1.45x10^{-6}$ were obtained in the steam reforming reaction at 250 ℃ with the catalyst containing 15.0 wt.% ZrO_2.

Experimental

Catalyst preparation. A mixed aqueous solution of copper nitrate trihydrate ($Cu(NO_3)_2.3H_2O$), zirconium oxychloride octethydrate ($ZrOCl_2.8H_2O$) and aluminum nitrate nonahydrate ($Al(NO3)_3.9H_2O$) and a solution of sodium carbonate are added slowly and simultaneously into 100ml of deionized water at 60℃ with vigorous stirring. The pH is kept constant at 7.0–7.2. The precipitates are aged at 60 ℃ for 30 min under vigorous stirring and then filtered and thoroughly washed with hot deionized water. The precipitates are dried overnight in air at 110℃ and calcined on a muffle oven at 500℃ for 3h . Each calcined catalyst are pelletized in a hydraulic press, crushed, and sieved into particle size ranging from 0.45–0.50mm and used as catalysts for the steam reforming of methanol reaction.

Activity measurement. Catalytic experiments were performed in a continuous flow fixed-bed microreactor (4mm i.d.) placed in an electrically heated furnace. The furnace temperature was controlled by a PID temperature controller through a K–type thermocouple inserted into the furnace. A separate thermocouple was used to monitor the temperature of the catalyst bed. This arrangement was capable of ensuring an accuracy of (±1℃) for the catalyst bed temperature. All run were conducted at reaction temperature in the range of 180-250℃ at atmospheric pressure. About 300–500mg of the catalyst was loaded in the reactor. A typical run for methanol–steam reforming (methanol space velocity of 3.28h^{-1} and feed consisting of a 1:1 molar mixture of methanol and water) was performed as follows: The catalyst was first reduced in situ in a premixed H_2/Ar (5/95(v/v)) flow of 80 ml min^{-1} from 120℃ to 300 ℃ with a heating rate of 1℃ min^{-1} and kept at this temperature for 3h before cooling to the reaction temperature. The feed was then pumped at the desired methanol space velocity to the vaporizer maintained at about 240℃. The vaporized feed from the vaporizer entered the reactor in a stream of Ar gas. The reaction products were analyzed on-line using HP 5890 gas chromatograph with thermal conductivity detector. The GC equipped with a 3m long Porapak-Q column and a 3m long Porapak-R column was able to detect the liquid products such as water, methanol, formaldehyde, methyl formate and dimethyl ether and the gaseous products such as H_2, CO, CO_2 and CH_4. The catalytic activity was evaluated from the data collected between 2h and 4h of the continuous operations. In order to check the stability of the catalyst, the reaction was also performed for a period of 200 h the continuous operation at 250℃. Blank run conducted with an empty reactor in the temperature range 180-250℃ did not show any detectable methanol conversion.

Results and Discussion

Table 1 Effect of ZrO_2 concentration on catalytic activity

No	ZrO_2 Wt. /%	$X(CH_3OH)$ /%	$Y(H_2)$/ mol(h.g)$^{-1}$	$S(H_2)$/ %	$y(H_2)$/ %	$y(CO)$/ 10^{-6}
1#	0	81.4	0.2509	100	75.0	1.60
2#	5	87.5	0.2697	100	75.0	1.65
3#	10	90.0	0.2774	100	75.0	1.47
4#	15	95.0	0.2928	100	75.0	1.45
5#	20	92.5	0.2851	100	75.0	1.44

Reaction conditions: p=0.1Mpa ; t=250℃ ; X is methanol molar conversion; Y is hydrogen productivity; S is selectivity ; y is molar fraction.

Table 1 shows a typical behavior of methanol conversion with catalyst ZrO_2 concentration. It is seen that initially shows an increase in methanol conversion with catalyst ZrO_2 concentration increasing between 0 wt.% and 15 wt.%, beyond 15.0 wt% ZrO_2, methanol conversion begins to fall. Maximum methanol conversion of 95.0 % is attained over the catalyst containing 15.0 wt.% ZrO_2. H_2 selectivity

is 100 mol.% in the experiment conditions, and CO concentration in reformed rich hydrogen gases is relatively little.

The effect of reaction temperature on catalytic performance is depicted in **Table 2**. Methanol conversion and hydrogen productivity increase with temperature increasing, methanol has almost converted into H_2, CO, CO_2 entirely at 280℃. In the temperature range180−250 ℃, hydrogen concentration and selectivity remain unchanged ,CO concentration is relatively little. On the other hand, CO concentration in reformed rich hydrogen gases increases with reaction temperature increasing.

Table 2 Effect of reaction temperature on catalytic activity

Temperature /℃	$X(CH_3OH)$ /%	$Y(H_2)$/ mol(h.g)$^{-1}$	$S(H_2)$/ %	$y(H_2)$/ %	y(CO)/ 10^{-6}
180	30.2	0.0931	100	75.0	1.06
200	56.4	0.1738	100	75.0	1.14
230	82.5	0.2543	100	75.0	1.21
250	95.0	0.2928	100	75.0	1.45
280	99.8	0.3076	100	75.0	4.46

Reaction conditions: the same as **Table 1**.

Figure 1 shows the effect of H_2O/CH_3OH molar ratio on the catalytic performance at 250℃. It can be observed that the methanol conversion and hydrogen productivity increase with H_2O/CH_3OH molar ratio increasing, beyond 1.3, methanol conversion increases relatively slowly. CO concentration decreases with H_2O/CH_3OH molar ratio increasing, water gas shift reaction accelerates with H_2O/CH_3OH molar ratio increasing according to equation (4), which promotes CO shifting to CO_2, so the experiment result displays that CO concentration decreases with H_2O/CH_3OH molar ratio increasing.

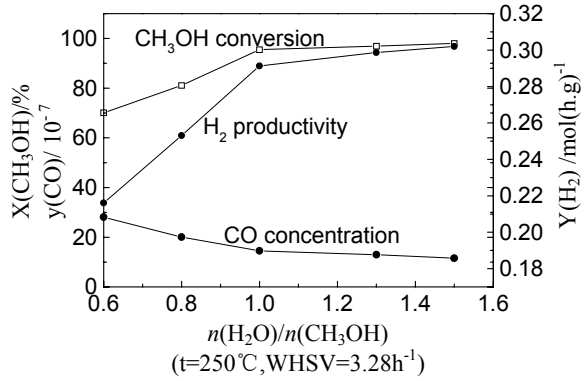

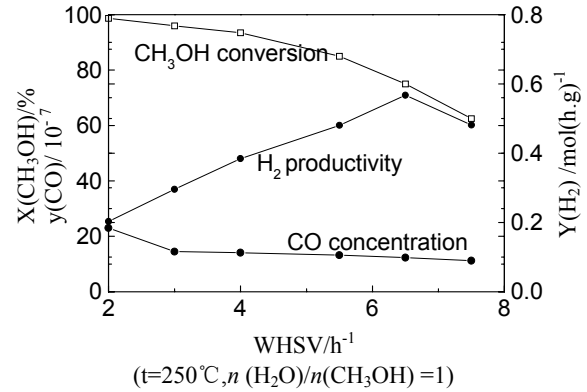

Figure1. Effect of H_2O/CH_3OH molar ratio on the reaction

Figure2. Effect of methanol space velocity on catalytic activity

Figure 2 shows the effect of methanol space velocity (WHSV) on the catalytic performance over $Cu/ZrO_2/Al_2O_3$ catalysts. Methanol conversion and CO concentration decrease with increasing methanol space velocity, hydrogen productivity has maximum in the experiment conditions. On the other hand, the methanol space velocity does not influence the selectivity of H_2, which remains 100% throughout the experiment. In the present study, a methanol space velocity of 3.28 h^{-1} has been chosen for the evaluation of the performance of the catalyst in the steam reforming reaction.

In order to investigate the stability of the catalyst during the steam reforming reaction, the continuous operation was performed at 250℃ over the catalyst with containing 15 wt. % ZrO_2 for a period of 200 h and the result is displayed in **Figure 3**. It can be seen that there is a small initial deactivation over the catalyst. After 30 hours of continuous operation, the methanol conversion remains almost unchanged throughout the period. As far as the product selectivity is concerned, there is no change in the selectivity of H_2, H_2 selectivity is still 100 mol.%.

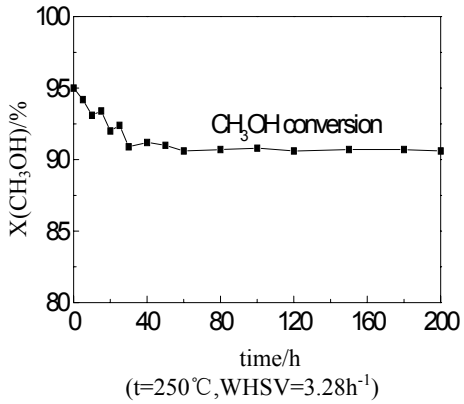

Figure 3.Effect of reaction time on catalytic activity

Conslusion

$Cu/ZrO_2/Al_2O_3$ ternary catalysts obtained from thermal decomposition of Cu/Zr/Al hydroxycarbonate precursors display great activity for methanol conversion and high selectivity for hydrogen and long stability. The catalytic activity increases with ZrO_2 concentration increasing between 0 wt.% and 15wt.%, the increase in the reaction temperature and H_2O/CH_3OH molar ratio also improves the catalytic activity, and the catalytic activity decreases with methanol space velocity increasing. Hydrogen selectivity and concentration remain unchanged in the experiment conditions, CO concentration in the reformed rich hydrogen gases is relatively little.

Acknowledgment

The authors acknowledge the financial support from the Guangyu Corp, China

References

1. Emonts B, Bogild J. *J Power Sources,* 1998**,** 71: 288-293.
2. Wies W,Emonts B. *J Power Sources,***1999**, 84: 187-193.
3. Amphlett J C, Mann R F. *J Power Sources,* **1998**, 71:179-184.
4. Velu S.Suzuki K, Kapoor M P. *Appl Catal A,* **2001**,213:47-64.
5. Dudfield CD,Chen R. *J Power Sources*, **2000**, 85:237-244.
6. Ledjeff−Hey K, Formanski V. *J Power Sources,* **1998**, 71:199.
7. Toshimasa U. Koshi S. *Appl Catal A*, **2000**,194:21-26.
8. Peppley B A, Amphlett J C. *Appl Catal A,* **1999**,179:21-29.

PRODUCTION OF SYN GAS / HIGH BTU GASEOUS FUEL FROM THE PYROLYSIS OF BIOMASS DERIVED OIL

S. Panigrahi, A. K. Dalai, and N. N. Bakhshi*

Catalysis and Reaction Engineering Laboratories
Department of Chemical Engineering
University of Saskatchewan
Saskatoon, SK. S7N 5C9, Canada
Phone: (306) 966-4771 Fax: (306) 966-4777
E- mail: Dalai@engr.usask.ca

Introduction

The gradual shortage of oil reserves has created considerable interest in using alternative source of energies, which are renewable in nature. As we enter the 21st century, new, clean burning, renewable fuels may revolutionize the energy industry. The renewable energy technologies (RET) of the European commission have the target of doubling their contribution from the present 5.6% to about 12% in the future[1]. Amongst all the renewable energy sources, biomass represents high potential and will play a vital role in the near future. Two approaches, namely pyrolysis and gasification of biomass, have been attempted to convert biomass into a useful form of energy[2,5]. The pyrolysis process is generally carried out by subjecting the biomass to a high temperature under an inert or oxygen deficient atmosphere. In the past, biomass was used for the production of hydrogen and medium Btu gas[6]. Extensive studies have been done on pyrolysis of cellulose, wood and biomass materials[7-12]. Waste biomass materials such as Kraft and Alcell lignins have been converted to hydrogen and medium Btu gas by steam gasification[6,13,14].

The fast pyrolysis process of biomass generally gives three products viz. gas, biomass-derived oil and char. The bio-oil thus produced contains unsaturated hydrocarbons and is thus highly unstable. This biomass-derived oil (BDO) has found a variety of applications in various areas. Unlike fossil fuels, BDO is renewable, cleanly burns, and is greenhouse gas neutral. It does not produce any SOx (sulfur dioxide) emission during combustion and produces approximately half the NOx (nitrogen oxide) emission in comparison with fossil fuels. Therefore, it is a potential raw material for renewable fuel and can be used as a fuel oil substitute[1-3]. However, several challenges are identified in bio-oil applications resulting from their properties. Extensive research on analyzing physical properties has been carried out earlier[15-20]. Rick and Vix have reviewed on product standards of BDO[21]. Most of the BDO are polar, viscous and corrosive, and contains 40-50 % oxygen. They have a high water content that is detrimental for ignition. Soltes and Lyn reported that most of the pyrolytic oils quickly form a solid mass when exposed to air[4]. Therefore, they can't be used as such as conventional fuel[5]. The conversion is due to the presence of organic acids in the oils. Over time, reactivity of some components in the oils leads to formation of larger molecules that result in high viscosity and in slower combustion[4]. Diebold and Czernik developed additives to stabilize the viscosity of biocrude during long-term storage, which demonstrated the ability to drastically reduce its aging rate, defined by the increase in viscosity with time[22].

Some research has been done on catalytic upgradation of BDO[14,23,24]. The product gas consisted of H_2 CO, CO_2. CH_4, C_2-C_4, higher hydrocarbons. The BDO has been converted to hydrogen via catalytic steam reforming followed by a shift conversion step[25,26]. The hydrogen yield was as high as 85%. Baker & Elliott have reported the catalytic upgrading of BDO produced at high-pressure conditions[27]. The yield of gasoline range hydrocarbons was 60-90%. The bio-oil thus produced contained unsaturated hydrocarbons and was highly unstable. An attempt has been made in this research to produce clean fuels including hydrogen, high Btu gaseous fuel and synthesis gas by pyrolysis of BDO in the absence of a catalyst. In this work, the reactor temperature and inert gas flow rate were varied from 650 to 800 ^{0}C, and from 18 to 54 ml/min, respectively. In all experiments, the BDO flow rate was maintained at 4.5-5.5 g/h.

Table 1. Properties of Biomass and BDO

Biomass Feedstock	Pine/ Spruce 100% wood[33]	Pine/ Spruce 53% Wood 47% bark [33]	Bagasse [33]	BDO (used in the present study)
Moisture, wt.%	2.4	3.5	2.1	- -
Ash Content, wt.%	0.42	2.6	2.9	
Bio-oil				
PH	2.3	2.4	2.6	2.5
Water Content, wt.%	23.3	23.4	20.8	21.5
Lignin Content, wt.%	24.7	24.9	23.5	25.0
Solids Content, wt.%	< 0.10	< 0.10	< 0.10	-
Ash content, wt.%	< 0.02	< 0.02	< 0.02	0.16-0.18
Density, g/cc @20^{o}C	1.20	1.19	1.20	1.18-1.24
Calorific Value, MJ/kg	16.6	16.4	15.4	17.5-19.1
Kinematic Viscosity				
cSt @20^{o}C	73	78	57	110
cSt @40^{o}C	-	-	-	45.6
cSt @80^{o}C	4.3	4.4	4.0	-

Experimental

Biomass-derived oil was obtained from DynaMotive, which was produced from Asphene wood materials using a patented technology[28]. On an average, 1 kg (dry) of biomass produces 0.75 kg of oil, 0.1 kg of char and 0.15 kg of gas[29]. Biomass derived oil is a liquid mixture of oxygenated compounds containing various chemical functional groups such as carbonyl, carboxyl and phenolic[30,31]. Biomass derived oil is made up of the following constituents: 20-25 % water, 25-30% water insoluble pyrolytic lignin, 5-12 % organic acids, 5-10% non polar hydrocarbons, 5-10% anhydrosugars and 10-25 % other oxygenated compounds[31].

The water includes those present in the wood 5-8% (see Table 1) as well as that is produced during the pyrolysis. Elemental analysis showed that the biomass-derived oil contained 43.6 wt % C, 8 wt. % H, 0.5 wt % N, and 47.9 wt% was O (obtained by difference). The viscosity of the fresh biomass-derived oil at 25 ^{0}C was 8x10^{-2} pa.s, which increased slowly upon storage[32].

Experimental Procedure. The experimental set-up used in our research consisted of an Inconel tubular continuous down flow micro reactor (12.7 mm i.d. and 200 mm long, placed co axially in the furnace). The reactor contained quartz chips (used for better temperature distribution and to avoid high pressure drop in the reactor) through which desired flow of an inert gas such as nitrogen was maintained through a Brooks mass flow controller (Model 0152/0154). The reactor temperature was controlled using a temperature controller using a thermocouple attached to the outer wall of the reactor and connected to the temperature controller. The temperature was measured by placing a thermocouple at the center of the quartz bed. A schematic diagram of the experimental set up used for the pyrolysis of BDO is shown in **Figure 1**. In this study, the reactor temperature was varied in the range of 650 to 800 ^{O}C where as the carrier gas flow rate was varied from 18 to 54 mL/min (STP). Biomass-derived oil was introduced at a predetermined rate using a micro metering syringe pump (Eldex, model A-60-S) at the rate of 4.5-5.5 ml/hr through a specially designed nozzle, which helped to spray liquids into the reactor along with the inert gas. Each experiment was performed at atmospheric pressure only for a period of 30-45 min, depending upon the operating conditions. In most cases, the run was terminated after 30 minute of operation. At the end of the run, the pump and the heating of furnace were shut off and the reactor was cooled down to the ambient temperature. The reactor was then removed from the reaction system and was weighed to determine the amount of coke formed. The product gas was cooled with a water-cooled heat exchanger and then with an ice-salt bath (to liquefy the condensable) before it was collected over saturated brine solution. The condensed liquid product was retained in a trap cooled by an ice-salt mixture and weighed. After each run, the mass of the gas, char and condensed liquid were calculated for bio oil conversion and mass balance.

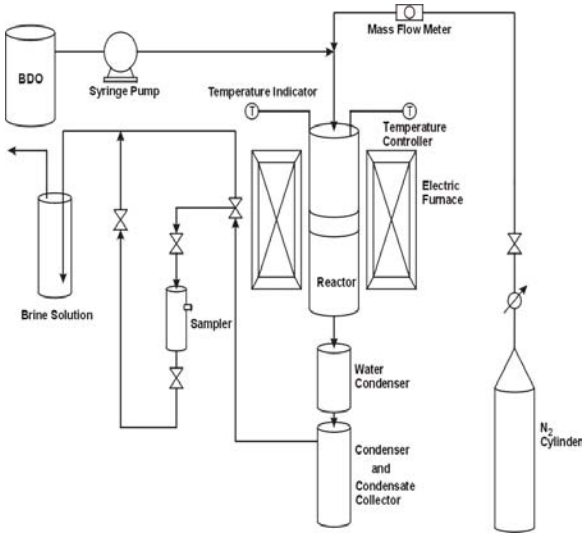

Figure 1: Schematic diagram of experimental setup for pyrolysis of BDO.

Product Gas Analysis. It may be noted that the reactor had a long preheating section. Thus, there was sufficient time for the BDO to achieve desired temperature in the reactor to crack and to produce gas, coke and liquid. The amount of the product gas was measured for each experiment, and was analyzed for its compositions using two GCs (Carle GC-500 series and HP5890). The HP5890 GC was equipped with a thermal conductivity detector and Carbosive S II column and analyzed H_2, CO, CO_2 and CH_4 where as the Carle GC, equipped with a flame ionization detector and combination of packed and capillary columns (Stable wax), analyzed hydrocarbons. Temperature programming of the oven was used in this case for analysis of the product gas.

Results and Discussion

The properties of BDO used in our study are compared to those reported in literature (see Table 1). The data in **Table 1** indicate that the properties of BDO are quite comparable to those obtained from other sources. In this investigation the effects of reactor temperature and the nitrogen flow rate on the BDO conversion and product gas composition was studied. The material balance for each experiment was found to be between 92-98wt.%.

Effect of Nitrogen Flow Rate. The effects of nitrogen flow rate (18 to 54 mL(STP)/min) on the conversion of BDO, product gas yield and its composition have been studied at constant pyrolysis temperature of 800 ^{0}C and contact BDO flow rate of 4.5 mL/h and the results are shown in **Figure 2**.

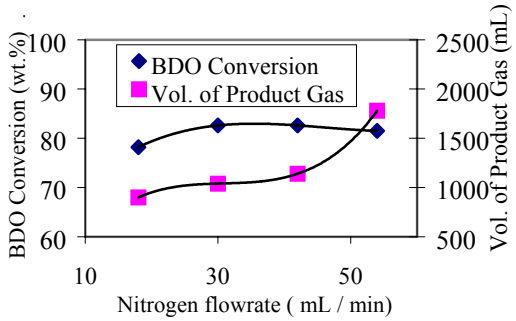

Figure 2 Effects of carrier (nitrogen) gas flow rate on conversion of BDO and volume of gas produced during pyrolysis of BDO at 800 0C and BDO flow rate of 4.5 mL/h

By varying nitrogen flow rate from 20 to 30mL/min, the conversion of BDO to gas and char was increased from 75 to 83wt.%. The increased conversion of BDO may be due to the increased heat and mass transfer caused due to the turbulences created by the higher flow rate of nitrogen. Beyond nitrogen flow rate of 30mL/min, the conversion of BDO was ~ 83wt.% and did not change with respect to nitrogen flow. It was also observed that with the increase in flow rate of nitrogen, the amount of gaseous product was increased. For example, the volume of product gas was increased from 900 to 1780 ml by changing the nitrogen flow rate from 18 to 54 ml/min i.e., from 100 grams of BDO, 39 l and 65 l of product gas were obtained at N_2 flow rates of 18 and 54 ml/min, respectively. Higher gas yield at higher nitrogen flow could be due to higher syn gas production, which is explained below.

The effect of nitrogen flow rate on product gas composition was also evaluated and is shown in **Figure 3**. It is observed that the production of hydrogen remained approximately constant with the

increase in nitrogen flow rate from 18 to 45 mL/min. However, there is a sharp increase in the hydrogen production with further increase in nitrogen flow rate. The formation of methane was high 30 mol% at lower nitrogen flow rate of 20 mL/min. Higher residence time due to low flow rate of nitrogen is responsible for cracking of BDO producing more methane. At higher flow rate (42-54 mL/min) of N_2, the concentration of methane was low (~20-24 mol%). At 800 ^{0}C methane could react due to partial oxidation and combustion producing more hydrogen. CO gas yield was increased when the nitrogen flow was increased from 18 to 54 ml and reached maximum for N_2 flow of 42 – 50 mL/min. This may be due to the reaction of CO_2 with carbonaceous material producing more CO. The total amount of synthesis gas (hydrogen and CO) also increased from 22 to 65 mol% as nitrogen flow increased from 18 to 54 mL/min. The effect of nitrogen flow rate on the production of other gases such as ethane and higher hydrocarbons was not very significant.

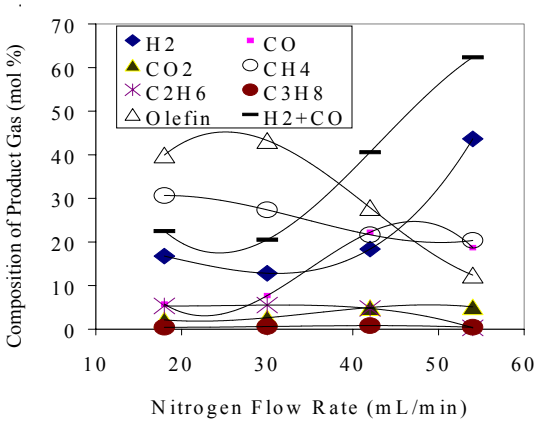

Figure 3. Effects of carrier (nitrogen) gas flow rate on product gas composition for pyrolysis of BDO at 800 0C and BDO flow rate of 4.5 ml/h

The effects of N_2 flow rate on total olefin production and its distribution are shown in **Figure 3** and **Table 2**, respectively. The production of olefins (mostly ethylene and propylene) initially after showing a slight increasing trend followed a decreasing pattern with nitrogen flow rate (see Figure 3). The olefin content of approximately ~ 43mol% was obtained corresponding to a nitrogen flow rate of 30mL/min (see Table 2). Probably at lower N_2 flow rate (20-30 mL/min) BDO had higher residence time for cracking and thus producing more olefins. At higher flow rate (42-54 mL/min) of N_2, the concentration of olefins was lower (~10-25 mol%) where as syn gas formation was higher.

Table 2. The Effects of N_2 Flow Rate on Total Olefin Production and its Distribution at a Reaction Temperature of 800 ^{0}C

Nitrogen flow	C_2H_4, mol%	C_3H_6, mol%	Higher C_3H_6 Olefins, mol%	Total olefins, mol%
18	31.5	3.8	3.6	38.9
30	31.1	3.1	9.0	43.2
42	18.4	2.4	7.1	27.9
54	6.9	0.1	4.4	11.4

The effect of nitrogen flow at 800 ^{0}C on the heating value of product gas is shown in **Figure 4**. Due to optimum production of hydrocarbons at a nitrogen flow rate of 30mL/min and 800 ^{0}C, the heating value of gas was high (1738 Btu/SCF). At these conditions, the conversions of bio-oil and olefin yield were as high as 83 wt.% and 43mol%, respectively. However, the syn gas yield of 65mol % was optimum at nitrogen flow rate of 54mL/min at 800 ^{0}C (See Figure 3).

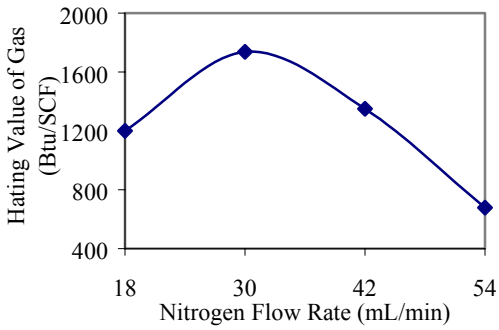

Figure 4. Effects of carrier (nitrogen) gas flow rate on total heating value of produt gas during pyrolysis of BDO at 800 ^{0}C

Effects of temperature. The effects of temperature (650-800 ^{0}C) on the conversion of bio-oil, gas yield and its composition have been studied keeping nitrogen and bio-oil flow rates constant, respectively, at 30mL/min and 4.5g/h. Effects of temperature on conversion of BDO and volume of gas produced are shown in **Figure 5**. The results show that as the temperature is increased from 650 to 800 ^{0}C, the conversion of bio-oil to gas and char is increased from 57 to 83 wt. %. Also, as expected, the production of gas is increased with temperature. For example, the product gas volumes obtained at 650 and 750 ^{0}C were 730 and 1020 mL, respectively. This corresponds to the fact that from 100 grams of BDO, 26 l to 45 l of gas could be produced with increase in temperature from 650 to 750 ^{0}C at constant N_2 flow rate of 30 mL/min. However, beyond this temperature, its effect on the gas production was negligible.

Table 3. The Composition Data as a Function on Temperature at Nitrogen Flow Rate of 30 mL/min

Temp., ^{0}C	H_2, mol %	CO, mol %	CO_2, mol %	CH_4, mol%	C_2H_6, mol%	C_3H_8, mol%	Total olefin, mol%	Total
650	12.8	17.0	2.5	19.2	7.2	0.9	40.3	99.9
700	16.3	9.2	3.4	21.6	7.2	1.1	41.2	99.8
750	9.3	6.5	2.1	23.2	9.0	1.3	48.5	99.9
800	12.8	7.7	2.6	27.4	5.5	0.6	43.2	99.8

The effects of temperature on the product gas composition and olefins formed from BDO are given in **Table 3**. It is also evident from data in this table that the production of maximum olefins is at 48.5 mol% at 750 ^{0}C. The methane concentration increases from 19.2 to 27.4 mol% as the temperature increases from 650 to 750^{0}C. Thus it is possible to produce a gas stream having an olefin content of as high as ~48-mol % from BDO. The results also show that the concentration of CO_2, C_2, C_3 paraffin do not change with temperature.

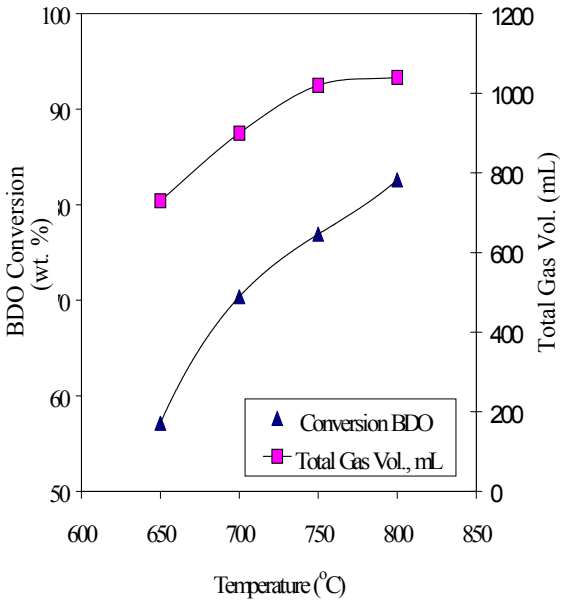

Figure 5. Effects of temperature on conversion of BDO and volume of gas produced during pyrolysis of BDO at a nitrogen flow rate of 30 mL (STP)/min

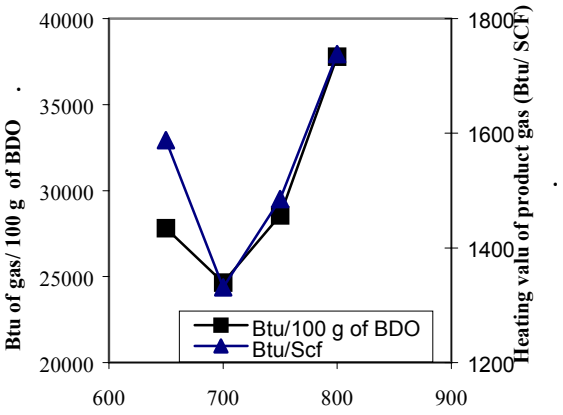

Figure 6. Effects of temperature on heating value of product gas for pyrolysis of BDO at nitrogen flow rate of 30 mL/min.

The effects of reaction temperature on the olefins composition are shown in **Table 4**. The effects of reaction temperature on the heating value and energy content of the gas produced at nitrogen flow rate of 30 mL/min are shown in **Figure 6**. The results indicate that the heating value of the product gas was increased from 1300 to 1700 Btu/SCF with increase in temperature from 700 to 800 ^{0}C. This could be due to increase in methane concentration from 19 to 27 mol % in the product gas.

Table 4. Effects of Temperature on Distribution Olefins Formed During the Pyrolysis of BDO at a Nitrogen Flow Rate of 30 mL/min and BDO Flow Rate of 4.5 –5.5 mL/h

Temperature ^{0}C	C_2H_4, mol%	C_3H_6, mol%	Higher C_3H_6Olefins, mol%	Total olefins, mol%
650	20.8	9.4	10.1	40.3
700	23.0	9.1	9.1	41.2
750	26.4	10.2	12.0	48.6
800	31.1	3.1	9.0	43.2

It is observed that the concentration of olefins (of which 60-70 mol % is ethylene) is varied in a range of 40 to 48mol % in the product gas with increase in temperature from 700 to 800 ^{0}C. However, syn gas production is decreased by 20 mol % in spite of higher production of hydrogen with the temperature increase. The increase in hydrogen production with increased temperature occurred probably because at high temperatures pyrolysis of the BDO sub-units, which evolved more hydrogen.

Conclusions

The present study identifies the pyrolysis of biomass-derived oil as a source of gaseous fuel. In this process, the product gases essentially consisted of H_2, CO, CO_2, CH_4, C_2H_4, C_2H_6, C_3H_8, and C_4^+ components. This process can be utilized for producing hydrocarbons and synthesis gas for various applications. By adjusting the parameters such as inert gas flow rate and reactor temperature, the composition of the product gas from biomass-derived oil can be tuned in the desired direction. The conversion of biomass-derived oil at a flow rate of 4.5 – 5.5 g/h could be increased from 57 to 83 wt.% due to increasing the reactor temperature from 650 to 800 ^{O}C at a nitrogen flow rate of 30

mL/min. At 800 ^{0}C and nitrogen flow rate of 30 mL/min, composition of various product gas components ranged between: Syn gas 16-30 mol %, CH_4 19-27 mol % and C_2H_4 23-31 mol %. A large amount of total product gas was obtained from BDO at 800 ^{0}C and N_2 flow rate of 30 mL/min. Heating values ranged between 1300 – 1700 Btu/SCF. Thus, the present study shows that there is a strong potential for making syn gas, methane, ethylene and high heating value gas from the pyrolysis of biomass-derived oil.

References

1. Chantal, P.D; Kaliaguine, S; Grandmaison, K.L; Mahay, A. *Appl. Catal*. **1984**, *10*, 317.
2. Sharma, R.K; Bakhshi, N.N. *DSS contract file # 23440-0-9467/01-SZ*, *Bio-energy Dev. Prog., Energy Mines and Resources, Ottawa,* **1992**
3. Diebold, J; Soltes, E.J; Miline, T.A. *ACS Symp. Ser.376, Amer. Chem. Soc., Washington, DC*, **1988**, 264.
4. Soltes, E.J; Lin, S.L. *ACS Symposium Series* **1987**, *264*, 178-185.
5. Churin, E.P; Grange, B. *Elseiver Appl. Sci., London, UK*, **1990**. *2,* 616
6. Chaudhari, S.T; Ferdous, D; Dalai, A.K; Bej. S.K; Thring, R.W; Bakhashi, N.N. *Fifth International conference on Biomass Conversion, Austria*, **2000**
7. Boutin, O; Ferrer, M; Lede, J. *J. Anal. Appl. Pyrol.* **1988** *47,* 13.
8. Radlein, A.G.D; Piskorz, J; Scott, S.D. *J.Anal. Appl. Pyrol.* **1987***,12*, 51.
9. Piskorz, J; Radlein, A.G.D; Scott, S.D; Czernik, S. J. *Anal. Appl. Pyrol.* **1989**, *16*, 127.
10. Liu, N.A; Fan, W.C. *Fire and Materials.* **1998**, *22,*103.
11. Koullas, D.P; Nikolaou, N; Koukios, E.G. *Bioresource Energy,* **1998**, 63: 261.
12. Maschio, G; Lucchesi, A; Stoppato, G. *Bioresource Technology,* **1994**, *48*, 119.
13. Iqbal, M; Dalai, A.K; Thring, R.W; Bakhshi N.N. *33rd International Engineering Conference on Energy Conversion, Colorado,* **1998**.
14. Bakhshi, N.N; Dalai, A.K; Thring R.W. *Division of Fuel Chemistry, 217th ACS National Meeting, California,* **1999**, *4,* 278.
15. Elliot, D.C. *IEA Co-operative project D1 Biomass liquefaction Test Facility project , Washington, Pacific Northwest Laboratory*, **1983,** *4*, 87.
16. Bridgwater, A.V; Kuester, J.L. *Research in thermo chemical biomass conversion, Phoenix, Arizona, New York: Elsevier Applied Science,* **1988,** 1177.
17. Milne, T.A; Brennan, A.H; Glenn, B.H. *Sourcebook of methods of analysis for biomass and biomass conversion process.* London, Elsevier Applied Science, **1990,** 327.
18. McKinley, J.W; Overend, R.P; Elliott, D.C. In *Proc. Biomass pyrolysis oil properties and combustion meetings,* Estes Park, CO. Golden, CO: NREL. NREL-CP-430-7215, **1994,** 34.
19. Diebold, J.P; Milne, T.A; Czernik, S; Oasmaa, A; Bridgwater, A.V; Cuevas, A; Gust, S; Huffman, D; Piskorz, J. *Development in thermo chemical biomass conversion. Banff.* Glasgow: Blackie Academic and professional, Eds.; **1997**,*1*, 533.
20. Piskorz, J; Radlein, D; Majerski, P; Scott, D.S. In *Proc. Biomass pyrolysis oil properties and combustion meetings*, Estes Park. CO. Golden. CO. NTIS, **1994**, 22.
21. Rick F, and Vix U. In Bridgwater, A.V; Grassi, G. *Biomass Pyrolysis liquids upgrading and utilization. London & New York: Elsevier Applied Science,* Eds.; **1991**. 177-218.
22. Diebold, J.P; Czernik, S. *Energy & Fuels,***1997***, 11(5)*, 1081.
23. Mathews JF, Tepylo MJ, Eager RL and Pepper JM. *Can. J. Chem. Eng.,* **1985**, *63*, 686.
24. Srinivas, S.T; Dalai, A.K; Bakhshi, N.N. Can. J. Chem. Eng., **1985,** *78*, 343.
25. Wang, D; Czernik, S; Montane, D; Mann, M; Chornet, E. *Industrial and Engineering Chemistry Research***, 1994,** *36(5)*, 1507.
26. Czernik, S; Wang, D; Chornet, E. *Proceedings of the 1998 U.S. DOE Hydrogen Program Review*, 28-30 April, Alexandria, Virginia. NREL/CP-570-25315. National Renewable Energy Laboratory,**1998,** *2*, 557.
27. Baker, E.G; Elliot, D.C. *Thermo chemical Biomass Conversion,* Eds.; Elsevier Appl. Sci., London UK, **1988,** 883-895.
28. Cottam, M.L; Bridgwater, A.V. *Thermo chemical Biomass Conversion,* Blackie Academic and Professional, London, Eds.; **1994**, *2*, 1343.
29. Bridgwater, A.V. *Advances in Thermo chemical Biomass Conversion* Blackie Academic and Professional, London,Eds.; **1994**, *2*, 1314.
30. Bridgwater AV, In *Fast Pyrolysis of Biomass: A handbook,* Eds.; PL Press. **1999**.
31. Morris, K.W. *4th Biomass conference of Americas,* **1999**.
32. Piskorz, J. *United States Patent* No. 5,728,271.
33. Morris, K.W; Johnson, W; Thamburaj, R**.** *1st World Conference and Exhibition on Biomass for Energy and Industry in Seville, Spain,* **2000**.

Reaction Behavior of Fischer-Tropsch Synthesis in Near Critical and Supercritical Hexane Media

*Xiwen Huang, Christine W. Curtis, Christopher B. Roberts**

Department of Chemical Engineering
Auburn University
Auburn, AL, 36849

Introduction

Supercritical fluids (SCFs) can offer certain advantages over traditional solvents for catalytic reactions including the ability to manipulate the reaction environment through simple changes in pressure to enhance solubility of reactants and products, to eliminate interphase transport limitations, and to integrate reaction and separation unit operations. SCF solvents offer attractive physical properties including; low viscosity and high diffusivity resulting in superior mass transfer characteristics; low surface tension enabling easy penetration into the pores of a solid matrix (catalyst) for extraction of nonvolatile materials from within the pores; high compressibility near the critical point inducing large changes in density with very small changes in pressure and/or temperature enabling separation of the dissolved material easily and completely. These unique properties of SCFs have been exploited to provide many opportunities for the design of heterogeneous catalytic reaction systems such as ethylene polymerization, ammonia synthesis and methanol synthesis.

The advantages of SCF-phase Fischer-Tropsch (FT) synthesis (SCF-FT) include gas-like diffusivities and liquid-like solubilities which together combine the desirable features of the gas- and liquid-phase FT synthesis routes[1-5]. The supercritical phase reaction can also (1) reduce production of undesirable products; produce less methane because of better distribution of heat in the reactor; (2) produce more long-chain olefins as a result of the enhanced solubility of these higher hydrocarbons in the SCF; (3) mitigate deactivation of the catalyst through better heat and mass transfer; (4) provide in-situ extraction of heavy hydrocarbons from the catalyst surface and their transport out of the pores thereby extending catalyst lifetimes; (5) enhance pore-transport of the reactants such as hydrogen to the catalyst surface thereby promoting desired reaction pathways; (6) enhance desorption of the primary products preventing secondary reactions that adversely affect product selectivity.

In this paper, we will investigate the FT reaction under supercritical hexane conditions in a continuous, high pressure, fix-bed reactor by employing a cobalt catalyst (15%Co-0.5%Pt-Al_2O_3). The effect of SCF conditions on syngas conversion, product distribution and olefin selectivity will be presented in order to demonstrate improvements in process parameters under SCF-FT operation versus gas phase operation. In addition, the effects of isothermal pressure-tuning on the catalyst activity, product distribution, and olefin selectivity will be examined. In the near critical and supercritical region, optimal combinations of product desorption and pore transport can be obtained. Finally, the syngas space velocity was varied to determine whether the primary and/or secondary reaction steps are diffusion controlled.

Experimental

Reactor Design. The reactor (HIP Equipment, Erie, Pa) used in this study is a conventional downflow fixed bed reactor. The cobalt catalyst (United Catalyst Inc.) is fixed in the middle of the fixed-bed. To fix the catalyst in place, a 15mm (diameter), 2-3mm (thickness) and 4-15micron (porosity) fused quartz disc (Quartz Plus, Inc.) is put inside the reactor. In order to position the disc in the middle of the reactor, the inner diameter of the reactor above the disc was machined exactly to match the disc diameter, which is a little larger than the section underneath the disc. The quartz disc was employed to avoid the use of any Fe-containing metal near the reaction zone. A profile thermocouple with 6 equally-spaced thermocouple probes(OMEGA) is located along the axial reactor tracking the temperature distribution in the reactor.

Delivery, Reaction and Analysis Systems. Syngas (AirProducts) flow rate was controlled by a mass-flow controller (5850E Brooks) and hexane was delivered through an HPLC pump (Acuflow Series III, Fisher). The hexane and syngas were combined in the static mixer (OMEGA) before entering the reactor. The reactor was situated in a furnace (Applied Test System Inc.) with a programmed temperature controller system. The reaction pressure is adjusted using a backpressure regulator (Tescom, Inc.) located between the reactor and a hot trap. After leaving the reactor, the products passed through a hot trap (200 ^oC) to condense some heavy components prior to the on-line GC analysis. All of the lines between the reactor outlet and the GC were heated to 200 ^oC preventing product condensation. Two GCs were used for the analysis system, which included; Varian 3300 GC with a capillary column (DB-5) and FID for the analysis of C2-C30 hydrocarbons and oxygenates; Varian CP-3800 with packed column (Hayes-DB100/120) and TCD for the analysis of permanent gases and C1-C3 hydrocarbons.

Reaction Procedure. The cobalt catalyst is so highly hygroscopic that it needed to be heated for an extended period of time (>24 h) at 150^oC to remove absorbed water. CO was used to reduce the catalyst at 280^oC, 100psi for 20hrs before the reaction initiated. Once the HPLC pump flow rate was checked to guarantee a steady-state flow rate, hexane flow is directed to the reaction system. With hexane flowing, the temperature and pressure of the reaction zone is raised to 250C and the particular pressure for the experiment. The hot trap and the transfer line to the GC were heated to 200C to absolutely insure the stream directed to the GC would experience no condensation while being directed to the GC.

Once the temperature and pressure were stabilized, the flow of syngas was initiated. The mass flow controller is set to the appropriate value and control commenced. All the reactions were continued until a steady-state with respect to conversion and selectivity are attained. When the reaction was halted, the syngas flow is stopped while maintaining the hexane flow. Once the FT products were no longer detected in the effluent, the pressure was reduced to 100psi and the flow of hexane is stopped, helium flow was started and the temperature of catalyst bed was allowed to drop to room temperature with helium flowing over it.

Reaction Conditions

Reactor	Stainless steel, D=1.27cm, L=25.4cm, V=32 cm^3
Catalyst	15%Co-0.5%Pt-Al_2O_3
Solvent	Hexane (Pc=29.7bar, Tc=233.7C), flowrate:1.0 ml/min
Syngas	Space velocity: 50 sccm/g cat; Ratio: H_2/CO: 2.0
Pretreatment	Reducing gas:CO; Flowrate: 50sccm; Time: 20 hr; Temperature: 280°C
Reaction Conditions	Temperature: 250^oC (1.07Tc); Pressure: 500psi, 600psi, 950psi, 1160psi Time: until steady state and keep steady state for 10h

Results and Discussion

1. Comparison of Gas-Phase and Supercritical Phase Fischer-Tropsch

1.1 Syngas Conversion. Figure 1 presents the syngas conversion in gas-phase and SCF-phase Fischer Tropsch synthesis. From this figure, we can see that the CO conversion is slightly higher in the supercritical phase than in the gas phase. This result suggests that the SCF-FT could increase the syngas conversion.

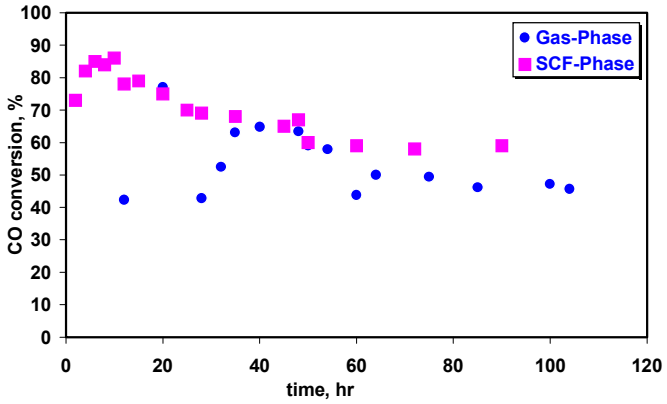

Figure 1. CO Conversion in Gas- and SCF-Phase Reaction. The pressure in the SCF phase reaction was 1160 psi and the pressure in the gas phase was 290 psi.

1.2 Hydrocarbon Distribution. Figure 2 and 3 presents the hydrocarbon distribution under gas- and SCF- phase operation. From these figures, we can see that in the supercritical phase, the whole hydrocarbon distribution diagram is shifted to a higher carbon number, and the methane content is decreased. Interestingly, the mass percents of C11 to C17 are fairly constant in the SCF experiment. The reason is that in the supercritical phase, the higher diffusivities and desorption rates of heavy hydrocarbons could cause the heavy product to diffuse easily from the catalyst bed along with the lighter compounds, rather than remaining in the catalyst.

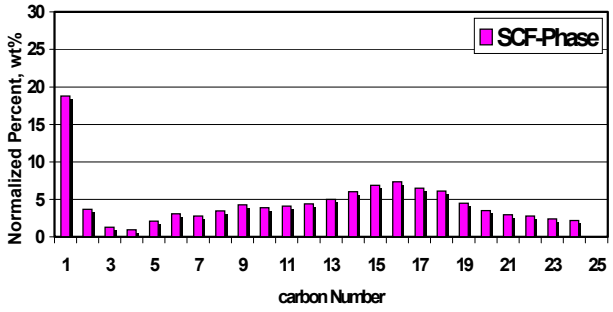

Figure 2. Hydrocarbon Distribution in SCF-Phase FT synthesis at 1160 psi.

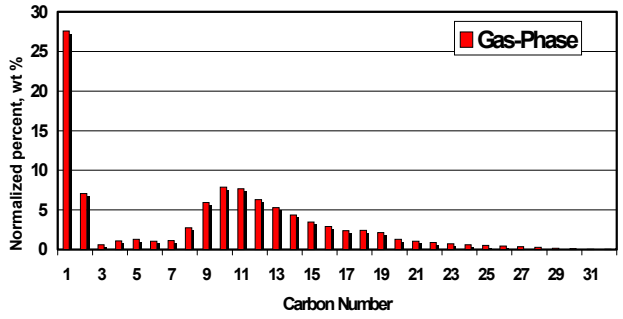

Figure 3. Hydrocarbon Distribution in Gas-Phase FT synthesis at 290 psi.

1.3 1-Olefin Selectivity. The initial product in the Fischer Tropsch reaction is the olefin species. In the case of mass transfer and heat transfer limitations, the olefin products can not flow out of the catalyst pores as soon as they are produced so as to cause many secondary reactions to take place, such as hydrogenation and isomerization to form paraffins. If the supercritical medium could improve the diffusivity and desorption rate of the product, then the secondary reactions would be reduced and the olefin selectivity would consequently increase. Figure 4 presents the olefin selectivity in the supercritical phase and gas phase. From this figure, we can see that the olefin selectivity in the SCF phase is obviously higher than in gas phase. This is in agreement with the situation discussed above. The enhanced selectivity of heavy olefins is due to the higher diffusivities and desorption rates. Without the intraparticle diffusion limitations, the primary products can leave the catalyst pores without undergoing secondary reactions.

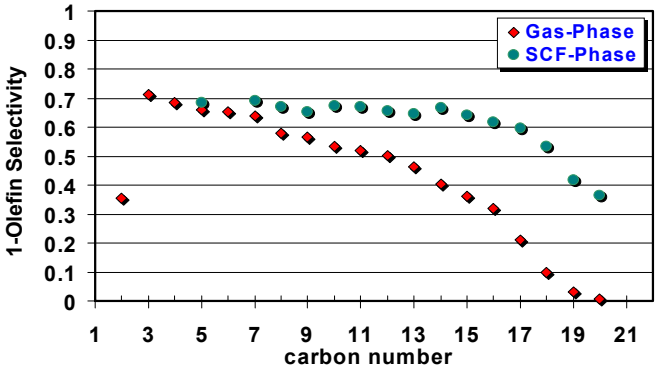

Figure 4. 1-Olefin Selectivity in Gas- and SCF-Phase FT synthesis

1.4 Temperature Distribution. The supercritical medium has a better heat removal ability compared to the gas phase. The FT reaction is an exothermic process in which a large amount of heat is given off during the reaction process. If the heat transfer process is so slow as to create excessive heat, then it will coke the catalyst shortening the catalyst lifetime. Figure 5 presents the temperature profile along the length of the reactor under both SCF phase and Gas phase operation. Thermocouple postion 3 is just above the catalyst bed and the distance between each thermocouple is 1.4 inches. The temperature deviation is from 247 to 261°C in the gas phase where the temperature deviation is only from 253 to 258°C in the SCF phase. Therefore, the temperature deviation is 3 times greater in the gas phase than in the SCF phase. It should also be noted that the CO conversion in the SCF phase experiment presented in Figure 5 was 70% where the conversion in the gas phase experiment was only 40%. Therefore, if the conversions were matched the temperature difference between the gas phase and SCF phase would be even more dramatic. From this we can conclude that a better heat transfer rate could be obtained in the supercritical reaction medium relative to the gas phase reaction.

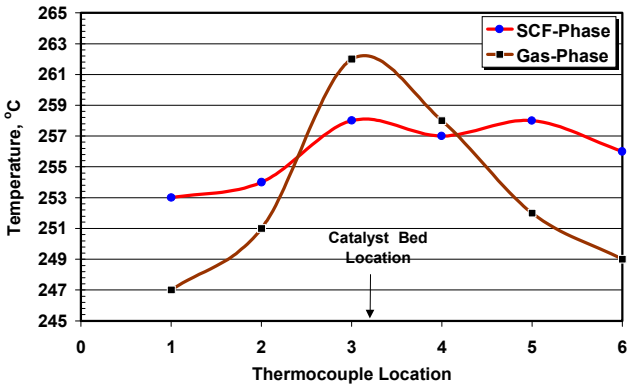

Figure 5. Temperature distribution in Gas- and SCF-Phase. The pressure in the SCF phase experiment was 1160 psi and the pressure in the gas phase experiment was 200 psi.

2. Effect of Pressure-tuning on the reaction behavior

According to Professor Subramaniam,[2] "the physical and transport properties of the fluid can be altered drastically from gas-like to liquid-like behavior, simply by isothermally varying the pressure around the critical pressure. At slightly above the critical pressure, while the fluid possesses roughly 70% of the liquid density, the diffusivity and viscosity are more gas-like. By pressure-tuning fluid properties around the critical pressure, optimal combinations of product desorption and pore transport can be obtained."

2.1 Syngas Conversion. Figure 6 presents the effect of pressure on the CO conversion. From this result we can see that the conversion increases with the pressure from 500psi to 950psi. As the pressure is increased the hexane medium posses a more liquid-like density enabling extraction of more heavy hydrocarbons from catalyst pores and maintains wider pore channels to reduce pore diffusion limitation. Meanwhile, this SCF environment maintains the high gas-like diffusivity. This combination results in the increase in conversion with increasing pressure up to 950psi. However, when the pressure is increased to a certain point (in our case 950psi), the conversion can not continue to increase. At this point it begins to decrease with a further increase in pressure. Beyond this transition point, the further increase in pressure still increased the hexane medium density which further increases the ability to extract heavy products. But, on the other hand, the bulk diffusivity decreases at these higher pressures and the comprehensive result is that the negative decrease in bulk diffusivity outweighs the positive enhancement in pore diffusivity. So, the conversion ceases to increase with further increases in pressure.

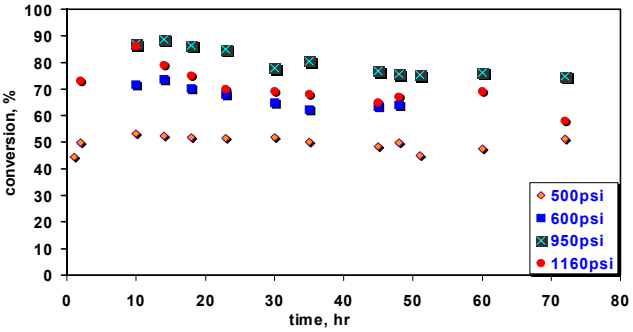

Figure 6. Effect of Pressure-Tuning on CO conversion.

2.2 Hydrocarbon Distribution Figure 7 presents the overall product carbon number distribution at different pressures in the SCF FT reaction. From this figure, we can see that at the higher operating pressure, more heavy hydrocarbon products could be obtained. This again supports the assertion that the decreased pore diffusion limitation at the high pressure is due to enhanced extraction of the heavier hydrocarbons by the more dense medium.

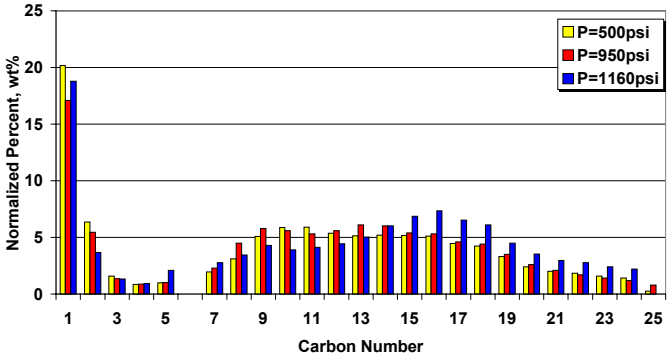

Figure 7. Effect of Pressure-Tuning on the Hydrocarbon Product Distribution in SCF FT synthesis.

2.3 1-Olefin Selectivity The effect of pressure on the olefin selectivity is also apparent in Figure 8. With an increase in pressure from 500 psi to 950 psi, the olefin content increases because of the improved extraction ability of the more dense medium. This results in an increase in pore diffusion efficiency, and an increase in the solubility of heavy products from the inner pores. This could result in a reduction in the readsorption of the 1-olefin thus reducing secondary reactions to form paraffin and 2-olefin products. Once the pressue was raised from 950 psi to 1160 psi, the 1-olefin content decreased. This also may be due to the decrease in bulk diffusivity of the product in the mole liquid-like medium at the highest pressure.

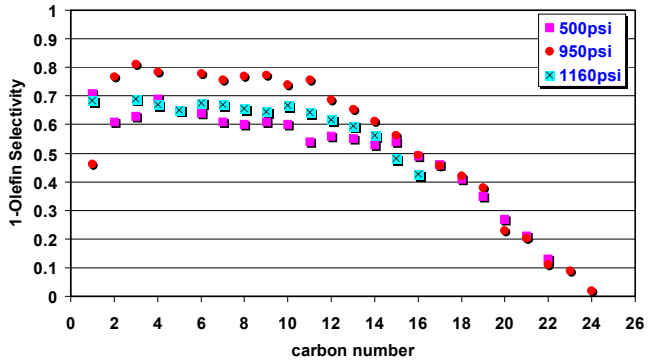

Figure 8. Effect of Pressure-Tuning on 1-olefin Selectivity

3. Gas Residence Time Effects

The effect of syngas residence time on the conversion was also examined. Figure 9 shows that there is no significant effect of syngas residence time on the CO conversion. This result is quite different from that obtained under gas-phase operation in which the conversion increases with a decrease in syngas residence time. The lack of effect of residence time on conversion in the supercritical phase reaction maybe a result of the improved pore diffusivity in the supercritical medium. Thus, the diffusion rate of product out of the catalyst pores is increase thereby leaving more active sites for CO and H2 causing the residence time effects become insignificant.

The effect of residence time on olefin selectivity is presented in Figure 10. Again, there is an insignificant effect of the residence time on the 1-olefin selectivity in the SCF phase. At high syngas

conversion, the effect of the solubility on the olefin selectivity is stronger than the effect of intraparticle diffusion. Therefore, there is little effect of residence time on the olefin selectivity. The olefin selectivity decreases with the increase in carbon number because the larger olefins spend more time in the catalyst pores than smaller ones due to the lower diffusivities. This increases the probability for secondary 1-olefin readsorption, double bond isomerization and hydrogenation reactions.[4] This suggests that the SCF-FT reaction is not diffusion controlled, however, the secondary olefin hydrogenation is diffusion limited.

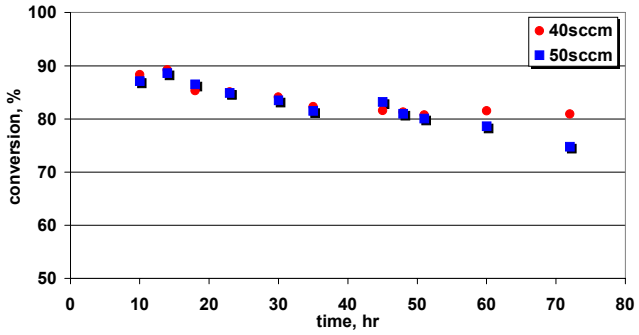

Figure 9. Effect of Syngas-Residence Time on CO Conversion at 950 psi.

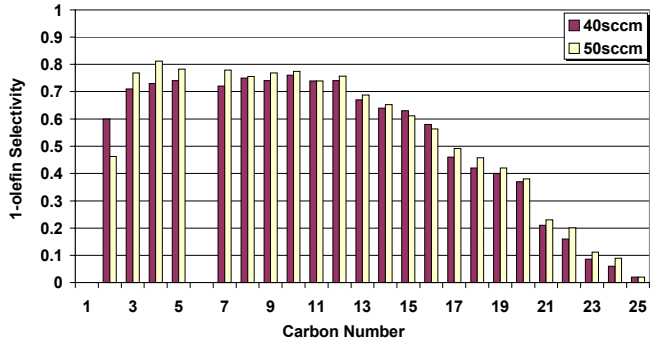

Figure10. Effect of Syngas-Residence Time on 1-olefin Selectivity at 950 psi.

Conclusions

Due to the increased diffusion and desorption rate of reactants and products in SCF phase Fischer Tropsch synthesis, the CO conversion and olefin content are higher than that in conventional FTS. Higher selectivity of the olefin products suggest that the SCF-FT operation results in higher pore diffusivities and more rapid removal of heavy 1-olefins from catalyst, thereby suppressing secondary hydrogenation and isomerization reactions. Over our experimental range, there exists an optimum operating pressure (P=950psi) that maximizes the conversion and the olefin selectivity. Better heat removal in SCF-FT compared to gas phase allows the catalyst bed temperature to be well controlled. There is little effect of syngas residence time on the syngas conversion and olefin selectivity in the SCF FT process. This demonstrates that the SCF-phase based Fischer-Tropsch reaction is not diffusion controlled.

Acknowledgement. Financial support by the U.S. Department of Energy, Fossil Energy Division, through the Consortium for Fossil Fuel Liquefaction Science is gratefully acknowledged. The authors would also like to thank Dr. Yoonkook Park for his valuable assistance in the reaction system built and other precious suggestions.

References

1. Li, F.; Fujimoto, K.; *Applied Catalysis A: General*; **1999**, 186, 343
2. Bala Subramaniam; *Energeia*; **1999**,10(3)1-4
3. Bala Subramaniam; *Industrial Engineering Chemistry Research;* **1997**, 36(10); 4413
4. Bukur, D.B.; Lang, X.; *Industrial Engineering Chemistry Research;* **1997;** 36(7); 2580-2587
5. Burt Davis; *Energeia*; **1997,** 8(3),1

Recent Developments in Autothermal Reforming and Prereforming for Synthesis Gas Production in GTL Applications

Kim Aasberg-Petersen, Thomas S. Christensen, Charlotte Stub Nielsen, Ib Dybkjær*

Haldor Topsøe A/S, Nymøllevej 55, DK-2800 Lyngby, Denmark

Introduction

Processes for conversion of natural gas into liquid fuels ("Gas-to-Liquids" or GTL) such as gasoline or diesel produced by Fischer-Tropsch (FT) synthesis are attracting increased attention. A GTL-plant for production of FT-products can be divided into three sections. In the first section, the natural gas is converted into synthesis gas – a mixture of hydrogen and carbon oxides. In the second part, the actual FT synthesis takes place and in the final section, product upgrading and separation occurs.

The most capital-intensive part of the GTL-plant is the preparation of synthesis gas, which may account for 50-75% of the capital cost [1]. Hence, there is a considerable incentive to optimise technologies for reducing the cost. Autothermal Reforming (ATR) has been identified as the preferred option for large-scale safe and economic synthesis gas production. This paper will focus on recent developments in the prereforming and ATR technology for synthesis gas production.

Process Concepts and Synthesis Gas Composition

A typical process concept for production of synthesis gas based on ATR is shown in Figure 1. The key steps in the process scheme are desulphurisation, adiabatic prereforming, autothermal reforming, and heat recovery.

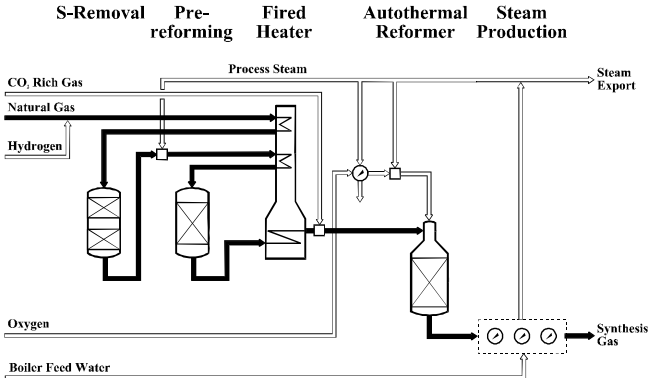

Figure 1. Process Concept for Synthesis Gas Production by Adiabatic Prereforming and Autothermal Reforming

The desired exit gas composition for most FT-applications is an H_2/CO-ratio of about 2. This ratio is achieved by recirculating CO_2. Reducing the amount of steam added to the hydrocarbon feedstock decreases the H_2/CO-ratio and the required recirculation of carbon dioxide. Operation at low steam-to-carbon (H_2O/C) ratio improves process economics, as illustrated in Table 1 [1]. Operation at H_2O/C-ratios of 0.6 has been proven industrially [3] and large-scale GTL projects for production of FT-fuels based on ATR have been publicized [4].

Table 1. Process Economics with Various H_2O/C-Ratios [1]

H_2O/C	0.2	0.6	1.0
Relative Energy Consumption	0.97	1.00	1.03
Relative Investment	0.9	1.0	1.1

The Air Separation Unit (ASU) for production of pure oxygen accounts for a large part of the investment of the production of synthesis gas. The use of a prereformer in the process scheme in Figure 1 upstream the ATR reactor reduces the oxygen consumption per unit of product produced.

Prereforming and ATR at Low H_2O/C-ratios

In the prereformer, all higher hydrocarbons (C_{2+}) are converted into a mixture of methane, hydrogen, and carbon oxides according to the following reactions:

$$C_nH_m + nH_2O \Rightarrow nCO + (n + m/2)H_2 \quad (1)$$

$$3\,H_2 + CO \Leftrightarrow CH_4 + H_2O \quad (2)$$

$$CO + H_2O \Leftrightarrow H_2 + CO_2 \quad (3)$$

The prereformer is an adiabatic fixed-bed reactor with highly active nickel catalysts.

The ATR reactor consists of a burner, a combustion chamber, and a fixed bed catalyst section contained in a refractory lined pressure shell [2]. The key elements in the ATR reactor is the burner and the catalyst bed [2]. The burner provides mixing of the feed streams and the natural gas is converted in a turbulent diffusion flame often simplified by the following reaction:

$$CH_4 + 3/2\,O_2 \Rightarrow CO + 2H_2O \quad (4)$$

The catalyst bed equilibrates the methane steam reforming (reverse of (2)) and the shift (3) reactions.

As shown in Table 1, there is a considerable economic incentive to reduce the H_2O/C-ratio in a GTL plant. However, operation with low H_2O/C-ratios involves the risk of soot formation in the ATR reactor and whisker carbon formation in the prereformer. In order to overcome this challenge, both fundamental studies and extensive pilot plant operation have been carried out to understand and push the limits towards lower H_2O/C-ratios.

In a prereformer, whisker carbon can be formed either from methane or higher hydrocarbons. The lower limit of the H_2O/C-ratio depends on a number of factors including the feed gas composition, the operating temperature and the choice of catalyst. In a prereformer operating at low H_2O/C-ratio, the risk of carbon formation [5] from methane is most pronounced in the reaction zone where the temperature is highest. Carbon formation from higher hydrocarbons can only take place in the first part of the reactor with the highest concentrations of C_{2+} compounds. In Figure 2, a measured temperature profile from a prereformer pilot plant run operating at an H_2O/C-ratio of 0.4 is presented. Post-test analysis of the catalyst showed that no carbon formation had occurred.

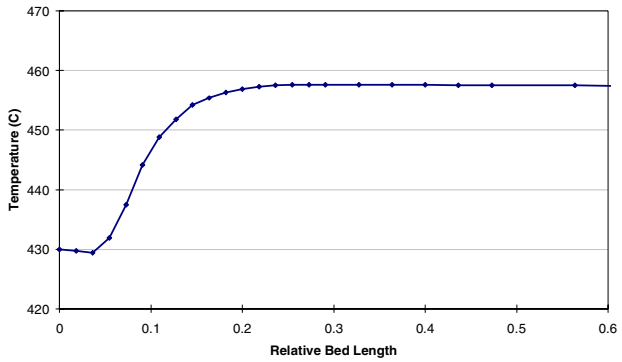

Figure 2. Temperature profile in Adiabatic Prereformer during pilot plant operation. $H_2O/C = 0.4$.

The risk of soot formation in an ATR reactor depends on a number of parameters including feed gas composition, temperature, pressure, and especially burner design. Soot precursors may be formed in the combustion chamber during operation. It is essential that the design of burner, catalyst and reactor is such that the precursors are destroyed by the catalyst bed to avoid soot formation. In Table 2, examples of operating conditions without soot formation in a pilot plant are given [2].

Table 2: Autothermal Reforming - Pilot Plant Demonstration Runs at Low H_2O/C-Ratios [2]

Test	**A**	**B**
Feed Ratios [1](mole/mole)		
H_2O/C	0.60	0.36
O_2/C [2]	0.58	0.57
Product Gas		
Temperature, (˚C)	1020	1022
Pressure, (bar)	28.5	28.5
H_2/CO, (mole/mole)	2.30	2.15
Total run hours	2235	920

Notes: 1) Mole per mole of hydrocarbon C-atoms
2) The O_2/C-ratio is approximately 5% higher than truly adiabatic reactors with same exit temperature.

Conclusion

The combination of adiabatic prereforming and autothermal reforming at low H_2O/C-ratios is a preferred layout for production of synthesis gas for large GTL-plants. Extensive testing and demonstration in pilot plants have proven that the technologies are ready for application in large industrial scale.

References

[1] Dybkjær, I. and Christensen, T.S., *Stud. Surf. Sci. Catal*., 136 (**2001**) 435.
[2] Christensen, T.S.; Østberg, M.; and Bak Hansen, J.-H., "Process Demonstration of Autothermal Reforming at Low Steam-to-Carbon Ratios for Production of Synthesis Gas", *AIChE Annual Meeting*, Reno, USA, Nov. 4-9, **2001**
[3] Ernst, W.S.; Venables, S.C.; Christensen, P.S.; and Berthelsen, A.C., *Hydrocarbon Proc*., 79(3) (**2000**), 100-C
[4] Rostrup-Nielsen, J.R.; Dybkjær, I.; and Coulthard, G.R.G., "Synthesis Gas for Large-Scale GTL-Plants", *AIChE Spring Annual Meeting*, Houston, USA, April 22-26, 2001
[5] Rostrup-Nielsen, J.R. and Sehested, J., *Stud. Surf. Sci. Catal.,* 139 (**2001**) 1.

Selective Oxidesulfurization of C1-Organosulfur Compounds over Supported Metal Oxide Catalysts

Sukwon Choi and Israel E. Wachs

ZCSS and Department of Chemical Engineering,
Lehigh University,
Bethlehem, Pennsylvania 18015

Introduction

Recent analyses by EPA[1, 2] concluded that one of the highest priority needs of the Pulp and Paper industry is a new alternative to combustion (burning in power boilers and lime kilns using fossil fuels) and incineration (thermal oxidation systems operating at ~1500 ^{o}F) of concentrated process streams of totally reduced sulfur (TRS) compounds (H_2S, CS_2, CH_3SH, CH_3SCH_3 and CH_3SSCH_3) as well as CO that are currently converted to SO_2, CO_2 and H_2O. Consequently, the toxic TRS and CO emissions from the pulp and paper mills are converted to an undesirable acid rain precursor, SO_2, and a major contributor to global warming, CO_2, in very energy intensive non-catalytic processes. A novel catalytic process scheme has been developed to convert the by-products from the pulp and paper mills (TRS compounds, SO_2, CO and CO_2) to valuable chemical intermediates (CH_3OH, H_2CO and H_2SO_4) that are consumed in the Pulp and Paper Industry. A key catalytic intermediate reaction step in the catalytic process scheme is the selective catalytic oxidation of C1-organosulfur compounds:

$$COS + O_2 \rightarrow CO + SO_2 \quad [1]$$
$$CS_2 + 5/2\ O_2 \rightarrow CO + 2\ SO_2 \quad [2]$$
$$CH_3SH + 2\ O_2 \rightarrow H_2CO + SO_2 + H_2O \quad [3]$$

These reactions are the subject of this paper. The objective of the current studies is to establish the fundamental kinetics and mechanism of the selective oxidation of C_1-organosulfur compounds (COS, CS_2, and CH_3SH) over sulfur-tolerant metal oxide catalysts.

Experimental

Catalyst Preparation. The catalysts used in this study were prepared by the incipient wetness impregnation method. This technique is described in detail elsewhere[3-5]. The support materials used in this study are TiO_2 (55 m^2/g), ZrO_2 (39 m^2/g), Nb_2O_5 (55 m^2/g), CeO_2 (36 m^2/g), Al_2O_3 (γ, 180 m^2/g), and SiO_2 (300 m^2/g). Concentrations of the supported metal oxides were all prepared to exhibit below monolayer coverage.

Characterization. *In Situ* Raman spectroscopy was performed with a system comprised of an Ar+ laser (Spectra Physics, model 2020-50) set at 514.5 nm, and a Spex Triplemate spectrometer (model 1877) connected to a Princeton Applied Research (model 143) OMA III optical multichannel photodiode array detector. Samples were dehydrated by heating to 300 °C prior to any analyses. The entire procedure was performed in flowing oxygen to achieve complete oxidation of the catalyst. The reactivities of the catalysts were obtained from an isothermal fixed-bed reactor system operating at atmospheric pressure. The feed gas contained 1000 ppm of the reactant (COS, CS_2, or CH_3SH), 18% O_2 in He balance, and was introduced into the reactor at a flow rate of 150 ml/min. Sample runs were performed between 200-450 ^{o}C. Analysis of the reaction products was accomplished using a FTIR, (model #101250 Midac) or an on-line gas chromatograph (HP 5890A) equipped with a thermal conductivity detector (TCD) and a sulfur chemiluminescence detector (SCD 355, Sievers). Temperature Programmed Surface Reaction Mass Spectrometry (TPSR-MS) was carried out with an AMI-100 system equipped with an online mass spectrometer (Dycor DyMaxion). The adsorption was performed between 35-100 ^{o}C using 200 mg of catalyst and was ramped to 500 ^{o}C at a heating rate of 10 ^{o}C/min in 5% O_2/He or He at 30 mL/min.

Results and Discussion

Steady-state reactivity data showed that COS and CS_2 are selectively oxidized to CO and SO_2 over the sulfur tolerant supported vanadia catalysts via reactions [1] and [2] between 290-330 ^{o}C and 230-270 ^{o}C, respectively. CO selectivities as high as 98% and 90% were achieved for COS and CS_2 oxidation, respectively. The major byproduct from CS_2 oxidation is COS, which can be further selectively converted to CO via reaction step [1]. For the selective oxidation of CH_3SH to H_2CO and SO_2 via reaction [3] over a series of redox supported metal oxide catalysts (supported vanadia, molybdate, tungstates and niobates) also did not exhibit deactivation and were sulfur tolerant. The most selective catalysts for reaction step [3] between 350-400 ^{o}C were vanadia supported on ZrO_2, TiO_2 and SiO_2 (in the 84-89% range at high conversions).

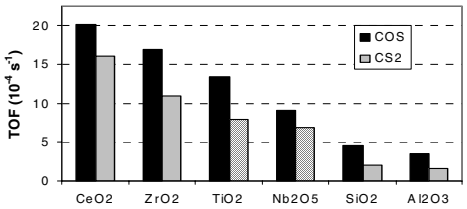

Figure 1. Variation of the TOF with the oxide support for COS and CS_2 oxidation at 330°C and 260°C, respectively, over supported vanadia catalysts with monolayer coverage.

Raman spectroscopy revealed that the supported metal oxide phases were 100% dispersed on the oxide substrate. Thus, the exclusive presence of surface metal oxide species allowed the determination of the number of active sites in the catalyst samples since dispersion was 100 %. As shown in **Figure 1** for monolayer surface vanadia coverage, where the oxide support cations are essentially not exposed to the reactant gases and are covered by the vanadia overlayer, the turnover frequencies (TOF: Activity per surface metal atom based on the yield of CO) for COS and CS_2 oxidation varied about one order of magnitude with the specific oxide support ($CeO_2 > ZrO_2 > TiO_2 > Nb_2O_5 > Al_2O_3 \sim SiO_2$). A similar phenomenon is shown in **Figure2** for TOFs (based on the yield of H_2CO) during CH_3SH oxidation over supported vanadia catalysts at 350 ^{o}C. The TOFs varied within one order of magnitude ($TiO_2 > ZrO_2 \sim Nb_2O_5 > Al_2O_3 \sim SiO_2$). These trends are inversely correlated with the electronegativity of the support cation in the bridging V-O-Support bond and suggests the bridging V-O-Support bond being the active site for these reactions since Raman revealed that the terminal V=O bonds were essentially the same in these supported vanadia catalysts[6]. Furthermore, all three reactions exhibited a zero-order dependence on the oxygen partial pressure

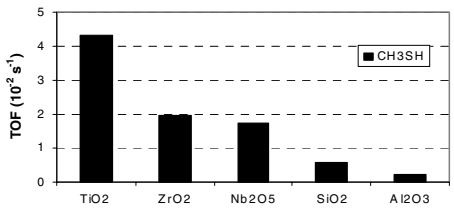

Figure 2. Variation of the TOF with the oxide support for CH_3SH oxidation at 350°C over supported vanadia catalysts (1% V_2O_5).

(0.5-20%) and a first-order dependence on the COS/CS_2 /CH_3SH partial pressures (<1%, due to safety concerns), which suggest that the surface vanadia species is essentially fully oxidized under the investigated reaction conditions. The apparent activation energies for COS, CS_2 and CH_3SH oxidation over the supported vanadia catalysts were found to be ~10, ~6 Kcal/mol and 17 Kcal/mol, respectively.

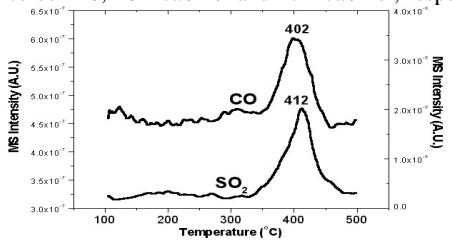

Figure 3. TPSR-MS profiles after *COS* adsorbed at 100 °C on the 5% V_2O_5/TiO_2 catalyst, under 5% O_2/He flow.

The desorption spectra of CO and SO_2 are shown in **Figure 3** from the 5% V_2O_5/TiO_2 catalyst following COS adsorption at 100 °C. The simultaneous desorption of CO and SO_2 suggests that the oxidation of COS proceeds via the rate-determining step involving cleavage of the C-S bond. The slight delay in the production of SO_2 is consistent with this conclusion since the remaining S(ads) requires the addition of two oxygen atoms. The above suggests the following mechanism for COS oxidation to CO and SO_2 over the 5 % V_2O_5/TiO_2 catalyst.

COS	↔	COS(ads)		[4]
COS(ads)	→	CO + S(ads)		[5] rds
S(ads) + O(ads)	→	SO(ads)		[6]
SO(ads) + O(ads)	→	SO_2		[7]

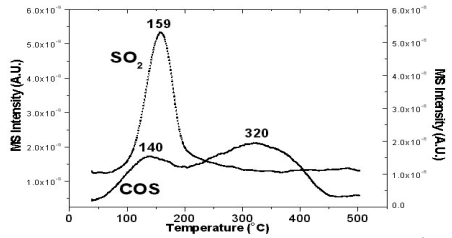

Figure 4. TPSR-MS profiles after *CS_2* adsorbed at 35 °C on the 5% V_2O_5/TiO_2 catalyst, under 5% O_2/He flow.

The desorption spectra of COS and SO_2 are shown in **Figure 4** from the 5% V_2O_5/TiO_2 catalyst following CS_2 adsorption at 35 °C. The presence of the COS species in the desorption spectra suggests CS_2 is oxidized to CO and SO_2 via the formation of COS as an intermediate species. Steady-state data obtained at low conversions also confirmed the presence of COS formation. In view of these findings the following mechanism is proposed for CS_2 oxidation.

CS_2 + O(ads)	↔	CS_2O(ads)		[8]
COS_2(ads)	→	COS + S(ads)		[9] rds
S(ads) + O(ads)	→	SO(ads)		[10]
SO(ads) + O(ads)	→	SO_2		[11]

The further oxidation of COS to CO and SO2 proceeds via reaction steps [4-7]. From comparison of the CH_3SH and CH_3OH TPSR desorption profiles in **Figures 5** and **6**, the peaks for H_2CO appear at the exact same temperature suggesting H_2CO is produced via the same surface reaction intermediate from both CH_3SH and CH_3OH.

The above suggests the following mechanism for reaction [3] over the 1 % V_2O_5/TiO_2 catalyst.

CH_3SH + O(ads)	↔	CH_3S(ads) + OH(ads)		[12]
CH_3S(ads) + O(ads)	→	CH_3SO(ads)		[13]
CH_3SO(ads)	→	CH_3O(ads) + S(ads)		[14]
CH_3O(ads)	→	H_2CO + H(ads)		[15] rds
H(ads) + OH(ads)	↔	H_2O		[16]
S(ads) + O(ads)	→	SO(ads)		[17]
SO(ads) + O(ads)	→	SO_2		[18]

The dissociative adsorption of CH_3SH to CH_3S(ads) and OH(ads), reaction step [12], was revealed by desorption of CH_3SSCH_3 into the gas phase during the adsorption step at 100 °C. All TPRS experiments repeated in the absence of flowing gas phase oxygen gave the same product desorption peaks, which demonstrate that the oxygen involved in the surface reaction steps [4-18] is oxygen from the surface vanadia species.

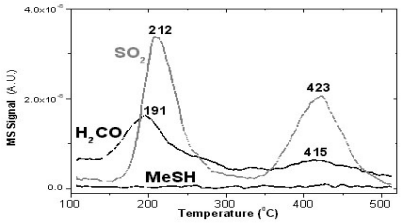

Figure 5. TPSR-MS profiles after *CH_3SH* adsorbed at 100 °C on the 1% V_2O_5/TiO_2 catalyst, under 5% O_2/He flow.

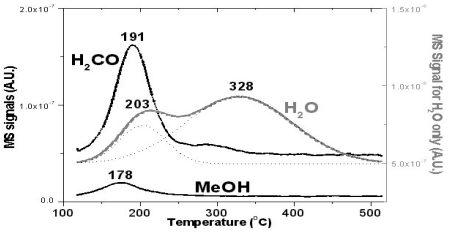

Figure 6. TPSR-MS profiles after *CH_3OH* adsorbed at 100 °C on the 5% V_2O_5/TiO_2 catalyst, under 5% O_2/He flow.

Acknowledgement

The authors gratefully acknowledge the National Science Foundation, Grant NSF-CTS-9626893, for financial support of this research.

References

1. "Pulp, Paper and Paperboard Industry - Background Information for Proposed Air Emission Standards," EPA, 453/R-93-050a (Oct. 23, 1993).
2. "Targeted Energy Performance Areas for 1999," American Forest and Paper Association Energy Performance Research Task Group (May 1998).
3. Deo, G., Wachs, I. E. J. Catal. 146 (1994) 323-334.
4. Wachs, I. E., Deo, G., Juskelis, M. V., Weckhuysen, B. M. in: Froment, G. F., Waugh (Eds.), K. C., Dynamics of Surfaces and Reaction Kinetics in Heterogeneous Catalysis, Elsevier, Amsterdam, 1997, pp. 305-314.
5. Wachs, I. E., in: Spivey(Ed.), J. J., Catalysis, vol. 13, The Royal Society of Chemistry, Cambridge, 1997, pp. 37-54.
6. Harcastle, F. D. and Wachs, I. E., J. Phys. Chem. **95** (1991) 5031-5041.

SELECTIVELY SYNTHESIZE ISOBUTENE FROM CO HYDROGENATION OVER ZRO_2 BASED CATALYSTS IN A SPECIALLY DESIGNED REACTOR

Yingwei Li, Dehua He*, Qiming Zhu

State Key Laboratory of C_1 Chemistry and Technology, Department of Chemistry, Tsinghua University, Beijing 100084, China

*Corresponding author. Email: hedeh@mail.tsinghua.edu.cn Fax: +86-10-6279-2122

Introduction

Isosynthesis is the reaction that selectively converts syn-gas ($CO+H_2$) to isobutene (and isobutane). It has been widely investigated over ZrO_2 based catalysts in recent years [1-3]. The common problems in the isosynthesis are that it is difficult to obtain high activity and i-C_4 selectivity at the same time and suppress the percentage of CO_2 in the products (>40%). In this study, we report an effective catalyst loaded in a specially designed reactor that could selectively convert synthesis gas to i-C_4 hydrocarbons and in the meantime surely maintain a relative high CO conversion. Furthermore, the percentage of CO_2 in the products was largely suppressed.

Experimental

Preparation of zirconia-based catalysts has been described in our previous work [4]. The hydrogenation of CO was carried out in two types of reactors at 5.0 MPa, 648-723 K and 650 h^{-1}. One was a stainless steel tube (marked as Reactor A) that was normally used in most researches that performed at a high pressure [2,3]. Another was a specially designed reactor that contains a stainless steel line in which a quartz line was tightly fixed (marked as Reactor B). A Viton O-ring pressed by a locking nut was used to prevent the gas from leaking into the ringed gap so as to eliminate the influence of the metal wall. The reactor effluent was reduced to atmospheric pressure and then injected into two on-line gas chromatographs.

Results and Discussion

The results are presented in Table 1. Under the reaction conditions in this study, the products consisted primarily of hydrocarbons, CO_2, methanol and dimethyl ether. About 19.6% CO was converted with 36.7% C_4 selectivity in total hydrocarbons over ZrO_2 catalyst in the stainless steel tube. However, the percentage of CO_2 in the products was exceeding 60%, as normally reported in the literatures and the formation of C_1–C_3 was also remarkable. This would likely indicate that the metal wall of the stainless steel tube affected seriously the reactivity of the catalysts in the isosynthesis. The blank reactivity of the stainless steel tube also accounted for it. It can be seen from Table 1 that C_1-C_3 hydrocarbons were the predominant hydrocarbons products in the blank experiments. In order to eliminate the influence of the metal wall on the isosynthesis, the reaction was performed on the specially designed Reactor B (quartz lined). The blank experiment of the Reactor B showed that much fewer amount of CO was converted (lower than 0.1%) compared with the activity conducted on the reactor A. Although the CO conversion was a little lower than the reactor A, the i-C_4 selectivity in total hydrocarbons was largely enhanced (about 52.5%) with a much lower percentage of CO_2 in the products (37.7%) over ZrO_2 catalyst conducted on the reactor B. This would suggest that the quartz line reactor (reactor B) could eliminate the influence of metal wall, improving the performance of the catalysts in the isosynthesis.

Table 1. Influence of the Type of Reactor On the Performance of the Isosynthesis [a)]

Reactor	Catalyst	CO conv. / %	Selectivity of Products / %			Distribution of hydrocarbons / (C mol%)			
			H.C.[b)]	CHO [c)]	CO_2	C_1-C_3	C_4	C_5^+	i-C_4
A	-	1.8	81.7	0	18.3	83.6	15.1	1.2	2.8
B	-	< 0.1	51.7	0	48.3	100	0	0	0
A	ZrO_2	19.6	38.8	0	61.2	50.8	36.7	12.5	26.9
B	ZrO_2	16.3	51.5	10.8	37.7	19.6	58.1	22.3	52.5

A: Stainless steel tube; B: Stainless steel tube in which a quartz line was tightly fixed.

a) Reaction conditions: 673 K, 5.0 MPa, GHSV = 650 h^{-1}, CO/H_2 = 1.

b) CH_3OH + CH_3OCH_3 c) Hydrocarbons

The percentage of CO_2 in the products could be even more decreased over 15.3%Al_2O_3-0.5KOH-ZrO_2 catalyst conducted in the reactor B at 673 K. The NH_3, CO_2-TPD experiments revealed that the performance of the catalysts strongly depended on the acid-base properties of the catalysts. An appropriate amount of moderately strong acid - base sites and ratio of basic to acidic sites on the catalysts are significant for an active catalyst to selectively produce isobutene and isobutane from CO hydrogenation.

Conclusion

The metal wall of the stainless steel tube reactor would affect seriously the reactivity of the catalysts in the isosynthesis. The quartz tube reactor would be favorable for the formation of i-C_4 and decrease CO_2 formation. The amount of acid - base sites and ratio of basic to acidic sites on the catalysts are significant for an active catalyst to selectively produce isobutene and isobutane from CO hydrogenation.

Acknowledgement

We acknowledge the financial support from the Basic Research Foundation of Tsinghua University and the Analytical Foundation of Tsinghua University.

References

(1). [1] Maruya, K.; Komiya, T.; Hayakawa, T.; Lu, L. H.; Yashima, M. *J. Mol. Catal. A-Chem.* **2000**, *159*, 97.

(2). [2] Postula, W. S.; Feng, Z. T.; Philip, C. V.; Akgerman, A.; and Anthony, R. G. *J. Catal.* **1994**, *145*, 126.

(3). [3] Su, C. L.; Li, J. R.; He, D. H.; Cheng, Z. X.; Zhu, Q. M. *Appl. Catal. A-Gen.* **2000**, *202*, 81.

(4). [4] Li, Y. W.; He, D. H.; Cheng, Z. X.; Su, C. L.; Li, J. R.; Zhu, Q. M. *J. Mol. Catal. A-Chem.* **2001**, *175* (1-2), 267.

STRUCTURAL EVOLUTION AND SITE REQUIREMENTS FOR FISCHER-TROPSCH SYNTHESIS CATALYSTS BASED ON Fe OXIDES PROMOTED WITH Cu, Ru, OR K

Senzi Li, Sundaram Krishnamoorthy, George D. Meitzner, and Enrique Iglesia

Department of Chemical Engineering, University of California at Berkeley, Berkeley, CA 94720

The effects of different promoters (Ru, Cu, ZnO, and K_2CO_3) on the density and structure of active sites for the Fischer-Tropsch synthesis (FTS) was studied. The structure, reduction and carburization behavior, and catalytic properties of the catalysts were examined using a combination of isothermal kinetic transient and spectroscopic methods including on-line mass spectroscopy, *in-situ* X-ray absorption spectroscopy, and steady-state FTS catalytic rate measurements. Isotopic jump and site titration methods were used to estimate the density of active sites, to establish the identity and reversibility of elementary steps, and to confirm the structure-function rules suggested by the kinetic and spectroscopic methods.

Fe-based catalysts were prepared by co-precipitation of Fe and Zn (Zn/Fe=0.1) nitrates with $(NH_4)_2CO_3$ to form porous mixed oxides, which were subsequently impregnated with Cu (Ru) nitrate or K carbonate solutions (M/Fe=0-0.04, M=Cu, K, or Ru), similar to the procedure used in another study [1]. Displacing intrapore water with alcohol before drying the precipitate and decreasing the treatment temperature from 673 K to 543 K increased the surface area of Fe-Zn-K-Cu oxides from 65 to 120 m^2/g. These procedures appear to prevent pore mouth pinching during by decreasing the surface tension of intrapore liquids.

The reduction of Fe_2O_3 to Fe_3O_4 in H_2 in Fe-Zn-K-Cu (Ru) precursors is faster than on Fe-Zn-K samples; Cu and Ru reduce at low temperatures and provide H_2 dissociation sites unavailable on Fe_2O_3. Oxygen removal and carbon introduction rates during exposure of Fe-Zn-K-Cu (Ru) oxides to CO showed that such processes occur sequentially via Fe_2O_3 reduction to Fe_3O_4, incipient removal of a minority of the O-atoms in Fe_3O_4, and rapid carburization of such oxygen-deficient species to form a □-$Fe_{2.5}C$ and □-Fe_3C mixture at 540 K or pure □-Fe_3C at around 720 K. Cu and Ru increased the rate of oxygen removal from Fe_2O_3 and Fe_3O_4 and thus the rate of formation of FeC_x. K, present as a carbonate, inhibited oxygen removal but increased the rate of carbon introduction, apparently by increasing CO dissociation rates on FeO_x or FeC_x surfaces.

Mass spectrometric analysis of the products formed during initial exposure of oxide precursors to H_2/CO mixtures at 523 K detected the initial removal of oxygen and a concurrent increase in FTS rates as oxygen was removed and carbon introduced. Steady-state rates were obtained after an initial induction period during which only 1-2 equivalent oxygen monolayers are removed (10^{19} O-atoms/m^2) from the Fe_2O_3 precursors. Pre-reduced (Fe_3O_4) and pre-carburized FeC_x (Fe/C=2.5~3) did not show the induction period or the rapid initial removal of oxygen as H_2O and CO_2 observed on Fe_2O_3 precursors. FTS remained constant even as slow removal of oxygen and introduction of carbon continued to occur on Fe_3O_4. This indicates that the formation of an active surface occurs within a few FTS turnovers, irrespective of the initial presence of Fe_3O_4 or FeC_x (Fe/C=2.5~3). The catalytic properties of the resulting surface are not influenced by the remaining presence of an oxide or carbide bulk. This active surface is likely to consist of a steady-state mixture of vacancies, adsorbed CO, and carbon and oxygen atoms formed in CO dissociation steps. Their relative concentrations are rapidly established by FTS elementary steps and depend on the redox properties of the contacting gas phase, the reaction temperature, and the surface concentrations of chemical promoters.

In-situ Fe K-edge X-ray absorption (XAS) studies confirmed the phase transformation from Fe_2O_3 to Fe_3O_4 and then to FeC_x during the initial stages of FTS reactions. Only the incipient conversion of Fe_2O_3 to Fe_3O_4 and Fe_xC was required in order to reach steady-state FTS rates. The extent of carburization increased with time on stream without a detectable increase in FTS reaction rates, confirming that the catalytic properties of Fe carbides are not influenced by a remaining Fe oxide core or by its ultimate carburization. Cu, K and Ru all increased the rate and the extent of carbide formation. The promoting effects of K, Cu, and Ru on FTS reaction rates (described below) appear to correlate with their ability to increase the rate and the extent of reduction and carburization of Fe_2O_3 precursors. Localized Fe_2O_3 surface regions influenced by the presence of Cu, Ru, or K species may provide multiple nucleation sites for reduction and carburization within each Fe_2O_3 precursor crystallite with the eventual formation of smaller oxide and carbide particles from larger Fe_2O_3 precursor particles. This proposal is consistent with the greater extent of carburization obtained when K and Cu (Ru) are present.

The effects of promoters (K, Cu and Ru) on FTS rate and selectivity were determined using a fixed-bed reactor in the 493-543 K temperature range and 5-31.6 atm pressure with a H_2/CO mixture (2/1). Addition of Cu considerably improves FTS activity of the catalyst by decreasing the temperature required for the formation of active Fe_xC structures. At 508 K and 21.4 atm for example, the CO rate doubled with the addition of Cu (Cu/Fe=0.01) to a Fe-Zn-K (Zn/Fe=0.1, K/Fe=0.01) catalyst (1.3 to 2.6 mol/h-mol Fe at 20% CO conversion). Copper also promotes the hydrogen availability on the catalyst surface and hence decreases product molecular weight. Potassium improves both the activity and the selectivity of the FTS by increasing the amount of chemisorbed CO and decreasing the amount of chemisorbed H_2 on Fe-based catalysts. The promotion effect of K, however, is much more pronounced on a Cu-promoted catalyst than on a Cu-free catalyst, suggesting a synergistic effect of Cu and K, in agreement with a previous study [1]. Cu and K also significantly promote CO_2 formation during the FTS reaction. Replacement of the Cu by Ru in the Fe-Zn-K system led to a significant promotion of the FT rate (CO rates being 2.7 and 6.7 mol/h-mol Fe respectively at 20% CO conversion and 508 K) with negligible change in the product selectivities. This effect can be attributed to the better dispersion of the Fe_xC structure in the presence of Ru. Furthermore, an increase in surface area in the case of the Fe-Zn-Cu-K catalyst also markedly increases FT rates (CO rates being 2.7 and 6.8 mol/h-mol Fe respectively at 20% CO conversion and 508 K) due to a corresponding increase in the availability of the active Fe_xC sites.

Iron-based catalysts with high Fischer-Tropsch synthesis (FTS) rates were prepared by using promoters (K, Ru, Cu) and synthesis and activation protocols that favor the nucleation of small Fe carbide crystallites and inhibit sintering of oxide catalyst precursors during synthesis and activation. The effect of promoters on reduction/carburization behavior, on Fischer-Tropsch synthesis (FTS) rates, and on the number of CO binding sites formed during reaction

were examined by combining steady-state and transient rate measurements, titration of active sites, and X-ray absorption spectroscopy. K, Ru, and Cu promoters increased reduction/carburization rates of Fe-Zn oxide precursors, steady-state FTS rates, and the number of CO binding sites present after activation and FTS. These promoters increased the number of active sites formed during activation by favoring the nucleation of smaller Fe_3O_4 and Fe_xC domains as Fe_2O_3 precursors convert to active catalysts during initial contact of oxide precursors with synthesis gas. These smaller crystallites, in turn, provide higher surface areas, a larger number of CO binding sites, shorter diffusion distances for oxide-carbide transformations, and higher steady-state FTS rates. The number of active sites and the rates of FTS reactions were also increased by using surface-active alcohols to minimize sintering of Fe-Zn oxide precursors during thermal treatment of precipitated oxide precursors. The hydrocarbon synthesis rates using Fe-Zn-Cu-K catalysts prepared by this method were similar to those on representative Co-based catalysts (at 473 K; 2.0 MPa) when compared on the basis of catalyst mass and significantly higher on a volume basis. Fe-Zn-Cu-K catalysts showed significantly lower CH_4 selectivities than Co-based catalysts and much weaker effects of temperature and of synthesis gas composition on CH_4 and C_{5+} selectivities. The CO_2 selectivity is lower than on previously reported Fe-based catalysts, predominately because of the lower reaction temperatures made possible by the high FTS reaction rates on the promoted Fe catalysts reported in this study

1. S. Soled, E. Iglesia, S. Miseo, B. A. DeRites and R. A. Fiato, *Topics in Catalysis* 2 (1995) 193.

STRUCTURAL REQUIREMENTS AND REACTION PATHWAYS FOR THE FISCHER-TROPSCH SYNTHESIS

Sundaram Krishnamoorthy, Senzi Li, Dario Pinna, Mai Tu, and Enrique Iglesia
Department of Chemical Engineering, University of California, Berkeley, CA 94720

Hydrocarbon synthesis from H_2/CO in the Fischer-Tropsch synthesis (FTS) is a critical step in the conversion of coal or natural gas to petrochemicals and fuels. On Co-based catalysts, crystallite size and support effects do not influence turnover rates, but small amounts of Ru increase rates and C_5+ selectivity. Co crystallites smaller than ~6 nm, however, tend to oxidize during FTS. Promotion by Ru requires its intimate contact with Co, induced by RuO_x migration and by formation of Co-Ru oxides. Ru domains on Co surfaces inhibit the formation of unreactive carbon species and preserve the initial number of Co surface atoms. Other promoters inhibit sintering (Re) or aid the reduction (Pt) of CoO_x precursors. Catalyst synthesis by contact of supports with saturated Co precursor solutions and the slow reduction of Co precursors without air treatment lead to small Co crystallites (6-10 nm), even at high Co concentrations.

Water is the primary oxygenate product during FTS reactions on Co-based catalysts. Higher water concentrations in the synthesis gas reactant stream lead to higher hydrocarbon synthesis rates. The C_{5+} selectivity and the olefin content in all hydrocarbons also increases with increases water content, while the CH_4 selectivity concurrently decreases. Kinetic isotope effects using CO/H_2 and CO/D_2 reactants showed that these changes do not arise from independent kinetically relevant steps introduced by water, since the observed isotope effects were not influenced by the reactant conversion level or by the water concentration. Reactant mixtures consisting of $CO/H_2/D_2$ and $CO/H_2O/D_2O$ were used in order to probe the reversibility of hydrogen dissociation and water desorption steps. H_2 dissociation are quasi-equilibrated during FTS reactions, but water desorption steps are reversible but far from equilibrium. This leads to oxygen chemical potentials at Co surfaces that significantly exceed those set by the H_2O/H_2 ratios in the prevalent gas phase. This surface chemical potential become the controlling variable in establishing the extent of oxidation of Co surfaces during FTS, a process that can lead to deactivation especially for well-dispersed Co catalysts.

In-situ infrared studies of the CO coverage during FTS showed that the number of CO binding sites is not influenced by the presence of water concentrations that lead to greater than two-fold increases in FTS reaction rates. Thus, it appears that the role of water is not to increase the density of catalytic sites during FTS, a process that would have led to a rate increase, possibly via the scavenging of unreactive carbon-containing adsorbed species. The intensity of the linear adsorbed CO band did not change as H_2O partial pressures increased from 0 to 300 kPa, but the band disappeared and reaction rates became very low at H_2O/H_2 ratios greater than 0.8, apparently as a result of surface oxidation. Chemical transients effected by switching from H_2/CO to H_2 streams were used in order to measure the concentration of reactive adsorbed species during steady-state catalysis on Co/SiO_2 and Co/SiO_2. The concentration of these carbon species was not influenced by the presence of water at concentrations leading to significant changes in FTS reaction rates and selectivity. In situ X-ray absorption spectroscopy showed that at typical reaction conditions, Co metal was the only Co-containing structure present on Co/SiO_2 catalysts.

FTS reactions proceed on Co and Fe via surface polymerization using surface alkyls as growing chains and CH_x species as monomers. Olefin readsorption influences C_{5+} and olefin selectivities by reversing chain termination to olefins. Intrapellet and gas-liquid diffusional constraints increase the extent of readsorption and introduce catalyst design parameters (e.g., pellet diameter and void fraction, Co site density) unavailable in kinetic-limited pellets. The higher reactivity and lower diffusivity of larger olefins lead to an increase in growth probability and in paraffin content with increasing chain size. The pellet structure and the Co site density also influence CO diffusional restrictions, which decrease local monomer concentrations and inhibit chain growth. As a result, maximum C_{5+} yields are achieved using catalyst pellets with intermediate transport restrictions. In packed-bed reactors, these optimum pellets require eggshell Co distributions, which decouple the size of the pellets from their characteristic diffusion distance. Smaller uniform pellets with higher site densities lead to optimum transport restrictions in bubble column reactors.

Fe-based catalysts exhibit more complex structure-function relationships than Co and significant structural promotion by oxides (ZnO), metals (Cu, Ru), and alkali (K). In situ X-ray absorption and transient product analysis methods confirmed FeC_x as the active species and probed the kinetic details of the structural changes occurring during reaction. Controlled pH co-precipitation, surface active agents added during drying, and promoters that convert Fe oxide precursors to high surface area FeC_x at low temperatures led to Fe-based catalysts with higher productivity than reported Co-based catalysts (at 473 K, 2 MPa, $H_2/CO=2.1$). Although these Fe catalysts give higher CO_2 selectivities than Co catalysts (6-10% vs. <1%), their lower selectivities to CH_4 and to C_2-C_4 paraffins make them attractive catalysts, even for the synthesis of liquid fuels from H_2/CO mixtures derived from natural gas.

STUDIES WITH A PRECIPITATED IRON FISCHER-TROPSCH CATALYST REDUCED BY H_2 OR CO

Guozhu Bian, Atsushi Oonuki, Norimasa Fujishita, Naoto Koizumi, Hiderou Nomoto, and Muneyoshi Yamada

Department of Applied Chemistry, Graduate School of Engineering, Tohoku University, Aoba 07, Aramaki, Aoba-ku, Sendai 980-8579, Japan

Introduction

Iron- based catalysts have been used in Fischer-Tropsch synthesis of hydrocarbons from syngas since 1923. It has been reported that the reducing pretreatments with H_2, CO or syngas often have significant effects on the catalytic activity and selectivity of the iron-based catalysts. For instance, for unsupported iron-based catalyst systems, H_2-reduced samples show obvious lower activities for FT synthesis than the CO- and syngas-reduced samples [1-2]. It has been regarded that reduction of the iron-based sample in hydrogen lead to a metallic state with serious sintering, and CO or syngas reduction lead to metallic state and small amounts of iron carbides without significant sintering. During performing FT synthesis, more iron carbides and iron oxides are formed. However, the purpose of the pretreatments of various catalyst systems have not been clearly understood, on which carefully investigations may deepen the understanding of the roles of the various iron phases in performing FT synthesis, and might be helpful to prepare catalysts with good activities.

Experimental

Precipitated Fe_2O_3 sample used in this study was prepared in the usual batch-wise manner by adding ammonia solution into a solution of $Fe(NO_3)_3 \cdot 9H_2O$. The obtained precipitates were calcined in air at 350°C for 2h. The reduced samples were obtained by calcination of the precipitated Fe_2O_3 samples in a 40ml/min flow of H_2 or CO/He (20/80) at 300°C and atmospheric pressure for 6h. The treated samples were obtained by calcination of the H_2-reduced sample in the CO/He flow or by calcination of the CO-reduced sample in the H_2 flow at 300°C for 6h.

The diffuse reflectance FTIR spectra were recorded with a resolution of 4cm^{-1} and accumulation of 20 on a Bio-Rad FTS 6000 FTIR spectrometer supplied with a MCT detector and a diffuse reflectance attachment. The infrared cell with ZnSe windows (Spectra-Tech Inc.) can be used at high pressures and high temperatures.

BET specific surface areas of the samples were measured by N_2 physisorption at 77K, using a QUANTACHROME MONOSORB surface area analyzer and one-point BET method.

Activities of the reduced and treated catalyst samples for FT synthesis from syngas were measured using a slurry phase reactor with a volume of 100ml. 30ml of n-$C_{16}H_{34}$ was used as liquid medium. 0.3g of oxidized catalyst sample was used for each experiment. The reaction was carried out in a 30ml/min flow of syngas with H_2/CO/Ar ratios of 62/33/5.0 at 1.0 MPa and 250°C. Analyses of the gas-phase products were performed by an on-line gas chromatography. The liquid products in the reactor and those collected in an on-line trap at 0°C were analyzed by an off-line gas chromatograph after the reaction. Chain growth probability, α, was calculated using the C_{10}-C_{25} data.

Results and Discussion

In- situ H_2-reduced iron sample was subjected to the adsorption experiment in a syngas flow (H_2/CO=2, 60ml/min) at 1.2MPa and room temperature. Figure 1a shows the spectrum recorded after the syngas adsorption was performed for 20min. Two very weak bands at 2013 and 2033cm^{-1} can be observed. With increasing time, the bands at 2013 and 2033 cm^{-1} slowly increase. According to the literature [3], these bands are assigned to linearly adsorbed CO on metallic iron particles.

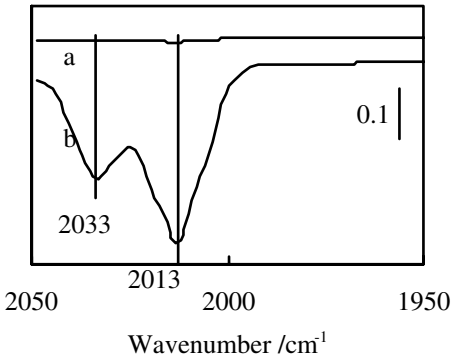

Figure 1. Infrared spectra recorded from syngas adsorption on H_2-reduced Fe catalyst at 1.2 MPa and room temperature for 20min (a), and followed by flashing the sample in the high-pressure syngas flow up to 100°C (b)

After syngas adsorption for 20 min, the sample was quickly heated up to 100°C in the high-pressure syngas flow. The bands at 2013 and 2033cm^{-1} become very stronger (Figure 1b). Thereafter, however, the bands gradually decrease in intensities. After remaining temperature at 100°C for 1h, the bands become as weak as those shown in Figure 1a. When the high-pressure syngas adsorption is directly performed at 100°C, the bands at 2013 and 2033cm^{-1} are even weaker than those observed by syngas adsorption at room temperature.

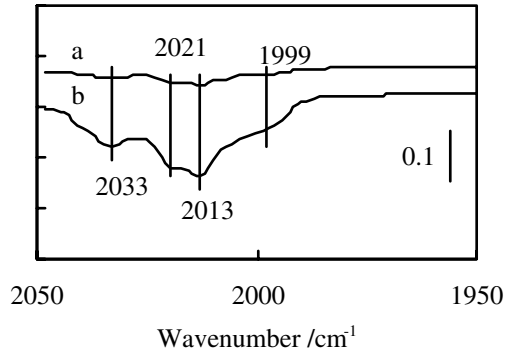

Figure 2. Infrared spectra recorded from syngas adsorption on CO-reduced Fe catalyst at 1.2MPa and room temperature for 20min (a), and followed by flashing the sample in the high-pressure syngas flow up to 100°C (b)

After high-pressure syngas adsorption at room temperature for 20min, pressure was reduced and then syngas was replaced by helium at atmosphere pressure. The bands of gaseous CO disappear by simple helium flushing for about 0.5min. The sample was flashed up to 100°C after helium flushing for 3min. By flashing sample to 100°C in the helium flow, the bands at 2013 and 2033cm^{-1} become stronger. It is

also seen that these bands quickly diminish in the helium flow at 100°C and disappear completely in about 2min.

These results suggest that the tremondous increase in intensities of the bands are not due to further adsorption of gaseous CO molecules, but due to recombination of the dissociative CO molecules bound on the catalyst surface at room temperature. The recombined CO molecules were initially adsorbed molecularly on the catalyst surface, followed by slowly desorption in the high-pressure syngas flow, or by quickly desorption in the helium flow at atmospheric pressure.

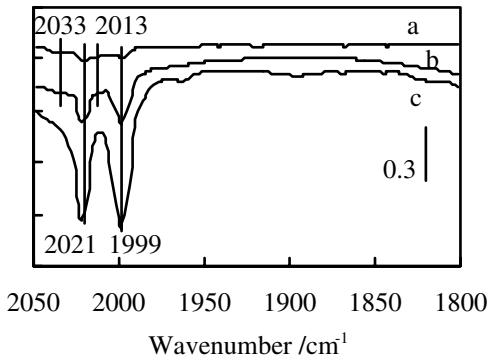

Figure 3. Infrared spectra recorded from syngas adsorption on H2-reduced Fe catalyst used for FT synthesis for 15min (a), 50min (b) and 3h (c). The adsorption was performed at 1.2MPa and room temperature for 20min.

As shown in Figure 2, on CO-reduced sample, high-pressure syngas adsorption at room temperature gives four weak bands at 1999, 2013, 2021 and 2033cm^{-1}. Compared to the spectra of syngas adsorption on the H_2-reduced sample, two new bands appear at 1999 and 2021 cm^{-1}. It is also observed that, as shown in Figure 2(b), quickly heating the sample up to 100°C in the syngas flow results in a great increase of all these four bands. Therefore, large quantities of CO molecules are dissociatively adsorbed on the CO-reduced catalyst at room temperature as well.

The bands at 1999 and 2021cm^{-1} may be assigned to CO adsorption on iron carbide species. The main reason for this assignment is that, as shown later in this paper, syngas adsorption on the samples used for FT synthesis gives rise to strong bands at 1999 and 2021cm^{-1}. This result strongly supports the above assignment, because during FT synthesis iron carbides are the only Fe^0 species to be formed in large quantities. More investigations were performed and it is found that iron carbides on the CO-reduced sample can be converted to metallic iron by H_2 treatment at 300°C, and metallic iron on the H_2-reduced sample can be partly converted to iron carbides by CO treatment at 300°C.

On the H_2-reduced sample used for FT synthesis for 15min, syngas adsorption gives rise to four obvious bands at 2013, 2033, 1999 and 2021cm^{-1}, as shown in Figure 3a, indicating that the metallic iron species on the surface are partly transformed to iron carbides. Figure 3b shows the spectrum of the syngas adsorption on the sample used for FT synthesis for 50min; the bands at 1999 and 2021cm^{-1} are growing, and the bands at 2013 and 2033cm^{-1} become very weaker. Figure 3c shows the spectrum of the syngas adsorption on the sample used for FT synthesis for 3h, the bands at 1999 and 2021cm^{-1} become very strong. These results clearly indicate that the metallic iron particles on the surface are gradually transformed to iron carbides. However, the iron carbides formed during FT synthesis exhibit very low ability for CO dissociation.

Syngas adsorption on the CO-reduced sample used for FT synthesis for 10min gives bands at 1999 and 2021cm^{-1} as well. Furthermore, it is noticed that the iron carbides formed on the CO-reduced samples during performing FT synthesis have relatively higher ability for CO dissociation than that on H_2-reduced sample.

BET surface area data are shown in Table 1. The surface area of the CO-reduced sample is near to that of the oxidized catalyst precursor, but the surface area of the H_2-reduced sample becomes very much low. The surface area of the CO-reduced sample is about 5 times higher than that of the H_2-reduced sample. After the H_2-reduced sample was treated with CO at 300°C, its surface area increases significantly. On the other hand, after the CO-reduced sample was treated with H_2, its surface area shows a slight decreae.

Table 1 BET surface areas of various iron samples

Sample	reduction conditions	Surface area (m^2*g^{-1})
Oxidized	-----	38
Reduced:	CO, 300°C	37
	H_2, 300°C	7
Treated:	CO, 300°C; H_2, 300°C	33
	H_2, 300°C; CO, 300°C	11

As shown in Table 2, H_2-reduced sample shows lower catalytic activity for FT synthesis than the CO-reduced sample. Over the CO-reduced sample treated with H_2, CO conversion becomes greatly reduced compared to that over the untreated sample. Conversely, over the H_2-reduced sample treated with CO, CO conversion shows a sharp increase. These results clearly indicate that high surface area of the CO-reduced sample is not the main cause for the sample to show high activity for FT synthesis. The fine iron carbides formed during CO reduction of the oxidized sample or during CO treatment of the H_2-reduced sample have played an important role in enhancing the activity of the sample.

Table 2 Activity data of the iron samples after reaction for 7h

Reduction Conditions	CO conv. (CO%)	Yields of CO_2 & HC (CO%) CO_2	C_1	C_2	C_{3-5}	α
H_2, 300°C	24.1	4.2	2.9	1.9	7.4	0.87
CO, 300°C	68.9	13.9	6.6	5.6	21.5	0.85
H_2, 300°C; CO, 300°C	46.9	8.6	4.1	3.6	16.7	0.85
CO, 300°C; H_2, 300°C	32.3	7.5	3.8	2.6	9.7	0.86

Acknowledgement. This work was supported by Research for the Future Program of Japan Society for the Promotion of Science under the project "Synthesis of Ecological High Quality Transportation Fuels" (JSPS-RFTF98P01001).

References

(1) Bukur, D. B.; Koranne, M.; Lang, X.; Rao, K. R. P. M.; Huffman, G. P. *Appl. Catal. A* **1995**, 126, 85.

(2) Bukur, D. B.; Lang, X.; Rossin, J. A.; Zimmerman, W. H.; Rosynek, M. P.; Yeh, E. B.; Li, C. *Ind. Eng. Chem. Res.* **1989,** 28, 1130.
(3) Guglielminotti, E. *J. Phys. Chem.* **1994**, 98, 4884.

Supercritical-phase process for selective synthesis of heavier hydrocarbons from syngas on cobalt catalysts

Jinglai Zhou[1] Shirun Yan[2] Zhixian Gao[1] Li Fan[3]
1: Institute of Coal Chemistry, Chinese Academy of Science. P.O. Box 165, Taiyuan, Shanxi030001, P.R. China
2: Department of Chemistry, Fudan University, Shanghai ,P.R. China
3: Department of Applied Chemistry, School of engineering, The University of Tokyo

Introduction

As an effective reaction for production of liquid fuels from coal and natural gas, Fischer-Tropsch (FT) synthesis has received great attention in past several decades. To be more promising and economically competitive, FT synthesis should be modified to shift the product spectrum from transportation fuel to valuable chemicals such as light olefin and heavier wax. Owing to its merits such as high melting point, low viscosity, as well as nitrogen-, sulfur-, and aromatics-free property, wax has been highly favored. However, selective synthesis of wax is not easy. It is believed that the readsorption and subsequent secondary reaction (hydrogenolysis, cracking, and reinsertion) of primary 1-olefin product are main reasons for the deviation from ASF distribution. To obtain an insight into secondary reactions of primary product, 1-olefin, and the mechanism of chain growing process, gas and liquid phase FT reaction over Fe, Co, Ru catalyst cofed with the 1-olefin ($C^{=}_2$, $C^{=}_3$, 1-$C^{=}_4$, 1-$C^{=}_6$, 1-$C^{=}_8$, 1-$C^{=}_{10}$, 1-$C^{=}_{20}$) have been studied extensively by many researchers[1-5]. It was found added 1-olefin, as a chain initiator, could combine CH_2 species on the catalyst surface, which lead to a decrease in methane formation and a increase in selectivity of hydrocarbons with one more carbon number than the added 1-olefin. But added olefin had no noticeable effect on the formation rate of heavier hydrocarbons and on the chain growth probability.

The supercritical phase FT synthesis cofed with medium-size 1-olefin (i.e. 1-tetradecene) over Co/SiO_2 catalyst, combining the characteristic of effective transportation of supercritical fluid and high readsorption probability of medium-size 1-olefin, have been carried out in our laboratory. Our results have shown that added 1-tetradecene could be remarkably involved in the chain growth process that was indistinguishable from the original chain growth. Consequently the formation rate of hydrocarbons larger than C_{14} increased markedly, while yield of C_1-C_{13} hydrocarbons decreased correspondingly. Effects of catalyst pore size, H_2/CO feed ratio, cofed olefin concentration were also investigated.

Experimental

Co/SiO_2 catalysts were prepared by impregnating SiO_2 with cobalt nitrate from its aqueous solution by incipient wetness method. The catalyst precursors were dried in air at 393K for 12hr and then calcined at 573K. Supercritical-phase FT reaction was carried out on a pressurized fixed-bed reactor system, accompanied with a high pressure pump which supplied the supercritical fluid (SCF) and 1-olefin during supercritical-phase reactions. Detailed description of reaction system was reported in our previous publication [6]. N-pentane was used as SCF., and Nitrogen was used as the balance material in gas phase reaction. The loading amount of catalyst was 0.5g. Prior to FT reaction, the catalyst was reduced with hydrogen under atmospheric pressure at 673K, 60ml/min for 12hr. Except noted, the reactions were conducted under standard conditions listed below. T=483K, P(total)=4.5Mpa, P(CO+H_2)=1.0MPa, W/F (syngas)=15g.h/mol. Argon was used as internal standard with concentration of 3% in the feed gas. The effluent gas was analyzed on line with two gas chromatographies. The condensed products were analyzed off-line with other two chromatographies.

Results and Discussion

1. Reaction Performance in Different Reaction Phase

Fig.1 and Table 1 present the effect of reaction phase on CO conversion and the hydrocarbon yield. It is found that CO conversion in supercritical phase was higher than that in gas phase and the yield of hydrocarbons, except methane, showed the same trend.

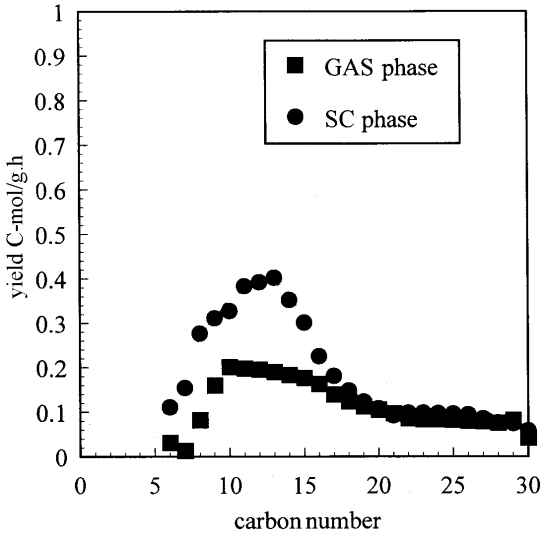

Fig.1. Phase effect on yield of hydrocarbons; Cat.3, W/F=15,210□, with out olefin addition

It is well known that in gas-phase FT reaction, after reaching the steady state, the catalyst pores were filled with heavier hydrocarbons in which CO and H_2 must be solved and subsequently diffused to reach the inner surface of catalyst. In supercritical phase FT reaction, due to the higher solubility of supercritical fluid, a large part of these heavier hydrocarbons could be solved and removed in situ by supercritical solvent whose density and viscosity are greatly smaller than those of the heavier hydrocarbons.

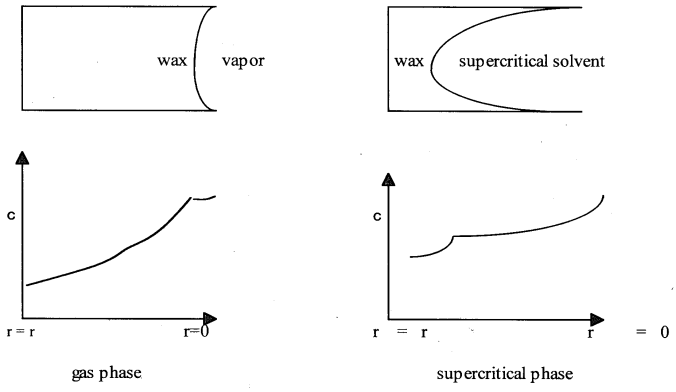

Fig.2. Visualized CO and H_2 concentration Profiles inside catalyst pores in different phases
Note: Represent the concentration of syngas inside pores

Consequently the transportation of CO and H_2 to the surface of catalyst was facilitated, and both the CO conversion and hydrocarbon yield were increased. CO and H_2 concentration profiles in different phase can be visualized in Fig.2. Meanwhile, because the large amount

of reaction heat could be removed efficiently by the SCF, formation of overheating spot on catalyst bed was prohibited and formation of methane, which was favored at high temperature, was also inhibited.

2. Effect of 1-tetradecene addition

Fig.3 and Table 2 exhibit the addition effect of 4 mole% (CO base) 1-tetradecene on CO conversion and hydrocarbons formation rate. It was found that CO conversion as well as light hydrocarbons (C_1-C_{13}) yield decreased, but the selectivity of hydrocarbons larger than C_{14} increased markedly with the addition of 1-tetradecene. As a result, C^+_{20} Yield was enhanced from 33.3% to 36.2% due to the addition of 1-olefin.

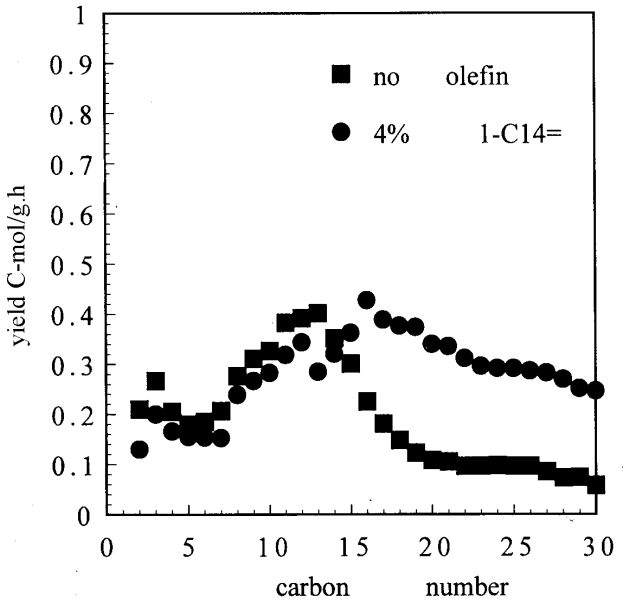

Fig.3. Effect of olefin addition on the distribution of products CO conversion: 85% (without olefin addition); 73% (with 4% 1-tetradecene addition);(CH_4 was not included)

Light olefin (C_2-C_{10}) addition to syngas and subsequent influence on reaction itself on cobalt catalysts had been well studied[17]. In recent years Iglesia[5] and kuipers[8,9] reported their cofeeding studies. Their results showed that 1-olefin addition of low concentration (5% mole) could inhibit the formation of methane but did not affect the value of the chain growth probability. But in our study where 1-olefin 4% mole was added increased the formation rate of heavier hydrocarbons noticeably as shown in Fig.3. The differences between previous olefin cofeeding studies and ours are molecule size of the added olefin and the reaction medium therein. In previous cofeeding studies, added light olefin was at gas phase under reaction conditions. In contrast, in our studies, supercritical fluid could greatly remove the wax in situ, which made the wax layer covered on the surface of catalyst much thinner than that for the gas phase reaction. And the added 1-tetradecene, which was at liquid state under reaction conditions, had higher solubility in wax layer than that of gaseous olefins. Thus the concentration of added 1-tetradecene in wax layer was relatively high and its adsorption probability on the catalyst surface and thus followed reinsertion reaction rate were also higher, which consequently increased the yield of hydrocarbons higher than C_{14}. Another interesting phenomenon in Fig.3 is that in the 1-tetradecene cofeeding experiment the yield of C_2 was much lower than that of C_3 while C_{16} were higher than C_{15}. This implies that probably species involved in growing chains was not limited to CH_2, and C_2H_4 may also be inserted. It is reported C_2H_4 is more active than C_3H_6[10], so the probability of being inserted was higher correspondingly. This phenomenon was also found by other investigators[3,11]. As for the CO conversion, since the adsorption of added 1-olefin would consume some H_2, and occupy some active sites which otherwise would be consumed and occupied by CO, the conversion level in the olefin-added reaction was lower than that of conventional reaction.

3. Influence catalyst pore size

The Co/SiO_2 catalysts with different pore size but the same amount of metal on specific surface area were also prepared and investigated. The properties and composition of catalysts and their reaction performance were compared in Fig.4 and Table 3. It is clear from the data in Fig.4 that the selectivity to the heavier hydrocarbons increased with increasing catalyst pore size, while the CO conversion decreased as shown in Table 3.

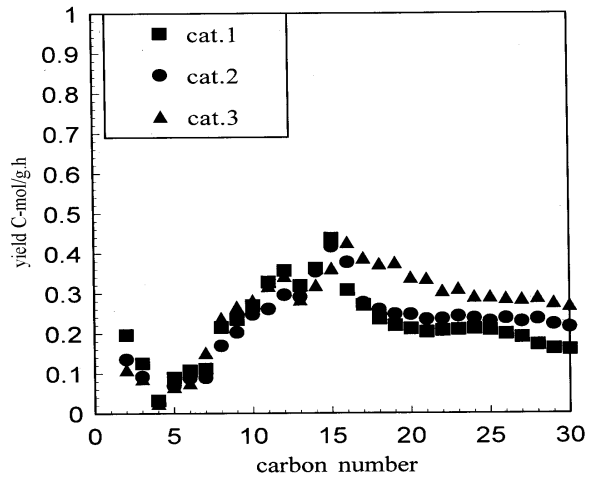

Fig.4. Catalyst pore size effect on yield of heavier hydrocarbon (see also Table3) Reaction conditions: T=483K, P(total)=4.5MPa, P($CO+H_2$)=1.0MPa, W/F=15g.hr/mol, 4% (CO base) 1-tetradecene added

Because more effective mass transfer could be realized on the catalyst with large pores, it can be inferred that with the increase of pore size, the percentage of wax extracted in situ by the supercritical fluid increased correspondingly, while the thickness of wax layer covered on the surface of catalyst was reduced. Thus the diffusion of added 1-olefin inside the large-pore catalyst and its concentration in the wax layer was relatively higher than those for the catalyst with small pores, which consequently led to the higher adsorption probability of cofed olefin onto the catalytic sites. As a result, the selectivity to heavier hydrocarbons increased. One of the present authors have investigated the pore size effect on the performance of Ru/Al_2O_3 catalyst in supercritical phase FT synthesis, which proved that the chain growth probability increase with the increasing pore diameter of catalyst [6]. Meanwhile the acceleration in the heavier hydrocarbon formation may inhibit the formation of CO_2. So the CO_2 yield on catalyst with large-pore was greatly less than that on the small-pore catalyst.

4. Effect of olefin cofeeding concentration

Fig.5 shows olefin cofeeding concentration effect on the CO conversion and carbon number distribution of products. It was found that the yield of hydrocarbons heavier than C_{14} increased with increasing concentration of added 1-tetradecene while the CO conversion shown a reverse trend. This could be ascribed to the different probability of adsorption and thus-hence chain growth reaction of different cofed olefin concentrations. It is clear from the above discussion that addition of 1-tetradecene could enhance the

formation of hydrocarbons larger than C_{14}, while the formation of C_1-C_{13} was inhibit, thus increased the selectivity to heavier hydrocarbons. It can be deduced that with the increasing concentration of 1-tetradecene in the system, the concentration within wax layer increased, the probability of participation in the chain growth process also increased, and consequently the selectivity of hydrocarbons larger than C_{14} increased. Because the more adsorption of olefin would occupy more active sites and consume more H species, CO conversion was lowered correspondingly.

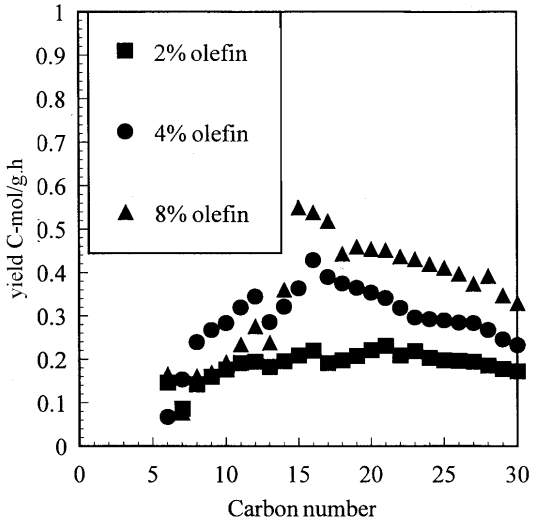

Fig.5 Olefin concentration effect on carbon number distribution of product Cat.3, T=210□, W/F=15g.hr/mol, P(total)=4.5MPa, P(CO+H_2)=1.0MPa, The percentages in figure are CO conversions

5. Investigation on the influence of H_2/CO feed ratio

Different gases with H_2/CO ratio of 1/1 and 2/1 have been used to investigated effect of H_2/CO ratio on the catalytic behavior of Co/SiO_2 catalyst. The main results are exhibited in Table 4. It can be found that for 1/1 syngas, CO conversion was obviously lower while the selectivity of wax was higher than that for 2/1 syngas. The reaction rate of FT synthesis is reported to be proportional to the partial pressure of H_2 over Co/SiO_2 catalyst[7]. The lower CO conversion may be interpreted easily by the stoichiometrical requirement of FT reaction as well as the properties of catalyst. The higher selectivity to wax in the case of 1/1 syngas might be ascribed to high surface concentration of CO, which would favor the adsorption and chain propagation reaction of added olefin[5].

6. Analysis and evaluation results of waxes

Table 5 presents some analytical results of wax. It could be found that the average molecule weight and the degree of saturation (H/C ratio) of wax increased greatly due to addition of 1-tetradecene. These strongly support that the incorporation of 1-tetradecene to chain growth reaction happened. This implies that added 1-tetradecene might inhibit the formation of oxygenates which is generally the products of hydroformylation reaction. Elemental analytical results also give some evidences to this point, because total percentage of (C+H) were increased from 98.65% to 99.55% after addition of 1-tetradecene. However, as for inhibition of oxygenates formation, the reaction mechanism was not clear.

Table 1. CO conversion and hydrocarbons distribution in different reaction phase

Reaction phase	CO conv. (%)	C_1-C_4 yield (C-mmol/g.hr)				C^+_{20} Selectivity (%)
		C_1	C_2	C_3	C_4	
Gas phase	70	2.91	0.218	0.551	0.607	13.4
SC phase	84	1.87	0.259	0.164	0.041	39.6

Rreaction conditions: T=483K, P(total)=45atm, W/F(CO+H_2)=15g/hr.mol

Table 2. Effect of 1-tetradecane addition

Item	CO conv. (%)	C_1-C_4 yield (C-mmol/g.hr)			
		C_1	C_2	C_3	C_4
Without 1-$C^=_{14}$	84	1.870	0.259	0.164	0.04
4% 1-$C^=_{14}$ added	73	1.235	0.128	0.302	0.16

tetradecane addition: 4 mol% CO base

Table 3. Effect of catalyst pore size on reaction performance of Co/SiO_2

Catalyst No.	Mean pore Diameter (Å)	Co loading (by weight) (%)	CO Conversion (%)	CO_2 Selectivity (%)	C^+_{20} Selectivity (%)
1	150	40	96	10	36.9
2	300	29	93	6	41.7
3	500	30	73	N.D*	49.5

Note: 4mol% 1-tetradecene added. * N.D. Non-detectable

Table 4. Effect of H_2/CO ratio on the reaction performance

H_2/CO	CO conv. (%)	Yield of C_1-C_4, C-mol/g.hr				C^+_{20} Selectivity
		C_1	C_2	C_3	C_4	
1/1	42	1.030	0.145	0.120	0.074	57.3
2/1	73	1.235	0.128	0.302	0.164	49.5

4 mol.% 1-tetradecene added

Table 5. Molecule weight and elemental composition of wax

Item	Sample 1	Sample 2
Mean molecule weight	873	1055
Composition (%)		
H	13.84	15.01
C	84.81	84.54
N	N. D	N. D
O	N. D	N.D
Ash	-	-
Total	98.65	99.55

Note: Sample 1: Co/SiO_2 catalyst, T=483K, W/F=15g.hr/mol; N. D: Non-detectable

Sample 2: reaction condition is same as the sample 1 except for 4% 1-tetradecene addition.

Molecule weight is the number mean molecule weight measured by Gel Permeation Chromatography (GPC).

Conclusions

1. Due to quick diffusion of reactant and product in supercritical phase, CO conversion and liquid hydrocarbon yield of the supercritical phase reaction are higher than those in gas phase reaction.
2. Added 1-tetradecene, as a chain initiator, could participate in the chain propagation process, and consequently promoted formation of hydrocarbons larger than C_{14}, inhibited the formation of C_1-C_{13} hydrocarbons, which made the carbon number distribution deviated from ASF distribution significantly.
3. Species involved in the chain growth process is not limited to the CH_2; it is found that C_2H_4 could be incorporated into carbon chain growth as well.
4. Because the effective transportation of reactant and product could be realized inside the larger pores, catalyst with large pores favored the formation of heavier hydrocarbons.
5. Because the high CO partial pressure could inhibit the hydrogenation and hydrogenolysis of olefin, CO-rich syngas favored the formation of heavier hydrocarbons.
6. In the studied cases, the more olefin added, the more wax produced.

References

1. Robert T. Hanlon and Carles N Satterfield, *Energy & Fuels*, 2 (1988), 196
2. Li-Min Tau, Hossein A. Dabbagh and Burtron H. Davis, *Energy & Fuels,* 4(1990)94
3. Ruichi Nakamura, Irura Takahashi, Chan Sieh Yong and Hiroo Niiyama, *9 th int. congr. Catal.*, 2(1988)759
4. A. T. Bell and P. Winslow, *Proc. 8 th Int. Congr. Catal.,* Berlin, 3(1984)175
5. Enrique Iglesia, Sebastain C. Reyes, Rostam J. Madon and Stuart L. Soled, *Advances in catalysis,* 39(1993)759
6. Li Fan, Kohshiroh Yokota, and Kaoru Fujimoto, *AIChE J.,* 38 (10), 1992, 1639
7. J. P. Hindermann, *Catal. Rev.-Sci. Eng.,* 35(1), 1993, 1
8. E. W. Kuipers, I. H. Vinkenburg and H Oosterbeek, *J. Catal.,* 152, 1995, 137
9. E. W. Kuipers, C. Scheper, J. H. Wilson, I. H. Vinkenburg and H. Oosterbeek, *J. Catal.,* 158, 1996, 288
10. Li-Min Tau, Hossein Dabbagh, Shiqi Bao et al., *9 th Int. Congr. Catal.,* 1988
11. Takashi Komaya and Alexis T. Bell, *J. Catal.*, 146, 1994, 237

SUPPORTED BINARY CATALYSTS FOR DEHYDROGENATION OF METHANE

Naresh Shah[1], Frank E. Huggins[1], Devadas Panjala[1], Gerald P. Huffman[1], A. Punnoose[2], M.S. Seehra[2]

[1]University of Kentucky, Lexington, KY 40508-4005
[2]West Virginia University, Morgantown, WV 26506-6315

Introduction

Production of pure hydrogen from hydrocarbons, particularly methane, the major component of natural gas, has great practical importance. Traditionally, reforming and partial oxidation of methane are employed to produce synthesis gas, which, when followed by water-gas shift conversion of the CO in synthesis gas to CO_2 and the consequent removal of CO_2, produces a relatively pure hydrogen stream. However, this hydrogen stream still contains enough CO to poison the catalysts used in PEM electrochemical fuel cells. A reverse methanation reaction has to be carried out to reduce the CO concentration to sub-ppm levels.

Catalytic decomposition of undiluted methane to pure hydrogen and carbon was carried out in absence of any oxidizing medium with a variety of alumina supported binary metal catalysts. Nanoscale, binary, 0.5%M-4.5%Fe (M = Pd, Mo or Ni) catalysts supported on alumina reduced the decomposition temperature of undiluted methane by 400-500 °C relative to non-catalytic thermal decomposition. The product stream comprised of over 75-volume % of hydrogen and unconverted methane at reaction temperatures of 700 °C. The efficient removal of carbon from the catalyst surface in the form of nanotubes is believed to be the key factor influencing catalyst performance.[1]

Figure 1 is a plot of hydrogen production by catalytic decomposition of methane at various reactor temperatures using pure Fe, pure Mo and binary Mo-Fe catalysts. The role that binary metals play in methane decomposition is clearly evident. Similar plots of hydrogen production by methane decomposition using other binary metal catalysts (Ni-Fe and Pd-Fe) show significantly higher activity than either Fe or the other secondary metal (Ni, Pd) alone.[1]

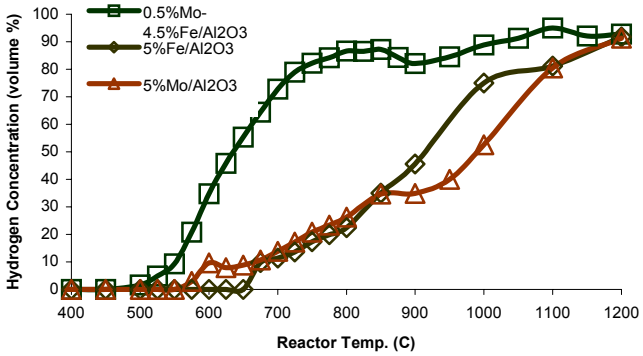

Figure 1. Comparison of alumina supported pure molybdenum and pure iron catalysts with binary Fe-Mo catalysts pre-reduced at 700 °C for hydrogen production.

This paper primarily deals with characterization of these highly active nanoscale binary alumina supported catalysts using a variety of analytical techniques, viz. x-ray absorption fine structure (XAFS) spectroscopy, x-ray diffraction (XRD), Mössbauer spectroscopy, and scanning (SEM) and transmission (TEM) electron microscopy. The synthesis and pre-treatment of the catalysts, as well as SEM/TEM characterization of the produced nanotubes, have been reported elsewhere[1].

As-prepared catalysts

Mössbauer and Fe K-edge XAFS spectroscopies confirmed that the iron in vacuum-dried, alumina-supported catalysts exists in the ferrihydrite structure.[2] The radial structure functions of the Pd and Ni EXAFS indicate the presence of only one nearest neighbor oxygen shell implying either very small particles of oxide on alumina or incorporation in ferrihydrite. XAFS analysis indicates that Mo exists in the +6 oxidation state, probably as MoO_4^{-2}.

Pre-reduced catalysts

The as-prepared or pre-oxidized catalysts were not active for methane decomposition[1]. The catalysts were activated by reduction at 700 °C for two hours and cooling in flowing hydrogen. However, Mössbauer and Fe EXAFS spectroscopic data showed that for all the catalysts, the reduction of Fe to the metallic state is not complete at 700 °C probably because iron reacted with the alumina support to form hercynite. Pre-reduction at 1000 °C is required to complete the reduction of all the Fe to metal. XRD studies of catalysts reduced at 700 °C only yielded lines due to the γ-alumina support, except for Pd-Fe, in which lines due to metallic Fe were also observed (figure 2). Both Pd XANES and Fe Mössbauer data showed that at 700 °C, Pd is easily reduced to metallic state and its presence appears to facilitate the reduction of Fe. Both Ni and Mo are partially reduced to the metallic state. Mössbauer spectroscopy showed the presence of a Fe_2Mo phase in Mo-Fe/Al_2O_3 catalysts and the enhanced formation of a NiFe austenitic phase in reduced Ni-Fe/Al_2O_3 catalysts. STEM investigation of the reduced catalyst further confirms the formation of alloy phase. Figure 3 shows a dark field STEM image and Al, Fe and Mo K-edge EDS maps of a pre-reduced Mo-Fe catalyst. Overlap of Mo and Fe images confirm formation of nanoscale Mo-Fe metallic alloy particles.

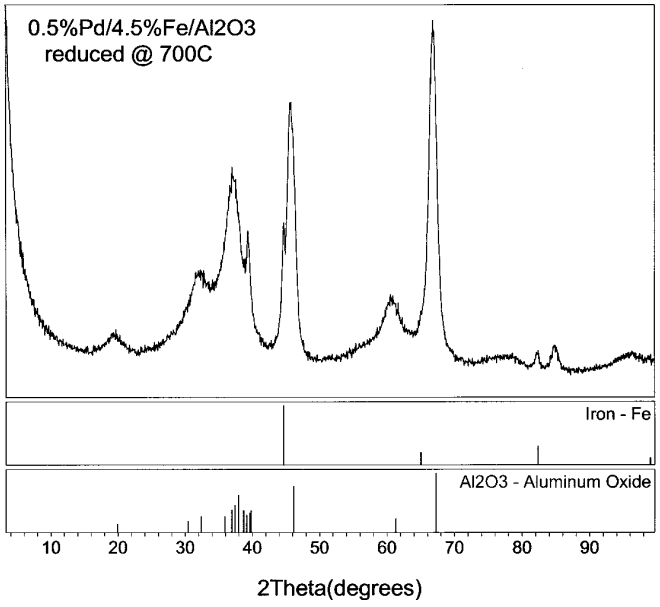

Figure 2. XRD spectra of 0.5%Pd/4.5%Fe/Al_2O_3 catalyst after reduction at 700C showing formation of metallic Fe phase.

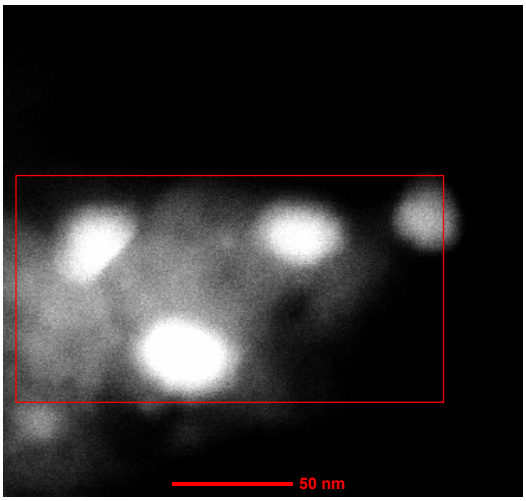

STEM image

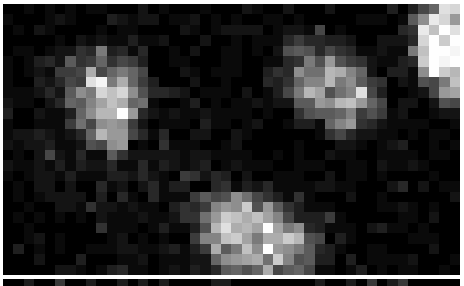

Fe K Map

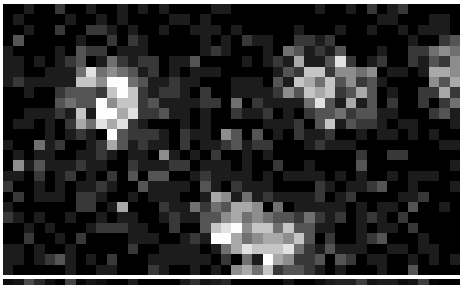

Mo K Map

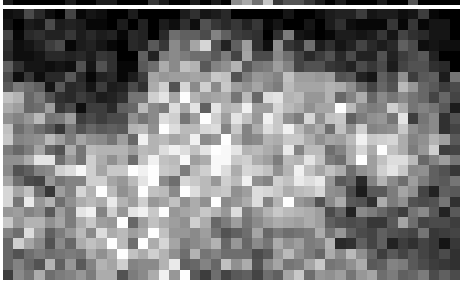

Al K Map

Figure 3. Dark field STEM image with Fe, Mo and Al K-edge EDS maps of the area mark in the STEM image of a Fe-Mo catalysts pre-reduced at 700 °C showing formation of nano-size binary metallic particles on alumina support.

Catalysts after on-stream exposure

Exposure of the pre-reduced catalysts to flowing methane at 700 °C did not result in any significant changes in the XAFS spectra. Although methane is a carburizing atmosphere and the catalysts are very active in decomposing methane to produce large amounts of elemental carbon in form of nanotubes, the catalysts retain their metallic states. As shown in figure 4, XRD studies indicate that γ-alumina undergoes a phase transformation to δ-alumina when the pre-reduction step is carried out at a higher temperature (1000 °C instead of 700 °C). Besides lines due to alumina, XRD studies showed lines due to graphite and Fe_3C in all samples after on-stream exposure. Mössbauer spectroscopy indicated formation of austenite phase possibly due to incorporation of carbon in iron and/or stabilization by the secondary metal. A small amount (0-20%) of iron was also found in metallic state. Substantial amounts of iron were still in unreduced Fe^{2+} state probably as hercynite ($FeAl_2O_4$) spinel due to reaction of the iron with the support.

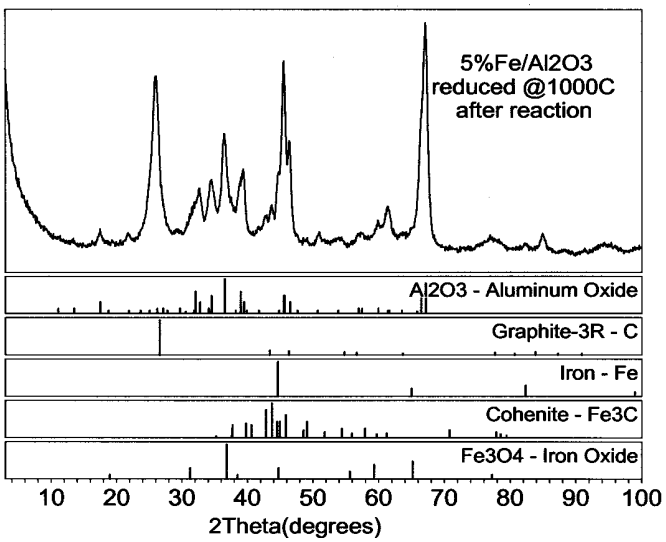

Figure 4. XRD spectra of 5%Fe/Al_2O_3 catalyst (reduced at 1000C) shows phase transformation of alumina support. Lines due to deposited graphitic carbon (in form of nanotubes) are also clearly evident. PDF files of different possible phases are also shown for comparison

Acknowledgement. This research was supported by the U.S. Department of Energy through both the Division of Fossil Energy (FE) under the National Energy Technology Laboratory (NETL) and the Division of Energy Efficiency and Renewable Energy (EE) under the Office of Advanced Automotive Technologies, under contract No. DE-FC26-99FT40540.

References

(1) Shah, N.; Panjala, D.; Huffman G. P. *Energy & Fuels,* **2001**, *15(6),* To be published.

(2) Shah, N.; Zhao, J.; Huggins, F. E.; Huffman, G. P. *Energy & Fuels*, **1996,** *10(2),* 417-420.

SURFACE REACTION MECHANISM DEVELOPMENT FOR PARTIAL OXIDATION OF METHANE TO SYNTHESIS GAS

Ashish B. Mhadeshwar[1], Preeti Aghalayam[2], Vasilis Papavassiliou[3], and Dionisios G. Vlachos[1]

[1]Department of Chemical Engineering, University of Delaware, Newark, DE 19716-3110
[2]Department of Chemical Engineering, University of Massachusetts-Amherst, MA 01003-3110
[3]Praxair Inc.

Introduction

Synthesis gas is an important chemical intermediate for many industrial processes. The need for synthetic fuels is increasing as the recovery of petroleum becomes increasingly difficult and expensive. Synthesis gas can be converted to paraffinic liquid fuels through Fischer-Tropsch synthesis. It helps to reduce environmental pollution, as fuels from synthesis gas are heteroatom free. Catalytic partial oxidation of methane (POX) offers a very promising route to convert natural gas to synthesis gas. POX over noble metal catalysts, including Pt and Rh, is in great demand due to the dual application for energy production[1] (complete combustion) and syngas production[2] (partial oxidation in short contact time microreactors). Although a considerable progress has been made in development of large detailed gas phase reaction mechanisms, the surface chemistry is not well established. In addition, surface reaction mechanisms proposed so far suffer from the disadvantage of violating thermodynamic consistency, lacking important reaction paths and surface coverage-dependent kinetic parameters.

In this work, an elementary surface reaction mechanism of methane oxidation is used, which is derived using a unique combination of surface science experiments, semi-empirical thermo chemistry calculations, and mathematical optimization. The ability of predicting experimental data over a wide range of operating conditions will be demonstrated. As an example, quantitative predictions of experimental data on fuel conversion vs. surface temperature, and selectivities to syngas will be shown.

Chemistry

Below we discuss the prominent features of our chemistry modeling.

Gas-phase Chemistry. The GRI 3.0 mechanism has been employed for gas phase chemistry[3]. This mechanism consists of 53 species and 325 chemical reactions. It is associated with a thermodynamic database as well as a transport database and is in the CHEMKIN format. This mechanism has been extensively validated against experimental data over a wide range of operating conditions and various types of experiments and is used without modifications.

Surface Chemistry. We have developed a C1 reaction mechanism for CH_4 oxidation on platinum consisting of 10 species among 62 surface reactions[4]. The surface reaction mechanism developed involves adsorption and desorption of reactants and intermediate species, pyrolytic hydrogen abstraction from CH_x species, oxygen-assisted and hydroxyl-assisted hydrogen abstraction from CH_x species as well as complete oxidation mechanisms of H_2 and CO on platinum[5,6]. The activation energies of the surface reactions are computed using the semi-empirical Bond Order Conservation (BOC), also known as Unity Bond Index Quadratic Exponential Potential (UBI-QEP) technique[7] that enables us to include the coverage dependence of activation energies in a systematic way. The entire BOC formulism has been incorporated within the SURFACE CHEMKIN Library itself for the first time to provide flexibility, clarity, and ease of use. Thermodynamic consistency is ensured, by using BOC for the calculations of activation energies.

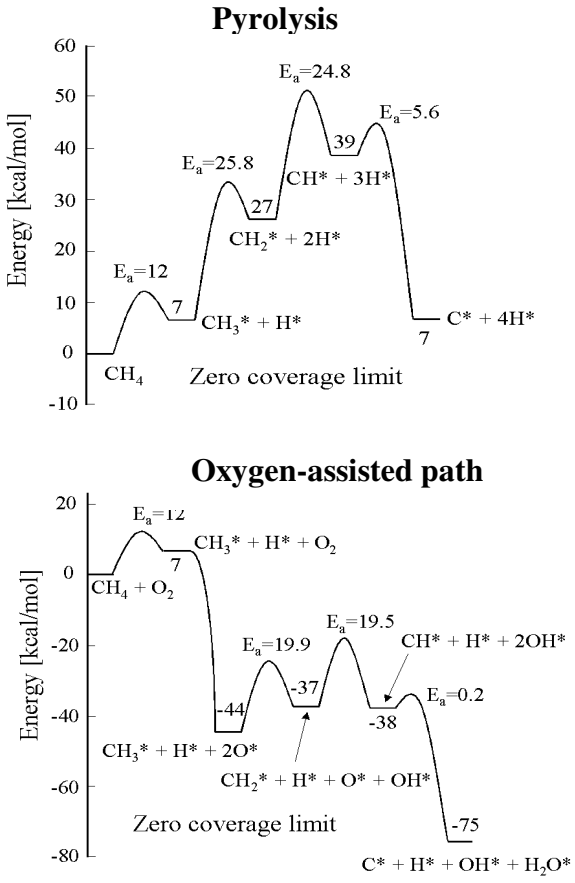

Figure 1. Selected energy diagrams for methane decomposition on Pt. The pyrolysis mechanism and oxygen-assisted mechanism are compared in terms of energetics at the zero coverage limit.

An example of reaction paths of the decomposition of methane on Pt is shown in Figure 1. In contrast to the previous assumption that methane decomposes in a simple step[2], $CH_4 \rightarrow C + 4H$, our energetics indicate that the rate determining step is the second or third hydrogen abstraction. Furthermore, in the presence of oxygen, lower activation energy paths will be preferred. The implications of these multiple reaction paths are that a change in the dominant path with composition as well as with operating conditions (e.g., prior and after ignition) have been observed in our simulations. Thus, the description of the all paths is essential to correctly describe both the entrance (prior to ignition) and main reactor zone (after ignition) of a monolith.

Numerics

In the case of steady state calculations, Newton's method and parametric arc-length continuation method are employed, whereas unsteady state simulations are carried out using the first order ordinary differential equation solver LSODA.

Reactor Scale Models

Depending on the reactor modeled, different reactor scale models have been implemented. Examples include a catalytic thin film plug flow reactor (PFR), a perfectly mixed fluidized bed reactor, a

temperature programmed desorption (TPD) model, and a catalytic stagnation flow micro-reactor.

Prediction of Conversion and Selectivity Data at Atmospheric Pressure

This section discusses the validation of the surface reaction mechanism by comparing with available experimental data in a fluidized bed reactor. In particular, Bharadwaj and Schmidt have carried out conversion and selectivity measurements as a function of operating temperature in a fluidized bed reactor with Pt-coated Al_2O_3 beads[8]. Figure 2 shows experimental as well as predicted methane conversion and selectivity to syngas for a mixture of 29.5% methane in air and conditions indicated in the figure caption.

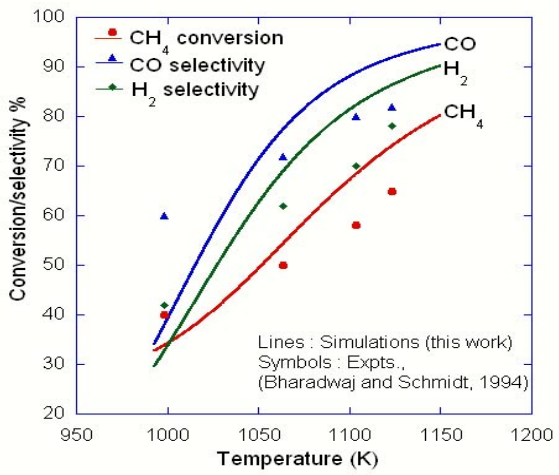

Figure 2. Comparison of predicted conversion and selectivity to syngas with experimental data of Bharadwaj and Schmidt.

The experiments have been conducted in a fluidized bed and the simulations using a catalytic CSTR, with an area per unit volume ratio of 15000 cm^{-1} and a residence time of 0.18 s. No optimization has been done for the reaction mechanism. Internal mass transfer limitations are not considered to be important. The concentration of OH, which is a main indicator of the role of gas phase chemistry, is very low ($<10^{-13}$) in this range. The negligible role of gas phase chemistry under these conditions has been further validated by excluding the gas phase chemistry from our calculations. The predicted data matches fairly well the experimental data except at lower temperatures, where the model underpredicts conversion as well as selectivities. Future work will address this last issue (see also below).

Surface Chemistry Optimization

From the preliminary simulations, we have observed fairly good agreement with available experimental data (see Figure 2). However, parameter optimization is necessary to accurately capture experimental data and have a reliable mechanism that can be used for reactor design. To accomplish the aim of optimizing the surface chemistry, we have concentrated on the ultra-high vacuum (UHV) conditions also where external mass transfer and heat effects are negligible. Developing a mechanism that is a valid over a wide range of pressure (pressure gap) is also important from a reactor design point of view, as most experiments have been conducted at relatively low pressures compared to the industrially desirable conditions. Results from these optimization studies along with illustration of the dominant reaction paths in syngas formation will be discussed.

Conclusion

A thermodynamically consistent detailed surface reaction mechanism with coverage-dependent activation energies and heats of reactions has been developed for methane oxidation simulations. Experimental data from literature are well captured by the proposed reaction mechanism.

Acknowledgement

This work was supported by the Department of Energy.

References

(1) Pfefferle, W. C.; and L. D. Pfefferle, *Prog. Energ. Combust. Sci.*, **1986**, 12, 25.
(2) Hickman, D. A.; and L. D. Schmidt, *J. Catal.*, **1992**, 138, 267.
(3) GRI-Mech 3.0 (1999) Gas Research- Institute mechanism for natural gas, taken from http://www.me.berkeley.edu/gri_mech.
(4) Aghalayam P.; Park Y.K.; Fernandes N.; Papavassiliou V.; and Vlachos D.G., *I&ECR*, **2001**, To be submitted.
(5) Aghalayam P.; Park Y.K.; and Vlachos D.G., *AIChE J.*, **2000**, 46(10), 2016.
(6) Aghalayam P.; Park Y.K.; and Vlachos D.G., *Symposium (International) on Combustion*, **2000**, 28, 1331.
(7) Shustorovich, E.; and Sellers, H., *Surf. Science Rep.*, **1998**, 31, 1.
(8) Bharadwaj S.S.; and Schmidt L.D., *J. Catal.* **1994**, 146, 11.

Temperature-Programmed Studies on Partial Oxidation of CH_4 to Syngas over a Ni/Al_2O_3 Catalyst

LI Chun-Yi [1], ZHANG Zhao-Bin [2],
YU Chang-Chun [2],and SHEN Shi-Kong [2]

1. National Key Lab of Heavy Oil Processing, College of Chemistry & Chemical Engineering, University of Petroleum, Dongying, Shandong Province 257061
2. Catalytic Key Lab of CNPC, University of Petroleum, Changping, Beijing 102200

Introduction

Partial oxidation of CH_4 to syngas has been a hotspot of research for the advantages comparing to steam reforming process, such as low H_2/CO ratio ($\approx$2), more energy-efficient, and high CH_4 conversion and selectivities to CO and H_2 with smaller reactor and short contact time ($\leqslant 10^{-2}$s), etc [1-3]. Many metal catalysts have been studied, such as supported Rh, Pt, Pd, Ru, Re, Ir, Ni, Fe and Co, etc. The supported noble Rh catalyst exhibits excellent activity and selectivity [4], but its price is too expensive. The supported Ni catalysts have similar performance with supported Rh, and the price of Ni is far lower than that of Rh. So the studies on supported Ni catalyst have attracted a great number of researchers [5-14].

About the reaction mechanism, some authors [15,16-18] pointed out that partial oxidation of CH_4 to syngas proceeds via indirect oxidation mechanism, namely: complete combustion of CH_4 to CO_2 and H_2O and subsequently reforming reaction of the residual CH_4 with CO_2 and H_2O to CO and H_2. However, other authors [9,19,20,21] claimed that the reaction proceeds via direct oxidation mechanism: H_2 is from the decomposition of CH_4 and CO is the product of the reaction between surface carbon species and surface oxygen species.

Our work [22] on the reaction over a Ni/Al_2O_3 catalyst supports direct oxidation mechanism. CH_4 firstly decomposes on active metal Ni sites to H_2 and Ni_xC, and then Ni_xC reacts with NiO formed by oxidation of metallic Ni by O_2 to CO or CO_2 depending on the concentration of NiO around Ni_xC. Steady and non-steady state isotopic transient experiments showed that most of CO_2 during the reaction is from the surface reaction between Ni_xC and NiO, not from disproportionation of CO or further oxidation of CO [23]. This also proves the mechanism we suggested.

Furthermore, metal Ni is active sites of the Ni/Al_2O_3 catalyst. So the catalyst must be kept in reduced state, or the reaction mechanism will change and the conversion of CH_4 and the selectivities to H_2 and CO will be very low for CH_4 can't decompose on NiO [24].

In this paper, the Ni/Al_2O_3 catalyst was evaluated and the effects of temperature and space velocity were investigated with on-line chromatography analysis. In addition, temperature-programmed technique was used to investigate the change of the catalyst surface state during the reaction at different temperature and its influence on the conversion and selectivities.

Experimental

The preparation of the 8%(mol, $\frac{Ni}{Ni+Al}$) Ni/Al_2O_3 catalyst has been depicted elsewhere [22,24]. The granularity range is 0.30-0.45mm to eliminate the effect of inner diffusion. The BET surface area and the dispersion of Ni measured by ASAP2010 are 280m^2/g and about 5%, respectively.

The reactor for catalyst evaluation is a quartz tube with inner diameter 12mm. 450mg catalyst was placed in the middle and the other space of the reactor was filled with 0.45~0.9mm quartz sand. Before reaction the catalyst was reduced with pure H_2 at 700^{o}C for 4h. The products were analyzed with on-line gas chromatography (GC) (HP5890). The analysis method called Double-column in Series Analysis was developed by Zhang et al [25], which permits to analyze all the effluents in partial oxidation of CH_4 to syngas with once sample injection.

The apparatus for temperature-programmed experiments has been introduced in the reference [22,24]. All experiments were carried out in a fixed bed quartz micro-reactor with inner diameter 5.5mm at atmospheric pressure, and the total flow rate was 30mL/min. For TPO (temperature-programmed oxidation) and TPR (temperature-programmed reduction), 200mg catalyst was used. For the other experiments, only 30mg catalyst was used. The effluents of the reactor were monitored by a quadrupole mass spectrometer (MS) (AMTEK QuadLink 1000) with the minimum dwell time of 3 milli-seconds.

Results and Discussion

Evaluation of the Ni/Al_2O_3 catalyst under different temperature and space velocity The performance of the catalyst for partial oxidation of CH_4 to syngas was investigated at 600^{o}C, 700^{o}C, and 800^{o}C with different space velocity 53.3 h^{-1}, 65.2 h^{-1}, 77.0h^{-1}, respectively. After the reaction had proceeded for 1h over the catalyst pre-reduced for 4h at 700^{o}C, we sampled and analyzed the products with on-line GC. The results of conversion and selectivity were listed in **table 1**. The conversion of CH_4 is all more than 80% except for at 600^{o}C and 53.3h^{-1}, and even more than 90 % at 800^{o}C. Apparently, high temperature is favorable for CH_4 conversion. The selectivities to H_2 are in the range of 94.8% to 97%, very high at all the conditions. At higher space velocity, the selectivity to CO may exceed 90% at or above 700^{o}C. At 800^{o}C and 77h^{-1}, the selectivity to CO is 95.2%, approaches 96% the thermodynamic equilibrium value at the temperature [16]. Obviously, the catalyst exhibits very good performance. Zhang [26] gave even better results: the conversion of CH_4 95.6%, the selectivity to H_2 99.7%, and to CO 94.5%. These show that Ni base catalyst is the most promising one for partial oxidation of CH_4.

Table1. Results of partial oxidation of CH_4 over the catalyst

T (^{o}C)	Space velocity (h^{-1}, wt/wt)	Conversion of CH_4 (%)	Selectivity to CO (%)	Selectivity to H_2 (%)
600	53.3	79.2	82.6	94.9
	65.2	81.1	85.4	94.8
	77.0	83.9	87.2	95.9
700	53.3	84.6	89.3	95.4
	65.2	85.8	90.5	95.5
	77.0	87.2	91.1	96.3
800	53.3	89.7	94.3	96.3
	65.2	91.0	94.8	96.8
	77.0	91.7	95.2	97.0

Based on the results listed in **Table 1**, temperature and space velocity affect the results significantly. At the same space velocity, the conversion of CH_4 and the selectivities to H_2 and CO all increase with temperature. From 600^{o}C to 800^{o}C, at space velocity 53.3h^{-1} they increase 10.5, 1.4, and 11.7 percentage points, respectively. At 77.0h^{-1}, however, they increase 7.8, 1.1, and 8.0 percentage points, respectively. Obviously, at low space velocity both the conversion and the selectivities are more sensitive to temperature, and the selectivity to H_2 is more inert to temperature. Furthermore, the conversion of CH_4 and the selectivities to H_2 and CO all increase with space velocity, too. At 600^{o}C, they increase 4.7, 1.0, and 4.6 percentage points from 53.3h^{-1} to 77.0h^{-1}, respectively. However, at 800^{o}C they increase only 2.0, 0.7, and 0.9 percentage points, respectively. So at low temperature they are sensitive to space velocity. Similarly, the selectivity to H_2 is insensitive to space velocity.

Temperature-programmed decomposition of CH_4 and temperature-programmed partial oxidation of CH_4 from 510^{o}C to 800^{o}C Temperature-programmed decomposition of CH_4

proceeded in pure CH_4 with the rate of 25°C/min over the catalyst that had been reduced in pure H_2 at 700°C for 4h. The results were shown in **figure 1**. When temperature increases to 330°C, that the intensities of CH_4 and H_2 begin to decrease and increase respectively shows that CH_4 can decompose at the temperature. Between 330°C and 490°C, CH_4 decomposed is only a little. When temperature exceeds 490°C, CH_4 can decompose quickly and a large quantity of H_2 is produced. With Ni on the surface of the catalyst converting to Ni_xC [18], CH_4 stops to decompose gradually.

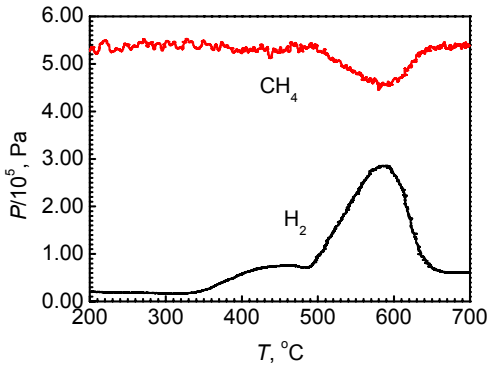

Figure 1. Curve for temperature programmed decomposition of CH_4 over the Ni/Al_2O_3 catalyst.

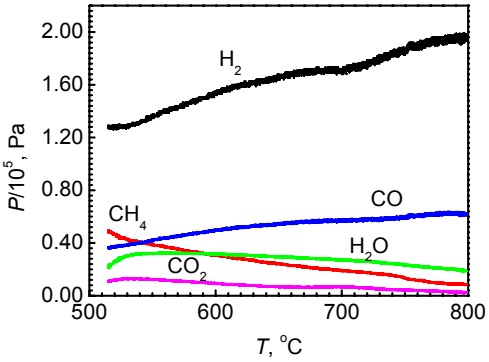

Figure 2. Curves for temperature-programmed partial oxidization of CH_4 from 500°C to 800°C over the Ni/Al_2O_3 catalyst reduced.

The catalyst was reduced firstly with pure H_2 for 4h at 700°C. In pure Ar, temperature was decreased to about 510°C, and then the atmosphere was switched from Ar to 2/1 (mol/mol) CH_4/O_2. After the switch, partial oxidation of CH_4 happens immediately. During the reaction, O_2 is consumed completely [15,26,27], and the conversion of CH_4 and the selectivities to H_2 and CO are changing with temperature. In **figure 2**, even at 510°C, the main products are H_2 and CO, but the conversion of CH_4 is very low (about 30%), and the selectivities to H_2 and CO are all not high (about 80% and 75%, respectively). With the increase of temperature, the conversion of CH_4 and the selectivities to H_2 and CO all increases gradually. At 800°C, the conversion of CH_4 and the selectivities to H_2 and CO are about 90%, 95% and 93%, consistent basically to that of catalyst evaluation.

The results of catalyst evaluation and **Figure 2** show that high temperature and high space velocity are all favorable for the conversion of CH_4 and the selectivities to CO and H_2. According to the mechanism we suggested, the decomposition of CH_4 over metal Ni sites to H_2 and Ni_xC is the precondition of the reaction [22]. In **figure 2**, No O_2 is detected during the process no matter how much the conversion of CH_4 is. As indicates that the conversion of CH_4 and the selectivities to H_2 and CO are dependent on the rate of CH_4 decomposition. High temperature can quicken the decomposition of CH_4 (**figure 1**), so the conversion of CH_4 increases with temperature. For CO and CO_2 are from the reactions between Ni_xC and NiO on the catalyst surface [22],

$$Ni_xC + NiO \rightarrow (x+1)Ni + CO$$

$$Ni_xC + 2NiO \rightarrow (x+2)Ni + CO_2$$

and O_2 is consumed completely. If the conversion of CH_4 is lower, CO_2 is easier to be produced due to more NiO and less Ni_xC on the catalyst surface. Therefore the selectivity to CO will be affected by the conversion of CH_4 seriously. H_2, however, is the product of CH_4 decomposition. The adsorption of H_2 on the catalyst is very weak at high temperature. Although more NiO on the catalyst surface will promote the reaction

$$H_{2(ad)} + NiO \rightarrow H_2O + Ni$$

to produce H_2O, the temperature effect on the selectivity to H_2 is very weak.

Partial oxidation of CH_4 is a mild exothermic reaction,

$$CH_4 + \frac{1}{2}O_2 \rightarrow 2H_2 + CO$$

$$\Delta H^o_{298K} = -35.7 kJ/mol$$

To enhance space velocity, the heat released per catalyst surface will increase. Although temperature of the catalyst bed is controlled, the increase of inner surface temperature of the catalyst granules is inevitable. It's obvious that enhancing space velocity is indirectly increasing the temperature. So the effect of space velocity on the reaction is similar to that of temperature.

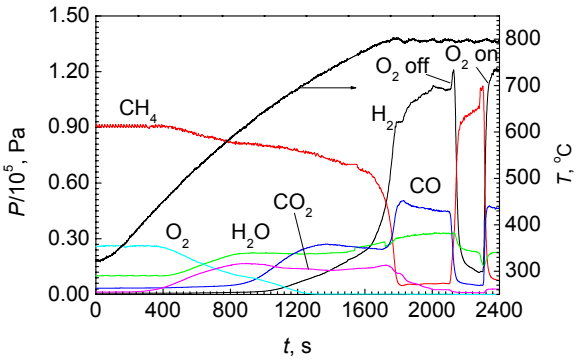

Figure 3. Curves for temperature-programmed reaction of partial oxidation of methane over the reduced Ni/Al_2O_3 catalyst under 30mL/min 2/1(mol/mol) CH_4/O_2 from room temperature to 800°C. Shut off O_2 for a few min and reopening at 800°C.

Transformation of the catalyst surface state during temperature-programmed partial oxidation of CH_4 If the other conditions were the same as that of **Figure 2** and temperature-programmed partial oxidation of CH_4 began from room temperature, the results are absolutely different from **Figure 2**. At about 430°C, CO_2 and H_2O are produced (**Figure 3**). When temperature increases to about 600°C, CO and H_2 appear. The intensities of these products increase with temperature. At 700°C, the conversions of CH_4 and the selectivities to H_2 and CO are about 8%, and 75%, 40% respectively, far lower than that in **Figure 2**. O_2 is not consumed completely here.

Continue to increase the temperature, when it exceeds 750 °C, the intensity of H_2 goes up quickly with temperature and O_2 is

consumed completely. Thereafter the intensity of CO also ascends rapidly. At 800 °C, the conversion of CH_4 and the selectivities to H_2 and CO reach or exceeds 90%. We closed O_2 for a while then reopened. It is can be seen that no evident change in the conversion of CH_4 and the selectivities to H_2 and CO happens before O_2 mass flow controller was closed and after it was reopened.

TPO and TPR of the catalyst show that the catalyst begins to be oxidized from about 250°C and the rate of oxidization is quickened with the increase of temperature, however, reducing the catalyst needs higher than 650°C. So the catalyst is easy to be oxidized and difficult to be reduced. In **figure 1**, CH_4 begins to decompose at 330°C. Thereby, if temperature-programmed partial oxidation of CH_4 begins from the temperature CH_4 can't decomposes rapidly, the catalyst surface will be oxidized. CH_4 can't decompose on the oxidized catalyst. We have discussed the effect of surface state and adsorbed oxygen on partial oxidation of CH_4 to syngas [24]. At or below 700°C, if the catalyst surface is oxidized, O_2 will not be able to be consumed completely and a certain amount of reversibly adsorbed oxygen will exist on the catalyst surface. Non-selective oxidation between CH_4 and reversibly adsorbed oxygen with high oxidation activity [28] occurs via Rideal-Eley mechanism, and both the conversion of reactants and the selectivities to H_2 and CO are very low.

With the increase of temperature, the reaction rate between CH_4 and adsorbed oxygen quickens. When temperature increases to around 750°C, O_2 is consumed completely, as can be seen clearly in **figure 3**. Then NiO on the catalyst surface has the chance to be reduced by hydrogen produced and metal Ni sites that are necessary for CH_4 decomposition form. Thereupon, CH_4 begins to decompose and the reaction mechanism changes to direct oxidation mechanism. Thus, when we closed O_2 for a while and then re-open, the conversion of CH_4 and the selectivities to H_2 and CO are almost unchanged for the catalyst surface has been reduced. Therefore, during partial oxidation of CH_4, the catalyst must be maintained in the reduced state, and CH_4 can react with O_2 via direct oxidation mechanism with high conversion and selectivity.

If partial oxidation of CH_4 proceeds at the temperature lower than 750°C, the catalyst must be kept reduced state. Otherwise, the conversion of CH_4 and the selectivities will be very low for CH_4 can't decompose and can only react with adsorbed oxygen on the oxidized catalyst surface via Rideal-Eley mechanism. However, if the reaction temperature is higher than 750°C, the catalyst is unnecessary to be reduced before reaction and metal Ni sites can form automatically during the reaction for O_2 is consumed completely.

Acknowledgement

This work is supported by the National Natural Science Foundation of China (Issue No. 29673027).

References

1 Tang S., Lin J., and Tan K.L. *Catal. Lett*. **1998**, *55*: 83.
2 Hickman D.A., Haupfear E.A., and Schmidt L.D. *Catal. Lett*. **1993**, *17*: 223.
3 Tsipouriari V.A., Zhang Z., and Verykios X.E. *J. Catal*. **1998**, *179*: 283.
4 Hickman D. A., and Schmidt L.D. *J. Catal.*, **1992**, *138*: 267.
5 Prettre M., Bichner C. H. and Perrin M. *Trans. Faraday Soc.*, **1946**, *43*: 335.
6 Hayakawa T., Anderson A. G., Shimizu M., and Suzuki K.. *Catal. Lett.*, **1993**, *22*: 307.
7 Lu Y., Deng C., Ding X.J., Shen S.K. *Chinese J. Catal.*, **1996**, *17(1)*: 28 (in Chinese).
8 Choudhary V. R., Rane V. H., and Rajput A. M. *Catal. Lett.*, **1993**, *22*: 289.
9 Choudhary V. R., Rajput A. M., and Prabhakar B. *J. Catal.*, **1993**, *139*: 326.
10 Choudhary V. R., Rajput A. M., and Prabhakar B. *Catal. lett.*, **1995**, *32*: 391.
11 Choudhary V. R., Rane V. H., and Rajput A. M. *Catal. Lett.*, **1992**, *16*: 269.
12 Choudhary V. R., Sansare S. D., and Maman A.S. *Appl. Catal.*, **1992**, *89*: 90.
13 Choudhary V. R., Rajput A. M., and Rane V. H. *J. Phys. Chem.*, **1992**, *96*: 8686.
14 Slagtern A., Swaan H.M., Olsbye U., Dahl I.M., and Mirodatos C. *Catal. Today*, **1998**, *46*: 107.
15 Ashcroft A. T., Cheetham A. K., Foord J. S., Green M. L. H., Grey C. P., Murrell A. J., and Vernon P.D. F. *Nature*, **1990**, *344*: 319.
16 Dissanayake D., Rosynek M.P., Kharas K.C.C., and Linsford J.H. *J. Catal*., **1991**, *132*: 117.
17 Looij F.V., Giezen J.C.V., Stobbe E.R., and Geus J.W. *Catal. Today*, **1994**, *21*: 495.
18 Ruiz A. G., Aparicio P. F., Baeza M.B. B., Ramos I. R. *Catal. Today*. **1998**, *46*: 99.
19 Hickman D. A., and Schmidt L.D. *Science*, **1993** , *259*: 343.
20 Mallens E.P.J., Hoebink J.H.B.J., and Marin G.B. *J. Catal*. **1997**, *167*: 43.
21 Matsumura Y., and Moffat J.B. *Catal. Lett*. **1994**, *24*: 59.
22 Shen S.K., Li C.Y. and Yu C.C. *Stud. Surf. Sci. Catal.*, **1998**, *119*: 765.
23 Li C.Y., Yu C.C., and Shen S.K. *Acta Physico-Chimica Sinica*, **2000**, *16*: 97.
24 Li C.Y., Yu C.C., and Shen S.K. *Catal. Lett.*, **2000**, *67(2-4)*: 139.
25 Zhang Z.B., Yu C.C., and Shen S.K. *Analysis and Measurement Technology & Instrument*, **1998**, *4*: 98. (in Chinese).
26 Zhang Z.B. *Studies on Ni Base Catalysts for Partial Oxidation of CH_4*, Ph. D. Thesis, University of Petroleum, Beijing, **1999** (in Chinese).
27 Huszar K. *Acta. Chim. Acad. Sci. Hungar*, **1971**, *70*: 287.
28 Li C.Y., Yu C.C., and Shen S.K. *Chinese J. Catal.*, **1998**, *19(5)*: 463 (in Chinese).

TRANSESTERIFICATION OF DIMETHYL OXALATE AND PHENOL OVER TS-1 CATALYST

Xinbin Ma, Shengping Wang, Hongli Guo, Genhui Xu

State Key Laboratory of C_1 Chemistry and Technology,
School of Chemical Engineering and Technology, Tianjin University,
Tianjin 30072, China

Introduction

Polycarbonates (PCs) are excellent engineering thermoplastics and substitutes for metals and glass because of their good impact strength and transparency [1]. In recent years, there has been an increasing demand for safer and environmentally friendly processes for PC synthesis. Non-phosgene based processes have been proposed to replace the traditional phosgene process [2]. One such process is composed of the synthesis of diphenyl carbonate (DPC) followed by the transesterification between DPC and bisphenol A. Several alternative methods for DPC synthesis have been developed or proposed. Among them, the transesterification of dimethyl oxalate (DMO) and phenol via three-step reaction has been considered as one of possible routes for DPC synthesis from the raw materials such as carbon monoxide, phenol and oxygen [3-4]. In the first step, dimethyl oxalate is produced by carbonylation of methanol, as shown in equation (1), and in the second step, diphenyl oxalate (DPO) is obtained from transesterification of dimethyl oxalate and phenol, as shown in equation (2), and in the third step, the decarbonylation of DPO, as shown in equation (3), is carried out to produce DPC and by-product carbon monoxide.

$$2CO + 2CH_3OH + 1/2O_2 \rightarrow (COOCH_3)_2 + H_2O \quad (1)$$

$$(COOCH_3)_2 + 2PhOH \rightarrow (COOPh)_2 + 2CH_3OH \quad (2)$$

$$(COOPh)_2 \rightarrow CO(OPh)_2 + CO \quad (3)$$

Usually, the transesterification of DMO and phenol in reaction (2) is carried out in the liquid phase using homogeneous catalysts such as Lewis acid and soluble organic Pb, Sn, or Ti compounds [3-4]. But the separation of the catalysts from the products will be complicated when these catalyst systems are applied to the industrial process. There are few reports on the development of active heterogeneous catalysts for the reaction. Hence we report that the titanium silicate molecular sieve TS-1 is an excellent solid catalyst for this reaction. It is well known that TS-1 is active in a variety of oxidation reactions. Reported herein is a new aspect of TS-1 as an acid catalyst.

Experimental

The TS-1 obtained from SINOPEC Research Institute of Petroleum Processing were dried in an oven at 393K for 2h to remove the absorbed water and calcined at different temperature for 2h in the air.

Ester change reactions were performed by mixing DMO, phenol and catalyst TS-1 1.8 g in a 250 ml glass flask equipped with a thermometer, a stirrer under refluxing conditions at atmosphere pressure. Identification and quantitative analysis of reaction products were carried out by a GC-MS spectrometer of HP 5890-HP5971MSD and a gas chromatograph equipped with a flame detector (FID). An OV-101 packed column was used to separate products for GC analysis.

The specific surface areas of the catalysts were determined using a constant volume adsorption apparatus (CHEMBET-3000) by the N_2 BET method at the liquid nitrogen temperature. Powder X-ray diffraction (XRD) measurements were conducted on a MAC Science Co. Model D/Max-2500 X-ray diffractometer using a radiation source of Cu Kα at 40 kV and 100 mA with a scanning rate of 8° min^{-1}.

Results and Discussion

In catalysts screening experiments, it was found that TS-1 is one of the most efficient catalysts for the transesterification of dimethyl oxalate and phenol. It was observed that methylphenyl oxalate (MPO) as an intermediate was produced, which is the same as the case with homogenous catalyst. It proved that DPO have been synthesized via a two-step reaction module from DMO and phenol since the direct synthesis of DPO is limited due to low equilibrium constants as the same as the transesterification of dimethyl carbonate and phenol. The first step, transesterification of DMO and phenol proceeds as shown in reaction (4) and formed MPO is disproportionated into DPO and DMO in reaction (5).

$$(COOCH_3)_2 + PhOH \rightarrow PhOOCOOCH_3 + CH_3OH \quad (4)$$

$$2PhOOCOOCH_3 \rightarrow (COOPh)_2 + (COOCH_3)_2 \quad (5)$$

The selectivity of the MPO and DPO (%) are defined as the moles of MPO and DPO produced per 100 mole of consumed DMO, and the yield of the MPO and DPO (%) are obtained from multiplication of phenol conversion by MPO selectivity and DPO selectivity, respectively.

It was observed that little by-products were anisole, which could be produced via methylation of phenol and DMO, when TS-1 was used in the ester change reaction of the DMO and phenol. The catalyst TS-1 performed significantly better than the other catalysts as shown in Table 1. The sum of the MPO selectivity and the DPO selectivity based on DMO of the catalyst TS-1 could reach 97.5% when the other catalyst only have 20~30%. Although the $Ti(OC_4H_9)_4$ and $AlCl_3$ showed good activities according to the conversion of the DMO, but the selectivity to MPO and DPO are poor. When the $Ti(OC_4H_9)_4$ was chosen as the catalyst of the transesterification of the DMO and phenol, the major by-products were n-butyl alcohol, n-butyl ether, butylphenyl oxalate and ethyl benzene, the selectivity to by-products was more than 76.5%. It was also observed the major by-products were anisole when the $AlCl_3$ and $MgCl_2$ as catalyst, the selectivity to anisole could reach 70%. Overall, the TS-1 was an efficient catalyst, giving a higher selectivity of MPO and little by-products were produced. However, the production of the DPO was much less than the MPO, indicating that DPO could not be obtained effectively through the disproportionation of MPO in the closed system.

Table 1. The Activities of the Different Materials

Catalyst	DMO conversion (%)	MPO selectivity (%)	DPO selectivity (%)
TS-1[a]	49.6	93.0	4.5
$Ti(OC_4H_9)_4$	92.5	20.6	2.8
$Zn(OAc)_2$	19.1	54.6	3.2
$MgCl_2$	30.5	19.7	0.0
$AlCl_3$	79.8	29.1	2.0

Reaction condition: 0.1 mol DMO, 0.5 mol phenol, 0.01 mol catalyst under refluxing conditions at 453K for 2h.
a: 1.8 g TS-1 calcined at 823K.

The activities of the transesterification reaction in the catalyst TS-1 calcined at 823K as function of the reaction time was shown in Table 2. The conversion of the DMO and the yield of MPO increased rapidly with the increase in the reaction time until 2 hours, beyond which the conversion of DMO didn't change and the yield of MPO decreased due to the disproportionation of MPO. The selectivity to

MPO was a constant of 92.6% at first, and then decreased slowly also due to the disproportionation of MPO. The yield and selectivity of DPO were not much more because the disproportionation of MPO is not favorable thermodynamically and the excessive phenol was used in the experiments. The yield and selectivity of DPO could be enhanced by combination of the common chemical method, such as the reactive distillation.

Table 2. Effect of the Reaction Time on the Activities for the Transesterification of DMO and Phenol over TS-1

Reaction time (h)	DMO conversion (%)	MPO selectivity (%)	MPO yield (%)	DPO selectivity (%)	DPO yield (%)
1	24.1	92.6	22.3	5.9	1.4
2	49.6	93.0	46.5	4.5	2.3
3	49.8	87.9	43.8	11.1	5.5
4	50.8	87.8	44.6	10.9	5.5

Reaction condition: 0.1 mol DMO, 0.5 mol phenol, 1.8 g TS-1 calcined at 823K under refluxing conditions at 453K.

Table 3 tabulates the activities of the catalysts TS-1for the ester change reaction of DMO and phenol as well as the calcination temperature. The selectivity to DPO decreased slowly with the increasing calcination temperature, and selectivity to MPO increased with the increase of the calcination temperature. The result showed that the conversion of DMO and the sum of selectivity to MPO and DPO did not show much variation with the calcination temperature. The conversion of DMO remained at 45~50%, and the sum of selectivity to MPO and DPO were more than 97.5%.

Table 3. Effect of the Calcination Temperature of TS-1 on the Activities for the Transesterification of DMO and Phenol

Calcination temperature (K)	DMO conversion (%)	MPO selectivity (%)	MPO yield (%)	DPO selectivity (%)	DPO yield (%)
723	47.7	86.8	41.4	11.9	5.7
773	50.6	89.0	45.0	9.0	4.6
823	49.6	93.0	46.5	4.5	2.3
873	45.1	93.0	41.9	4.6	2.1

Reaction condition: 0.1 mol DMO, 0.5 mol phenol, 1.8 g TS-1 under refluxing conditions at 453K for 2 hours.

It was also observed that the calcination temperature had not influence on the specific area of the catalyst TS-1, maybe one reason was because the TS-1 was also calcined at 773K for 4h in the factory in the past prior to catalyst thermal treatment by ourselves. The specific area of the catalyst TS-1 was generally 345 m^2/g. But after reaction the specific area of the catalyst TS-1 at calcined at 823K decreased to 295.5 m^2/g. The loss of the specific area of the catalyst TS-1 could be attributed to the carbon deposit. Studies on the influence of the coking on the activities of the catalyst TS-1 are ongoing to enhance and preserve the activity of the catalyst.

There are a large number of studies in the literature on the structure of TS-1 [5]. The XRD patterns of the sample TS-1 are similar too, and the calcination temperatures have no influence on the structure of the catalyst TS-1. The relation between the catalyst TS-1 structures and the activities for transesterification of dimethyl oxalate and phenol will be investigated in the future.

Conclusions

The titanium silicate molecular sieve TS-1 was an active heterogeneous catalyst for the transesterification of dimethyl oxalate and phenol. The sum of the methylphenyl oxalate selectivity and the diphenyl carbonate selectivity based on dimethyl oxalate of the catalyst TS-1 could reach 97.5%, with smaller by-product. The calcination had not obvious influence on the conversion of dimethyl oxalate and the sum of selectivity to methylphenyl oxalate and diphenyl oxalate.

Acknowledgement. This work was supported by foundation for University Key Teacher by the Ministry of Education and the Department of Science and Technology of Yunnan Province for the project on Technology Collaboration and Development in China.

References

(1) Freitag, D.; Grigo, U.; Müler, P.R.; Nouvertné, W. in: Mark, H.F.; Bikales, N.M.; Overberger, C.G.; Menges, G. (Eds.). Encyclopeia of Polymer Science and Engineering, Second ed., Vol. 11, Wiley, New York, 1988, p. 648
(2) Ono, Y. *Pure Appl. Chem*. **1996**, 68, 367.
(3) Keigo, N.; Shuji, T.; Katsumasa, H.; Ryoji, S.; U.S. Patent 5834651 (1998).
(4) Keigo, N.; Shuji, T.; Katsumasa, H.; Ryoji, S.; Akinori, S.; Katsutoshi, W.; U.S. Patent 55922827 (1999).
(5) Notari B. *Stud. Surf. Sci. Catal.* **1987**, 37, 413.